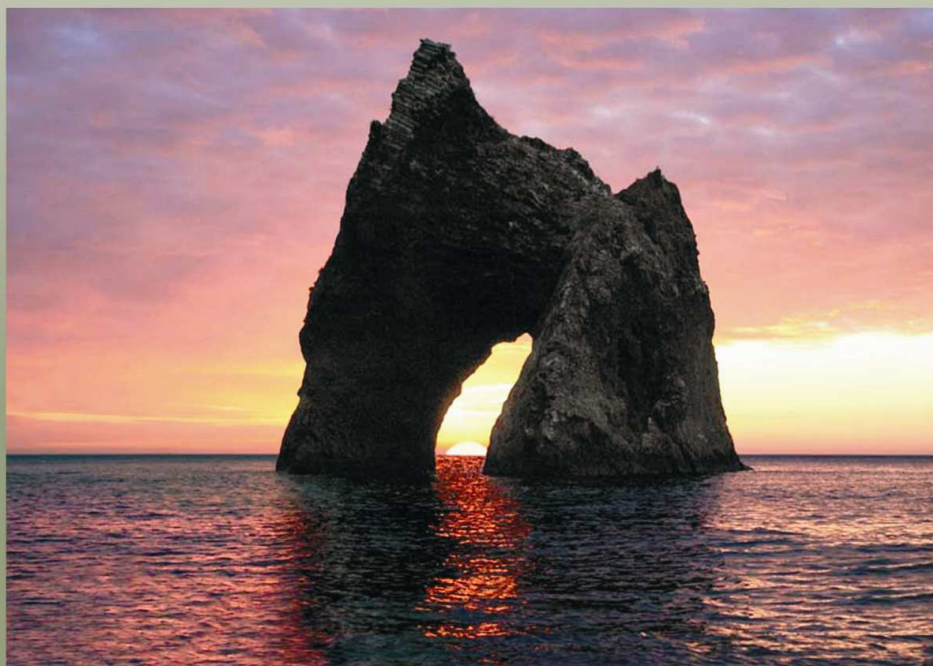




# **DEEP SEATED MAGMATISM, Its sources and plumes**

**Глубинный магматизм, его источники и плюмы**



**IRKUTSK  
2010**

*Russian Academy of Sciences  
Vinogradov Institute of Geochemistry  
Siberian Branch  
Russian Foundation of Basic Research*



# **Deep-seated magmatism, its sources and plumes**

**(Глубинный магматизм, его источники и плюмы)**

**PROCEEDING**  
*of X International Workshop  
«Deep-seated magmatism, its  
sources and plumes»*

*Edited by Dr. N.V. Vladykin*

IRKUTSK

2010

**Deep-seated magmatism, its sources and plumes**

Proceedings of the X International Conference. Publishing House of the Institute of Geography SB RAS, 2010, 209 p., ISBN 978-5-94797-154-5. Vol.1

The materials of the 10<sup>th</sup> periodic workshop are presented in this volume. The fundamental problems of deep-seated magmatism are discussed. The fugacity of oxygen is one of the main parameters responsible for the Earth and other planets evolution. It controls the behaviour of some elements in the processes of protoplanetary nebula condensation, planets accretion and formation of their metallic cores. The red-ox reactions with participation of the deep material determined the primary atmosphere composition and, supposedly, played an important part in life's origin. Based on the paragenetic analysis of minerals (magnetite, ilmenite, titanite, pyroxene) temperature and red-ox conditions of the Khibiny alkaline massif rocks crystallization were estimated. Particular attention has been given to the study of the melt inclusions. Mean compositions of the basitic magmas and the sources of island arches and active continental margins have been calculated and the data on the chemical composition, volatile components and trace elements of magmatic melts of the Kuraminskiy ore area have been obtained based on the evidence derived from the melt inclusions study. The chemical compositions, contents of volatile components and rare elements of melts of some Kamchatka volcanoes are given. On kimberlites themes, the first data on the three new diatremes of Nionok field of the Onega peninsula have been reported. Unusual xenolyths of mica-bearing rocks and garnet piroxenites of the Udachnaya pipe have been described. New data on nanominerals in Yakutian diamonds are given. The geochemical features of lamprophyres of Sikhote-Alin and Bielorusia have been discussed.

The book is of great importance for petrologists, geochemists, and specialists studying deep alkaline and kimberlite magmatism, students and teaching staff of Universities.

*Published following the decision of the Scientific Council  
of Vinogradov Institute of Geochemistry SB RAS*

**Editor: Prof. N.V. Vladykin**

**Reviewers: Prof. V.S. Antipin**

**Original-model: M.D.Sedunova**

Institute of Geography SB RAS  
664033, Irkutsk, Ulanbatorskaja str. 1

Published in Glazkovskaya printing House

Irkutsk, Gogol str., 53.

Order № 2353. Edition 100 copies.

**ISBN 978-5-94797-154-5**

© Institute of Geochemistry SB RAS, 20

© Irkutsk Geography SB RAS, 2010

## TABLE OF CONTENTS

<b>Foreword</b>	<b>4</b>
<b>1. Keith Bell.</b> Carbonatites, isotopes and mantle plumes - some comments	<b>5</b>
<b>2. V. I. Kovalenko, V. B. Naumov, A. V. Girnis, V. A. Dorofeeva, and V. V. Yarmolyuk.</b> Average Composition of Basic Magmas and Mantle Sources of Island Arcs and Active Continental Margins Estimated from the Data on Melt Inclusions and Quenched Glasses of Rocks	<b>21</b>
<b>3. I. D. Ryabchikova and L. N. Kogarko.</b> Thermodynamic analysis of mineral assemblages in magnetite-bearing nepheline syenites (Khibiny Pluton)	<b>52</b>
<b>4. V. B. Naumov, V. A. Kovalenker, and V. L. Rusinov.</b> Chemical Composition, Volatile Components, and Trace Elements in the Magmatic Melt of the Kurama Mining District, Middle Tien Shan: Evidence from the Investigation of Inclusions in Quartz	<b>73</b>
<b>5. Logvinova A.M., Wirth R.</b> Black cluster microinclusions in the core of Yakutian diamonds: Implications for diamond nucleation	<b>91</b>
<b>6. V. B. Naumov, M. L. Tolstykh, E. N. Grib, V. L. Leonov, and N. N. Kononkova.</b> Chemical Composition, Volatile Components, and Trace Elements in Melts of the Karymskii Volcanic Center, Kamchatka, and Golovnina Volcano, Kunashir Island: Evidence from Inclusions in Minerals	<b>102</b>
<b>7. Pokhilenko L.N., Pokhilenko N.P., Vladykin N.V.</b> Garnet Orthopyroxenites from the Udachnaya Kimberlite Pipe (Yakutia); Features of Their Composition and Origin	<b>126</b>
<b>8. Sablukov S.M., Belov A.V. and Sablukova L.I.</b> The alkaline ultrabasic magmatism of the Onega peninsula Nenoksa fields - reflection (display) of the plume and subduction processes in Belomorsky region (Arkhangelsk diamond province)	<b>143</b>
<b>9. Ashchepkov I.V., Ntaflos T., Vladykin N.V., Ionov D.A., Kuligin S.S., Malygina L.V., Mityukhin S.I., Palessky S.V., Khmelnikova O.S.</b> Deep seated xenoliths from the Phlogopite-bearing brown breccia of Udachnaya pipe	<b>162</b>
<b>10. Mikhailov N. D., Laptsevich A. G., Vladykin N.V.</b> Alkali lamprophyres of the Palaeozoic igneous complex of Belarus	<b>185</b>
<b>11. Petukhova L.L., Prihod'ko V.S.</b> Lamprophyres of South Sikhote-Alin	<b>198</b>

## FOREWORD

The fact is well accepted that alkaline rocks represent unique formations on the Earth. They have been long attractive for research because large Nb, Ta, Zr, Y, TR, Cu and P deposits, gemstones of charoite, Cr-diopside, dianite are associated with them. For instance, in Australia diamonds are recovered in lamproites. The complicated processes of their formation provoked scientific disputes still going on. The newly developed analytical methods and techniques provided abundant information on the composition of alkaline rocks. The data on geochemistry of isotopes confirm the evidence on the mantle sources of the substance of alkaline rocks. The new concepts of plume tectonics are applied by scientists when studying alkaline rocks as the deep-seated geodynamics of the Earth is interpreted based on these data. These problems were discussed at the international workshops held in 2001 at the Institute of Geochemistry in Irkutsk; in 2002 at the Far-East Geological Institute, Vladivostok; in 2003 at the Institute of Tectonics and Geophysics in Khabarovsk, in 2004 at Geological Institute in Ulan-Ude, in 2005 at the Institute of Volcanology and Seismology in Petropavlovsk-Kamchatsky), in 2006 in TSNIGRI JC "ALROSA" in Mirny, in 2007 in Irkutsk and Naples (Italy) in 2008 at the Far-East Geological Institute, Vladivostok, in 2009 was held at the Mineralogical Institute, Uralian Branch, in Miass. The materials of the 10<sup>th</sup> periodic workshop are presented in this volume. The fundamental problems of deep-seated magmatism are discussed. The fugacity of oxygen is one of the main parameters responsible for the Earth and other planets evolution. It controls the behaviour of some elements in the processes of protoplanetary nebula condensation, planets accretion and formation of their metallic cores. The red-ox reactions with participation of the deep material determined the primary atmosphere composition and, supposedly, played an important part in life's origin. Based on the paragenetic analysis of minerals (magnetite, ilmenite, titanite, pyroxene) temperature and red-ox conditions of the Khibiny alkaline massif rocks crystallization were estimated. Particular attention has been given to the study of the melt inclusions. Mean compositions of the basitic magmas and the sources of island arches and active continental margins have been calculated and the data on the chemical composition, volatile components and trace elements of magmatic melts of the Kuraminskiy ore area have been obtained based on the evidence derived from the melt inclusions study. The chemical compositions, contents of volatile components and rare elements of melts of some Kamchatka volcanoes are given. On kimberlites themes, the first data on the three new diatremes of Nionok field of the Onega peninsula have been reported. Unusual xenoliths of mica-bearing rocks and garnet piroxenites of the Udachnaya pipe have been described. New data on nanominerals in Yakutian diamonds are given. The geochemical features of lamprophyres of Sikhote-Alin and Bielorrussia have been discussed.

The book might present interest to specialists involved in petrological and geochemical investigations as well as those studying deep alkaline and kimberlite magmatism.

Chairman of Organizing Committee,  
Chief Editor

Dr. N.V. Vladykin

## **Carbonatites, isotopes and mantle plumes - some comments**

Keith Bell

*Ottawa-Carleton Geoscience Centre, Dept. of Earth Sciences,  
Carleton University, Ottawa, Ontario, Canada, Email: [kib@magma.ca](mailto:kib@magma.ca)*

### **ABSTRACT**

Carbonatitic parental melts have low viscosities and low dihedral wetting angles and therefore they become interconnected at very low melt fractions in the mantle and can migrate to the Earth's surface rapidly. Although volumetrically insignificant, the ease with which carbonatites can be identified (high REE and Sr abundances, light REE enrichment, isotope signatures) present a simple and unique way of documenting mantle instabilities that might include plume/hot spot activity, slab roll-back, major rifting/translithospheric faulting, and lithospheric delamination. Some carbonatites, especially those of the Cape Verdes and the Canary Islands, provide robust evidence for plume involvement. Others carbonatites are associated, both spatially and temporally, with flood basalts, e.g. Deccan, Paraná-Etendeka, Siberian, and Keeweenawan LIPs (large igneous provinces) events. Other carbonatites are considered to be plume-related because of their spatial distribution, age, and isotopic chemistry even though they are not associated with flood basalts, e.g. East Africa, and the Kola Peninsula, Russia. Further evidence for carbonatite-plume involvement is the similarity of Hf, Nd, Pb and Sr isotopic data between most young carbonatites and OIBs, and their primitive noble gas signatures (Ar, Ne, Xe). The favoured model involves melting of entrained material in the upper, volatile-rich parts of plumes below a thickened lithosphere. Such a model might also be extended to include rocks of kimberlitic affinity and the wide diversity of alkaline silicate rocks commonly associated with carbonatites.

### **INTRODUCTION**

Although they are among the most volumetrically insignificant of igneous rocks found at the Earth's surface, carbonatites provide unrivalled insights into the chemical evolution of the sub-continental upper mantle. The high Sr, Nd and in some cases Pb abundances of carbonatites provide unique probes into the mantle, and because they extend back into the Archean they can be used to monitor the secular evolution of the mantle over much of the Earth's history. Whether carbonatitic melts are primary or whether they are derived from carbonated silicate melts was contested for many years, but recent evidence has shown that carbonatites can be generated by a variety of processes involving both primary and differentiated melts [9, 53 and reference therein].

Carbonatitic melts are unusual. Not only are they chemically reactive but they differ from most other magmas because of their extremely low viscosity. Measured apparent viscosities of aphyric natrocarbonatitic melts from Oldoinyo Lengai, the only active carbonatite volcano, are more than an order of magnitude lower than the most fluid basaltic melt [55]. With such low viscosities, melts can separate from regions as thick as 100 km in only a few million years, even at small melt

fractions [51]. At melt fractions  $<0.05$  wt %, carbonatitic melts can become interconnected in carbonated olivine-rich mantle with grain sizes of the order of 1 mm [52]. Estimates of ascent rates based on fluid-flow calculations suggest rapid migration (20-65m/s) to the surface [29].

Small degrees of partial melting of carbonated mantle lherzolite can generate carbonatitic as well as alkali silicate liquids that lie very close to the mantle solidus. Such melts, if they escape, can provide sensitive indicators of perturbations in the mantle brought about by processes such as mantle upwellings (plumes/hotspots/hot fingers/diapiric upwelling), continental fragmentation, slab roll back and lithospheric delamination. Whether carbonatitic melts reach the crust depends on the velocity of migration and whether they survive interaction with other mantle phases without undergoing "chemical death" [14]. Reaction between mantle wall-rock and carbonatitic melts can significantly alter the overall chemistry of the mantle and even the melt itself during metasomatism.

## **OIBs AND ISOTOPES**

Are the isotopic compositions of carbonatites similar to those found in oceanic basalts? The isotopic data from OIBs show that the mantle is isotopically heterogeneous, and that such heterogeneities must have existed for substantial periods of time. Several isotopic components have been identified from OIBs, including HIMU (mantle material with a high, time-integrated U/Pb ratio), EMI (enriched mantle I), and EMII (enriched mantle II). For further details the reader is referred to Zindler and Hart [81], Hart [33] and Hofmann, [39]. Another component, with the acronym FOZO, is based on a region of convergence of pseudo-linear arrays in Pb, Sr and Nd isotope space [35]. This component, considered common to all OIBs, is not as well defined as some of the others. The original definition of FOZO ("FOCUS ZONE") set by Hart and co-workers involved a component characterised by depleted Sr and Nd and fairly radiogenic Pb; it is more primitive, yet depleted, than many of the other mantle components. Subsequently defined by the point of convergence of linear arrays from oceanic basalts and associated rocks in three-dimensional isotope ratio diagrams involving EM1, EM2, HIMU and DMM, the various estimates of this common OIB component show considerable differences e.g. FOZO1 [35], FOZO 2 [36], FOZO 3 [68]. The origin of FOZO is traditionally interpreted as a widespread plume component common in OIB and located in the lower mantle [35, 36]. A recent interpretation considers FOZO to be a ubiquitous component in the source of MORB and OIB produced by the continuous recycling and aging of unmodified, oceanic crust [68]. A common component, virtually identical to FOZO, is "C", which has been defined on the basis of the convergence of MORB isotopic arrays [31]. In contrast to OIBs, the isotopic data from normal mid-ocean ridge basalts (MORBs) are relatively uniform, reflecting the most depleted of all the known mantle sources (DMM, depleted MORB mantle) underlying oceanic regions.

DMM rarely appears in isotopic arrays, but has low  $^{87}\text{Sr}/^{86}\text{Sr}$ , high  $^{143}\text{Nd}/^{144}\text{Nd}$  and relatively low  $^{206}\text{Pb}/^{204}\text{Pb}$  ratios.

All of the mantle heterogeneities reflected in OIBs have been attributed to addition of crustal material by subduction, much of which is considerably old, and may go back to at least 2 Ga but this idea has been challenged by Stracke et al. [67]. If the isotopic heterogeneity in the mantle, however, is produced by subducted material then it has been stored for considerable periods of time either within the lowermost mantle or at the 660 km discontinuity.

With the substantial isotopic data base that now exists for carbonatites there is no doubt of their mantle origin [6, 54], and that many young carbonatites (<200 Ma), especially those from East Africa, reflect binary mixing between HIMU and EMI [6, 69, 10, 12]. Most young carbonatites can be divided into two groups, one corresponding to those that involve HIMU and EMI and the other to a group of so-called “Reference Carbonatites” that involve FOZO and HIMU as end-members [13]. The widespread nature of the “Reference Carbonatites” suggests that both FOZO and HIMU are of world-wide distribution [13].

Defining plumes and their products solely on the basis of isotopes, either radiogenic or stable, is difficult. Although some plumes may contain a dominant HIMU or EMI component or high  $^3\text{He}/^4\text{He}$  ratios, more typically there is a significant isotopic variation either within the same group of islands or even within the same island, and this requires isotopic heterogeneity in the upwellings plume [20]. Both the Hawaiian and the Icelandic plumes are good examples. Isotopic trends from individual volcanoes in Hawaii or Iceland, based on He, Hf, Sr, Nd, Pb and Os isotopic data require the presence of isotopically distinct end-members [40, 16, 1]. It thus appears that there is no such thing as a “pure” plume component. Instead, plumes are isotopically and chemically heterogeneous, perhaps even zoned, carrying with them entrained material from various mantle depths (i.e. different source regions). As a consequence of these observations, it appears that the isotopic composition of plumes can change with time, depending on the type of material entrapped within the plume or the degree of interaction of the plume with continental lithosphere. For a detailed review of OIB components, their association with plumes, and melting relationships, the reader is referred to Kogiso [42].

## **CARBONATITES ASSOCIATED WITH KNOWN LIPs**

More than 30 active hotspots are now documented [66], and in the geological record (back to 3.5 Ga) at least 200 potential paleo-plumes are recognized [24, 25, 27, and reference therein). Some hotspots and plumes are associated with alkaline rocks and carbonatites, while others are not. LIPs (large igneous provinces) marked by continental flood basalts and giant, radiating dyke swarms [58, 23] are perhaps the best markers of plume activity, indicating the site of arrival of plumes within

the continental crust and subsequent melting of plume heads. Some flood basalts are associated with carbonatites and alkaline rocks, including the Paraná (Brazil), Etendeka (southwest Africa), Keeweenawan (Canada,) as well as the Siberian and Deccan (India) flood basalts. Ernst and Bell [26] have cited and discussed several examples of carbonatite-LIP associations. One example is discussed below in detail.

Several models relate the Deccan flood basalts of India to the Réunion plume [56]. The main period of basaltic activity at ca. 65 Ma ago marked the first major, surface expression of the Réunion plume on the Indian sub-continent, with outpourings that might have taken place over a very short time interval, perhaps < 1 Ma [18]. Alkaline volcanism both preceded and followed the relatively short-lived outpourings of the Deccan flood basalts [4]. At Amba Dongar, the Deccan flood basalts were cut by carbonatites [75, 63, 76] dated at  $65 \pm 0.3$  Ma which is an event essentially co-eval with Deccan volcanism [57]. On the basis of Pb isotope ratios, Simonetti et al. [63] proposed that the carbonatites at Amba Dongar were petrogenetically linked to the Réunion plume. This model was later modified to include plume-lithosphere interaction for the generation of the carbonatites and alkaline rocks from Bhuj, Barmer and Mundwara [64]. At least three mantle sources were involved in the formation of the Deccan carbonatites and related alkaline silicate rocks, [64], i.e. continental lithosphere, asthenosphere and the Réunion plume.

One way of viewing the isotopic data from flood basalts and carbonatites is to relate them to the mantle plane described by the model end-members HIMU, EMI and DMM in two-dimensional space. The plane can be depicted as a straight line by combining  $^{143}\text{Nd}/^{144}\text{Nd}$  and  $^{206}\text{Pb}/^{204}\text{Pb}$  values into a term plotted against  $^{87}\text{Sr}/^{86}\text{Sr}$  [80].  $f(\text{Nd,Pb})$  [after 80] =  $[(^{143}\text{Nd}/^{144}\text{Nd})^2 + (^{206}\text{Pb}/^{204}\text{Pb})^2]^{1/2} \times \{\sin[\arctan((^{143}\text{Nd}/^{144}\text{Nd}) / (^{206}\text{Pb}/^{204}\text{Pb})) + 0.000064]\}$ . The equation for the mantle plane as given by Tilton et al. (1998) is:  $-0.42881(^{87}\text{Sr}/^{86}\text{Sr}) - 1.358437(^{143}\text{Nd}/^{144}\text{Nd}) - 8.75115 \times 10^{-5} (^{206}\text{Pb}/^{204}\text{Pb}) + 1 = 0$ . Such an approach is useful not only in assessing the data in terms of the mantle plane but it can be used to assess the possible role that the three mantle end-members may have had in producing the isotope data from the carbonatites, the flood basalts and the plume basalts.

Most of the data from the flood basalts form a converging array towards HIMU and the data points from Réunion, and all of the flood basalt data lie well above the mantle plane (see Fig. 14, [5]). The lowest  $^{87}\text{Sr}/^{86}\text{Sr}$  ratios are shown by the data from Réunion that cluster close to the HIMU section of the projection of the mantle plane while the two carbonatites, Amba Dongar and Barmer, although isotopically quite different from one another, overlap with the data from the flood basalts. The isotopic findings are consistent with the involvement of HIMU and EMI plus an additional old, enriched, source.

On the basis of the isotopic data from India, as well as from South Africa and Brazil, it seems that carbonatites are neither unusual nor extreme when compared

to the Sr, Nd and Pb isotopic compositions of flood basalts. Although the data from Réunion and the carbonatites show little overlap, there are enough isotopic characteristics in common between the carbonatites and the flood basalts to argue for similar source involvements. The isotopic ratios from the Amba Dongar carbonatite and some of the flood basalts require the involvement of a component more enriched than HIMU, and EMI, that might well be related to the DUPAL anomaly, a Pb and Sr isotope mantle anomaly encircling the southern hemisphere [32], or by enriched continental lithosphere [64].

There are no compelling arguments, as far as the isotope data are concerned, to conclude that the carbonatites from India, as well as Brazil and Namibia [5] were generated from sources other than those that generated many of the flood basalts. Isotopic similarities to some of the most primitive flood basalts, coupled with the close spatial and temporal relationships, are consistent with a model for carbonatite generation that involves partial melting of source material associated with the flood basalts. Furthermore, these sources can be related to mantle plumes.

### **CARBONATITES ASSOCIATED WITH KNOWN PLUMES**

Although carbonatites are very rare in oceanic environments, the Cape Verdes and the Canary Islands off the west coast of Africa are prime candidates for understanding plume-related carbonatites. Geographic variations of isotopically distinct components in the magma sources on a scale of 100 to 200 km are observed [30], which are similar in size to those estimated for other oceanic islands. The seminal study of the Cape Verde Islands [30] not only related the magmatic products to plume activity but attempted to relate the magmatism to variable degrees of partial melting, spatial distribution within the plume itself and scale lengths of melting within the mantle. Requirements involved three isotope components [30], a HIMU, an EM component, and an “intermediate HIMU” component each one marking the involvement of different mantle “sources”. Attempts to interpret the origin of the different magmatic products to plume geometry placed the earliest lavas and also the basement intrusive rocks, including carbonatites, to the cooler, marginal areas of the plume, whereas later lavas (EM±HIMU±DMM) involving higher degree of partial melting were interpreted to be generated near the proposed plume center [30]. It was thought that the geographic age and geophysical constraints as well as the trace element and isotope variations were due to variable partial melting of a heterogeneous plume (HIMU + depleted mantle) in the northern Cape Verdes, and mixing of plume-derived melts with lithospheric melts (EM) in the southern Cape Verdes. An alternative explanation also involved mixing at the plume margins, but between an EM plume and low degree partial melts derived from entrained pre-existing HIMU components in a heterogeneous DM + HIMU upper mantle. With progressive melting, the effect of the HIMU component seems to have played a diminishing role.

Subsequent studies of the Cape Verde and Canary Islands [37, 38, 21] all supported the heterogeneous nature of the mantle sources and in all of these studies HIMU played an important and consistent role especially during the generation of the calciocarbonatites [38]. This component was attributed to the melting of recycled, carbonated oceanic crust (eclogite) with a recycling age of ~1.6 Ga [38]. Compared with the Cape Verde calciocarbonatites, the less radiogenic Nd and Pb isotopic ratios and the negative  $\Delta 7/4$  of the magnesiocarbonatites require a separate mantle component, perhaps recycled subcontinental lithosphere.

In earlier studies, continental carbonatites were thought to be isotopically much more variable than oceanic, and this was attributed by Hoernle et al. [38] to the involvement of additional enriched components during generation of the continental carbonatites. One of the key ingredients in the Hoernle et al. model is Phanerozoic through to Proterozoic marine carbonates (e.g. limestone) that are recycled either by metasomatism of the lithospheric mantle or by subducting slabs of oceanic crust + marine carbonates into the deep mantle where they can be transported back to the surface by plume activity. However, this idea that continental carbonatites show much greater variation in radiogenic isotopic composition than do their oceanic carbonatites, seems not to hold in the light of the considerable amount of new isotopic data. In both oceanic and continental carbonatites HIMU certainly plays an important role along with an enriched component.

The much simpler model proposed by de Agnacio et al. [21] for the alkaline-carbonatite association of Fuerteventura, Canary Islands, requires only two main components, one a deep-seated, FOZO component, which can account for Sr and Nd compositions, and a HIMU component that can explain the Pb compositions. Fuerteventura, it should be noted, is one of the oldest of oceanic islands, and has been active for the last 80 Ma, a time range comparable to the entire age span of the Hawaii island - Emperor seamount chain [49]. Fuerteventura also contains the oldest known oceanic carbonatite (ca. 60 Ma). A heterogeneous mantle plume with a deep-seated (FOZO) signature that mixed with HIMU at a very specific time (around 25 Ma), forms the basis of the de Agnacio et al. model for the evolution of Fuerteventura.

### **INFERRED PLUMES**

Some carbonatites of continental setting have been attributed to plume activity in spite of the fact that they are neither spatially nor temporally associated with continental flood basalts. Among the best known are those of East Africa and the Kola Alkaline Province.

Most of the East African carbonatite complexes are younger than 120 Ma, and all are associated with nephelinites and phonolites, or their plutonic equivalents. The isotope systematics from these complexes are remarkably simple, and well-behaved given that these carbonatite complexes are found over an extensive geographic region. Sr and Nd isotope ratios define the so-called East African

Carbonatite Line (EACL), a linear array involving only HIMU and EMI [6]. With the addition of Pb to the isotopic data base, the same two-end members were involved in generating a series of binary mixing curves [12]. This simple result from the EACL may have more general application. The similarity of these findings to the LoNd array of Hart et al. [34] defined by basalts from Tubuaii, St. Helena, New England Seamounts, Comores, San Felix and the Walvis Ridge suggests that HIMU-EMI mixing is a widespread process during the production of a range of magmatic products of quite different chemical compositions.

The EACL was attributed to the mixing in different proportions of the two mantle components, HIMU and EMI, and this observation was subsequently incorporated by Bell and Simonetti [10] into a model that involved interaction between a HIMU plume and enriched lithosphere (EMI). However, the latest interpretation of the data involves melting of a heterogeneous, “streaky” or “marble-like” mantle, but still within the framework of a plume model [11].

The voluminous outpourings of plateau phonolites, the three-dimensional geophysical data, crustal uplift as reflected in the Kenya Dome, and the marked zonal arrangement of alkalic rocks, carbonatites and alkali basalts [47, 48] is consistent with plume-related activity. This vast, up-domed magmatic province, 1000 km across, with central and peripheral zones, was considered by Le Bas [48] to reflect an upwelling from a deep mantle source. Although the carbonatites require mixing between HIMU and EMI, one additional mantle component is needed, such as DMM or PREMA, to help explain the isotope systematics of some of the associated silicate rocks [8, 10]. A similar requirement was also proposed by Gerlach et al. [30] for the silicate rocks of the Cape Verde archipelago.

Bell and Tilton [12] restricted the HIMU and EMI components to the sublithospheric mantle but located at deep-seated levels, perhaps the lower 1000 km. It was recognized, too, that such signatures are not restricted to East Africa. Many young, continental carbonatites of world-wide distribution require both HIMU and EMI [69], although others require the involvement of FOZO instead of EMI. Bell and Tilton [13] thought it unlikely that metasomatism of the lithosphere (a possible mechanism for generating EMI), could be so uniformly widespread, not only in East Africa, but elsewhere on Earth and that such a signature could be preserved within the lithosphere for long periods of time.

One of the best examples of plume-related, alkaline rock-carbonatite activity is the extensive igneous province of the Kola Peninsula, eastern part of the Baltic Shield. Considered to be the largest alkaline province on Earth, the Kola event covers a wide tract of ground that extends from the shores of the White Sea north towards the Barents Sea and west into Finland. Reviews of the geology and the various models proposed for the Kola Alkaline Province (KAP) are given in Verhulst et al. [74], Zaitsev and Wall [79 and references therein] and Downes et al. [22]. The KAP includes the Kovdor and Turiy carbonatites as well as the Sokli carbonatite, one of the largest known. On the basis of noble gas data, Marty et al.

[50] was one of the first to point out the importance of plume components in the generation of the Kola carbonatites.

In addition to the noble gas data (see later discussion), additional support for a plume origin for the KAP is marked by the short episode during which magmatism took place; the period from 360 to 380 Ma seems to cover most of the alkaline and carbonatitic magmatism in Kola [44, 79, 22]. Whether the KAP was associated with flood basalt activity remains unclear, but remnants of flood basalts along the northeastern coast, normally attributed to the opening of the Barents Sea during the late Proterozoic, may be Devonian in age and hence may represent LIP-type magmatism [65, 26].

Carbonatites in the Kola Peninsula involved mantle sources with quite different isotopic compositions. For a review of the isotope systematics and the geochronology the reader is referred to Bell and Rukhlov [9] and Rukhlov and Bell [60]. Kramm [43] was first to point out a near-linear array of Nd and Sr isotope data from several of the Kola carbonatites that he attributed to binary mixing involving an enriched end-member (the supposed Devonian equivalent of EMI) and a second with a depleted isotope signature tentatively correlated with an end-member similar in isotopic composition to some of the Canadian carbonatites. Subsequent data showed that binary mixing was insufficient as an explanation, and that at least three end-members were needed [9]. Initial Hf, Sr and Nd data from some rare-metal deposits in Kola also indicate the presence of more than one end-member, consistent with the findings from the carbonatites [41].

## THE NOBLE GAS STORY FOR CARBONATITES

Although the amount of noble gas data from carbonatites is somewhat sparse, some of the Ar, Xe, and Ne data indicate a relatively primitive mantle source. Noble gas data from Canadian (Borden, Prairie Lake) and Brazilian (Jacupiranga) carbonatites support the view that carbonatitic melts are deep-seated, and probably plume-related [61]. Excess  $^{129}\text{Xe}$  in carbonatites, along with  $^{20}\text{Ne}/^{22}\text{Ne}$  and  $^{21}\text{Ne}/^{22}\text{Ne}$  ratios [61] further constrain the origin of carbonatites, and perhaps the sources of HIMU and EMI. The primordial  $^{129}\text{Xe}/^{130}\text{Xe}$  signature in carbonatites, comparable to those in diamonds, is presumably found only in the deeper and hence more primitive parts of the mantle. If the carbon in carbonatites is related to subducted materials then the subducted material must have exchanged gases with those residing in the deep mantle. Sasada et al. [61] made the interesting observation that carbonatites of different age have quite different Sr and Nd signatures, reflecting both enriched and depleted sources, yet their  $^{129}\text{Xe}/^{130}\text{Xe}$  ratios ( $>7$ ) and  $^{40}\text{Ar}/^{36}\text{Ar}$  ratios are similar. This suggests derivation of Sr and Nd from different mantle sources, yet a common source for the primitive volatiles.

Noble gases from Kola carbonatites also show a contribution from a deep plume source [50, 19, and 71]. Measured abundances of  $^3\text{He}$  and  $^4\text{He}$  indicate a large excess of  $^3\text{He}$  and fluids extracted from the carbonatites show  $^4\text{He}/^3\text{He}$  ratios

down to 38,000, which are lower than those of MORBs and in the range of ratios observed in  $^3\text{He}$ -rich OIBs related to mantle plumes. In addition,  $^{20}\text{Ne}/^{22}\text{Ne}$  ratios are much higher than those in the atmosphere implying the occurrence of solar-type Ne in the carbonatite source. The ultrabasic and alkaline rocks from Kola and associated carbonatites thus contain a contribution from a source that has a lower time-integrated  $(\text{U}+\text{Th})/{}^3\text{He}$ ,  $^{22}\text{Ne}$  and  $^{40}\text{K}/{}^{36}\text{Ar}$  ratios than those of the asthenosphere, the sub-continental lithosphere and the continental crust, indicating a source deeper than the convecting mantle that supplied MORB magmas [50].

Even N from the Lesnaya Varaka, Kovdor and Seblyavr carbonatites of the Kola Peninsula [19] indicate a source more enriched in heavy nitrogen than the Earth's surface and the shallow mantle. These data require either a source deep within the mantle that was either contaminated by oceanic crust or the N was affected during core formation by metal-silicate partitioning.

Tolstikhin et al. [71] also worked with carbonatites, and their findings agree, in part, with those of Marty et al. [50]. Included among these are low  $^4\text{He}/{}^3\text{He}$  values well below the mean ratio in mid-ocean ridge basalts, a regression line for  $^{20}\text{Ne}/^{22}\text{Ne}$  versus  $^{21}\text{Ne}/^{22}\text{Ne}$  which is indistinguishable from those typical of plumes, such as Loihi (Hawaii), an inferred source with a  $^{40}\text{Ar}/{}^{36}\text{Ar}$  ratio of about 4000 which is 10 times lower than that of the MORB source end-member and an estimated  $({}^3\text{He}/^{22}\text{Ne})\text{PRIM}$  of about 10, a value that approaches the solar ratio implying a non-fractionated solar-like rare gas pattern within a plume source.

## **MULTIPLE CARBONATITE EMPLACEMENTS**

The main criticism leveled against possible plume sources for carbonatites has been the repeated carbonatite activity over thousands of millions of years within the same crustal segment e.g. Greenland. Bailey [2, 3] has argued vehemently against any plume involvement citing as evidence the localization of activity by old lesions in the lithosphere, the plate-wide synchronicity and the repetition of carbonatite activity.

The large amount of isotopic data, both radiogenic and non-radiogenic, from carbonatites, suggests derivation from a mantle source considerably deeper than the lithosphere. Of the features cited by Bailey [2, 3] as arguments against plume activity, many are actually compatible with a plume model. Any impacting plume would certainly take advantage of lithospheric weaknesses, would be associated with continental rifting and would be involved in concentrating volatiles and incompatible elements during upward migration. Given the estimated size of many plume heads (up to 2000 km in diameter), it is perhaps not too surprising that carbonatites are synchronous over considerable parts of plate regions e.g. Kola alkaline province, and its possible broader distribution in the eastern and southern parts of the East European craton [26].

Repeated episodes of carbonatitic activity in a restricted areas such as that in Greenland [46] implies one of the following: i. that the source for the carbonated melts was attached (or became attached) to the lithosphere and was carried along with the lithosphere during plate migration, or ii. that the same points of weaknesses, such as persistent tranlithospheric faults, were preferentially favoured for transport of carbonated melts through the lithosphere. Reactivation of a fossil plume-head, as another alternative, has been proposed by Toyoda et al. [72] for some Brazilian carbonatites and by Black and Liegeois [15] for localization of alkaline magmatism in Africa.

Repeated magmatism impinging at the same spot on the Earth's surface can be accommodated within a plume model providing that the weaknesses within the lithosphere remain unhealed. Plumes are not rare, isolated, phenomena but are numerous and widespread, and have occurred repeatedly throughout most of the Earth's history [24 and references therein].

## **DISCUSSIONS AND CONCLUSIONS**

Carbonatites clearly provide valuable insights into mantle evolution that few other rocks offer. Carbonatites occur in various tectonic environments, and are not solely restricted to rift zones. This point was emphasized by Woolley and Kjarsgaard [77]. Less than half of all known carbonatites occur in or are associated with graben structures, and many others are associated with major faulting and updoming. It is tempting to relate these tectonic environments and their associated magmatism to plume activity. The typical association with flood basalts, and more broadly with LIPs also supports a plume origin for carbonatites, reflecting perhaps different evolutionary pathways in a single magmatic process/system.

There are two alternatives to generating melts associated with plume activity. Melts can be generated either within the plume itself, involving both primitive and entrained material, or within the overlying mantle by decompression melting induced by the forceful emplacement of the plume head during lithospheric thinning and/or by lowering of the mantle solidus by the introduction of volatiles into the overlying mantle. Modelling of melting within the Hawaiian plume depends on the volatile contents of the plume and the temperature distribution across its boundaries [78]. At the outer portions of any major mantle upwelling, volatile-rich melts are carried towards the C-H-O solidus with release of vapour at depths of about 75-85 km that may generate cracks in the lithosphere accompanied by the escape of low-melt, volatile-rich melts. Higher degrees of partial melting nearer the plume axis will generate more silica-saturated melts. Implied in this model is a symmetrical distribution of rock types with the more silica-enriched, rocks in the centre and the small volume, more volatile-rich rocks at the margins. On the basis of the isotopic data from carbonatites and what is known about plumes, a general model can be formulated in which an isotopically heterogeneous plume with volatile-rich portions and high CO<sub>2</sub>/H<sub>2</sub>O ratios undergoes discrete

partial melting generating low volume, low degree melts that are isotopically different. Such low volume melts might also be generated above the plume during its initial impingement on the lithosphere [26].

Examples of low-volume, isotopically-distinct melts are found within individual East African complexes including Shombole [8], Napak [62], and Oldoinyo Lengai [7, 10]. The scale of melting is consistent with the 25 to 50 km distances proposed for source regions involved in generating the individual shield volcanoes above the active Hawaiian plume [28].

Owing to a substantial increase in viscosity with depth, entrainment of deep-mantle material is to be expected in plume heads [20]. If a continuous supply of material from a hot source is assumed, then a large spheroidal plume head first rises and adjacent mantle melts become incorporated into the plume [17]. Because the temperature of the conduit is appreciably higher than that of the plume head, its composition approximates that of the boundary layer from which the plume originates. Once at the top of the plume head, the conduit material flows radially and forms a thin sheet with a large surface area. The composition of the plume head becomes compositionally and thermally zoned, in keeping with what is known of the of the Hawaiian and Iceland plumes [36, 40]. Assuming that the starting material is OIB-type mantle then the plume head should be zoned with layers of enriched OIB-type mantle separating regions of entrained, normal mantle [17]. Partial melting of isotopically distinct regions within a plume on a scale greater than the heterogeneities might explain some of the isotopic differences observed from many carbonatite complexes. Estimates based on inter-shield geochemical differences among Hawaiian volcanoes point to melt production regions similar in size to those estimated for the source variations [28]. On the basis of He isotopic data, the melting zone of the Hawaiian plume is considered to be  $< 40$  km in radius [45].

Returning to the concerns expressed about the carbonatite-plume relationship and the repeated incursions of carbonatitic melts into the same portions of the Earth's crust over periods of time considerably longer than the average life span of a mantle plume, such localized incursions might be related to mechanical weaknesses within the sub-continental lithosphere, which once established remain active as “chemical-free pathways” for low viscosity melts.

It might be unwise to attribute all carbonatites to plume activity given that some carbonatites are probably related to other types of mantle upwellings, such as those associated with extension at continental margins, large-scale overturns, slab break-off and crustal delamination. Establishing a set of criteria that could be used to separate one group of carbonatites from the other, requires a thorough evaluation of ages, field relationships, petrology, geochemistry and mineralogy in those areas where plume impingement is generally accepted such as the Cape Verde and Canary Islands.

In summary, the following features of carbonatites are consistent with a plume model:

- i. the similarity of isotopic signatures between OIBs and many carbonatites,
- ii. the primitive nature of the noble gas data from some carbonatites,
- iii. the association of carbonatites with known plumes (Cape Verde and Canary Islands) and
- iv. the temporal and spatial relationships of some carbonatites to LIPs.

The vertical and lateral stratification of plume heads, the thermal effects of three-dimensional flow, and the ability of the upper parts of the plume to distribute and retain volatile-rich materials are all features important to our understanding of the generation of carbonated melts. The extremely low degrees of partial melting required to generate melts of alkaline and carbonatitic affinity probably reflect magma generation from the cooler parts of a plume where volatiles have been retained in quantities sufficient to generate carbonatitic and alkaline magmatism.

## ACKNOWLEDGEMENTS

Thanks go to my former graduate students and post-doctoral fellows who taught me a great deal and made my scientific life considerably more exciting. Thanks to A. Simonetti and R. Ernst for discussions during the writing of this overview.

## REFERENCES

1. **Abouchami, W., Hofmann, A.W., Galer, S.J.G., Frey, F.A., Eisele, J. and Feigenson, M.** Pb isotopes reveal bilateral asymmetry and vertical continuity in the Hawaiian mantle plume: *Nature*, 2005, v. 434, pp. 851-856.
2. **Bailey, D.K.** Carbonate magmas: *Journal of the Geological Society of London*, 1993a, v.150, p. 637-651.
3. **Bailey, D.K.** Petrogenetic implications of the timing of alkaline, carbonatite, and kimberlite igneous activity in Africa: *South African Journal of Geology*, 1993b, v. 96, p. 67-74.
4. **Basu, A.R., Renne, P.R., DasGupta, D.K., Teichmann, F. and Poreda, R.A.** 1993, Early and late alkali igneous pulses and a high-<sup>3</sup>He plume origin for the Deccan flood basalts: *Science*, v. 261, p. 902-906.
5. **Bell, K.** Carbonatites: Relationships to mantle-plume activity: *in* Ernst, R.E. and Buchan, K.L., eds., *Mantle plumes: their identification through time*. Geological Society of America Special Paper 352, 2001, p. 267-290.
6. **Bell, K. and Blenkinsop, J.** Nd and Sr isotopic compositions of East African carbonatites: implications for mantle heterogeneity: *Geology*, 1987, v. 15, p. 99-102.
7. **Bell, K., and Dawson, J. B.** Nd and Sr isotope systematics of the active carbonatite volcano, Oldoinyo Lengai: *in* Bell, K., and Keller, J., eds., *Carbonatite Volcanism: IAVCEI Proceeding in Volcanology 4*, Springer-Verlag, Berlin, 1995, p. 100-112.
8. **Bell, K. and Peterson, T.D.** Nd and Sr isotope systematics of Shombole volcano, East Africa, and the links between nephelinites, phonolites and carbonatites: *Geology*, 1991, v. 19, p. 582-585.
9. **Bell, K. and Rukhlov, A.S.** Carbonatites from the Kola Alkaline Province: origin, evolution and source characteristics: *in* Zaitsev A, Wall F (eds) *Phoscorites and*

- carbonatites from mantle to mine: the key example of the Kola Alkaline Province, vol 10. The Mineralogical Society, 2004, London, United Kingdom, pp 421-455.
10. **Bell, K. and Simonetti, A.** Carbonatite magmatism and plume activity: implications from the Nd, Pb and Sr isotope systematics of Oldoinyo Lengai: *Journal of Petrology*, 1996, v. 37, p. 1321-1339.
  11. **Bell, K. and Simonetti, A.** Source of parental melts to carbonatites – critical isotopic constraints: *Mineralogy and Petrology*: 2010, v.98, p.77-89
  12. **Bell, K. and Tilton, G.R.** Nd, Pb and Sr isotopic compositions of East African carbonatites: evidence for mantle mixing and plume inhomogeneity: *Journal of Petrology*, 2001, v.42, p. 1927-1945.
  13. **Bell, K., and Tilton, G.R.** Probing the mantle: the story from carbonatites: EOS, American Geophysical Union, 2002, v. 83, p. 273, 276-277.
  14. **Bell, K., Kjarsgaard, B.A. and Simonetti, A.** Carbonatites - into the twenty-first century: *Journal of Petrology*, 1998, v. 39, p. 1839-1845.
  15. **Black, R. and Liegeois, J.-P.** Cratons, mobile belts, alkaline rocks and continental lithospheric mantle: the Pan-African testimony: *Journal of the Geological Society of London*, 1993, v. 150, p. 89-98.
  16. **Blichert-Toft, J., Weis, D., Maerschalk, C., Agranier, A. and Albarede, F.** Hawaiian hot spot dynamics as inferred from the Hf and Pb isotope evolution of Mauna Kea volcano: *Geochemistry Geophysics Geosystems* <sup>3</sup>G, 4, 8704, doi:10.1029/2002GC000340, 2003.
  17. **Campbell, I.H. and Griffiths, R.W.** Implications of mantle plume structure for the evolution of flood basalts: *Earth and Planetary Science Letters*, 1990, v. 99, p. 79-93.
  18. **Courtillot, V., Feraud, G., Maluski, H., Vandamme, D., Moreau, M.G. and Besse, J.** Deccan flood basalts and the Cretaceous/Tertiary boundary: *Nature*, 1988, v. 333, p. 843-846.
  19. **Dauphas, N. and Marty, B.** Heavy nitrogen in carbonatites of the Kola Peninsula: a possible signature of the deep mantle: *Science*, 1999, v. 286, p. 2488-2490.
  20. **Davies, G.F.** Plates, plumes, mantle convection and mantle evolution: *in* Jackson, I. (ed), *The Earth's mantle*, Cambridge University Press, 1998, pp.228-258.
  21. **De Agnacio, C., Munoz, J. Sagredo, S. Fernandez-Santin, and Johansson, A.** Isotope geochemistry and FOZO mantle component of the alkaline-carbonatitic association of Fuerteventura, Canary Islands, Spain: *Chemical Geology*, 2006, v. 232, p. 99-113.
  22. **Downes, H., Balaganskaya, E., Beard, A., Liferovich, R P. and Demaiffe, D.** Petrogenetic processes in the ultramafic, alkaline and carbonatitic magmatism in the Kola Alkaline Province: a review: *Lithos*, 2005, v. 85, p. 48-75
  23. **Ernst, R.E. and Buchan, K.L.** Giant radiating dyke swarms: their use in identifying pre-Mesozoic large igneous provinces and mantle plumes: *in* Mahoney, J.J. and Coffin, M.F. *Large Igneous Provinces: Geophysical Monograph 100*, 1997, p. 297-333.
  24. **Ernst, R.E. and Buchan, K.L.** Mantle plumes: their identification through time: *GSA Special Paper 352*, 2001, pp. 593.
  25. **Ernst, R.E., and Buchan, K.L.** Large igneous provinces (LIPs) in Canada and adjacent regions: 3 Ga to present: *Geoscience Canada*, 2004, v. 31 p.103-126.
  26. **Ernst, R.E. and Bell, K.** Large igneous provinces (LIPs) and carbonatites: *Mineralogy and Petrology*, 2010, v. 98, 55-76.
  27. **Ernst, R.E., Wingate, M.T.D., Buchan, K.L., and Li, Z.X.** Global Record of Large Igneous Provinces (LIPs) during evolution of the Rodinia supercontinent (1600-700 Ma): *Precambrian Research*, 2008, 160, 159-178
  28. **Frey, F.A. and Rhodes, J.M.** Intersield geochemical differences among Hawaiian volcanoes: implications for source compositions, melting process and magma ascent paths: *in* Cox, K.G., McKenzie, D.P. and White, R.S. (eds.). *Melting and melt movement in the*

- Earth: Philosophical Transactions of the Royal Society of London, Series A, 1993, v. 342, p.121-136.
29. **Genge, M.J., Price, G.D. and Jones, A. P.** Molecular dynamics simulation of CaCO<sub>3</sub> melts to mantle pressures and temperatures: implications for carbonatite magmas: Earth and Planetary Sciences, 1995,v. 131, p. 225-238.
  30. **Gerlach, D.C., Cliff, R.A., Davies, G.R., Norry, M. and Hodgson, N.** Magma sources of the Cape Verdes archipelago: isotopic and trace element constraints: Geochimica et Cosmochimica Acta, 1988, v. 52, p. 2979-2992.
  31. **Hanan, B.B. and Graham, D.W.** Lead and helium isotopic evidence from oceanic basalts for a common deep source of mantle plumes. Science, 1996, v. 272, p. 991-995.
  32. **Hart, S.R.** A large scale isotope anomaly in the southern hemisphere mantle: Nature, 1984, v. 309, p. 753-757.
  33. **Hart, S.R.** Heterogeneous mantle domains: signatures, genesis and mixing chronologies: Earth and Planetary Science Letters, 1988,v. 90, p. 273-296.
  34. **Hart, S. R., Gerlach, D.C. and White, W.M.** A possible new Sr-Nd-Pb mantle array and consequences for mantle mixing: Geochimica et Cosmochimica Acta, 1986, v. 50, p. 1551-1557.
  35. **Hart, S.R., Hauri, E.H., Oschmann, L.A. and Whitehead, J.A.,** Mantle plumes and entrainment: isotopic evidence: Science, 1992, v. 256, p. 517-520.
  36. **Hauri, E.H., Whitehead, J.A. and Hart, S.R.** Fluid dynamic and geochemical aspects of entrainment in mantle plumes: Journal of Geophysical Research, 1994, v. 99, p. 24275-24300.
  37. **Hoernle, K.A.and Tilton, G.R.** Sr-Nd-Pb isotope data for Fuerteventura (Canary Islands) basal complex and subaerial volcanics: applications to magma genesis and evolution: Schweizerische Mineralogische und Petrographische Mitteilungen: 1991, v. 71, p. 3-18.
  38. **Hoernle, K., Tilton, G., Le Bas, M.J., Duggen, S. and Garbe-Schöneberg, D.** Geochemistry of oceanic carbonatites compared with continental carbonatites: mantle recycling of oceanic crustal carbonate: Contribution to Mineralogy and Petrology, 2002, v. 142, p.520-542.
  39. **Hofmann, A.W.** Sampling mantle heterogeneity through oceanic basalts: isotopes and trace elements: *in* Carlson, R.W. (ed) The Mantle and Core Vol. 2. Treatise on Geochemistry, Elsevier-Pergamon, Oxford, 2005, pp. 61-101.
  40. **Kempton, P.D., Fitton, J.G., Saunders, A.D., Nowell, G.M., Taylor, R.N., Hardarson, B.S. and Pearson, G.** The Iceland plume in space and time: a Sr-Nd-Pb-Hf study of the North Atlantic rifted margin: Earth and Planetary Science Letters, 2000, v.177, p. 255-271.
  41. **Kogarko, L.N., Lahaye, Y. and Brey, G.P.** Plume-related mantle source of super-large rare metal deposits from the Lovozero and Khibina massifs on the Kola peninsular, eastern part of the Baltic Shield: Sr, Nd and Hf isotope systematics. Mineralogy and Petrology, 2010, v. 98. 197-208.
  42. **Kogiso, T.** A geochemical and petrological view of mantle plume: *in* Superplumes: Beyond Plate Tectonics, edited by D.A. Yuen, S. Maruyama, S. Karato and B.F. Windley, 2007, pp 165-185. Springer, The Netherlands.
  43. **Kramm, U.** Mantle components of carbonatites from the Kola Alkali Province, Russia and Finland: European Journal of Mineralogy, 1993, v. 5, p. 985-989.
  44. **Kramm, U., Kogarko, L.N., Kononova, V.A. and Vartiainen, H.** The Kola alkaline province of the CIS and Finland: precise Rb-Sr ages define 380-360 age range for all magmatism: Lithos, 1993, v. 30, p. 33-44.
  45. **Kurz, M.D.** Mantle heterogeneity beneath oceanic islands: some inferences from isotopes: *in* Cox, K.G., McKenzie, D.P. and White, R.S. (eds.). Melting and melt movement in the

- Earth: Philosophical Transactions of the Royal Society of London, Series A, 1993, v.342, p. 91-103.
46. **Larsen, L.M. and Rex, D.C.** A review of the 2500 Ma span of alkaline-ultramafic, potassic and carbonatitic magmatism in West Greenland: *Lithos*, 1992, v. 28, p. 367-402.
  47. **Le Bas, M.J.** Per-alkaline volcanism, crustal swelling and rifting: *Nature*, 1971, v. 230, p. 85-87.
  48. **Le Bas, M.J.** The East African Cenozoic magmatic province: *Accademia Nazionale dei Lincei*, 1980, v. 47, p. 111-122.
  49. **Le Bas, M.J., Rex, D.C. and Stillman, C.J.** The early magmatic chronology of Fuerteventura, Canary Islands: *Geological Magazine*, 1986, v. 123, p. 287-298.
  50. **Marty, B., Tolstikhin, I., Kamensky, I.L., Nivin, V., Balaganskaya, E. and Zimmerman, J-L.** Plume-derived rare gases in 380 Ma carbonatites from the Kola region (Russia) and the argon isotopic composition in the deep mantle: *Earth and Planetary Science Letters*, 1998, v. 164, p. 179-192.
  51. **McKenzie, D.** The extraction of magma from the crust and mantle: *Earth and Planetary Science Letters*, 1985, v. 74, p. 81-91.
  52. **Minarik W.G. and Watson, E.B.** Interconnectivity of carbonate melt at low melt fraction: *Earth and Planetary Science Letters*, 1995, v. 133, p. 423-437.
  53. **Mitchell R.H.** Carbonatites and carbonatites and carbonatites: *Canadian Mineralogy*, 2005, v. 43, p. 2049-2068.
  54. **Nelson, D.R., Chivas, A.R., Chappell, B.W. and McCulloch, M.T.** Geochemical and isotopic systematics in carbonatites and implications for the evolution of ocean-island sources: *Geochimica et Cosmochimica Acta*, 1988, v. 52, p. 1-17.
  55. **Norton, G.E. and Pinkerton, H., 1997,** Rheological properties of natrocarbonatites from Oldoinyo Lengai, Tanzania: *European Journal of Mineralogy*, v. 9, p. 351-364.
  56. **Peng, Z.X. and Mahoney, J.** Drillhole lavas from the northwestern Deccan Traps, and the evolution of the Réunion hotspot mantle: *Earth and Planetary Science Letters*, 1995, v. 134, p. 169-185.
  57. **Ray, J.S. and Pande, K.** Carbonatite alkaline magmatism associated with continental flood basalts at stratigraphic boundaries: causes for mass extinctions: *Geophysical Research Letters*, 1999, v. 26, p. 1917-1920.
  58. **Richards, M.A., Duncan, R.A. and Courtillot, V.E.** Flood basalts and hot spot tracks: plume heads and tails: *Science*, 1989, v. 246, p. 103-107.
  59. **Ritsema, J., van Heijst, J. and Woodhouse, J.H.** Complex shear wave velocity structure imaged beneath Africa and Iceland: *Science*, 1999, v. 286, p. 1925-1928.
  60. **Rukhlov, A.S. and Bell, K.** Geochronology of carbonatites from the Canadian and Baltic Shields, and the Canadian Cordillera: clues to mantle evolution: *Mineralogy and Petrology*, 2010, v.98, p.11-54.
  61. **Sasada, T., Hiyagon, H., Bell, K. and Ebihara, M.** Mantle-derived noble gases in carbonatites: *Geochimica et Cosmochimica Acta*, 1997, v. 61, p. 4219-4228.
  62. **Simonetti, A. and Bell, K.** Nd, Pb and Sr isotopic data from the Napak carbonatite-nephelinite centre, eastern Uganda: an example of open-system crystal fractionation: *Contributions to Mineralogy and Petrology*, 1994, v. 115, p. 356-366.
  63. **Simonetti, A., Bell, K. and Viladkar, S.** Isotopic data from the Amba Dongar carbonatite complex, west-central India: evidence for an enriched mantle source: *Chemical Geology (Isotope Geoscience Section)*, 1995, v. 122, p. 185-198.
  64. **Simonetti, A., Goldstein, S.L., Schmidberger, S.S. and Viladkar, S.L.** Geochemical and Nd, Pb, and Sr isotope data from Deccan alkaline complexes - inferences for mantle sources and plume-lithosphere interaction: *Journal of Petrology*, 1998, v. 39, p. 1847-1864.

65. **Sinitsyn, V.A. and Kushev, V.G.** Devonian traps of the Timan-Kola region: Academy of Sciences USSR, Doklody, (Earth Science Section), 1968, v. 178, p. 86-87.
66. **Sleep, N.H.** Hotspots and mantle plumes: some phenomenology: *Journal of Geophysical Research*, 1990, v. 95, p. 6715-6736.
67. **Stracke, A., Bizimis, M. and Salters, V.J.M.** Recycling oceanic crust: quantitative constraints: *Geochemistry Geophysics Geosystems* <sup>3</sup>G, 8003, doi:10.1029/2001GC000223, 2003.
68. **Stracke, A., Hofmann, A.W. and Hart, S.R.** FOZO, HIMU and the rest of the mantle zoo: *Geochemistry Geophysics Geosystems* <sup>3</sup>G, 2004GC000824, 2005.
69. **Tilton, G.R. and Bell, K.** Sr-Nd-Pb isotope relationships in late Archean carbonatites and alkaline complexes-applications to the geochemical evolution of Archean mantle: *Geochimica et Cosmochimica Acta*, 1994, v. 58, p. 3145-3154.
70. **Tilton, G.R., Bryce, J.G. and Mateen, A.** Pb-Sr-Nd isotope data from 30 and 300 Ma collision zone carbonatites in northwest Pakistan: *Journal of Petrology*, 1998, v. 39, p. 1865-1874.
71. **Tolstikhin, I.N., Kamensky, I.L., Marty, B., Nivin, V.A., Vetrin, V.R., Balaganskaya, E.G., Ikorsky, S.V., Gannibal, M.A., Weiss, D., Verhulst, A., and Demaiffe, D.** Rare gas isotopes and parent trace elements in ultrabasic-alkaline-carbonatite complexes, Kola Peninsula: identification of lower mantle plume component: *Geochimica et Cosmochimica Acta*, 2002, v. 66, p. 881-901.
72. **Toyoda, K., Horiuchi, H. and Tokonami, M.** Dupal anomaly of Brazilian carbonatites: geochemical correlations with hotspots in the South Atlantic and implications for the mantle source: *Earth and Planetary Science Letters*, 1994, v. 126, p. 315-331.
73. **Van der Hilst, F.D., Widiyantoro, S. and Engdahl, E.R.** Evidence for deep mantle circulation from global tomography: *Nature*, 1997, v. 386, p. 578-584.
74. **Verhulst, A., Balaganskaya, E., Kirnarsky, Y. and Demaiffe, D.** Petrological and geochemical (trace elements and Sr-Nd isotopes) characteristics of the Paleozoic Kovdor ultramafic, alkaline and carbonatite intrusion (Kola Peninsula, NW Russia): *Lithos*, 2000, v.51, p.1-25.
75. **Viladkar, S. G.** The carbonatites of Amba Dongar, Gujarat, India: *Bulletin of the Geological Society of Finland*, 1981, v. 53, p. 17-28.
76. **Viladkar, S.G.** Geology of the carbonatite-alkalic diatreme of Amba Dongar, Gujarat: International workshop. GMDC Science and Research Centre, 1996, Ahmedabad. 74 p.
77. **Woolley, A.R. and Kjarsgaard, B.A.** Carbonatite occurrences of the world: Map and database: Geological Survey of Canada, 2008, Open File 5796
78. **Wyllie, P.J.** Solidus curves, mantle plumes, and magma generation beneath Hawaii: *Journal of Geophysical Research*, 1988, v. 93, p. 4171-4181.
79. **Zaitsev, A., and Wall, F., eds.** Phoscorites and Carbonatites from Mantle to Mine: the key example of the Kola Alkaline Province: *Mineralogical Society Series 10*, 2004, London, p. 421-455.
80. **Zindler, A., Jagoutz, E. and Goldstein, S.** Nd, Sr and Pb isotopic systematics in a three-component mantle: a new perspective: *Nature*, 1982, v. 298, p. 519-523.
81. **Zindler, A. and Hart, S. R.** Chemical dynamics: *Annual Reviews of Earth and Planetary Sciences*, 1986, v. 14, p. 493-571.

UDK 550.442

## **Average Composition of Basic Magmas and Mantle Sources of Island Arcs and Active Continental Margins Estimated from the Data on Melt Inclusions and Quenched Glasses of Rocks**

V. I. Kovalenko<sup>1</sup>, V. B. Naumov<sup>2</sup>, A. V. Giris<sup>1</sup>, V. A. Dorofeeva<sup>2</sup>,  
and V. V. Yarmolyuk<sup>1</sup>

<sup>1</sup> *Institute of Geology of Ore Deposits, Petrography, Mineralogy, and Geochemistry, Russian Academy of Sciences, Staromonetnyi per. 35, Moscow, 119017 Russia, E\_mail: vik@igem.ru;*

<sup>2</sup> *Vernadsky Institute of Geochemistry and Analytical Chemistry, Russian Academy of Sciences, ul. Kosygina 19, Moscow, 119991 Russia; E\_mail: naumov@geokhi.ru.*

### **ABSTRACT**

Based on the generalization of data on melt inclusions and quenched glasses, the average compositions of subduction (island arc and active continental margin settings) basic magmas were estimated. The main geochemical features of the average composition of these magmas are significant depletion in Nb and Ta, less significant depletion in Ti, Zr, and Sm, and enrichment in Cl, H<sub>2</sub>O, F, and P in the primitive mantle normalized patterns. The average normalized contents of moderately incompatible HREE in these magmas are close to those in the basic magmas of other geodynamic settings. Subduction basic magmas exhibit negative correlation of Li, Y, Dy, Er, Yb, Lu, and Ti contents with MgO content. Most of incompatible elements (Nb, Ta, U, Th, LREE) do not correlate with MgO, but correlate with each other and K<sub>2</sub>O. Variations in element contents are related to crystallization differentiation, magma mixing, and possibly, participation of several sources. The water content in the island arc basic magmas varies from almost zero value to more than 6 wt %. Most compositions are characterized by weak negative correlation between H<sub>2</sub>O and MgO contents, but some compositions define a negative correlation close to that in magmas of mid ocean ridges (MOR). Considered magmas demonstrate distinct positive correlation between MgO content and homogenization temperature, practically coinciding with those of MOR magmas. Modeling of phase equilibria revealed widening of crystallization field of olivine in the magmas of subduction zones compared to MOR magmas. This can be related to the high water content in subduction magmas. Simultaneous liquidus crystallization of olivine and clinopyroxene in subduction magmas occur at pressure approximately 5 kbar higher than that of MOR magmas. Based on the average ratios of trace element to K<sub>2</sub>O content, we determined the average compositions for subduction magma sources. Relative to depleted mantle, they are enriched in all incompatible elements, with positive anomalies of U, Rb, Ba, B, Pb, Cl, H<sub>2</sub>O, F, and S, and negative anomalies of Th, K, Be, Nb, Ta, Li, Nd, Pb, and Ti. A general elevated content of incompatible elements indicates a reworking of the rocks of mantle wedge by fluids and melts that were released from the upper layers of subducted plate.

## INTRODUCTION

It is considered that the basic and ultrabasic magmas of island arcs (IA) and active continental margins (ACM) are formed in mantle wedge metasomatized by fluids or melts that were released from subducted oceanic lithosphere [3]. This explains the water enrichment of these magmas, as well as their elevated oxidation state and some specifics in the behavior of trace elements (for instance, Nb, Ti, and Zr). Kelemen and others [23] estimated the average contents of major and some trace elements in the basic and intermediate rocks of subduction zone in the light of problems of magma formation in island arc systems. At the same time, it is known that the average compositions of mantle magmas and source of IA and ACM have not been considered in detail. In this paper, we attempted to estimate these compositions using data on the melt inclusions in the minerals and quenched glasses of the rocks. The advantage of this approach is the possibility to study the behavior of volatiles and perfectly mobile components, which cannot be determined from the rock composition [23].

In this paper, the IA and ACM magmas are considered together and will be termed as “subduction” magmas, because their differences are insignificant. At present, a great body of melt inclusion data has been accumulated, including determinations of volatiles and numerous trace elements. Our data base of compositions of melt inclusions [45] includes more than 480000 determinations for 73 elements, which will be used in this paper. In this work, we do not distinguish petrochemical series (tholeiitic, calc\_alkaline, and others), but consider all entirety of compositions together. More detailed analysis is the subject of future studies.

## APPROACH TO THE SOLUTION OF THE PROBLEM

The factual base for this study is the data set of compositions of melt inclusions from phenocryst minerals and quenched glasses of the rocks from subduction settings [45]. Based on these data, we calculated the average composition of basic magmas that are formed in mantle subduction zones. The contents of rock-forming components of magmas were calculated as arithmetic mean compositions, while that of trace elements, as geometric mean, because they define a lognormal distribution [32].

The average contents of incompatible elements in magma sources could be estimated from their ratios to the average content of element, whose concentration in the suprasubduction zones are known. In the previous studies [31, 33, 34, 29], it was demonstrated by the example of midocean ridges (MOR) and within-plate geodynamic settings that ratios of highly incompatible elements to K<sub>2</sub>O content in basic magmas and their sources are close. More accurate contents of ratios of elements to K<sub>2</sub>O in source with allowance for difference in degree of incompatibility can be determined using equations:

$$\log(C_0^{K_2O} / C_0) = \log(C^{K_2O} / C) - (D^{K_2O} - D) \log(1 - M), \quad (1)$$

where  $C_0^{K2O}$  and  $C_0$  are concentrations of K2O and any incompatible element in source (mantle),  $C^{K2O}$  and  $C$  are contents of these elements in magma derived from this source,  $D^{K2O}$  and  $D$  are the crystal/melt bulk partition coefficient for K2O and incompatible element,  $(1 - M)$  is degree of melting of source or magma differentiation.  $D$  was taken to be constant and equals to values estimated for MOR magmas in the paper [68]. The average K2O content in mantle of subduction settings is unknown. However, one can suggest [34] that the content of moderately incompatible Dy in all types of mantle is close to its average content in depleted mantle (0.531 ppm). Thus, using equation

$$C = C_0(1 - M)^{D-1}, \quad (2)$$

we can estimate the melting degree for the average composition of basic magmas from Dy content, and then, the average K2O content in mantle of subduction settings. The average contents of other incompatible elements in source of basic subduction magmas can be calculated using equation (1).

As was shown earlier [32], in spite of the allowance for differences in incompatibility of trace elements, the described procedure seems to be valid for the most incompatible elements having bulk partition coefficient less than 0.05. The average contents of elements with  $D > 0.05$  (Ti, P, S, Y, and HREE) in source are better to determine from their ratios to Dy with  $D \sim 0.8$  [68].

This approach was used for estimating mantle compositions of MOR, oceanic islands, and withinplate oceanic settings [33, 34, 29, 30], suggesting that  $D$  values for basic magmas of these settings are close to those in MOR magmas. This assumption is based on the relative stability of mineral composition of mantle sources. Under subduction settings, the mineral composition of mantle could be modified owing to influx of components released from subducted plate. However, these changes concern mainly trace elements, whereas partition coefficients of major rock-forming components remain unchanged.

## **COMPOSITIONS OF SUBDUCTION BASIC MAGMAS**

Unlike MOR and within-plate oceanic settings, the subduction magmatic complexes contain significant amounts of felsic and intermediate rocks (Fig. 1). In this paper, we consider mainly compositions with SiO<sub>2</sub> content less than or equal 54 wt %, which corresponds to the boundary of the first maximum in the histogram (Fig. 1a). For sake of brevity, these magmas were termed basic magmas, though some of them have intermediate and ultrabasic compositions. The second maximum in the histogram corresponds to felsic magmas, which were discussed by us previously in relation with the problem of formation of agpaitic melts [28]. Intermediate (andesitic) magmas play subordinate role in subduction settings, which is reflected in the presence of the corresponding minimum in the histogram (Fig. 1), though andesites play significant, occasionally predominant role among the IA and ACM rocks [14]. This paradox was noted by us previously [44; 62] and explained by the fact that most andesites are cumulate rocks that crystallized from felsic magmas.

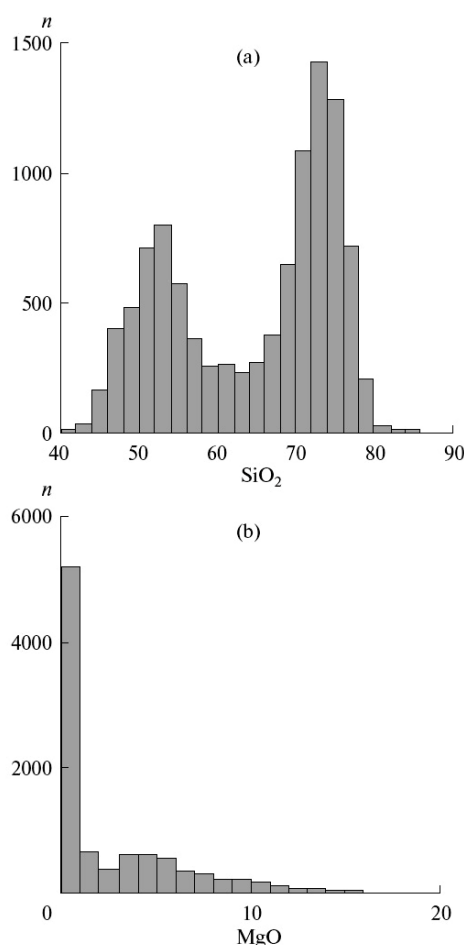


Fig. 1. Histogram of SiO<sub>2</sub> (a) and MgO (b) contents (wt %) in the subduction magmas (10385 determinations on melt inclusions and quenched glasses from the rocks).

A set of data on IA and ACM includes analyses from 411 papers. Below, we list only those works that report more than 100 analyses of melt inclusions or quenched glasses. During 1992–2004, there were only eleven of such works: 2, 64, 58, 11, 59, 60, 61, 65, 12, 16, 21. Fourteen works were published for the last five years (2005–2009): 7, 67, 8, 37, 38, 43, 10, 24, 47, 20, 39, 48, 56, 51. The geographical distribution of objects represented in data set (modern subduction settings and their paleoanalogues) is shown in Fig. 2.

The average composition of subduction basic magmas is represented in Table 1, while Fig. 3 demonstrates spider-diagrams for incompatible elements, including volatile components (H<sub>2</sub>O, Cl, F, B, and S). For comparison, this diagram also shows the average compositions of basic magmas of MOR and within-plate continental settings from our previous papers [33, 34, 29, 30]. As for magmatic rocks, the main geochemical feature of subduction magmas of intermediate composition is deep negative Nb–Ta anomaly, and less significant negative anomalies of Ti, Zr, and Hf. The contents of Nb, Ta and most moderately incompatible elements in them are lower than those in MOR magmas. In general,

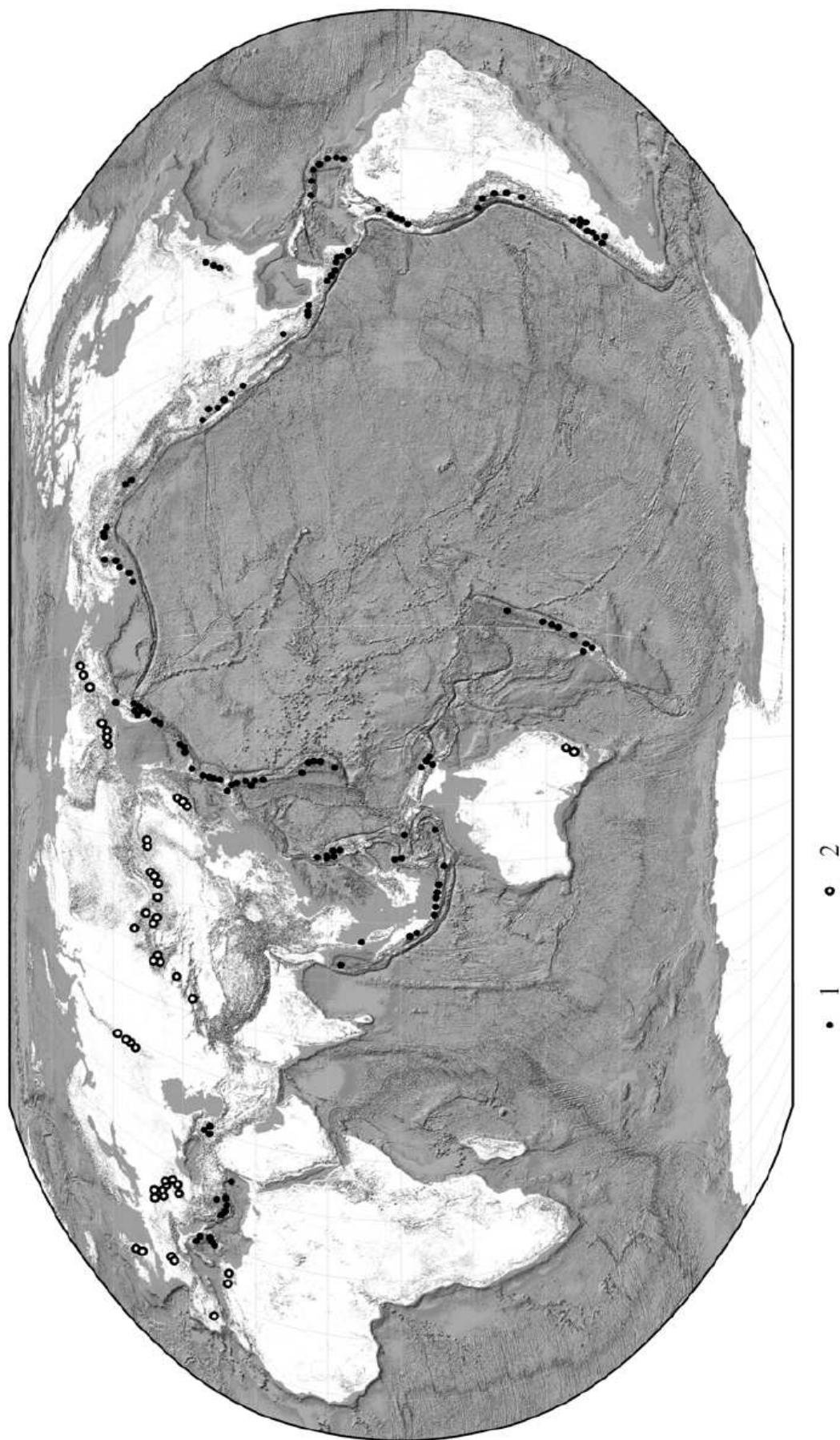


Fig. 2. Geographic distribution of areas of studying the melt inclusions and quenched glasses of subduction geodynamic settings: (1) in the areas of modern volcanism, (2) in the areas of ancient magmatism (paleoanalogues of IA + ACM).

Table 1.

**Average contents of major (wt %), H<sub>2</sub>O (wt %), volatiles and trace elements (ppm) in the basic ultrabasic mag-matic melts (SiO<sub>2</sub>=40-54 wt %) of island arcs and active continental margins**

Components	MgO > 0		MgO > 10	
	<i>n</i>		<i>n</i>	
SiO <sub>2</sub>	2485	50.76	452	49.51
		+3.03/-2.86		+3.20/-3.00
TiO <sub>2</sub>	2431	1.00	436	0.53
		+0.80/-0.44		+0.54/-0.27
Al <sub>2</sub> O <sub>3</sub>	2419	15.82	423	12.61
		+3.24/-2.69		+3.26/-2.59
FeO	2433	9.00	423	8.25
		+3.21/-2.36		+1.92/-1.56
MnO	1872	0.17	271	0.15
		+0.12/-0.07		+0.08/-0.05
MgO	2437	6.32	452	11.92
		+4.66/-2.68		+2.30/-1.93
CaO	2419	10.18	423	11.83
		+3.50/-2.60		+3.01/-2.40
Na <sub>2</sub> O	2419	2.54	423	1.56
		+1.50/-0.94		+0.79/-0.53
K <sub>2</sub> O	2434	0.76	423	0.38
		+1.04/-0.44		+0.68/-0.24
P <sub>2</sub> O <sub>5</sub>	2002	0.21	299	0.11
		+0.33/-0.13		+0.22/-0.07
H <sub>2</sub> O	1089	1.80	172	1.64
		+1.51/-0.82		+0.79/-0.53
Cl	1356	990	143	1010
		+870/-460		+1260/-560
F	462	370	75	360
		+770/-250		+610/-230
S	1129	1220	133	1610
		+1470/-670		+860/-560
CO <sub>2</sub>	239	430	8	1280
		+1670/-340		+9970/-1130
Total		98.86		98.92
<i>T</i> , °C	722	1180	140	1267
		+101/-93		+64/-61
Li	434	6.06	46	4.58
		+4.48/-2.57		+2.76/-1.72
Be	292	0.55	41	0.52
		+0.28/-0.18		+0.31/-0.20
B	494	11.97	53	12.67
		+8.92/-5.11		+6.10/-4.12
Sc	77	32.6	12	35.2
		+21.3/-12.9		+29.0/-15.9
V	213	317	24	270
		+93/-72		+51/-43
Cr	469	232	182	432
		+656/-171		+454/-221
Co	23	48.2	—	—
		+28.1/-17.8		
Ni	57	65.4	—	—
		+157/-46.2		
Rb	201	13.1	45	11.6
		+32.7/-9.3		+28.7/-8.3
Sr	510	375	99	286
		+335/-177		+386/-164
Y	630	19.9	122	15.6
		+8.0/-5.7		+5.8/-4.2

Table.1 Contd.

Components	MgO > 0		MgO > 10	
	<i>n</i>		<i>n</i>	
Zr	626	64.3 +57.6/-30.4	112	44.7 +40.9/-21.3
Nb	550	1.57 +1.89/-0.86	100	1.13 +1.58/-0.66
Cs	117	0.79 +2.66/-0.61	28	0.62 +0.72/-0.33
Ba	643	212 +292/-123	103	184 +252/-106
La	583	6.07 +6.96/-3.24	122	4.35 +5.70/-2.47
Ce	493	13.5 +16.4/-7.4	99	9.62 +12.82/-5.50
Pr	113	1.89 +1.65/-0.88	24	1.48 +1.67/-0.78
Nd	424	10.14 +8.74/-4.70	96	7.01 +7.14/-3.54
Sm	434	2.73 +1.66/-1.03	111	2.11 +1.63/-0.92
Eu	404	1.04 +0.56/-0.36	90	0.97 +1.05/-0.50
Gd	249	3.55 +1.72/-1.16	61	3.17 +2.13/-1.28
Tb	54	0.53 +0.11/-0.09	8	0.42 +0.08/-0.06
Dy	398	3.30 +1.28/-0.92	94	2.53 +1.12/-0.78
Ho	51	0.77 +0.26/-0.20	8	0.57 +0.11/-0.10
Er	398	1.99 +0.76/-0.55	94	1.40 +0.61/-0.43
Tm	76	0.28 +0.12/-0.08	24	0.23 +0.05/-0.04
Yb	446	1.89 +0.80/-0.56	112	1.42 +0.56/-0.40
Lu	82	0.38 +0.22/-0.14	9	0.24 +0.06/-0.05
Hf	292	1.74 +1.02/-0.64	74	1.22 +0.43/-0.32
Ta	99	0.24 +0.36/-0.14	16	0.15 +0.24/-0.09
Pb	259	2.17 +2.48/-1.16	46	1.75 +2.03/-0.94
Th	471	0.62 +0.66/-0.32	78	0.58 +0.79/-0.34
U	330	0.35 +0.42/-0.19	62	0.28 +0.25/-0.13

**Note:** The table lists average geometrical mean, the confidence interval (first numeral is plus to the average values, and second numeral is minus of the average value) corresponds to standard deviation of the logarithms of concentrations. *n* is the number of analyses. *T*<sup>°C</sup> is the temperature of homogenization of melt inclusions.

melts from inclusions are somewhat depleted in incompatible elements as compared to rock compositions, which is presumably related to the higher average degree of rock differentiation. In addition, compositions of magmas are

characterized by more significant negative Nb and Th anomalies as compared to the rock compositions. The reason of anomalous depletion of the melts is unclear yet.

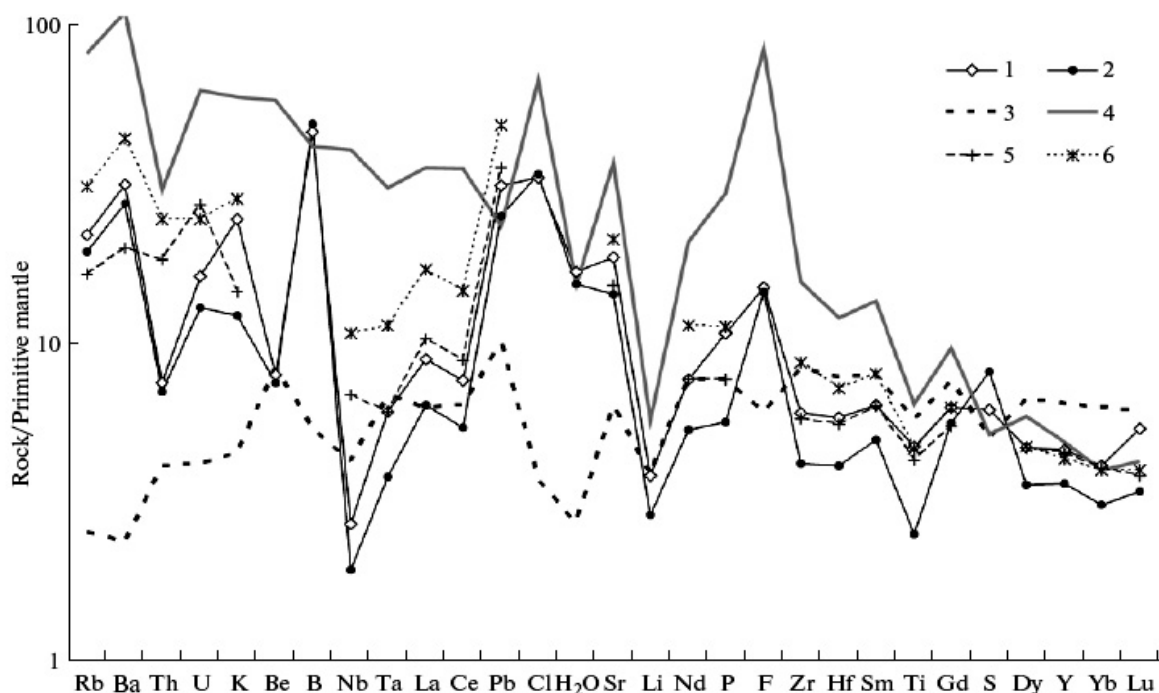


Fig. 3. Abundances of incompatible trace and volatile components normalized to primitive mantle [46] for average compositions of (1) basic magmas ( $\text{SiO}_2 < 54$  wt %) and (2) primitive magmas ( $\text{MgO} > 10$  wt %) of subduction settings. Average compositions of the melts of mid-ocean ridges (3) and (4) within-plate continental areas, as well as average composition of basic rocks of oceanic (5) and (6) continental island arcs are shown for comparison [23].

Other important geochemical feature of subduction basic magmas, which was revealed only from melt inclusions, is positive anomalies of Cl, H<sub>2</sub>O, F, and P (Fig. 3). An elevated content of H<sub>2</sub>O in subduction basic magmas was supposed from many indirect evidence, in particular, from the presence of hydrous minerals (amphiboles, biotite), and abundance of pyroclastic rocks. Melt inclusions provide direct evidence for high contents of H<sub>2</sub>O, Cl, and F in subduction basic magmas (Fig. 3). High H<sub>2</sub>O content in such magmas was known from melt inclusions in the rocks from separate regions of IA and ACM. Melt inclusions with water content more than 5.5 wt % were found in olivines, plagioclases, and clinopyroxenes [57, 50, 49, 54, 15, 39, 63, 6 and others). At the same time, some subduction magmas contain no more than 0.3 wt % H<sub>2</sub>O. Such inclusions were found in olivines, plagioclases, and clinopyroxenes [1, 57, 42, 41, 9, 66, 26, 13, 17, 47, 39, 36]. The spidergrams (Fig. 3) demonstrate positive Cl, H<sub>2</sub>O, and F anomalies for average composition of subduction basic magmas, which indicates that, in general, melts of IA and ACM were enriched in volatiles.

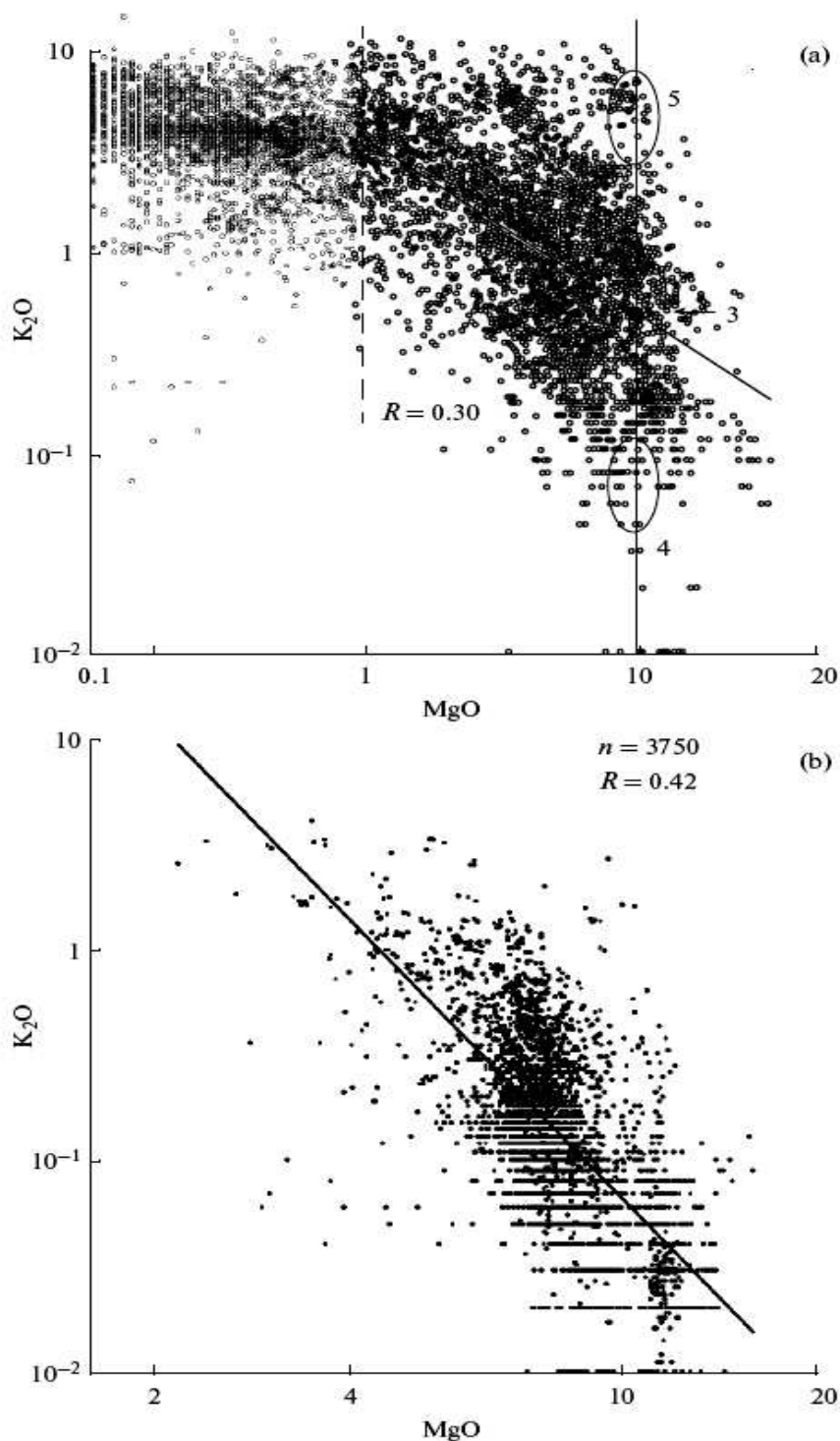


Fig. 4. Variations of  $K_2O$  versus  $MgO$  (wt %) in subduction (a) and MOR magmas (b). Numbers in Fig. 4a: (3) average composition of subduction magmas at  $MgO = 10$  wt %, (4) the same for minimal contents of  $K_2O$  and some other incompatible elements; (5) the same for maximal contents of  $K_2O$  and other incompatible elements.  $n$  is the number of compositions in our data base. The compositions of subduction magmas with  $MgO$  contents  $> 1$  wt % and  $< 1$  wt % are separated by dashed line. Trends of linear correlation were calculated for compositions with  $MgO > 1$  wt %.

The third geochemical feature of compositions of subduction basic magmas is relatively low average contents of moderately incompatible HREE (Fig. 3), which appeared to be close for basic magmas of all geodynamic settings. This served as evidence for assumption of comparatively constant contents of these elements in all types of mantle. Sulfur can be also ascribed to this group of elements (Fig. 3).

In order to estimate the variations of incompatible trace elements in subduction magmas and their reasons, we studied correlations between contents of MgO and various incompatible trace elements and temperature. Figure 4 shows variations of K<sub>2</sub>O versus MgO in basic magmas of subduction zone (Fig. 4a) and MOR (Fig. 4b), with known average contents of incompatible elements in source [DM: 60 ppm K<sub>2</sub>O and 38.73 wt % MgO, and primitive mantle: 650 ppm K<sub>2</sub>O, 9.74 wt % MgO,  $(1 - M) = 0.08$ ,  $D \sim 0$  [0.0013 after [68]]. In spite of a large scatter, data on considered geodynamic settings define significant correlation between MgO and K<sub>2</sub>O. This dependence is described by equation  $\log \text{MgO} = 0.77 - 0.18 \log \text{K}_2\text{O}$  ( $R^2 = 0.16$ ) for basic magmas (melt inclusions and quenched glasses) of subduction settings and  $\log \text{MgO} = 0.79 - 0.13 \log \text{K}_2\text{O}$  ( $R^2 = 0.42$ ) for MOR magmas. Correlation coefficient for subduction basic magmas is statistically significant with probability more than 95% ( $n = 2128$ ). The close slopes of regression lines for basic magmas of subduction zones and MOR indicate that the bulk partition coefficients for K<sub>2</sub>O are close to zero over entire range of evolution of basic magmas. Assuming that the MgO content in near-primary subduction melts equals that in similar MOR magmas (~10 wt %), the K<sub>2</sub>O content in such basic subduction magma will be about 560 ppm (Fig. 4a). An increase in K<sub>2</sub>O content with decreasing MgO corresponds to crystallization differentiation of primary magma up to MgO content ~3 wt %. At this level, the slope of MgO–K<sub>2</sub>O correlation line sharply changes, which indicates a significant change of bulk partition distribution coefficient for K<sub>2</sub>O between solid phases and melts. This drop is related to the appearance of K-bearing solid phases (amphibole or biotite), whose crystallization retards the accumulation of K<sub>2</sub>O in the residual melt (Fig. 4a). In order to estimate K<sub>2</sub>O variations, Figure 4 demonstrates also minimal (ellipse 4 in Fig. 4a) and maximal (ellipse 5 in Fig. 4a) contents of this component in basic magmas at ~10 wt % MgO.

Proposed mechanism of differentiation of subduction basic magmas is confirmed by correlation of F, Zr, Y, Yb, and TiO<sub>2</sub> contents with MgO (Fig. 5). The contents of these components in the intermediate and felsic subduction magmas (MgO < 3%) decrease with decreasing MgO, which indicates the fractionation of their mineral carriers (amphibole, biotite, oxides). The most incompatible trace elements (Nb, U, Th), which are accumulated in residual melts with decreasing MgO content, show a significant scatter without notable correlation with MgO (Fig. 6). At the same time, there are distinct correlations (Figs. 7a, 7b) between contents of most incompatible elements including canonical pairs (Nb–K<sub>2</sub>O, Nb–U, Th–Ta, Nb–Zr, Nb–Th, Cl–K<sub>2</sub>O, and Ce–Pb) [27]. The presence of this correlation indicates that bulk partition coefficients of these

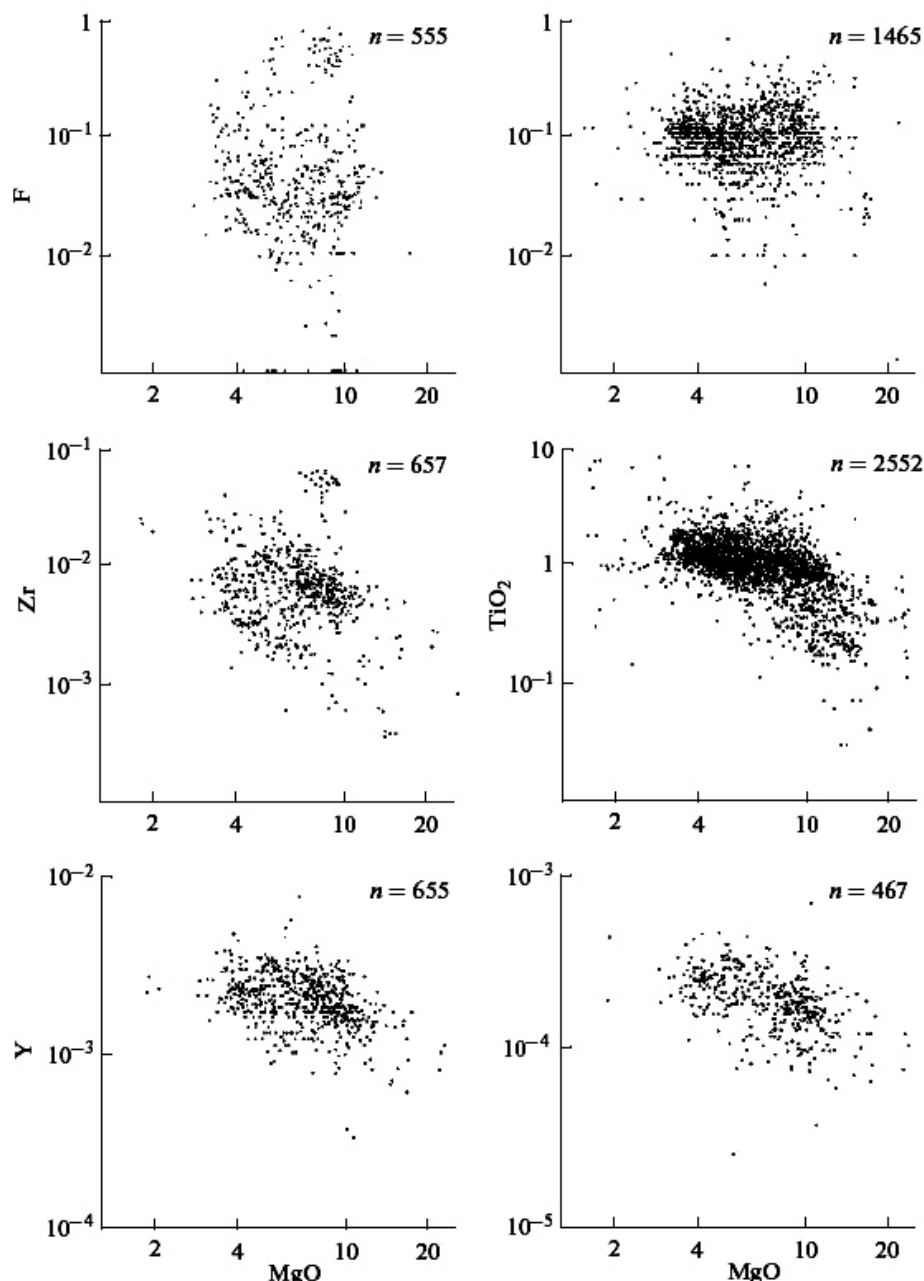


Fig. 5. Variations of F, Cl, Zr, TiO<sub>2</sub>, Y, and Yb versus MgO (wt %) in the subduction basic magmas.

elements are constant over entire interval of evolution of basic magmas for subduction zone. In our opinion, the absence of the correlation of highly incompatible elements with MgO, which is well expressed in the basic magmas of MOR, indicates transport of these elements in a fluid phase and initial heterogeneity of magma sources.

Single incompatible component, which is not correlated with contents of K<sub>2</sub>O and other incompatible elements, is water (Fig. 8). Two trends are observed for subduction basic magmas in the MgO–H<sub>2</sub>O diagram. Most of compositions show a weak negative correlation at minimal water content (few wt %) and MgO content more than 10 wt %; remained compositions define a distinct negative correlation

with the lowest water content about 0.01 wt % and MgO content about 10 wt %. With decreasing MgO content, these trends converge. Taking water content in initial magmas to be hundredths percents (at ~ 0.5 wt % K<sub>2</sub>O), the H<sub>2</sub>O content of 1 wt % will be reached in the most differentiated potassic magmas. High K subduction magmas are typically formed in the frontal zones of island arcs, and, judging from figure, these magmas seem to be drier than normal subduction basic magmas with K<sub>2</sub>O content no more than 2 wt %. Proportions shown in the figure could be related to the degassing of subduction basic magmas under subsurface conditions or with different water contents in the initial basic magmas. The compositions of MOR magmas are shown for comparison. It is seen that H<sub>2</sub>O – MgO correlation observed for minimal water contents is close to those in MOR magmas.

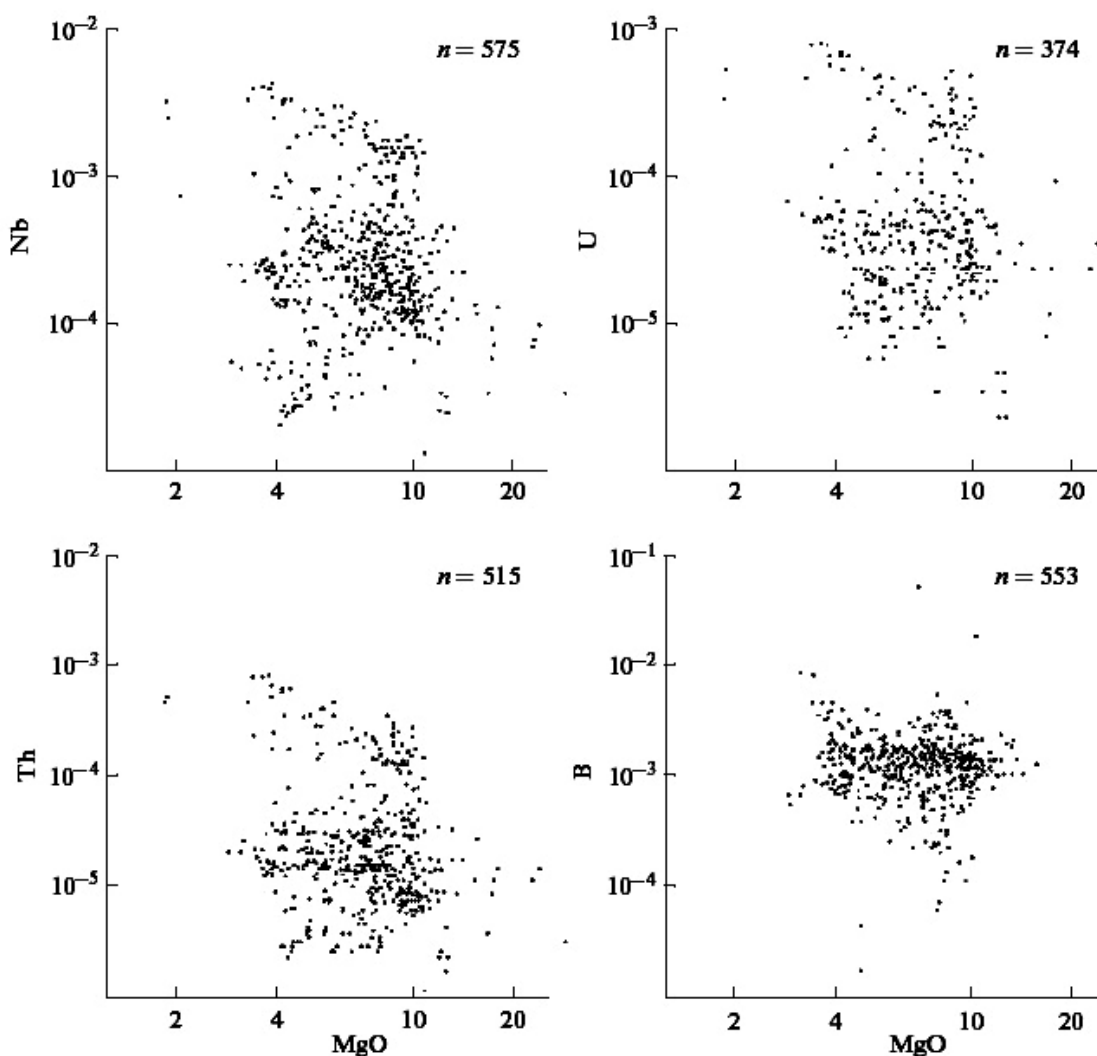


Fig. 6. Variations of Nb, U, Th, and B versus MgO (wt %) in the subduction basic magmas.

### ESTIMATION OF POSSIBLE CONDITIONS OF GENERATION OF BASIC MAGMAS

The MgO contents in the subduction-related basic magmas correlate with homogenization temperatures of melt inclusion (Fig. 9a). The correlation lines of temperature and MgO for subduction basic magmas are close to those for basic magmas of MOR. The average compositions of basic melts of both the settings are also similar (Table 1). Insignificant differences in MgO contents (6.3 wt % for subduction settings and 7.9 wt % for MOR) could be related to the different degree of crystallization differentiation. Most interesting are their differences in H<sub>2</sub>O and K<sub>2</sub>O contents. This raises the question how observed differences could affect the conditions of generations of primary magmas. In order to estimate the possible effects related to the differences in compositions of subduction and MOR basic magmas, we simulated crystallization of average magma compositions using COMAGMAT-3.57 program [5].

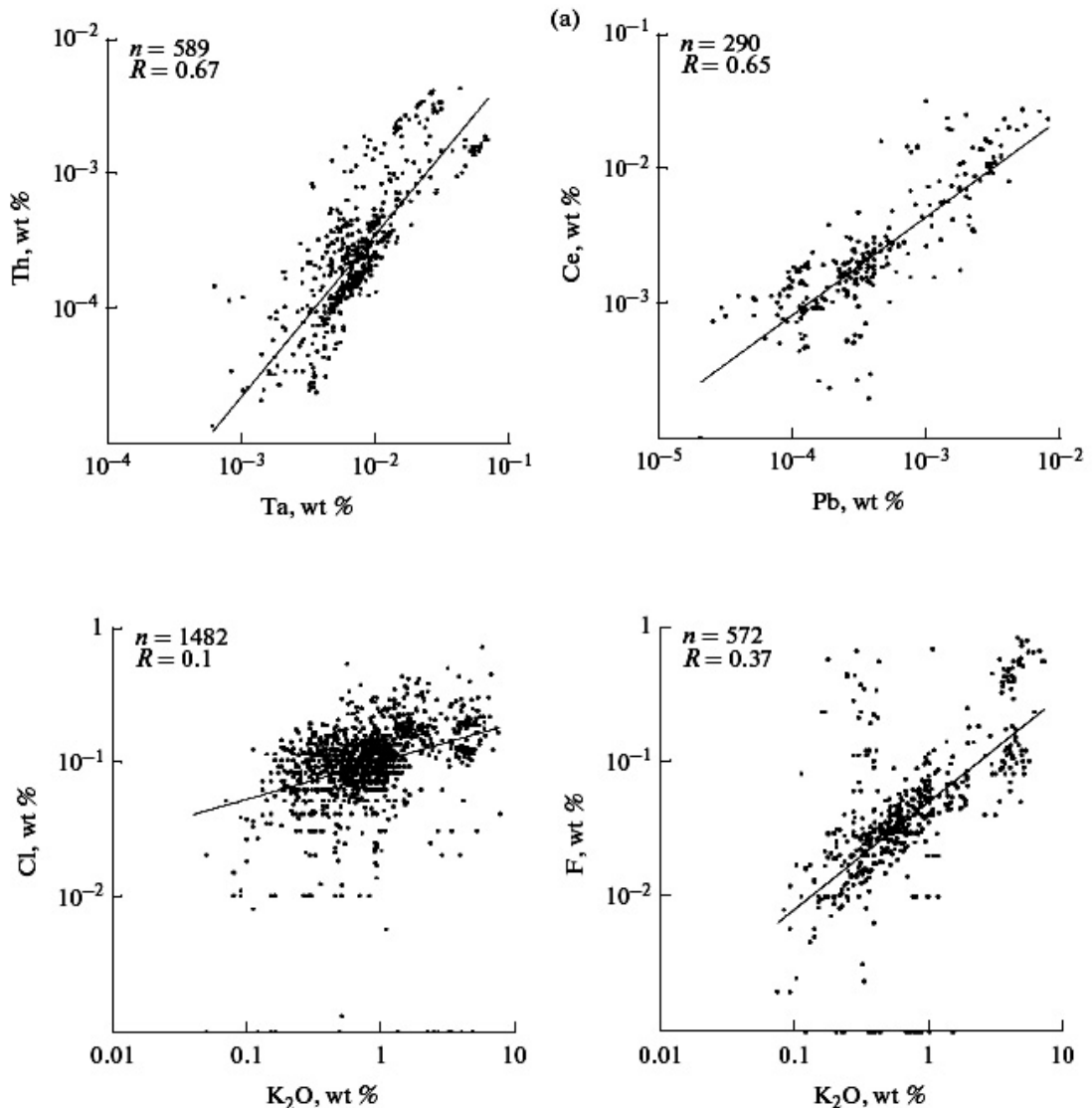


Fig. 7. Covariations of contents of highly incompatible elements (Th-Ta, Ce-Pb, Cl-K<sub>2</sub>O, F-K<sub>2</sub>O, Fig. 7a), (Nb-K<sub>2</sub>O, Nb-U, Nb-Th, Nb-Zr, Fig. 7b) in subduction basic magmas.

Calculations were conducted for isobaric equilibrium crystallization at oxygen fugacity corresponding to the quartz–fayalite–magnetite buffer and pressure up to 25 kbar, which is significantly higher than recommended maximum pressure of 12 kbar [5]. Since modeling is aimed at comparison of near-liquidus equilibria of compositionally close magmas, such a widening in pressure range will hardly lead to significant errors. Taking into account that the average compositions of magmas correspond to variably differentiated melts, they were added by some amount of olivine up to MgO content in the melts of 8, 11, and 12 wt % and further modeling was conducted with recalculated compositions.

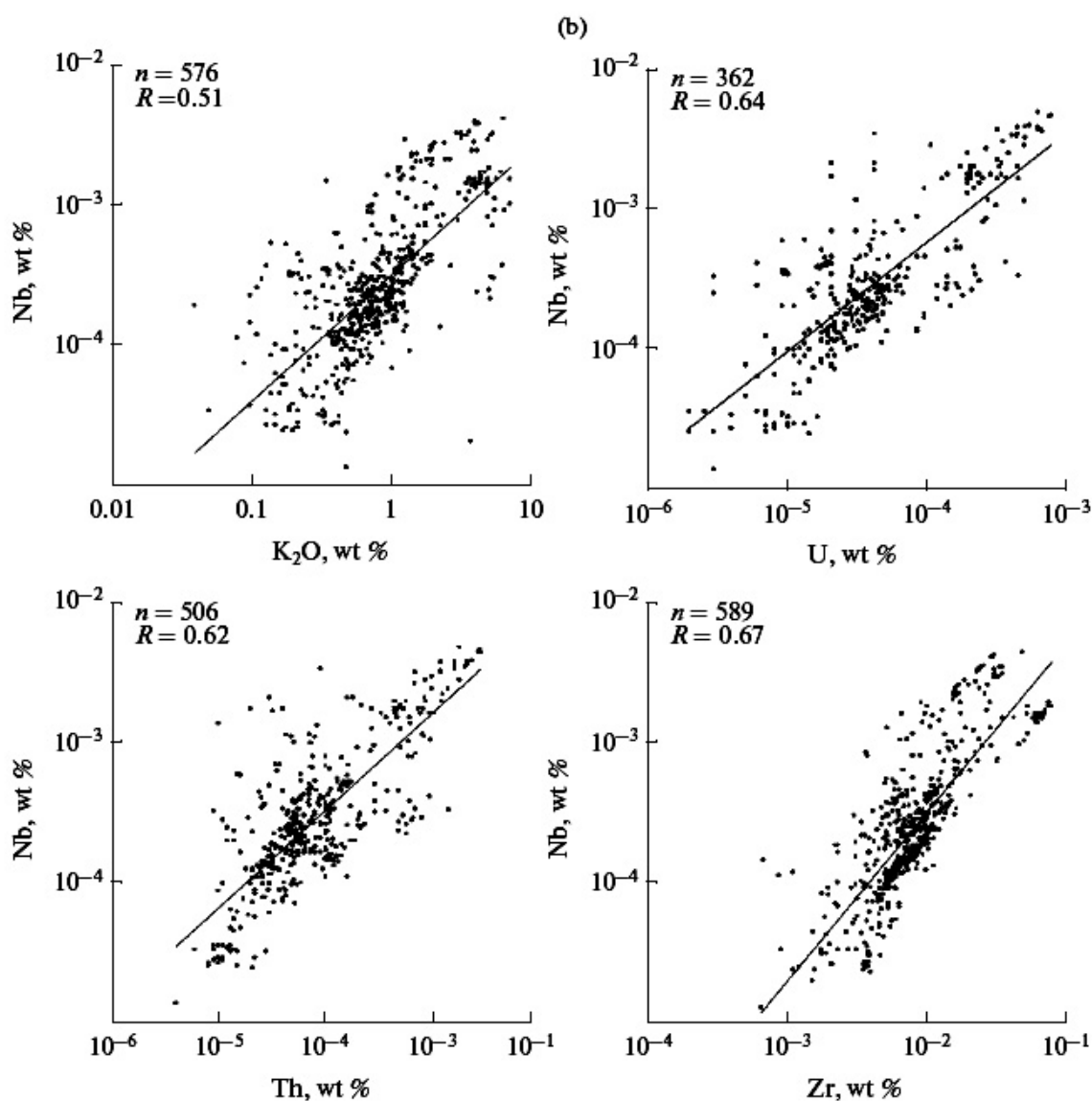


Fig. 7. Contd.

The calculation results are shown in Fig. 10. It should be emphasized that obtained diagrams are used to compare phase relations of close compositions, and, in this respect, the results of modeling are reliable. At the same time, certain physicochemical parameters of phase equilibrium should be used with some

caution, because boundaries of phase fields strongly depend on used models of melt mineral equilibria. The examination of diagram in Fig. 10 shows the following:

1. Topology of phase diagrams is mainly determined by mutual position of crystallization fields of olivine (low pressure) and clinopyroxene (high pressure). The liquidus line shows a sharp slope change in the point of simultaneous crystallization of these two phases. Diagrams are complicated by fields of lowpressure plagioclase crystallization and orthopyroxene for subduction magmas.

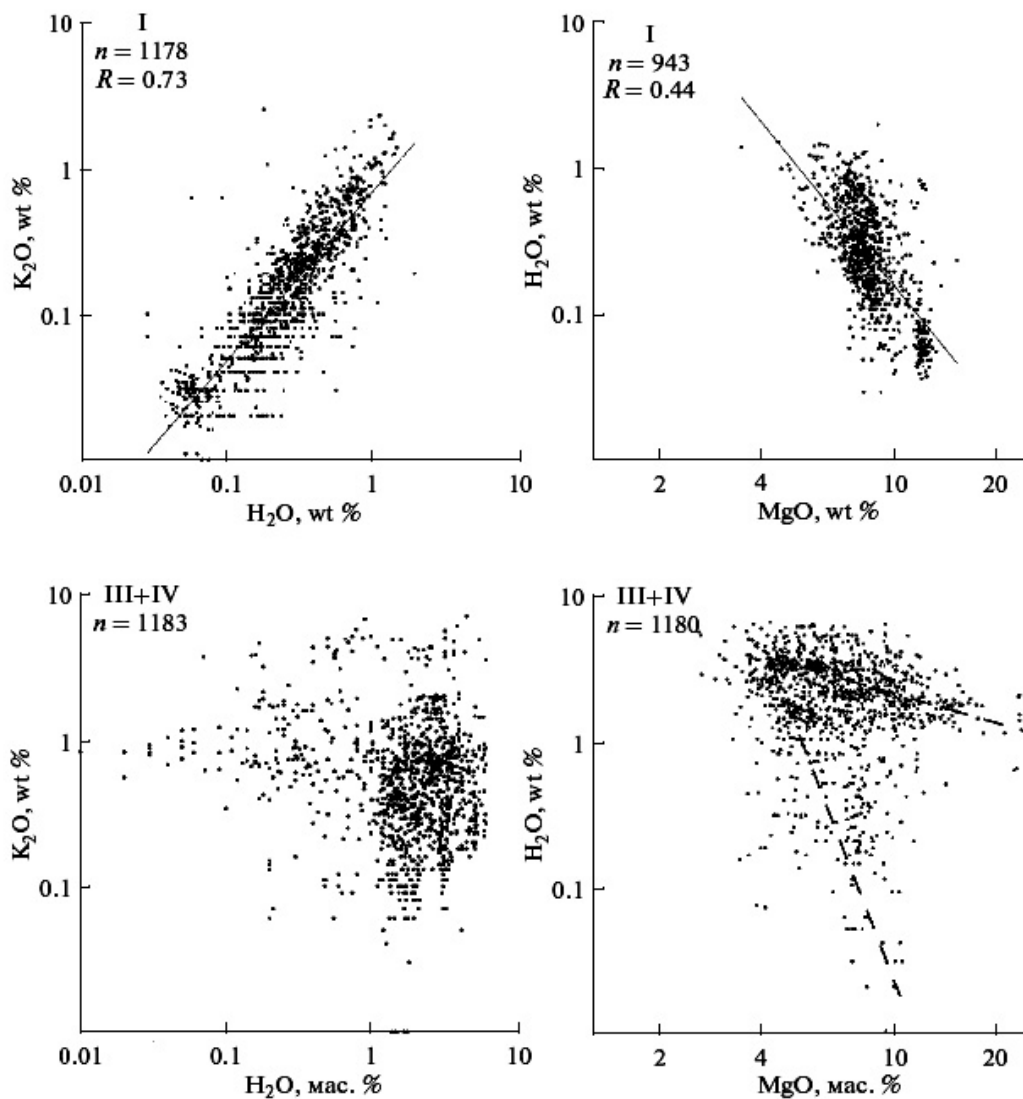


Fig. 8. Covariations of K<sub>2</sub>O, MgO, and H<sub>2</sub>O in MOR magmas (I) and subduction basic magmas (III + IV).

2. Under conditions of liquidus olivine stability, the liquidus temperatures of magmas of the considered settings practically coincide at the similar MgO

contents. This denotes that decrease in melting temperature owing to increase of H<sub>2</sub>O content in subduction magmas is compensated by small change in the contents of other components (Al, Ti, Ca).

3. Olivine crystallization fields in the magmas of subduction zones are somewhat wider as compared to those in MOR magmas. This effect could be caused by increase of water content in subduction magmas. As a result, the simultaneous liquidus crystallization of olivine and clinopyroxene in subduction magmas occur at pressure about 5 kbar higher than that in MOR magmas.

4. The crystallization field of plagioclase in subduction magmas is significantly smaller than that in MOR magmas, which can be caused by the higher water content in subduction magmas.

Some conclusions concerning the magma generation conditions can be drawn from modeling results. Close temperatures of olivine liquidus for magmas of subduction settings and MOR not always indicate similar temperatures of magma generation. Assuming that MgO contents in primary melts of both settings were similar, the pressure of generation (pressure of stability of polymineral liquidus assemblage) of subduction magmas should be approximately 5 kbar higher than that of MOR setting. Taking into account insignificant slope of liquidus line at conditions of olivine crystallization, subduction magmas should be generated at temperatures 50–100°C lower than MOR magmas at the same depth. On the other hand, the temperature difference may be lower if primary MOR magmas were higher in MgO than subduction magmas. In this case, the difference between magma compositions should reflect the different generation depth (deeper for MOR magmas) at similar temperature regime of mantle. There are also intermediate variants, i.e., primary magmas of subduction settings were simultaneously colder at fixed pressure and less magnesian as compared to MOR magmas. The difference in temperature of mantle sources in this case should be insignificant, about 50°C at equal pressure.

### **ESTIMATION OF CONTENTS OF INCOMPATIBLE TRACE ELEMENTS IN THE SOURCE OF SUBDUCTION MAGMAS**

Estimation of the average contents of incompatible trace elements in source of subduction basic magmas is based on assumption that the average Dy contents in suprasubduction mantle and MOR mantle are similar (0.531). Using equation (2),  $DDy = 0.079$  [68], and average Dy content in the initial basic magma (3.3 ppm), the average degree of melting and differentiation of basic subduction magma with 10 wt % MgO is estimated as  $(1-M) = 0.15$ . According to equation (1) and obtained above average K<sub>2</sub>O content in the primitive mantle of subduction basic magma (4074 ppm at MgO = 10 wt %, Fig. 4a, point 3), we obtain average K<sub>2</sub>O content in the supra subduction mantle  $C_0^{K2O} = 560$  ppm. This value is used to estimate the average contents of incompatible trace elements in suprasubduction mantle using equation (1) at values  $C^{K2O}/C$  from Table 1 and values  $\Delta D (D^{K2O} - D)$  from [68] (Table 2). By the same way, we calculated the minimal and maximal

contents of K<sub>2</sub>O in subduction magma at MgO = 10 wt % (Fig. 4a, points 4 and 5): K<sub>2</sub>O = 316ppm, Dy = 1.6 ppm, Dy<sub>0</sub> = 0.531 ppm, (1-M) = 0.30, K<sub>2</sub>O<sub>0</sub> = 96 ppm (point 4 in Fig. 4a, column 4 in Table 2) and K<sub>2</sub>O = 10000 ppm, Dy = 3.5 ppm, Dy<sub>0</sub> 0.531 ppm, (1 - M) = 0.11, K<sub>2</sub>O<sub>0</sub> = 1120 ppm (point 5 in Fig. 4a, column 5 in Table 2). The contents of moderately incompatible elements in sources of subduction basic magmas were deduced from proportion C/Dy = C<sub>0</sub>/Dy<sub>0</sub> for each element.

These estimates were conducted for the “most primitive” compositions of melt inclusions in olivine containing more than 10 wt % MgO: K<sub>2</sub>O = 3800 ppm, Dy = 2.5 ppm, Dy<sub>0</sub> = 0.531 ppm; (1 - M) = 0.18, K<sub>2</sub>O<sub>0</sub> = 699 ppm (column 2 in Table 2), as well as for the average composition of all subduction basic magmas: K<sub>2</sub>O = 7600 ppm, Dy = 3.3 ppm, Dy<sub>0</sub> = 0.531 ppm, (1 - M) = 0.14, K<sub>2</sub>O<sub>0</sub> = 1050 ppm (column 1 in Table 2).

Figures 11 and 12 demonstrate spidergrams of incompatible trace and rare-earth elements, respectively, for sources of subduction basic magmas, shown in Table 2, and MOR magmas [34, 68, 53]. Analysis of these figures showed that the average compositions of subduction magmas obtained by different methods are close. Note specially the similarity of compositions obtained from average compositions of all subduction basic magmas and primitive melts with MgO > 10 wt %.

This fact indicates that composition of subduction magma source could be estimated from the average composition of all subduction basic magmas, not only from the highest magnesian melts. Note that the average compositions of basic magmas were previously used by us for estimating the compositions of magma sources of MOR, oceanic islands, and within-plate continental settings [31, 33, 34, 29, 30].

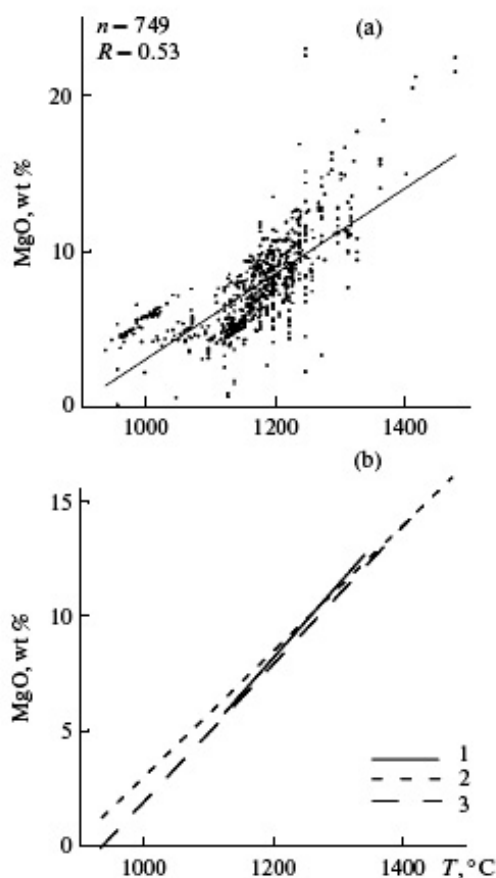


Fig. 9. Correlation between MgO content and homogenization temperature of melt inclusions (a) for subduction basic magmas and (b) comparison of correlation lines of these parameters for magmas of MOR (1), ocean islands (2), and subduction zones (3).

Diagrams of normalized trace element contents (Figs. 11, 12) characterize a general features of the average composition of mantle of suprasubduction wedge.

This material as compared to DM is enriched in all incompatible elements, but to a variable degree, which results in the positive (U, Rb, Ba, B, Pb, Cl, H<sub>2</sub>O, F,

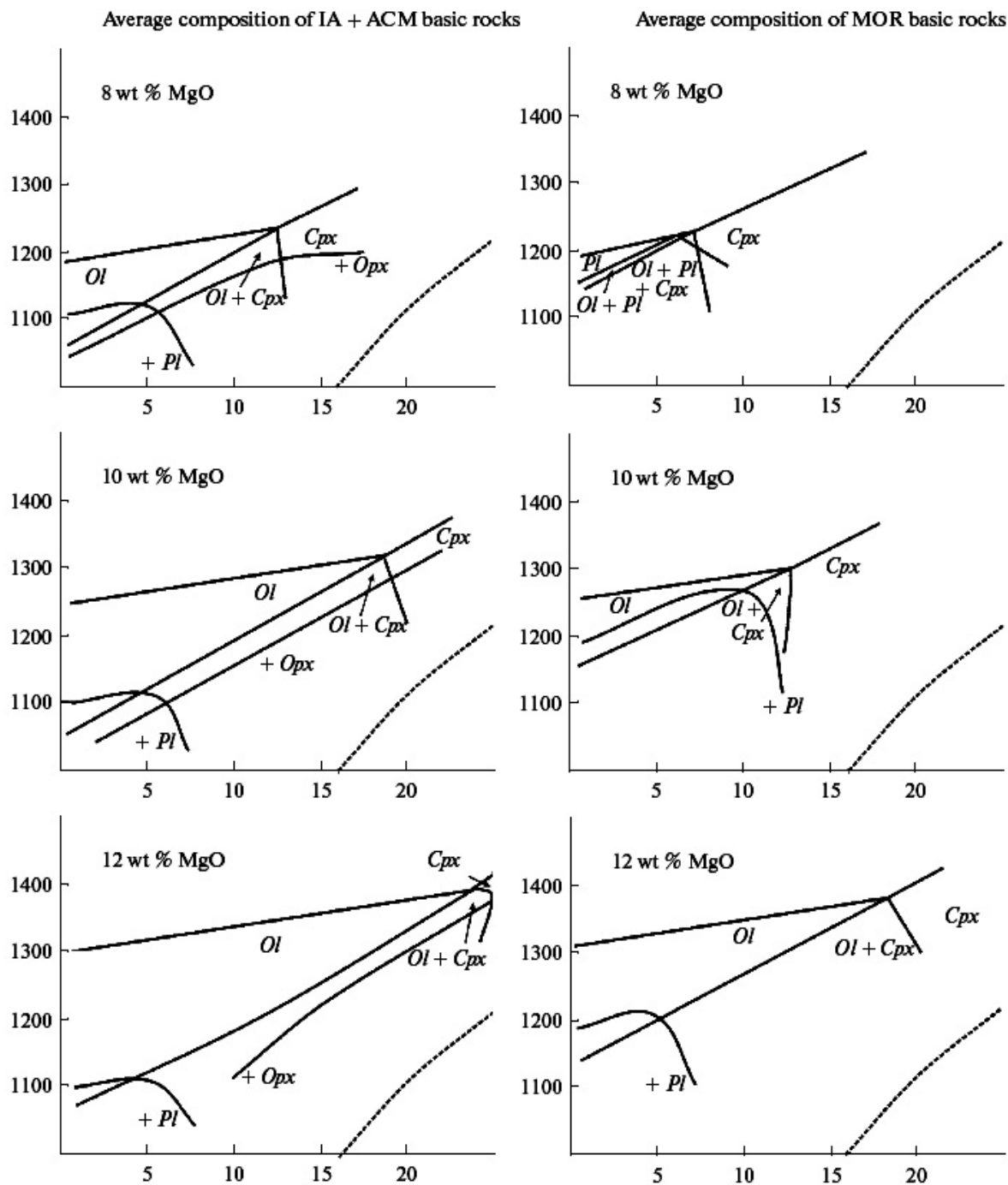


Fig. 10. Phase relations in near-liquidus area of average compositions of basic rocks of subduction settings (IA + ACM) and mid-ocean ridges.

Crystallization fields of minerals were calculated using a program COMAGMAT-3.57 [5,4] at oxygen fugacity corresponding to quartz—fayalite—magnetite buffer. Calculations were conducted for average compositions with addition of equilibrium olivine up to MgO contents of 8, 10, and 12 wt %. Melt occurs in all phase fields of the diagrams. Dashed line is geotherm of oceanic areas after [40].

Table 2.  
Average contents (ppm) of incompatible elements in mantle (sources) of subduction settings

Components	1	2	3	4	5	6	7
<b>K<sub>2</sub>O</b>	1050	700	560	96	1120	72	18000
<b>TiO<sub>2</sub></b>	1530	1060	1090	070	1200	153010	7000
<b>P<sub>2</sub>O<sub>5</sub></b>	380	250	230	33	960	100	1000
<b>H<sub>2</sub>O</b>	2600	3100	2600	100	3300	160	-
<b>F</b>	57	66	56	10	620	11	553
<b>Cl</b>	140	190	140	33	350	6.5	244
<b>S</b>	200	340	260	33	380	123	404
<b>Li</b>	0.84	0.84	0.72	0.66	1.35	0.64	16
<b>Be</b>	0.076	0.096	0.082	0.076	0.110	0.032	1.9
<b>B</b>	1.7	2.3	1.7	0.3	2.2	0.083	11
<b>Rb</b>	1.9	2.1	1.8	1.0	5.6	0.073	49
<b>Sr</b>	58	55	54	10	120	7.3	320
<b>Y</b>	3.5	3.3	2.8	1.1	3.4	3.1	19
<b>Zr</b>	9.5	8.7	9.4	3.1	12	5.2	132
<b>Nb</b>	0.23	0.21	0.44	0.30	1.4	0.20	8
<b>Ba</b>	29	34	35	4.6	234	0.83	456
<b>La</b>	0.81	0.81	0.85	0.17	3.6	0.23	20
<b>Ce</b>	1.9	1.8	1.9	0.6	6.6	0.61	43
<b>Nd</b>	1.5	1.4	1.5	0.6	3.0	0.57	20
<b>Sm</b>	0.41	0.42	0.41	0.18	0.49	0.20	3.9
<b>Eu</b>	0.15	0.19	0.16	0.150	0.20	0.07	1.1
<b>Gd</b>	0.55	0.64	0.54	0.51	0.63	0.47	3.7
<b>Tb</b>	0.10	0.09	0.08	-	-	-	0.6
<b>Dy</b>	0.531	0.531	0.531	0.531	0.531	0.531	3.6
<b>Yb</b>	0.33	0.32	0.24	-	-	0.32	1.9
<b>Lu</b>	0.066	0.050	0.035	-	-	0.046	0.3
<b>Hf</b>	0.26	0.24	0.21	0.20	0.33	0.13	3.7
<b>Ta</b>	0.033	0.028	0.033	0.0330	0.063	0.014	0.7
<b>Pb</b>	0.31	0.33	0.31	0.17	0.65	0.026	11
<b>Th</b>	0.09	0.11	0.09	0.03	0.11	0.018	5.6
<b>U</b>	0.05	0.05	0.05	0.02	-	0.0047	1.3

**Note:** (1) source composition calculated for average composition of all basic magmas of subduction settings; (2) source composition for average composition of basic magmas with MgO > 10 wt %; (3—5) composition of subduction setting magma source s containing 10 wt % MgO ((3) for average composition of basaltic magmas, (4) the same for the minimal contents of K<sub>2</sub>O and other incompatible elements and (5) for maximal contents of K<sub>2</sub>O). (6) average composition of depleted mantle [34]; (7) average composition of continental crust [52].

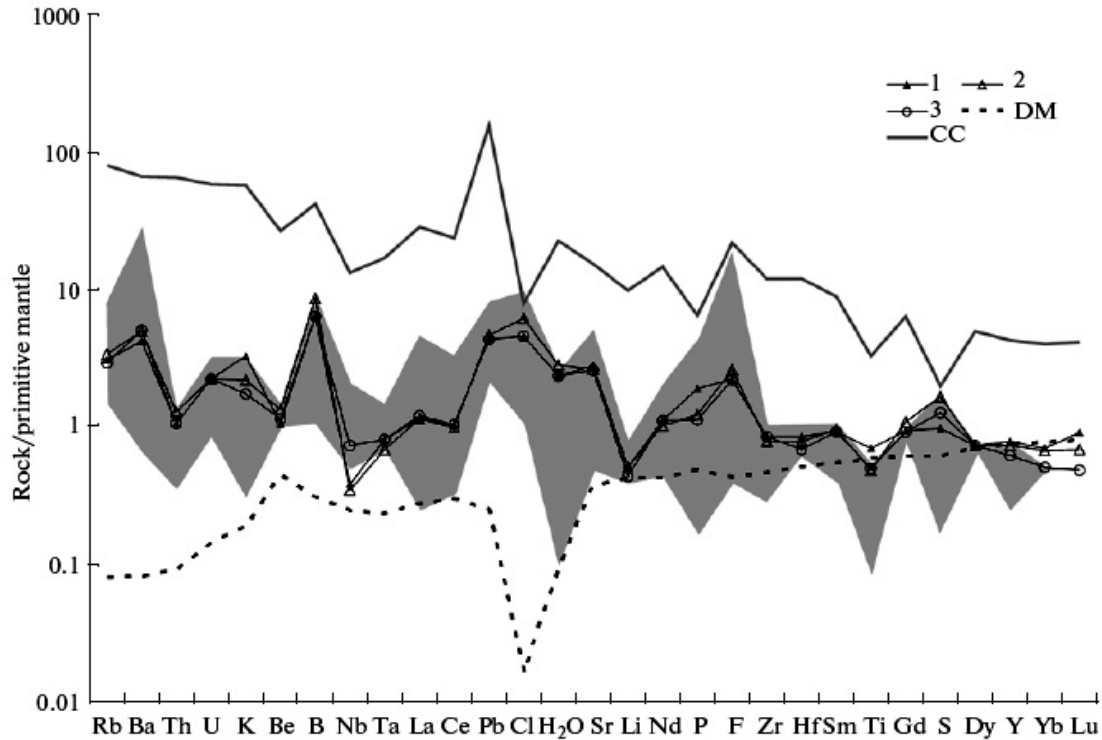


**Fig. 11. Spidergrams for calculated average compositions of magma sources of subduction settings.**

(1) source composition calculated for the average composition of all basic magmas of subduction settings; (2) source composition for the average composition of basic magmas with MgO > 10 wt %; (3) magma source composition for subduction settings containing 10 wt %, gray field shows the interval between minimal and maximal abundances of incompatible elements in magma source with 10 wt % MgO; DM is the composition of source of MOR basalts (depleted mantle) after [34]; (CC) average composition of continental crust after [52]. The contents of components are normalized to primitive mantle composition [46].

and S) and negative (Th, K, Be, Nb, and Ta, Li, Nd, P and Ti) anomalies in the spidergrams. There is a general decrease in normalized abundances from highly incompatible (Fig. 11, left) to the moderately incompatible (Fig. 11, right). The positive anomalies are primarily formed by elements which were supposedly introduced in mantle wedge from subducted plate. The negative anomalies in the spidergrams of source of subduction basic magmas (primarily, Nb, Ta, and Ti) are usually considered to be related to the specifics of such fluids and melts. The presence of these negative anomalies in the mantle wedge indicates that minerals accumulating these elements are present in dehydrated subducted lithospheric plate, which produced fluids and melt that modify mantle wedge. One of the possible phases is rutile that efficiently retain Nb and Ta in residue (Fig. 13), but practically shows no effect on the contents of other incompatible elements in the melt (for instance, [23]). A general elevated content of incompatible elements in mantle wedge as compared to MORB indicates the contribution of not only fluids

that transport Rb, Ba, B, Pb, Cl, H<sub>2</sub>O, F, and S, but also melts that were released from the upper layers of subducted plate and contain all incompatible elements.

The average normalized contents of some incompatible trace elements (Th, Be, LREE, P, Zr, and Hf) in suprasubduction mantle are close to those in primitive mantle (especially, LREE, Fig. 12). This suggests fertilization of mantle wedge with these elements, similarly to processes in mantle of oceanic plumes [33, 34]. However, there are significant differences in composition between suprasubduction mantle and mantle of oceanic plumes: the suprasubduction mantle is characterized by positive anomalies of Ba, K, B, (Cl, H<sub>2</sub>O, and F), whereas mantle of oceanic plumes demonstrates negative anomalies of B, H<sub>2</sub>O, and Cl. On the other hand, mantle of the oceanic plumes has positive Nb, Na, and LREE anomalies and negative S anomaly, which are absent in the suprasubduction mantle.

Third conclusion concerns variations of the average contents of incompatible trace elements in mantle of suprasubduction wedge (Fig. 11) and their reasons. The highest contents of these elements presumably characterize magma sources that experienced most intense reworking by fluids and melts. Then, almost minimal contents of incompatible elements should characterize the composition of mantle wedge least altered by fluids and magmas, i.e. composition approaching DM. The REE distribution (Fig. 12) is consistent with this assumption. Complete spidergram (Fig. 11) is characterized by serrated shape. The positive anomalies of Rb, B, and Cl are high enough to suggest the input of these elements. The positive and negative anomalies of other elements for minimal contents of incompatible elements in subduction basic magmas differ from DM composition by 2–3 times. Based on our experience in estimating the composition of mantle of different geodynamic settings, these variations are within determination error of average compositions, and, hence, the compositions with the lowest contents of the most incompatible elements in source of subduction magmas (Fig. 11) can be considered to be close to DM. In this case, we may conclude that the variations in the average compositions of suprasubduction wedge are determined by mixing of DM-like composition of initial mantle wedge with fluid and melt influx from oceanic plate. Thus, the examination of magma compositions confirm the most popular model of the formation of subduction basic magmas. This substantiates that the negative correlation of contents of moderately incompatible elements in subduction magmas with MgO indicates crystallization differentiation of magma (or variable degree of source melting), while the absence of this correlation with highly incompatible elements results from their fluid transportation, which obliterates variations related to crystallization differentiation.

Mantle sources of MOR and oceanic island basalts have negative H<sub>2</sub>O and Cl anomalies related to the separation of World Ocean from primary mantle, whereas subduction basic magmas show positive anomalies of these volatile components. In this respect, the subduction magmas played an important role in circulation of H<sub>2</sub>O and Cl between inner and outer shells of the Earth [35, 70].

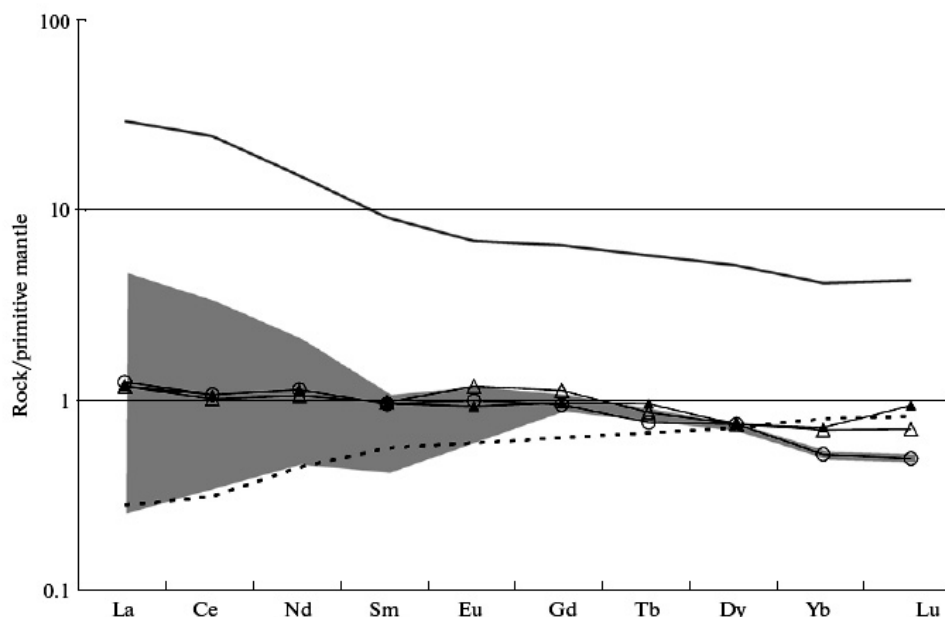


**Fig. 12. REE distribution patterns for calculated composition of magmas sources of subduction settings.**

Element abundance is normalized to primitive mantle [46]. Symbols are shown in Fig. 11.

### SUBDUCTION PROCESSES AND CANONICAL RATIOS OF INCOMPATIBLE ELEMENTS

Hoffman and other researchers [19] established that some incompatible element ratios in mantle magmatic rocks remain relatively constant or close to ratios in their sources regardless of degree of magma differentiation or source melting. The estimation of behavior of these canonical ratios in all compositional spectra of subduction magmas based on compositions of melt inclusions and quenched glasses have not been conducted yet. The average values of some incompatible trace element ratios for subduction basic and felsic magmas are reported in Table 3, while

Figure 14 displays variations of the canonical ratios versus SiO<sub>2</sub> content.

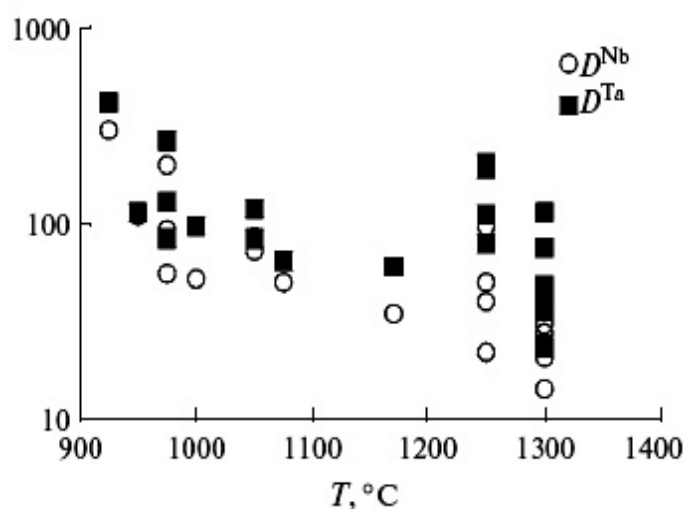


**Fig. 13. Experimental data on rutile/silicate melt partition coefficients for Nb and Ta [22, 55, 25, 69] showing strong compatibility of Nb and Ta in the rutile and their practically identical D values.**

Taking into account the bimodal compositions of subduction magmas, it is reasonable to compare these ratios separately for basic and felsic compositions. As follows from Table 3 and Fig. 14, the average values of the considered ratios in subduction magmas sharply differ from those in mantle magmas of oceanic settings. In particular, the H<sub>2</sub>O/Ce ratio in subduction magmas is approximately five times more than that in MOR magmas. The differences between felsic and basic subduction magmas are less significant, but some features deserve attention. In particular, the ratios of Nb/U, Ce/Pb, TiO<sub>2</sub>/Dy, K<sub>2</sub>O/H<sub>2</sub>O, and K<sub>2</sub>O/Cl in felsic subduction magmas are lower than those in basic magmas. This may indicate that source of subduction magmas changed from basic to felsic compositions. The Nb/U ratio in subduction basic magmas is lower than that in the oceanic basic magmas owing to reworking of mantle wedge by Nb-depleted fluids and melts. Further decrease of Nb/U ratio in felsic magmas could be related to anatexis of basic crust under subduction settings with preservation of the Nb carriers in residue. The same explanation could be proposed for variations in TiO<sub>2</sub>/Dy ratio. A decrease in Ce/Pb ratio in the felsic subduction magmas relative to basic ones is probably related to the contribution of mature continental crust in the source.

Figure 15 demonstrates variation plots for different canonical ratios in subduction and MOR magmas. As in Fig. 14, most compositions are characterized by Nb/U < 10. The deviations toward the higher Nb/U ratios (Figs. 14, 15) presumably correspond to scarce compositions of mantle wedge practically unmodified by fluids and melts (close to DM). Among magmas with Nb/U < 10, some compositions are characterized by wide variations in some other canonical ratios: Ce/Pb > 10, Zr/Nb > 50, La/Yb > 20, K<sub>2</sub>O/Cl > 20, H<sub>2</sub>O/Ce > 5000, and TiO<sub>2</sub>/Dy > 5000. This is likely related to the variations of the considered ratios in subduction source, indicating its compositional heterogeneity. The causes of the latter remain unclear yet. We can only suggest that variations in Nb/U and Zr/Nb ratios are related to variably incomplete extraction of Nb by its mineral carriers during dehydration of subducted plate.

## CONCLUSIONS

1. The average composition of subduction (IA and ACM) basic magmas, including their most primitive varieties (MgO > 10 wt %) was estimated using data on the melt inclusions.

2. As for subduction magmatic rocks, the main geochemical peculiarity of the average composition of subduction basic magmas is deep negative Nb–Ta anomaly, less significant negative anomalies of Nd, Ti, Zr, and Sm, and positive anomalies of Cl, H<sub>2</sub>O, F, and P, as well as relatively low normalized contents of moderately incompatible heavy REE, which seem to be close for basic magmas of all mantle sources.

Table 3.

## Average canonical and some other ratios of incompatible trace elements in sources of subduction basic and felsic magmas

Components	1	2	3	4
H <sub>2</sub> O/Ce	1740	1700	1360	870
Ce/Pb	5.5	6.2	6.1	2.5
K <sub>2</sub> O/H <sub>2</sub> O	0.22	0.23	0.40	1.27
K <sub>2</sub> O/Cl	3.8	3.8	7.6	25.8
La/Yb	2.5	3.0	2.5	8.3
Nb/U	4.2	4.0	4.8	2.2
Nb/Yb	0.66	0.79	0.70	2.51
Zr/Nb	41	40	41	11
Th/Ta	3.9	3.8	2.6	13.9
Th/Yb	0.34	0.41	0.26	3.41
Ba/Rb	16	16	15	4.4
P <sub>2</sub> O <sub>5</sub> /F	3.8	3.1	6.6	1.0
TiO <sub>2</sub> /Dy	2000	2100	2900	760
Nb/Ta	7.5	7.4	7.0	12.6
Zr/Hf	36	37	37	30
K <sub>2</sub> O/Rb	330	320	550	290

**Note:** (1) for source of basic magmas with MgO > 10 wt % and with allowance for differences in the incompatibility of trace elements; (2) the same, but without allowance for difference in the incompatibility of trace elements; (3) for source of the average composition of all basic magmas (column 1 in Table 2); (4) for source of the average composition of subduction felsic magmas.

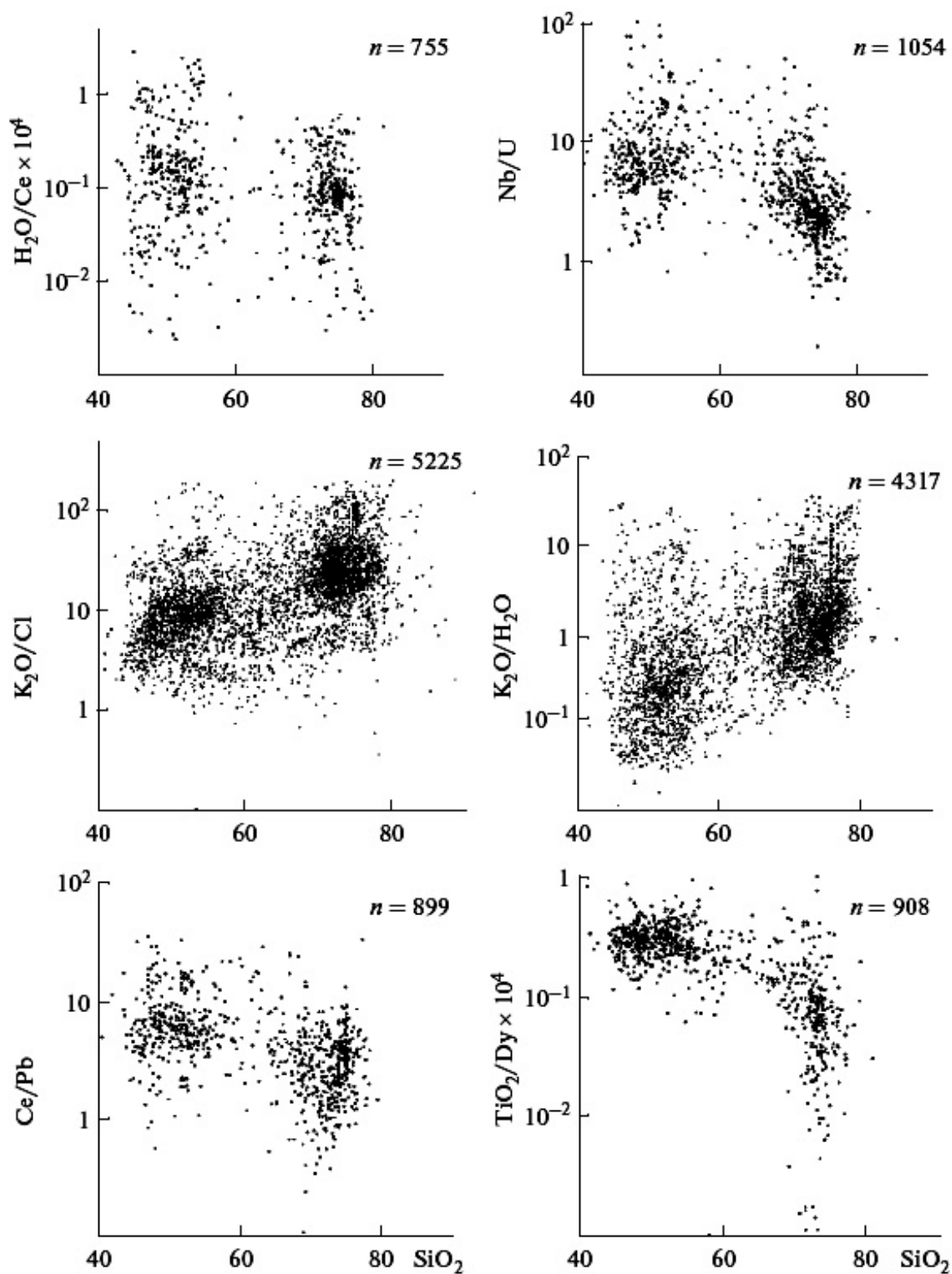


Fig. 14. Dependence of canonical ratios of incompatible elements in subduction magmas versus  $\text{SiO}_2$  content (wt %).

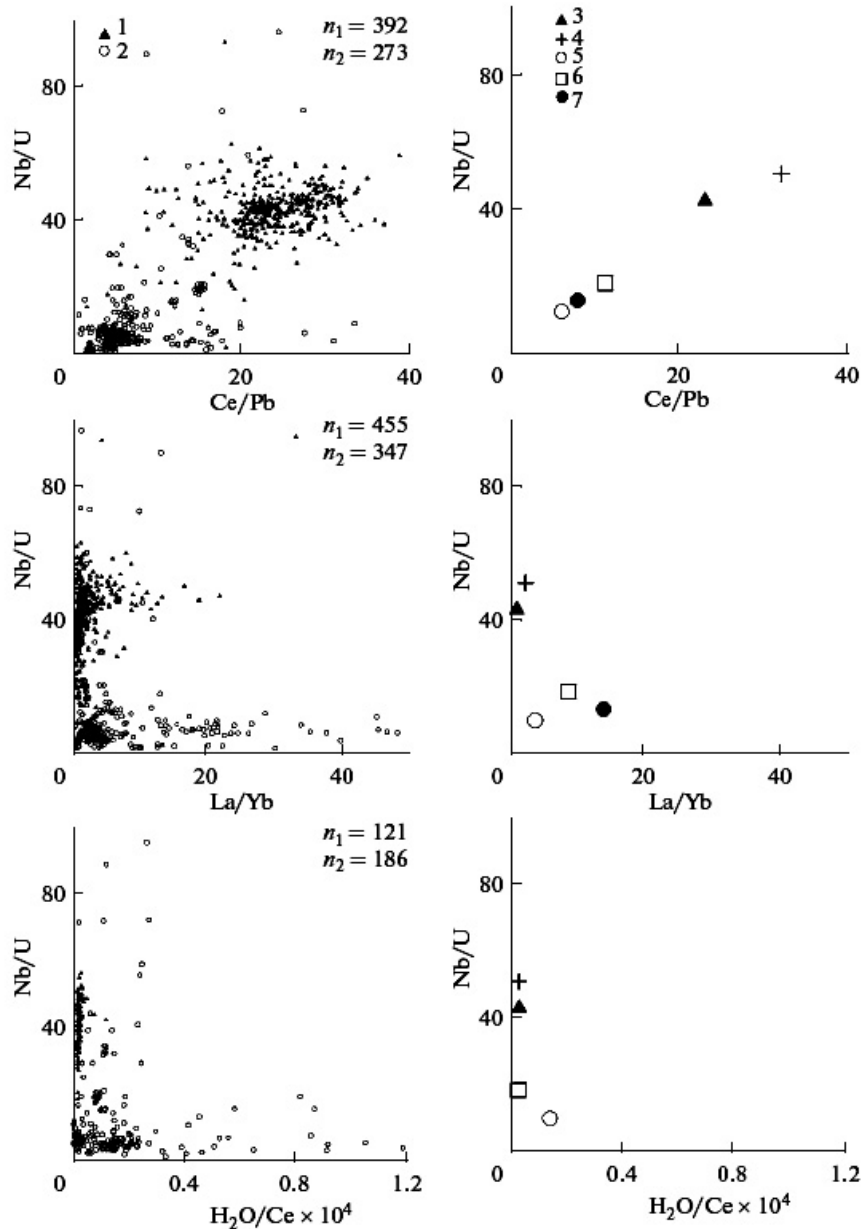


Fig. 15. Covariations of canonical ratios of elements in magmas of MOR (1) and subduction zones (2).

The average canonical ratios of elements in the melts of mid-ocean ridge (3), ocean islands (4), island arcs and active continental margins (5), continental rifts and hot spots (6), as well as average composition of continental crust [52] (7) are shown on the right-hand side.

3. Subduction basic magmas are characterized by correlation of contents of Li, Y, Dy, Er, Yb, Lu, and Ti with MgO. At the same time, the most incompatible trace elements (Nb, Ta, U, Th, and LREE), which should be accumulated in residual magmas with decreasing MgO contents, show significant scatter, no correlation with MgO, but correlation with each other and K<sub>2</sub>O. This indicates, first, that the bulk partition coefficients of these elements were constant over entire evolution of basic magmas, and, second, that variations of the elements of the first group were mainly determined by crystallization differentiation, while those of the second group depended mainly on magma or source heterogeneity.

4. The H<sub>2</sub>O content in the island arc magmas varies practically from zero values to more than 6 wt %. Most part of the compositions show weak negative correlation with MgO at low content of H<sub>2</sub>O and MgO > 10 wt %; few compositions demonstrate a negative correlation with minimal water content about 0.01 wt % at MgO about 10 wt %. With decreasing MgO content, these trends converge.

5. Subduction basic magmas are characterized by distinct positive correlation between MgO contents and homogenization temperatures of melt inclusions. The correlation lines MgO–temperature for subduction and MOR magmas practically coincide, which presumably indicates a close differentiation regime. The average compositions of basic melts of subduction settings and MOR are similar, but differ in K<sub>2</sub>O and H<sub>2</sub>O contents. Modeling the phase equilibria showed the widening of olivine crystallization field in the magmas of subduction zone as compared to MOR magmas. Simultaneous liquidus crystallization of olivine and clinopyroxene in magmas of subduction zones occurs at pressure approximately 5 kbar higher than that in MOR magmas. These effects could be caused by elevated water content in subduction magmas.

6. Assuming similar average Dy contents in suprasubduction and MOR mantles, we calculated the average compositions of sources of subduction magmas (mantle wedge reworked by fluids and melts). The average composition of this mantle is enriched in all incompatible elements as compared to DM composition, with positive anomalies for U, Rb, Ba, B, Pb, Cl, water, F, and S, and negative anomalies for Th, K, Be, Nb, Ta, Li, Nd, P, and Ti at a general decrease of normalized contents from highly incompatible to moderately incompatible elements. The positive anomalies are typical of elements, which were supplied in mantle wedge with fluids (or melts) released during dehydration of subducted plate. The presence of negative anomalies of the elements in the normalized patterns of mantle wedge indicates the preservation of their mineral carriers in the dehydrated subducted plate.

## **ACKNOWLEDGMENTS**

We are grateful to V.A. Kononova (Institute of Geology of Ore Deposits, Petrography, Mineralogy, and Geochemistry, Russian Academy of Sciences) for careful reading of manuscript and constructive comments. This work was supported by the Russian Foundation for Basic Research (project nos. 07-05-00497, 0805-00472), Research Programs of the Earth Science Division of Russian Academy of Sciences, and Program for the Support of Leading Scientific Schools.

## **REFERENCES**

1. **Anderson, A. T.** The Before-Eruption Water Content of Some High-Alumina Magmas, *Bull. Volcanol.* 37, 530-552 (1973).

2. **Arculus, R. J. and Bloomfield, A. L.** Major-Element Geochemistry of Ashes from Sites 782, 784, and 786 in the Bonin Forearc, Proc. Ocean Drilling Program, Sci. Res. 125, 277-292 (1992).
3. **Arculus, R. J.** Island Arc Magmatism in Relation to the Evolution of the Crust and Mantle, Tectonophysics 75, 113-133 (1981).
4. **Ariskin, A. A.** Phase Equilibria Modeling in Igneous Petrology: Use of COMAGMAT Model for Simulating Fractionation of Ferro-Basaltic Magmas and the Genesis of High-Alumina Basalt, J. Volcanol. Geotherm. Res. 90, 115-162 (1999).
5. **Ariskin, A. A., Barmina, G. S., Frenkel, M. Ya. and Nielsen, R. L.** COMAGMAT: a Fortran Program To Model Magma Differentiation Processes, Comput. Geosci. 19, 1155-1170 (1993).
6. **Auer, S., Bindeman, I., Wallace, P., et al.**, The Origin of Hydrous, High- $\delta^{18}\text{O}$  Voluminous Volcanism: Diverse Oxygen Isotope Values and High Magmatic Water Content within the Volcanic Record of Klyuchevskoy Volcano, Kamchatka, Russia, Contrib. Mineral. Petrol. 157, 209-230 (2009).
7. **Blundy, J. and Cashman, K.** Rapid Decompression-Driven Crystallization Recorded by Melt Inclusions from Mount St. Helens Volcano, Geology 33, 793-796 (2005).
8. **Blundy, J., Cashman, K. and Humphreys, M.** Magma Heating by Decompression-Driven Crystallization Beneath Andesite Volcanoes, Nature 443, 76-80 (2006).
9. **Cervantes, P. and Wallace, P.** Magma Degassing and Basaltic Eruption Styles: a Case Study of ~2000 Year BP Xitle Volcano in Central Mexico, J. Volcanol. Geotherm. Res. 120, 249-270 (2003).
10. **Churikova, T., Worner, G., Mironov, N. and Kronz, A.** Volatile (S, Cl and F) and Fluid Mobile Trace Element Compositions in Melt Inclusions: Implications for Variable Fluid Sources across the Kamchatka Arc, Contrib. Mineral. Petrol. 154, 217-239 (2007).
11. **Clift, P. D., Layne, G. D., Najman, Y. M. R., et al.**, Temporal Evolution of Boron Flux in the NE Japan and Izu Arcs Measured by Ion Microprobe from the Forearc Tephra Record, J. Petrol. 44, 1211-1236 (2003).
12. **Danyushevsky, L. V., Leslie, R. A., Crawford, A. J. and Durance, P.** Melt Inclusions in Primitive Olivine Phenocrysts: the Role of Localized Reaction Processes in the Origin of Anomalous Compositions, J. Petrol. 45, 2531-2553 (2004).
13. **Elburg, M. A., Kamenetsky, V. S., Foden, J. D. and Sobolev, A.** The Origin of Medium-K Ankaramitic Arc Magmas from Lombok (Sunda Arc, Indonesia): Mineral and Melt Inclusion Evidence, Chem. Geol. 240, 260-279 (2007).
14. **Gill, J.** Orogenic Andesites and Plate Tectonics (Springer, Berlin, 1981).
15. **Gurenko, A. A., Belousov, A. B., Trumbull, R. B. and Sobolev, A. V.** Explosive Basaltic Volcanism of the Chikurachki Volcano (Kurile Arc, Russia): Insights on Pre-Eruptive Magmatic Conditions and Volatile Budget Revealed from Phenocryst-Hosted Melt Inclusions and Groundmass Glasses, J. Volcanol. Geotherm. Res. 147, 203-232 (2005).
16. **Halter, W. E., Heinrich, C. A. and Pettke, T.** Laser-Ablation ICP-MS Analysis of Silicate and Sulfide Melt Inclusions in An Andesitic Complex II: Evidence for Magma Mixing and Magma Chamber Evolution, Contrib. Mineral. Petrol. 147, 397-412 (2004).
17. **Hamada, M. and Fujii, T.** H<sub>2</sub>O-Rich Island Arc Low-K Tholeiite Magma Inferred from Ca-Rich Plagioclase Melt Inclusion Equilibria, Geochemical Journal 41, 437-461 (2007).
18. **Hart, S. R. and Gaetani, G. A.** Mantle Pb Paradoxes: the Sulfide Solution, Contrib. Mineral. Petrol. 152, 295-308 (2006).
19. **Hofmann, A. W.** Sampling Mantle Heterogeneity Through Oceanic Basalts: Isotopes and Trace Elements, in Treatise on Geochemistry (Elsevier, Amsterdam, 2003), Vol. 2, pp. 61-101.
20. **Humphreys, M. C. S., Blundy, J. D. and Sparks, R. S. J.** Shallow-Level Decompression Crystallisation and Deep Magma Supply at Shiveluch Volcano, Contrib. Mineral. Petrol. 155, 45-61 (2008).
21. **Izbekov, P. E., Eichelberger, J. C. and Ivanov, B. V.** The 1996 Eruption of Karymsky Volcano, Kamchatka: Historical Record of Basaltic Replenishment of An Andesite Reservoir, J. Petrol. 45, 2325-2345 (2004).
22. **Jenner, G. A., Foley, S. F., Jackson, S. E., et al.** Determination of Partition Coefficients for Trace Elements in High Pressure-Temperature Experimental Run Products by Laser Ablation Microprobe-Inductively Coupled Plasma-Mass Spectrometry (LAM-ICP-MS), Geochim. Cosmochim. Acta 58, 5099-5103 (1994).

23. **Kelemen, P. B., Hanghøj, K. and Greene, A. R.** One View of the Geochemistry of Subduction-Related Magmatic Arcs, with An Emphasis on Primitive Andesite and Lower Crust, in *Treatise on Geochemistry* (Elsevier, Amsterdam, 2003), Vol. 3, pp. 593-659.
24. **Kimura, J.-I. and Nagahashi, Y.** Origin of a Voluminous Iron-Enriched High-K Rhyolite Magma Erupted in the North Japan Alps at 1.75 Ma: Evidence for Upper Crustal Melting, *J. Volcanol. Geotherm. Res.* 167, 81-99 (2007).
25. **Klemme, S., Prowatke, S., Hametner, K. and Gunther, D.** Partitioning of Trace Elements Between Rutile and Silicate Melts: Implications for Subduction Zones, *Geochim. Cosmochim. Acta* 69, 2361-2371 (2005).
26. **Kohut, E. J., Stern, R. J., Kent, A. J. R., et al.** Evidence for Adiabatic Decompression Melting in the Southern Mariana Arc from High-Mg Lavas and Melt Inclusions, *Contrib. Mineral. Petrol.* 152, 201-221 (2006).
27. **Kovalenko, V. I., Naumov, V. B., Giris, A. V., et al.** Canonical Ratios of Trace Element in Basic Magmas of Various Geodynamic Settings: Estimation from Compositions of Melt Inclusions and Rock Glasses, *Dokl. Akad. Nauk* 426 (2), 222-225 (2009b) [*Dokl. Earth Sci.* 426, 611-614 (2009b)].
28. **Kovalenko, V. I., Naumov, V. B., Giris, A. V., et al.** Peralkaline Silicic Melts of Island Arcs, Active Continental Margins, and Intraplate Continental Settings: Evidence from the Investigation of Melt Inclusions in Minerals and Quenched Glasses of Rocks, *Petrologiya* 17 (4), 437-456 (2009a) [*Petrology* 17, 410-428 (2009a)].
29. **Kovalenko, V. I., Naumov, V. B., Giris, A. V., et al.** Volatiles in Basaltic Magmas of Ocean Islands and Their Mantle Sources: I. Melt Compositions Deduced from Melt Inclusions and Glasses in the Rocks, *Geokhimiya*, No. 2, 131-149 (2007c) [*Geochem. Int.* 43, 105-122 (2007c)].
30. **Kovalenko, V. I., Naumov, V. B., Giris, A. V., et al.** Volatiles in Basaltic Magmas of Ocean Islands and Their Mantle Sources: II. Estimation of Contents in Mantle Reservoirs, *Geokhimiya*, No. 4, 355-369 (2007d) [*Geochem. Int.* 45, 313-326 (2007d)].
31. **Kovalenko, V. I., Naumov, V. B., Giris, A. V., et al.** Estimation of the Average Contents of H<sub>2</sub>O, Cl, F, and S in the Depleted Mantle on the Basis of the Compositions of Melt Inclusions and Quenched Glasses of Mid-Ocean Ridge Basalts, *Geokhimiya*, No. 3, 243-266 (2006a) [*Geochem. Int.* 44, 209-231 (2006a)].
32. **Kovalenko, V. I., Naumov, V. B., Giris, A. V., et al.** Composition and Chemical Structure of Oceanic Mantle Plumes, *Petrologiya* 14 (5), 482-507 (2006b) [*Petrology* 14, 452-476 (2006b)].
33. **Kovalenko, V. I., Naumov, V. B., Giris, A. V., et al.** Average Contents of Incompatible and Volatile Components in Depleted, Oceanic Plume, and Within-Plate Continental Mantle Types, *Dokl. Akad. Nauk* 415 (3), 389-393 (2007a) [*Dokl. Earth Sci.* 415, 880-884 (2007a)].
34. **Kovalenko, V. I., Naumov, V. B., Giris, A. V., et al.** Average Compositions of Magmas and Mantle Sources of Mid-Ocean Ridges and Intraplate Oceanic and Continental Settings Estimated from the Data on Melt Inclusions and Quenched Glasses of Basalts, *Petrologiya* 15 (4), 361-396 (2007b) [*Petrology* 15, 335-368 (2007b)].
35. **Kovalenko, V. I., Naumov, V. B., Yarmolyuk, V. V., et al.** Balance of H<sub>2</sub>O and Cl between the Earth's Mantle and Outer Shells, *Geokhimiya*, No. 10, 1041-1070 (2002) [*Geochem. Int.* 40, 943-971 (2002)].
36. **Kratzmann, D. J., Carey, S., Scasso, R. and Naranjo, J.-A.** Compositional Variations and Magma Mixing in the 1991 Eruptions of Hudson Volcano, Chile, *Bull. Volcanol.* 71, 419-439 (2009).
37. **Larsen, J. F.** Rhyodacite Magma Storage Conditions Prior To the 3430 YBP Caldera-Forming Eruption of Aniakchak Volcano, Alaska, *Contrib. Mineral. Petrol.* 152, 523-540 (2006).
38. **Liu, Y., Anderson, A. T., Wilson, C. J. N., et al.** Mixing and Differentiation in the Oruanui Rhyolitic Magma, Taupo, New Zealand: Evidence from Volatiles and Trace Elements in Melt Inclusions, *Contrib. Mineral. Petrol.* 151, 71-87 (2006).
39. **Maria, A. H. and Luhr, J. F.** Lamprophyres, Basanites, and Basalts of the Western Mexican Volcanic Belt: Volatile Contents and a Vein-Wallrock Melting Relationship, *J. Petrol.* 49, 2123-2123 (2008).
40. **Mercier, C., J.-C.** Single-Pyroxene Thermobarometry, *Tectonophysics* 70, 1-37 (1980).
41. **Metrich, N., Bertagnini, A., Landi, P. and Rosi, M.** Crystallization Driven by Decompression and Water Loss at Stromboli Volcano (Aeolian Islands, Italy), *J. Petrol.* 42, 1471-1490 (2001).

42. **Mironov, N. L., Portnyagin, M. V., Plechov, P. Yu. and Khubunaya, S. A.** Final Stages of Magma Evolution in Klyuchevskoy Volcano, Kamchatka: Evidence from Melt Inclusions in Minerals of High-Alumina Basalts, *Petrologiya* 9, 51-69 (2001) [*Petrology* 9, 46-62 (2001)].
43. **Mustard, R., Ulrich, T., Kamenetsky, V. and Mernagh, T.** Gold and Metal Enrichment in Natural Granitic Melts During Fractional Crystallization, *Geology* 34, 85-88 (2006).
44. **Naumov, V. B., Kovalenko, V. I., Babanskii, A. D. and Tolstykh, M. L.** Genesis of Andesites: Evidence from Studies of Melt Inclusions in Minerals, *Petrologiya* 5 (6), 654-665 (1997) [*Petrology* 5, 586-596 (1997)].
45. **Naumov, V. B., Kovalenko, V. I., Dorofeeva, V. A. and Yarmolyuk, V. V.** Average Concentrations of Major, Volatile, and Trace Elements in Magmas of Various Geodynamic Settings, *Geokhimiya*, No. 10, 1113-1124 (2004) [*Geochem. Int.* 42, 977-987 (2004)].
46. **Palme, H. and H. St. C. O' Neill,** Cosmochemical Estimates of Mantle Composition," in *Treatise on Geochemistry* (Elsevier, Amsterdam, 2003), Vol. 2, pp. 1-38.
47. **Portnyagin, M., Hoernle, K., Plechov, P., et al.** Constraints on Mantle Melting and Composition and Nature of Slab Components in Volcanic Arcs from Volatiles (H<sub>2</sub>O, S, Cl, F) and Trace Elements in Melt Inclusions from the Kamchatka Arc, *Earth Planet. Sci. Lett.* 255, 53-69 (2007).
48. **Reubi, O. and Blundy, J** Assimilation of Plutonic Roots, Formation of High-K Exotic Melt Inclusions and Genesis of Andesitic Magmas at Volcan De Colima, Mexico, *J. Petrol.* 49, 2221-2243 (2008).
49. **Roggensack, K.** Sizing Up Crystal and Their Melt Inclusions: a New Approach To Crystallization Studies, *Earth Planet. Sci. Lett.* 187, 221-237 (2001).
50. **Roggensack, K., Hergig, R. L., McKnight, S. B. and Williams, S. N.** Explosive Basaltic Volcanism from Cerro Negro Volcano: Influence of Volatiles on Eruptive Style, *Science* 277 (5332), 1639-1642 (1997).
51. **Rowe, M. C., Kent, A. J. R. and Nielsen, R. L.** Subduction Influence on Oxygen Fugacity and Trace and Volatile Elements in Basalts across the Cascade Volcanic Arc," *J. Petrol.* 50, 61-91 (2009).
52. **Rudnick, R. L. and Gao, S.** Composition of the Continental Crust, in *Treatise on Geochemistry* (Elsevier, Amsterdam, 2003), Vol. 3, pp. 1-64.
53. **Salter, V. J. M. and Stracke, A.** The Composition of the Depleted Mantle, *Geochem. Geophys. Geosyst* 5 (5), 1- 27 (2004).
54. **Schiano, P., Clochiatti, R., Boivin, P. and Medard, E.** The Nature of Melt Inclusions Inside Minerals in An Ultramafic Cumulate from Adak Volcanic Center, Aleutian Arc: Implications for the Origin of High-Al Basalts, *Chem. Geol.* 203, 169-179 (2004).
55. **Schmidt, M. W., Dardon, A., Chazot, G. and Vannucci, R.** The Dependence of Nb and Ta Rutile-Melt Partitioning on Melt Composition and Nb/Ta Fractionation During Subduction Processes, *Earth Planet. Sci. Lett.* 226, 415-432 (2004).
56. **Shane, P., Smith, V. C. and Nairn, I.** Millennial Timescale Resolution of Rhyolite Magma Recharge at Tarawera Volcano: Insights from Quartz Chemistry and Melt Inclusions, *Contrib. Mineral. Petrol* 156, 397-411 (2008).
57. **Sisson, T. W. and Layne, G. D.** H<sub>2</sub>O in Basalt and Basaltic Andesite Glass Inclusions from Four Subduction-Related Volcanoes, *Earth Planet. Sci. Lett.* 117, 619-635 (1993).
58. **Sobolev, A. V. and Chaussidon, M.** H<sub>2</sub>O Concentrations in Primary Melts from Supra-Subduction Zones and Mid-Ocean Ridges: Implications for H<sub>2</sub>O Storage and Recycling in the Mantle, *Earth Planet. Sci. Lett.* 137, 45-55 (1996).
59. **Stix, J., Layne, G. D. and Williams, S. N.** Mechanism of Degassing at Nevado Del Ruiz Volcano, Colombia, *J. Geol. Soc.* 160, 507-521 (2003).
60. **Straub, S. M. and Layne, G. D.** Decoupling of Fluids and Fluid-Mobile Elements During Shallow Subduction: Evidence from Halogen-Rich Andesite Melt Inclusions from the Izu Arc Volcanic Front, *Geochem. Geophys. Geosyst.* 4 (7), 1-24 (2003).
61. **Sun, W. D., Arculus, R. J., Bennett, V. C., et al.** Evidence for Rhenium Enrichment in the Mantle Wedge from Submarine Arc-Like Volcanic Glasses (Papua New Guinea), *Geology* 31, 845-848 (2003).

62. **Tolstykh, M. L., Naumov, V. B., Babanskii, A. D., et al.** Chemical composition, Volatile Components, and Trace Elements in Andesitic Magmas of the Kurile-Kamchatka Region, *Petrologiya* 11 (5), 451-470 (2003) [*Petrology* 5, 407-425 (2003)].
63. **Vigouroux, N., Wallace, P. J. and Kent, A. J. R.** Volatiles in High-K Magmas from the Western Trans-Mexican Volcanic Belt: Evidence for Fluid Fluxing and Extreme Enrichment of the Mantle by Subduction Processes, *J. Petrol.* 49 (9), 1589-1618 (2008).
64. **Vogel, T. A. and Aines, R.** Melt Inclusions from Chemically Zoned Ash Flow Sheets from the Southwest Nevada Volcanic Field, *J. Geophys. Res.* 3, 5591-5610 (1996).
65. **Walker, J. A., Roggensack, K., Patino, L. C., et al.** The Water and Trace Element Contents of Melt Inclusions across An Active Subduction Zone, *Contrib. Mineral. Petrol.* 146, 62-77 (2003).
66. **Witter, J. B., Kress, V. C., Delmelle, P. and Stix, J.** Volatile Degassing, Petrology, and Magma Dynamics of the Villarrica Lava Lake, Southern Chile, *J. Volcanol. Geotherm. Res* 134, 303-337 (2004).
67. **Witter, J. B., Kress, V. C. and Newhall, C. G.** Volcan Popocatepetl, Mexico. Petrology, Magma Mixing, and Immediate Sources of Volatiles for the 1994 - Present Eruption, *J. Petrol.* 46, 2337-2366 (2005).
68. **Workman R. K. and Hart, S. R.** Major and Trace Element Composition of the Depleted MORB Mantle (DMM), *Earth Planet. Sci. Lett.* 231, 53-72 (2005).
69. **Xiong, X. L., Adam, J., and Green, T. H.** Rutile Stability and Rutile/Melt HFSE Partitioning During Partial Melting of Hydrous Basalt: Implications for TTG Genesis, *Chem. Geol.* 218, 339-359 (2005).
70. **Yarmolyuk, V. V., Kovalenko, V. I. and Naumov, V. B.** Geodynamics, Flows of Volatile Components, and Their Exchange between the Mantle and the Earth's Upper Shells, *Geotektonika*, No. 1, 45-63 (2005) [*Geotectonics* 39, 39-55 (2005)].

## Thermodynamic Analysis of Mineral Assemblages in Magnetite–Bearing Nepheline Syenites (Khibiny Pluton)

I. D. Ryabchikov<sup>a</sup> and L. N. Kogarko<sup>b</sup>

<sup>a</sup> *Institute of Geology of Ore Deposits, Petrography, Mineralogy, and Geochemistry, Russian Academy of Sciences, Staromonetnyi per. 35, Moscow, 119017 Russia;*

<sup>b</sup> *Vernadsky Institute of Geochemistry and Analytical Chemistry, Russian Academy of Sciences, ul. Kosygina 19, Moscow, 119975 Russia.*

### ABSTRACT

The temperature and redox conditions of the crystallization of rocks from the Khibiny alkaline pluton have been estimated based on an analysis of coexisting magnetite, ilmenite, titanite, and pyroxene. Under redox conditions characteristic of the Khibiny Complex, CO<sub>2</sub> is contained in fluid and carbonate anions are contained in melt at high temperature; then graphite is released and an appreciable amount of hydrocarbons appear at a lower temperature as products of reaction of graphite with fluid. Abiogenic hydrocarbons can arise in igneous complexes owing to a processes distinct from Fischer-Tropsch synthesis.

### INTRODUCTION

Oxygen fugacity is one of the major parameters that determine the evolution of the Earth and other cosmic bodies. This parameter controls the behavior of certain elements during the condensation of protoplanetary nebula, accretion of planetesimals and planets, and the formation of their metallic cores. Redox equilibriums with the participation of matter from deep shells controlled the composition of the primordial atmosphere and were probably crucial to the origin of life.

Oxygen fugacity is also important in the evolution of magmatic systems. The mineral assemblages that arise in the course of magma solidification and the paths of crystal fractionation depend on this parameter. The most indicative result of the action of this factor is the fast growth of iron content in the melt under a constant silica content during crystallization of tholeiitic basalts (Fenner trend) and the fast growth of silica content owing to the early magnetite crystallization (Bowen trend in calc-alkaline series) under more oxidative conditions [29, 35]. In alkaline magmatic systems, the oxidative conditions facilitate crystallization of acmite-rich clinopyroxene, whereas alkali amphiboles appear at lower  $f_{O_2}$  values.

In some cases,  $f_{O_2}$  controls partitioning trace elements between the melt and solid phases. This is primarily related to elements with variable valence, in particular, Eu, V, and Cr, under magmatic conditions. For example, the behavior of vanadium in komatiites and other igneous series proved a very efficient indicator of redox conditions [6, 7, and 8].

Oxygen fugacity also controls the molecular composition of the gas phase, which affects magma generation and crystal fractionation. In particular, it was suggested that a reduced gas gives rise to the melting of mantle rocks after their ascent from a great depth and oxidation at the upper levels of the mantle [13]. In

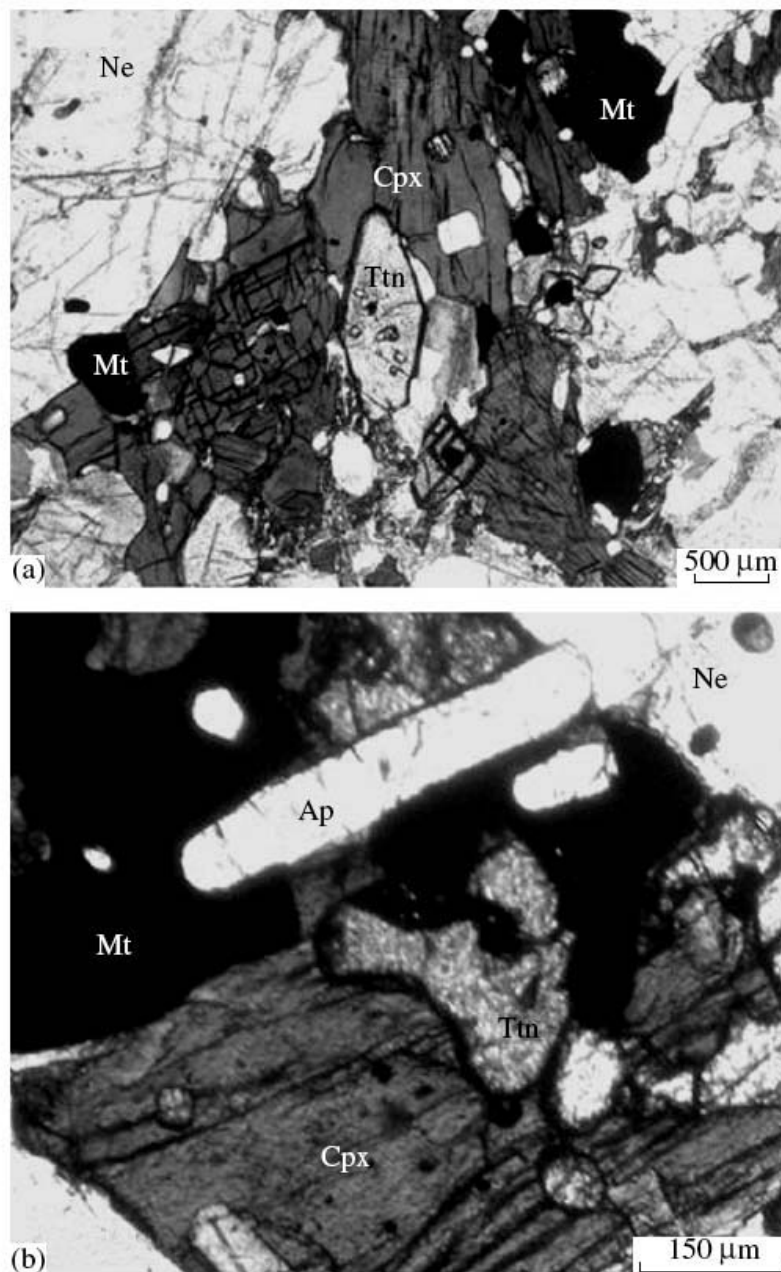


**Fig. 1. Relationships between titanite (Ttn), clinopyroxene (Cpx), and magnetite (Mt) in rocks of the Khibiny pluton, Sample Khib-50. Ne, nepheline; Ap, apatite.**

alkaline magmatic systems, oxygen fugacity determines the occurrence of hydrocarbons and hydrogen, which are detected in many alkaline and especially peralkaline rocks [3, 23, 26, 27, 33, 34; 41, 18, 19, 20, 32).

To estimate oxygen fugacity in magmatic system, various approaches have

been applied. Some of them are based on equilibrium constants of the reactions

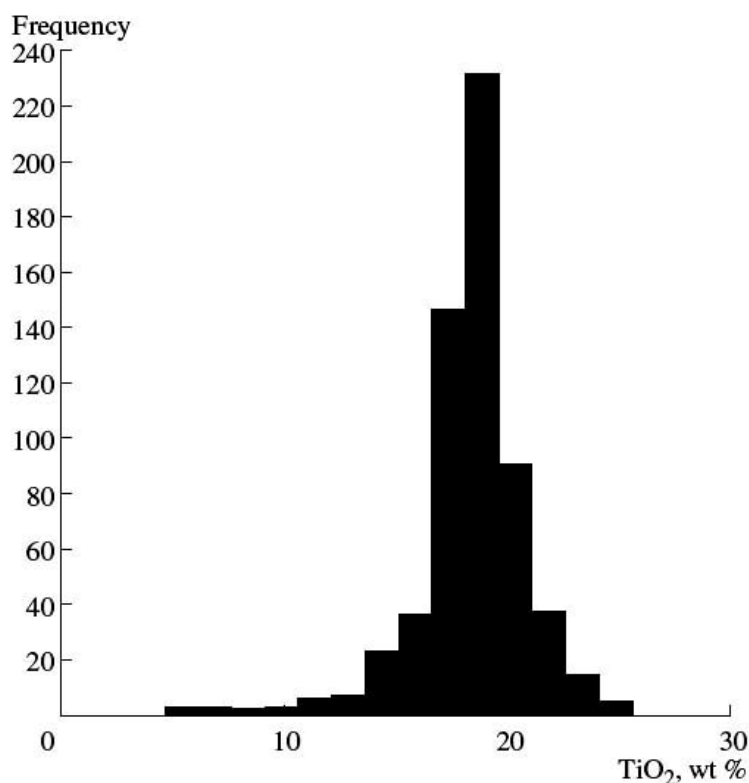


Fig. 2. Bar chart of TiO<sub>2</sub> content in magnetites from the Khibiny pluton, Borehole 1312.

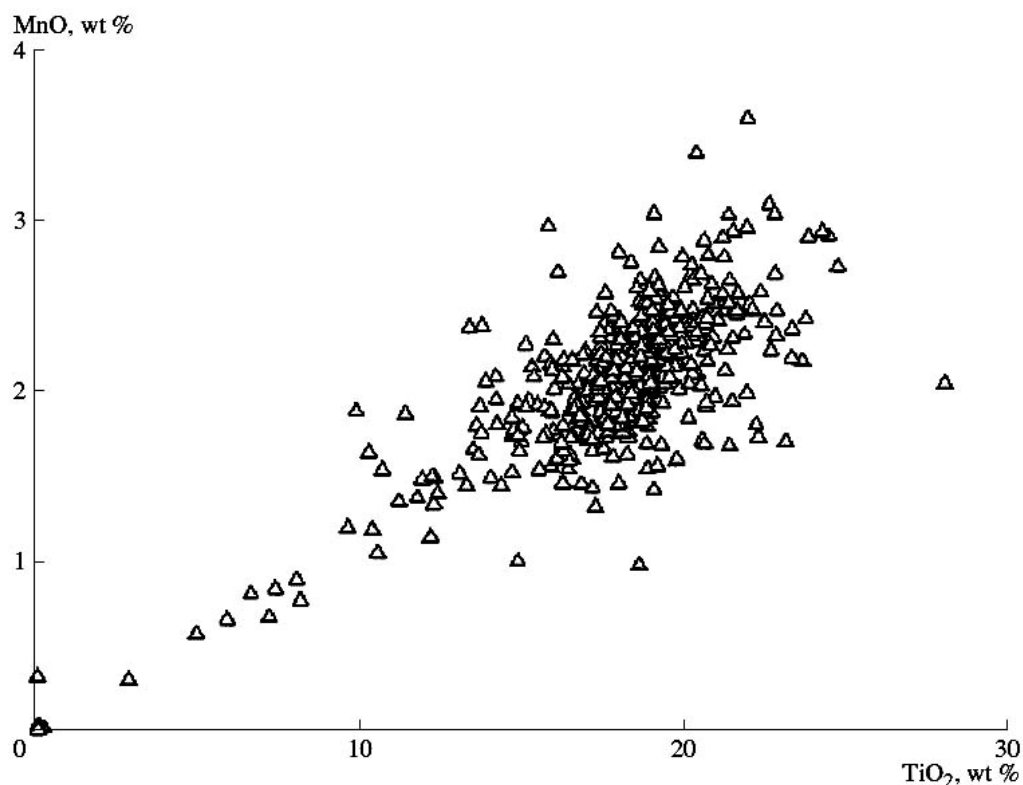


Fig. 3. MnO vs. TiO<sub>2</sub> in magnetites from the apatite-bearing Khibiny pluton, Borehole 1312 between solid solutions with the participation of ferrous and ferric ions. The

experimental data on equilibrium between titanomagnetite and ilmenite, which make it possible to estimate temperature and oxygen fugacity simultaneously from compositions of coexisting iron and titanium oxides, were obtained as early as in the 1960s [5]. Later on, this method was improved in order to apply it to spinels and ilmenites of more complex composition on the basis of thermodynamic models of these phases within multicomponent systems [11, 12]. This method was successfully applied to fresh volcanic rocks but were unfit for plutonic mineral assemblages due to the fast diffusion re-equilibration of iron and titanium oxides during slow cooling.

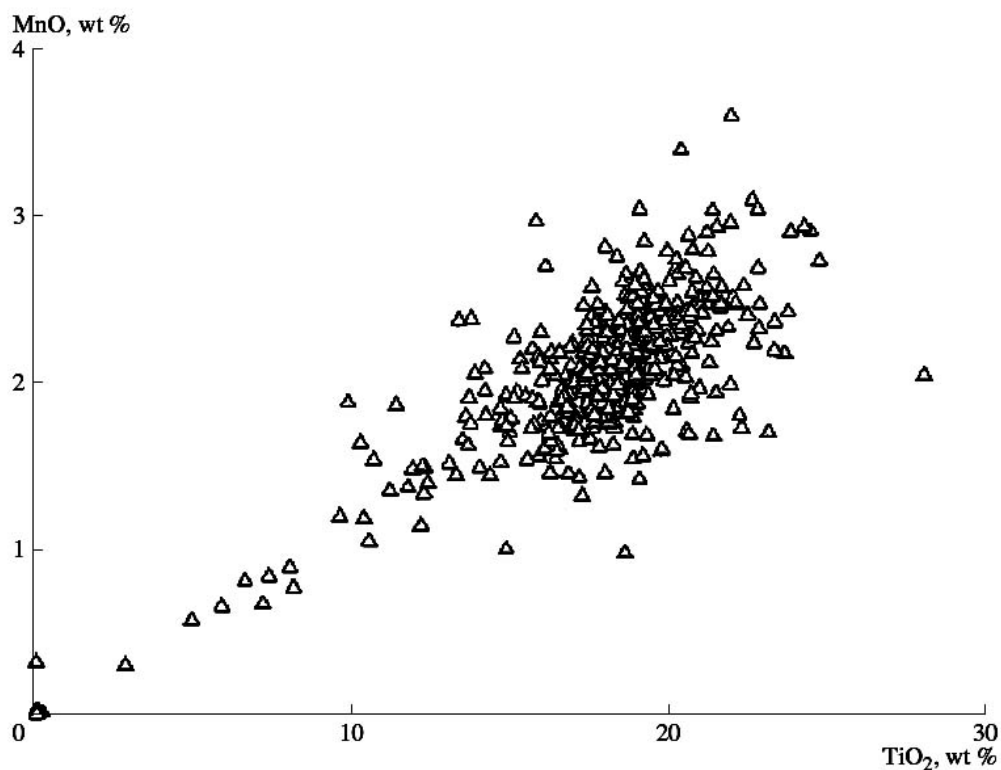


Fig. 4.  $V_2O_3$  vs.  $TiO_2$  in magnetites from the apatite-bearing Khibiny pluton, Borehole 1312.

It was proposed to use equilibria of magnetites and ilmenites with Fe-Mg silicates for this purpose [10, 9]. Wones (1989) pointed out important implications of the titanite-magnetite-quartz assemblage. He calculated the equilibrium temperature and oxygen fugacity for reactions with the participation of titanite with pure phases in the  $CaO-FeO-Fe_2O_3-TiO_2-SiO_2$  system at atmospheric pressure. Subsequently, these reactions were studied in experiment [47]. The experimental data were used for specifying thermodynamic characteristics of titanite, which made it possible to calculate the complete  $T-f_{O_2}$  diagrams [48]. These results were used to estimate  $f_{O_2}$  and the temperature of mineral equilibria in certain igneous rocks [49].

Numerous estimates of the oxygen fugacity in mantle peridotites and basaltic magmas have been carried out on the basis of redox reactions between components of magnetite-bearing spinels, olivine, and orthopyroxenes [1, 2, 28, 46, 38].

Estimates on oxygen fugacity in alkaline rocks were given in a number of

publications. The experimental study of stability of alkali pyroxenes, amphiboles, and aenigmatite in the subliquidus interval of nepheline syenite [19] indicated that

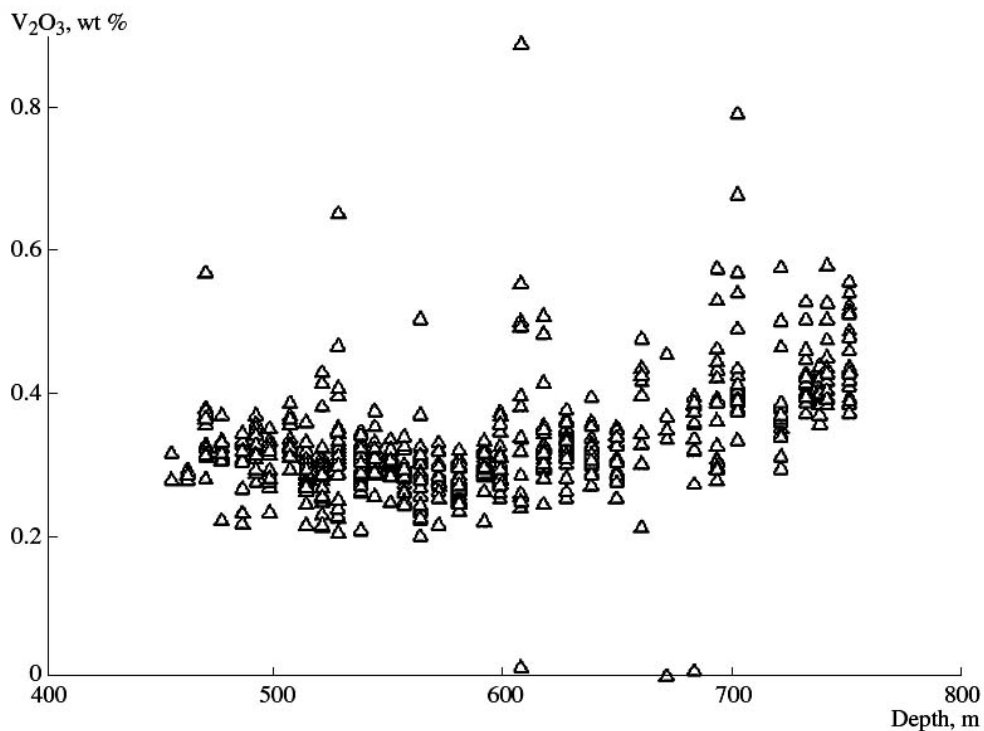


Fig. 5. V<sub>2</sub>O<sub>3</sub> in magnetites from the apatite-bearing Khibiny pluton vs. formation depth, Borehole 1312.

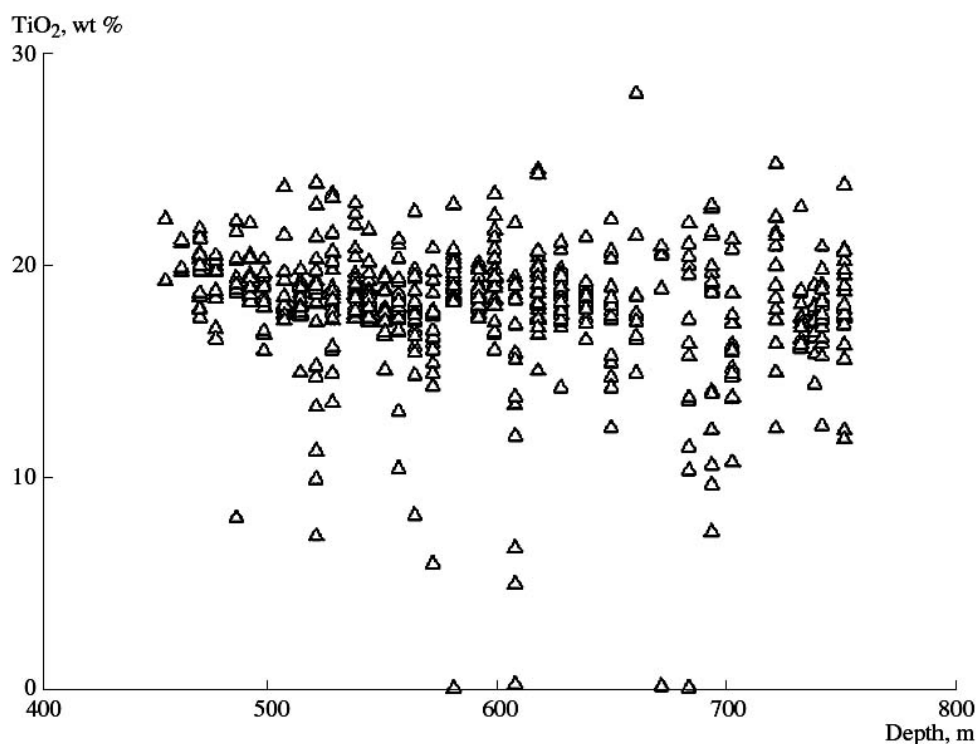
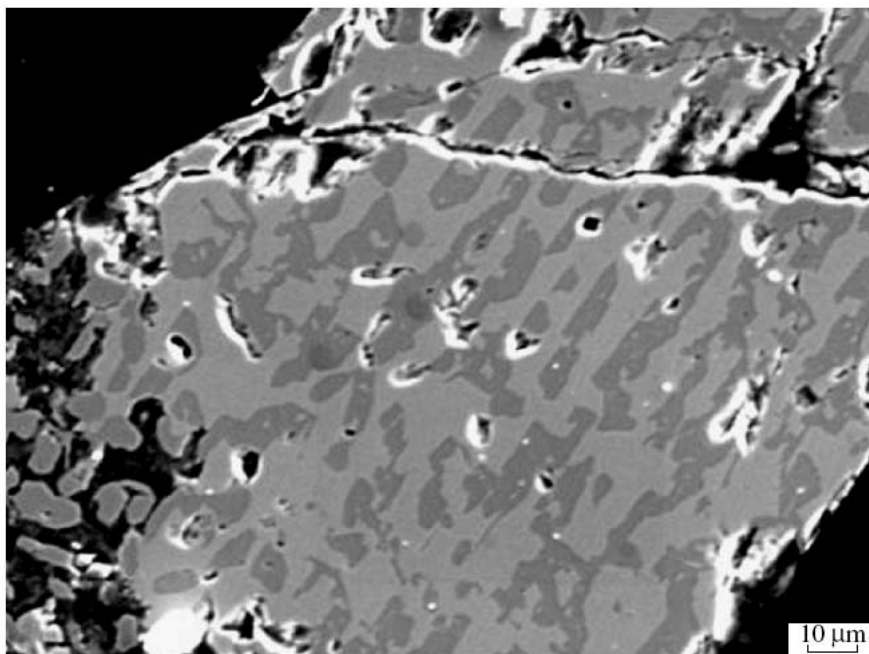


Fig. 6. TiO<sub>2</sub> in magnetites from the apatite-bearing Khibiny pluton vs. formation depth, Borehole 1312.

redox conditions characteristic of the Lovozero pluton were close to the quartz-fayalite-magnetite (QFM) buffer. The data on spinels in volcanic rocks of within-plate oceanic islands, which in many cases include alkali basalt, nephelinite, and



**Fig. 7. Intergrowths of magnetite (light matrix) and ilmenite (dark grains): exsolution-oxidation structure of solid solution. BSE image.**

melilitite, show a higher oxygen fugacity, varying from the QFM buffer to 2 log units higher than this level [1]. Volcanic rocks from Trindade Island, including evolved hyperalkaline varieties, also yielded high  $f_{O_2}$  values [36]. Extremely high  $f_{O_2}$  values were established for high-Mg lavas and dikes of the Mai-mecha-Kotui province of alkaline ultramafic rocks and carbonatites [39, 42]. Still higher oxygen fugacity has been estimated for the Gronnedal-Ika carbonatite-syenite complex in southern Greenland [14]. Very high oxygen fugacities were noted for Katzenbuckel volcano in southwest Germany [22]. Low oxygen fugacities, probably approaching the field of stability of Fe-Ni alloys, were estimated for the early phase of augite syenite from the Ilimaussaq pluton of hyper-alkaline rocks in southern Greenland [23, 24]. This estimate is based on an extremely high content of ulvospinel component in titanomagnetite from this rock. In various phases of the Tamazegt alkaline pluton in Morocco, the estimates on oxygen fugacity vary within several orders from the hematite-magnetite buffer to 2 log units below the QFM buffer [25]. Thus, redox conditions of alkaline magmas vary within a wide range.

## COMPOSITIONS OF MINERALS

The chemical compositions of 618 titanomagnetites, 238 titanites, and 470

clinopyroxenes were determined with an electron microprobe from samples taken from boreholes 1312 and 1880 drilled in rocks of the apatite-bearing intrusion of the Khibiny Complex near the Koashva deposit. The microprobe analyses were mostly performed for individual mineral grains recovered from rocks. In addition, the coexisting minerals from sample Khib-50 have been analyzed; the structural relationships between minerals in this sample indicate that magnetite, pyroxene, and titanite crystallized synchronously (Fig. 1). Representative analyses of the studied minerals are given in the table.

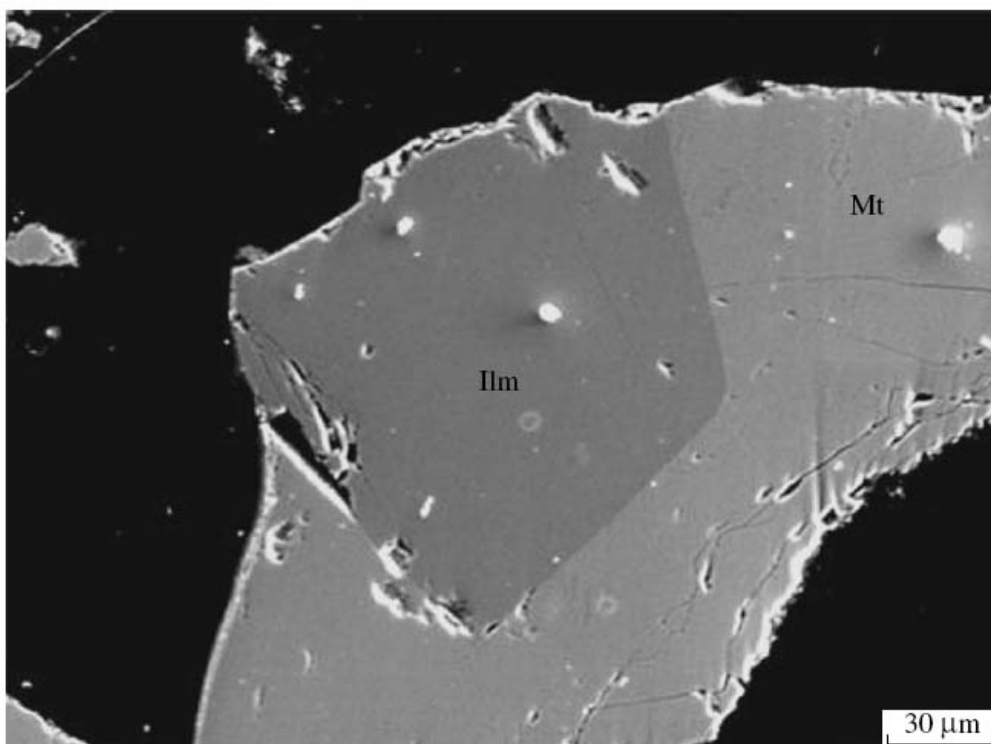


**Fig. 8. Intergrowths of large separate grains of magnetite (Mt) and ilmenite (Ilm).**

Most titanomagnetites are high-Ti varieties (Fig. 2). The prevalent ulvospinel contents are close to 55 mol % and occasionally reach 80 mol %. The MgO and Al<sub>2</sub>O<sub>3</sub> contents are not high and remain much lower than the MnO content, which reaches 3 wt % in high-Ti varieties. The MnO contents correlate very closely with TiO<sub>2</sub> concentrations (Fig. 3), whereas V<sub>2</sub>O<sub>3</sub> contents do not reveal such a correlation (Fig. 4). The vanadium content in magnetite tends to decrease upsection to a height of 600 m, and remains approximately constant at higher levels (Fig. 5). The TiO<sub>2</sub> contents are independent of depth within the observed range (Fig. 6).

Most of the analyzed titanomagnetites are homogeneous at the micrometer level. In rare cases, magnetite-ilmenite intergrowths with exsolution-oxidation structures are noted (Fig. 7). Sporadically, large separate magnetite and ilmenite grains are intergrown (Fig. 8).

Clinopyroxene compositions vary from varieties enriched in diopside (80 mol

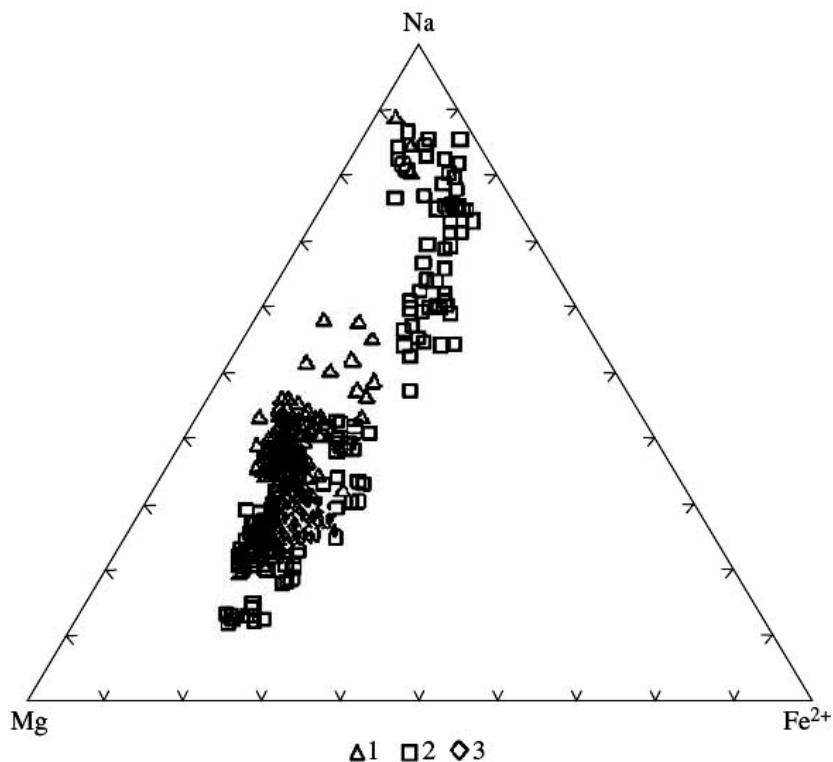


Fig. 9. Chemical compositions of clinopyroxenes from the studied rocks of the Khibiny pluton plotted in the ternary Mg-Na-Fe diagram, atomic amounts. (1) Borehole 1312, (2) Borehole 1880, (3) Sample Khib-50 from Borehole 1312.

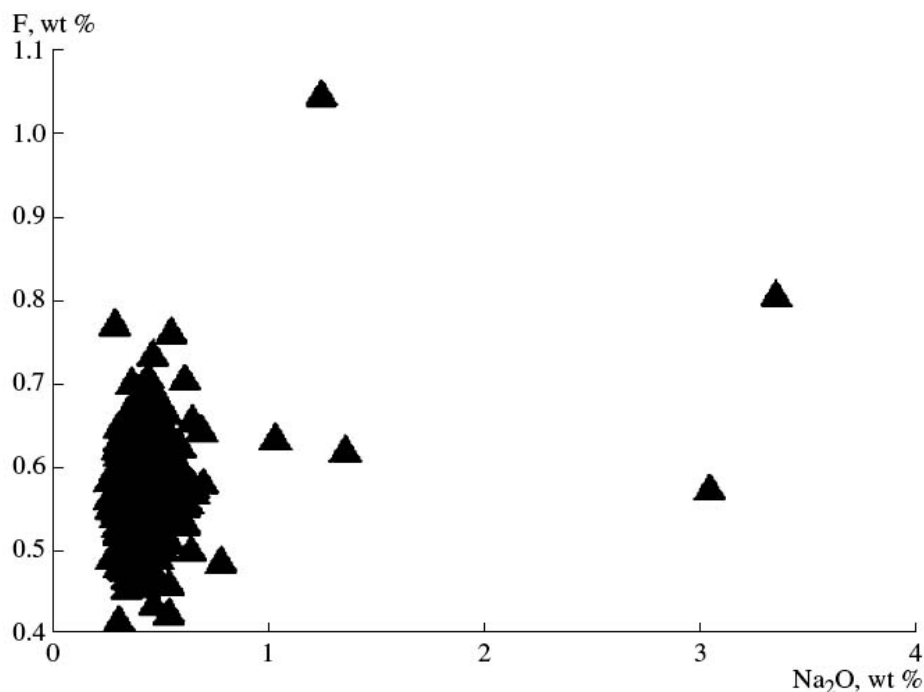


Fig. 10. F vs. Na<sub>2</sub>O in titanites from the apatite-bearing Khibiny pluton, Borehole 1312.

% diopside) to varieties enriched in acmite (80 mol % acmite). The hedenbergite content remains almost constant at ~20 mol % and drops only in acmite-rich

pyroxenes (Fig. 9).

Titanites are characterized by a relatively constant chemical composition. They contain, together with Ca, Ti, and Si, 0.3-0.8 wt % Na<sub>2</sub>O (0.48 wt %, on average), 0.1-0.8 wt % Al<sub>2</sub>O<sub>3</sub> (0.32 wt %, on average), 1-2 wt % FeO (1.25 wt %, on average), 0.1-0.7 wt % SrO (0.41 wt %, on average), and 0.4-1.0 wt % F (0.57 wt %, on average). Titanites also may contain 0.5-1.0 wt % Nb<sub>2</sub>O<sub>5</sub> + Ta<sub>2</sub>O<sub>5</sub>, about 0.5 wt % REE, 0.2-0.4 wt % ZrO<sub>2</sub>, and probably are water-bearing (Fig. 10).

## THERMODYNAMIC CALCULATIONS

To estimate  $f_{\text{O}_2}$  in rocks of the apatite-bearing intrusion, we used experimental and calculated data for the magnetite + ilmenite + titanite + hedenbergite + SiO<sub>2</sub> phase assemblage [47, 48, 49], which correspond to the reaction



These published results were obtained under  $a_{\text{SiO}_2}=1$  and hedenbergite activity close to unity. Equilibrium (1) was recalculated to conditions of lower silica and hedenbergite activities that fit nepheline-bearing mineral assemblages and compositions of clinopyroxenes occurring in the Khibiny rocks. For this purpose, the activities of silica and hedenbergite components have been estimated.

To estimate  $a_{\text{SiO}_2}$ , the equilibrium constant of the reaction



was used.

Nepheline and albite activities were estimated taking into account the compositions of nepheline and K-feldspar solid solutions from the Khibiny melteigite [4, 21], the published data on excess thermodynamic properties of tectosilicates [31], and the free energy of end member of these solid solutions [17].

At 900°C and 0.1 GPa, the  $a_{\text{SiO}_2}$  estimated in this way is 0.23 and coincides with the silica activity in the titanite + perovskite phase assemblage under the same conditions. Keeping in mind that perovskite is absent in rocks of apatite-bearing intrusion (except for sporadic loparite in pegmatites), this value should be accepted as a lower limit of silica activity.

The calculation from the equilibrium constant of the reaction



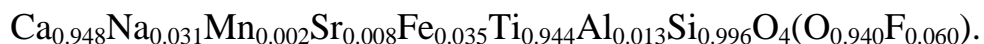
at the same NaAlSiO<sub>4</sub> activity as for reaction (2) and at the jadeite activity calculated from the composition of typical Khibiny clinopyroxene and the formulas for the activity coefficients proposed by Holland (1990) yields  $a_{\text{SiO}_2}=0.41$  for 900°C and 0.1 GPa, which is appreciably higher than the value presented

above = ( $a_{\text{SiO}_2} = 0.23$ ).

It cannot be ruled out that this discrepancy is caused by a certain disagreement in the thermodynamic data used. At the same time, this may be related to the arbitrarily chosen pressure, because the results of calculations from the equilibrium constants of reactions (2) and (3) draw together at a higher pressure. Anyway, the constant of reaction (1) increases only by 0.5 when  $\log f_{\text{O}_2}$  changes from 0.23 to 0.41.

In most Khibiny clinopyroxenes, the hedenbergite mole fraction is close to 0.2 [4, 21], see Fig. 9. In clinopyroxene solid solutions with replacement of  $\text{Ca}^{2+}$  with  $\text{Na}^{1+}$  and  $\text{Fe}^{2+}$  or  $\text{Mg}^{2+}$  with  $\text{Al}^{3+}$ , the activity coefficients at high temperatures are close to unity [30, 44]. As a first approximation, it is assumed that the mixing parameters in pyroxenes  $\text{CaMgSi}_2\text{O}_6$ - $\text{CaFeSi}_2\text{O}_6$ - $\text{NaFeSi}_2\text{O}_6$  are close to ideal as well ("molecular" model), so that  $a_{\text{Hed}} = 0.2$  was used in all calculations. The formulas for the activities of components in pyroxene solid solutions published by Holland (1990) yields values that are close to the molecular model. For the composition of pyroxene from a three-mineral aggregate in sample Khib-50 (table, analysis 19) at 900°C, this model yields a hedenbergite activity of 0.18, while the Holland's molecular model, 0.2. At 600°K, these values are 0.19 and 0.20, respectively.

The compositions of titanates in the studied rocks are relatively stable and are close, on average, to the formula



Assuming that the thermodynamics of this phase is described by the model of a multiposition ideal solid solution, the  $\text{CaTiSiO}_4\text{O}$  activity is 0.85. The substitution of this value into the equilibrium constant of reaction (1) drops the calculated oxygen fugacity only by 0.2 log units relative to the pure end member of titanite. Actually, the ordering of cations and anions by structural sites shifts titanite activity in the solid solution still closer to unity.

The  $\Delta\text{QFM}$  values for various temperatures ( $\Delta\text{QFM} = \lg(f_{\text{O}_2}(\text{rock})/f_{\text{O}_2}(\text{QFM}))$ ), were taken from the diagram at a pressure of 1 bar[48]. The  $\text{Fe}_2\text{TiO}_4$  and  $\text{Fe}_3\text{O}_4$  concentrations and activities were calculated from equation systems based on expressions for equilibrium constants of the following reactions:



where  $a_{\text{usp}}$  and  $a_{\text{mt}}$  were calculated on the basis of the previously published mixing functions and thermodynamic characteristics of end members of solid solutions [11, 12]. The  $a_{\text{usp}}$ , and  $a_{\text{mt}}$  values and  $\Delta\text{QFM}$  from [48] were used to calculate the equilibrium constant of the reaction



at each given temperature.

This equilibrium constant was used to calculate the  $\Delta\text{QFM}$ , composition, and activities of components in both Fe-Ti oxides at  $a_{\text{Hed}} < 1$  and  $a_{\text{SiO}_2} < 1$ . This equilibrium constant allows us to find the relationship of ilmenite and ulvospinel activities for two cases, when (1)  $a_{\text{Hed}} = 1$  and  $a_{\text{SiO}_2} = 1$  ( $a_{\text{usp}(0)}$  and  $a_{\text{ilm}(0)}$ ) and (2) silica and hedenbergite activities are less than unity ( $a_{\text{usp}}$  and  $a_{\text{ilm}}$ ):  $a_{\text{usp}}^2/a_{\text{ilm}}^3 = a_{\text{usp}(0)}^2/(a_{\text{ilm}(0)}^3 (a_{\text{hed}}/a_{\text{SiO}_2})$ .

Using a new  $a_{\text{usp}}^2/a_{\text{ilm}}^3$  value, we solve the system of equations proceeding from equilibrium constants of reactions (4) and (5) and obtain the compositions of magnetite and ilmenite solid solutions and  $\Delta\text{QFM}$  for the magnetite + ilmenite + titanite + hedenbergite + nepheline + K-feldspar phase assemblage at  $a_{\text{Hed}} < 1$  and  $a_{\text{SiO}_2} < 1$ . The  $\Delta\text{QFM}$  for the magnetite + ilmenite + titanite + hedenbergite + nepheline + K-feldspar phase assemblage are shown as the solid line in Fig. 11.

At a higher oxygen fugacity, magnetite appears in equilibrium with titanite + hedenbergite + nepheline + K-feldspar but ilmenite is unstable. The latter appears in a magnetite-free field at a lower oxygen fugacity.

In the field free of ilmenite above the monovariant line in Fig. 11, oxygen fugacity is fixed for each temperature and magnetite composition. To find  $f_{\text{O}_2}$  values for variable temperature,  $\Delta\text{QFM}$  values for the magnetite + ilmenite + titanite + hedenbergite + nepheline + K-feldspar phase assemblage were recalculated to new magnetite compositions on the basis of equation for equilibrium constant of the reaction



using the formula  $\Delta\text{QFM} = \Delta\text{QFM}(i) + 2\lg(a_{\text{usp}}(i)/a_{\text{mt}}(i)/a_{\text{usp}} \cdot a_{\text{mt}})$ , where  $\Delta\text{QFM}(i)$ ,  $a_{\text{usp}}(i)$ , and  $a_{\text{mt}}(i)$  are the values for phase assemblage with magnetite and ilmenite, whereas  $\Delta\text{QFM}$ ,  $a_{\text{usp}}$ , and  $a_{\text{mt}}$  are related to the given magnetite composition in the ilmenite-free assemblage. The calculated isopleths of magnetite compositions are shown in Fig. 11 as dashed lines.

## REDOX CRYSTALLIZATION CONDITIONS OF THE Khibiny Magma

For the most abundant magnetites with 55 mol % ulvospinel, Fig. 11 yields crystallization temperature above 880°C and oxygen fugacity close to the QFM buffer ( $\Delta\text{QFM} = -0.1$  at 880°C and  $\Delta\text{QFM} = +0.3$  at 1100°C).

The observed variations of magnetite compositions testify to the crystallization of this mineral within a range of temperatures and oxygen fugacities. According to Fig. 11, the Ti-rich magnetites with 25 wt %  $\text{TiO}_2$  (70 mol

% ulvospinel, see table, analysis 5) should crystallize above 1030°C and at  $\Delta QFM$  close to -0.2. The intergrowths of separate magnetite grains (40 mol % ulvospinel) and ilmenite (table, analyses 8 and 13) give 740°C and  $\Delta QFM = -0.1$ . Magnetite grains with exsolution-oxidation structure (table, analyses 1 and 12) were formed at a still lower temperature.

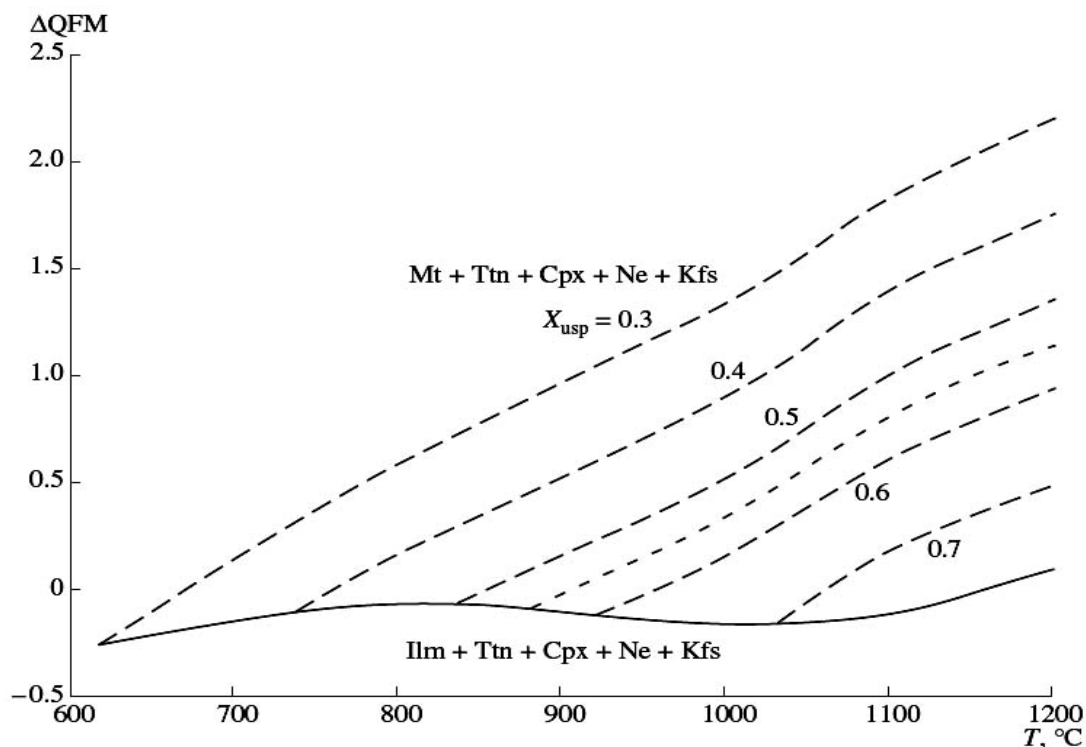


Fig. 11. Isopleths of magnetite compositions in equilibrium with ilmenite, titanite, clinopyroxene, nepheline, and alkali feldspar vs.  $\Delta QFM$ .

The obtained estimate of magnetite crystallization temperature for the most abundant composition of this mineral from Borehole 1312 (~880°C) is consistent with the data on melt inclusions in nepheline and apatite from the Khibiny intrusion (850-950°C) [19].

Our calculations have shown that oxygen fugacity for the apatite-bearing intrusion of the Khibiny Complex was close to the QFM buffer. The same conclusion was drawn for peralkaline rocks of the Lovozero pluton neighboring the Khibiny pluton based on a comparison of the relative stabilities of aegirine, arfvedsonite, and aenigmatite [19].

### EQUILIBRIUM GAS PHASE OF THE Khibiny INTRUSION

The composition of the gas phase in the C-H-O system has been calculated at oxygen fugacities characteristic of the Khibiny apatite-bearing intrusion. The equilibrium constants of the following reactions were used for this purpose:

Table. 1

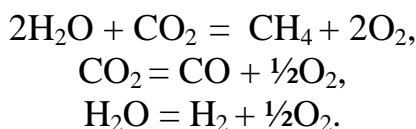
## Representative chemical compositions of minerals from rocks of the Khibiny pluton.

Component, wt %	1	2	3	4	5	6	7	8	9	10
	Mt	Mt	Mt	Mt	Mt	Mt	Mt	Mt	Mt	Mt
SiO <sub>2</sub>	0.42	0.28	0.36	0.33	0.33	0.38	0.67	0.33	0.05	0.05
TiO <sub>2</sub>	2.85	17.76	19.67	10.34	24.19	18.17	28.91	13.99	20.34	22.31
Al <sub>2</sub> O <sub>3</sub>	0.09	0.10	0.01	0.08	0.05	0.11	0.03	0.090	0.05	0.04
Cr <sub>2</sub> O <sub>3</sub>	0.07	0.05	0.08	0.04	0.05	0.05	0.04	0.07	0.09	0.06
Fe <sub>2</sub> O <sub>3</sub>	61.99	35.95	33.86	50.06	23.71	35.47	12.19	40.12	28.95	24.03
FeO	33.93	42.36	42.3642	37.98	47.68	43.42	54.66	42.55	47.33	48.21
MgO	0.00	0.55	0.01	0.15	0.26	0.28	0.08	0.08	0.11	0.09
MnO	0.29	2.082	2.43	1.17	2.12	2.12	2.10	1.48	2.08	2.18
ZnO	0.07	0.13	0.23	0.07	0.0	0.17	0.05	0.01		
V <sub>2</sub> O <sub>3</sub>	0.40	0.33	0.65	0.26	0.33	0.31	0.22	0.39		
<b>Total</b>	100.13	99.53	99.61	100.47	99.72	100.48	98.97	99.03	99.04	97.11
<i>Structural formula (number of cations)</i>										
Si	0.016	0.01	0.014	0.013	0.002	0.014	0.025	0.013	0.002	0.002
Ti	0.082	0.506	0.563	0.295	0.686	0.514	0.0820	0.403	0.582	0.650
Al	0.004	0.004	0.0040	0.004	0.002	0.005	0.001	0.0040	0.002	0.002
Cr	0.002	0.001	0.002	0.001	0.001	0.001	0.001	0.002	0.003	0.002
Fe <sup>3+</sup>	1.785	1.025	0.969	1.428	0.672	1.003	0.346	1.229	0.829	0.700
Fe <sup>2+</sup>	1.086	1.342	1.346	1.204	1.502	1.5	1.725	1.289	1.506	1.560
Mg	0.000	0.031	0.01	0.008	0.005	0.016	0.005	0.005	0.006	0.005
Mn	0.010	0.065	0.078	0.038	0.093	0.067	0.067	0.048	0.067	0.071
Zn	0.002	0.004	0.006	0.002	0.006	0.005	0.001	0.000		
V	0.012	V0.012	V0.012	0.008	V0.012	0.009	0.007	0.012		
ox	4	4	4	4	4	4	4	4	4	4
sc	3	3	3	3	3	3	3	3	3	3
<b>Component</b>	<b>11</b>	<b>12</b>	<b>13</b>	<b>14</b>	<b>15</b>	<b>16</b>	<b>17</b>	<b>18</b>	<b>19</b>	<b>20</b>
	<b>Mt</b>	<b>Ilm</b>	<b>Ilm</b>	<b>Cpx</b>	<b>Cpx</b>	<b>Cpx</b>	<b>Cpx</b>	<b>Cpx</b>	<b>Cpx</b>	<b>Ttn</b>
SiO <sub>2</sub>	0.06	0.24	0.24	52.33	52.09	51.58	51.18	51.14	51.92	30.00
TiO <sub>2</sub>	17.90	52.87	53.26	3.70	2.46	0.78	1.15	1.11	1.19	37.68
Al <sub>2</sub> O <sub>3</sub>	0.08	0.080	0.080	0.54	0.45	0.44	1.07	0.78	0.80	0.37
Cr <sub>2</sub> O <sub>3</sub>	0.04	0.05	0.03	0.01	0.00	0.04	0.00	0.00	0.00	0.00
Fe <sub>2</sub> O <sub>3</sub>	32.79			21.89	25.45	14.38	6.72	9.14	8.42	
FeO	45.04	41.25	43.18	4.86	2.92	7.81	7.19	6.38	7.12	1.42
MgO	0.05	0.13	0.21	0.75	1.09	4.67	9.29	8.55	8.31	0.00
CaO			0.00	3.33	2.76	13.23	20.24	17.90	18.00	26.94
Na <sub>2</sub> O				11.78	12.00	6.20	2.58	3.70	3.80	0.28
K <sub>2</sub> O				0.01	0.00	0.00	0.00	0.00	0.01	
NiO			0.01	0.010	0.010	0.02	0.01			
MnO	1.68	6.08	3.99	0.78	0.45	0.52	0.57	0.43	0.50	0.07
<b>Total</b>	97.72	100.73	100.93	99.98	99.67	99.67	100.00	99.14	100.07	97.43

Table. (Contd.)

Component, wt %	11	12	13	14	15	16	17	18	19	20
	Mt	Ilm	Ilm	Cpx	Cpx	Cpx	Cpx	Cpx	Cpx	Ttn
	<i>Structural formula (number of cations)</i>									
Si	0.002	0.006	0.006	2.003	1.998	1.990	1.942	1.956	1.968	1.014
Ti	0.520	0.994	0.998	0.107	0.071	0.03	0.03	0.032	0.034	0.958
Al	0.004	0.0040	0.0040	0.024	0.0240	0.0240	0.048	0.035	0.036	0.015
Cr	0.001	0.001	0.001	0.000	0.000	0.001	0.000	0.000	0.000	0.000
Fe <sup>3+</sup>	0.954	0.000	0.000	0.631	0.734	0.418	0.192	0.263	0.240	0.000
Fe <sup>2+</sup>	1.456	0.863	0.900	0.155	0.094	0.22	0.228	0.204	0.226	0.040
Mg	0.003	0.005	0.008	0.043	0.062	0.269	0.526	0.488	0.470	0.000
Ca			0.000	0.137	0.113	0.547	0.823	0.734	0.731	0.976
Na			0.000	0.874	0.892	0.464	0.190	0.274	0.279	0.018
K			0.000	0.000	0.000	0.000	0.000	0.000	0.000	0.000
Ni			0.000	0.000	0.000	0.001	0.000	0.000	0.000	0.000
Mn	0.055	0.129	0.084	0.025	0.015	0.017	0.018	0.014	0.016	0.002
OX	4	3	3	6	6	6	6	6	6	5
SC	3	2	2	4	4	4	4	4	4	3

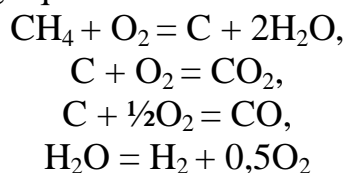
**Notes:** OX is the number of oxygen atoms in structural formula; SC is the number of cations for the given number of oxygen atoms. Mt, magnetite; Ilm, ilmenite; Ttn, titanite; Cpx, clinopyroxene. Ferrous and ferric components were calculated from microprobe analyses proceeding on the assumption of ideal stoichiometry of minerals. Analyses 1 and 12 are magnetites and ilmenites from the aggregates, which are products of exsolution-oxidation of titanomagnetite solid solution (Fig. 7). Analyses 8 and 13 are compositions of large coexisting magnetite and ilmenite grains (Fig. 8). Analyses 9 and 11 and 18-20 are coexisting minerals from sample Khib-50, Borehole 1312. Titanite (analysis 20) contains 0.35 wt % SrO and 0.56 wt % F.



The equilibrium constants were calculated using the internally consistent thermodynamic data set [17]. The activities of pure components participating in the above-mentioned reactions were taken from Holland and Powell [16]. The activity coefficients of components in a fluid of complex composition were estimated with allowance for the data published by Shmulovich [42] for the H<sub>2</sub>O-CO<sub>2</sub> system and by Zhang et al. [50] for the CH<sub>4</sub>-H<sub>2</sub>O system. To approximate the relationships of excess thermodynamic functions in these binary systems, two-parametric Margules equations had been used, and the obtained parameters of these equations were then applied to calculate the activity coefficients of the components in the ternary CO<sub>2</sub>-H<sub>2</sub>O-CH<sub>4</sub> mixture using the equations published by Ryabchikov [37]. It was suggested that CO<sub>2</sub> and CH<sub>4</sub> are mixed as ideal solutions and the parameter of simultaneous interaction of all three components is zero. It was suggested that the

activity coefficients for H<sub>2</sub> and CO occurring in small amounts were the same as for methane. This suggestion is consistent with the statement that parameters of interaction of nonpolar gases with water are very close to one another [42]. Simpler calculations, for example, assuming that interactions of CO<sub>2</sub> and methane with water are identical, lead to a result close to our model of the three-component solution, and at a temperature above 500°C, our result differs little from the model of an ideal gas solution. This implies that uncertainties related to the approximate thermodynamic model of a high-temperature fluid are too small to change the most important conclusions concerning the behavior of the gas phase equilibrated with mineral assemblages of alkaline rocks.

Calculations were carried out for the given atomic H/C ratios in gas phase. The expressions for equilibrium constants with fugacities of components substituted therein as products of activities by fugacities of pure components, together with the condition of equality of the sum of mole fractions of components to unity and the condition  $(4X_{\text{CH}_4} + 2X_{\text{H}_2\text{O}} + 2X_{\text{H}_2}) / (X_{\text{CH}_4} + X_{\text{CO}_2} + X_{\text{CO}}) = R_{\text{H/C}}$ , where  $R_{\text{H/C}}$  is the fixed atomic H/C ratio, give us five equations with five unknown quantities. The solution of this equation system yields the mole fractions of the components of the gas phase. In parallel, the graphite activity was calculated from constant of the reaction  $\text{C} + \text{O}_2 = \text{CO}_2$ . When the system is cooling, the graphite activity increases, and after the saturation with elementary carbon, the composition of gas phase was computed using equilibrium constants of four reactions:



in combination with condition of  $\sum X_i = 1$ .

As is seen from Fig. 12, at an oxygen fugacity close to the QFM buffer, H<sub>2</sub>O and CO<sub>2</sub> are dominant in the fluid from magmatic temperatures to ~450°C. At 900°C, the hydrogen concentration is somewhat less than 1 mol % and drops in the course of cooling. The methane concentrations at 900 to 500°C are very low and then begin to grow above 1 mol % with cooling.

At 470°C, graphite starts to be released from the fluid, largely due to the reaction  $\text{CO}_2 = \text{C} + \text{O}_2$ . With a further decrease in temperature, the mole fraction of CO<sub>2</sub> and the atomic fraction of carbon in the fluid decrease owing to fixation of carbon in graphite (Fig.13). At approximately 360°C, the atomic fraction of carbon goes through a minimum and then begins to grow. Graphite ceases to precipitate and undergoes resorption with the formation of appreciable amounts of CH<sub>4</sub>.

In most recent publications devoted to abiogenic synthesis of hydrocarbons in igneous rocks [27, 34, to name only a few), the Fischer-Tropsch reaction is regarded as the main mechanism:



Our calculations show, however, that within the equilibrium model, the reactions of water with previously formed graphite play the leading role, e.g.,

$C + H_2O = CH_4 + O_2$ ,  
 where  $f_{O_2}$  is buffered by melt and solid phases coexisting with the fluid.

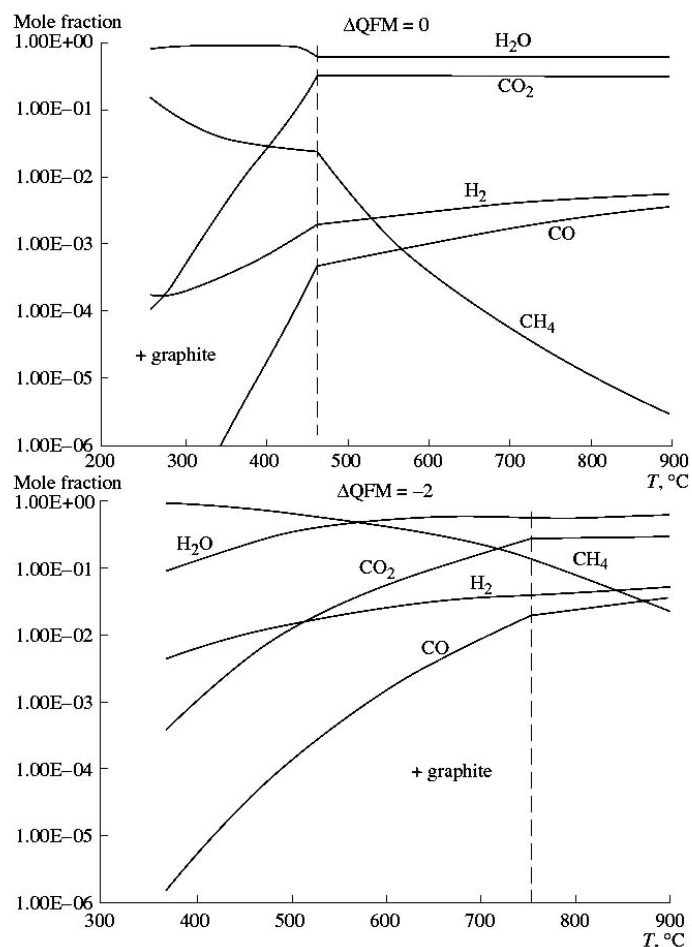


Fig. 12. Relationships of volatile components in fluid vs. temperature at  $H/C = 4$  and  $P = 0.1$  GPa.

The results of calculations at constant  $H/C = 4$  in the system are shown in Fig. 12. The calculations at other  $H/C$  values indicate that the temperature range of release of graphite from the fluid during its cooling changes relatively little at the given  $\Delta QFM$  and pressure. At  $\Delta QFM = 0$  and  $P = 0.1$  GPa, approximately corresponding to the condition of the emplacement of the apatite-bearing intrusion of the Khibiny Complex, the release of graphite from fluid starts at 450-470°C and ceases at 360°C (Fig. 14). The relatively low-temperature conditions of the graphite formation is consistent with the fact that this mineral was found largely in pegmatites and carbonatite of the Khibiny.

Thus, at the redox conditions characteristic of the Khibiny Complex, the evolution of carbon species looks as follows: CO<sub>2</sub> occurs in fluid and carbonate anions occur in melt at a high temperature; then graphite is being released, and an appreciable amounts of hydrocarbons appear at a lower temperature due to the reaction of fluid with graphite.

As was mentioned above, magmatic systems are known that are characterized by more reductive conditions than those estimated for the Khibiny Complex. To establish the evolution of carbon speciation in the course of cooling of magmatic

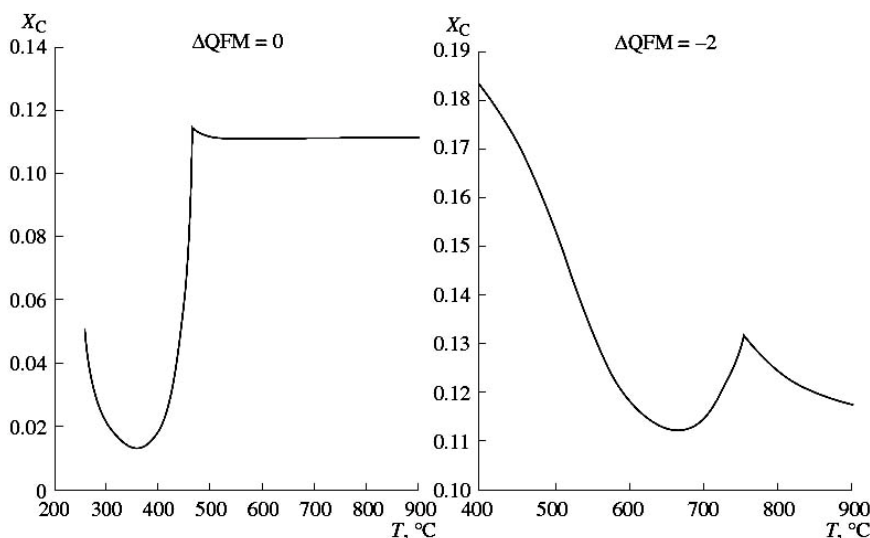


Fig. 13. Atomic fraction of carbon in fluid vs. temperature at  $H/C = 4$  and  $P = 0.1$  GPa. The abrupt decrease in  $X_c$  below  $500^\circ\text{C}$  is related to the onset of graphite release. At the temperature below a minimum point, graphite ceases of being released from fluid.

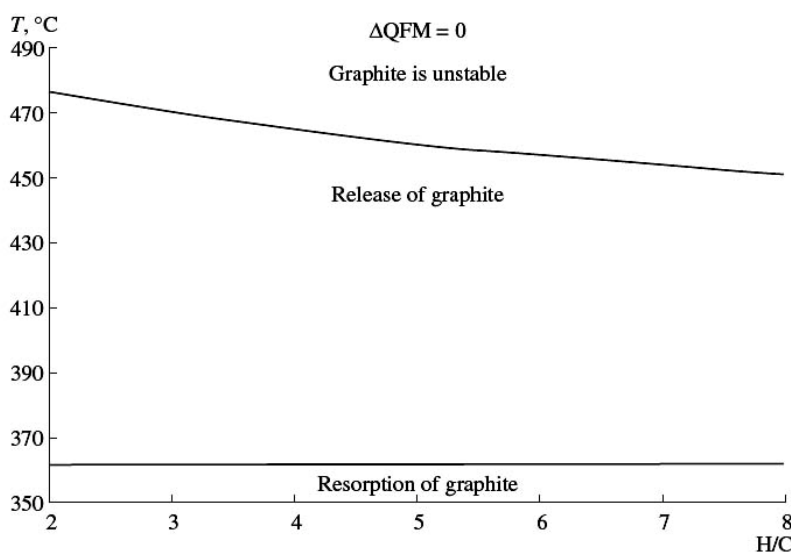


Fig. 14. The temperature of the onset of graphite release from cooling fluid vs.  $H/C$  in the bulk composition of the system at  $P = 0.1$  GPa and  $\Delta QFM = 0$ . The boundary of initial graphite resorption is shown in the low-temperature part of the diagram.

fluid under reductive conditions, the calculation was made at  $\Delta QFM = -2$  (Fig. 12).

Under more reductive conditions, the hydrogen concentration in the fluid is much higher (about a few mole percents); appreciable amounts of methane appear at a higher temperature, and the onset of graphite precipitation and the cessation of this process are shifted toward the region of higher temperature in comparison with  $\Delta QFM = 0$  (Fig. 13).

Taking into account that at a high temperature, the H<sub>2</sub> content in fluid even when  $\Delta QFM = 0$  exceeds 1 mol % and the diffusion rate of H<sub>2</sub> in the melt, through crystal lattices of mineral, and along crystalline grain boundaries is very high, it may be suggested that H<sub>2</sub> migrates from hot parts of the magmatic system into its cold portions. If the H<sub>2</sub> migration under a temperature gradient is sufficiently intense, then synthesis of hydrocarbons is possible in the colder part of the system due to interaction of H<sub>2</sub> with previously formed graphite and by such reactions as Fischer-Tropsch synthesis.

## CONCLUSIONS

1. Most magnetites in the Khibiny alkaline igneous complex sampled within a vertical interval of 500 m are distinguished by high Ti concentrations and contain approximately 55 mol % ulvospinel component. Occasionally, the ulvospinel content reaches 80 mol %.
2. As follows from the  $f_{O_2}$ - $T$  diagram, magnetites containing 55 mol % ulvospinel in equilibrium with clinopyroxene and titanite crystallized at a temperature above 900°C and at an oxygen fugacity slightly lower than that of the QFM buffer. Magnetites with higher Ti content crystallized at higher temperatures and lower AQFM values, whereas Ti-depleted magnetites were formed below 650°C.
3. At temperatures higher than 400°C, carbon occurred in the Khibiny magma either as carbonate ions in melt or as CO<sub>2</sub> in magmatic fluid. Graphite is released during further cooling, and an appreciable amount of hydrocarbons appear at still lower temperature due to the reaction of fluid with graphite. As well, abiogenic hydrocarbons can arise in igneous complexes as products of the processes distinct from Fischer-Tropsch synthesis.
4. It cannot be ruled out that hydrogen occurring in the gas phase at magmatic temperature migrated to colder portions of the solidified magma chamber and participated in the formation of hydrocarbons according to the Fischer-Tropsch reaction.

## ACKNOWLEDGMENTS

This study was supported by the Russian Foundation for Basic Research (project nos. 08-05-00356 and 08-05-00054), the International Association for the Promotion of Cooperation with Scientists from the Independent States of the Former Soviet Union (project no. 05-1000008-7938), and the Division of Earth Sciences of the Russian Academy of Sciences (program nos. 4 and 7).

## REFERENCES

1. **C, Ballhaus**, "Redox States of Lithospheric and Asthenospheric Upper Mantle," *Contrib. Mineral. Petrol.* 114, 341-348 (1993).
2. **C, Ballhaus, R. F., Berry, and D. H., Green**, "Oxygen Fugacity Controls in the Earth's Upper

- Mantle," *Nature* 348, 437-440 (1990).
3. **B., Beeskow, P. J., Treloar, A. H., Rankin, et al.**, "A Reassessment of Models for Hydrocarbon Generation in the Khibiny Nepheline Syenite Complex, Kola Peninsula, Russia," *Lithos* 91, 1-18 (2006).
  4. **B. E., Borutsky**, *Rock-Forming Minerals of High-Alkaline Complexes* (Nauka, Moscow, 1988) [in Russian].
  5. **A. F., Buddington and D. H., Lindsley**, "Iron-Titanium Oxide Minerals and Synthetic Equivalents," *J. Petrol.* 5, 310-357 (1964).
  6. **D., Canil**, "Vanadium Partitioning and the Oxidation State of Archean Komatiite Magmas," *Nature* 389, 842-845 (1997).
  7. **D., Canil**, "Vanadium Partitioning between Orthopyroxene, Spinel and Silicate Melt and the Redox States of Mantle Source Regions for Primary Magmas," *Geochim. Cosmo-chim. Acta* 63, 557-572 (1999).
  8. **D., Canil**, "Vanadium in Peridotites, Mantle Redox and Tectonic Environments: Archean to Present," *Earth Planet. Sci. Lett.* 195, 75-90 (2002).
  9. **B. R., Frost and D. H., Lindsley**, "Occurrence of Iron-Titanium Oxides in Igneous Rocks: Oxide Minerals: Petrologic and Magnetic Significance," *Rev. Mineral.* 25, 433-467 (1991).
  10. **B. R., Frost, D. H., Lindsley, and D. J., Andersen**, "Fe-Ti Oxide-Silicate Equilibria: Assemblages with Fayalitic Olivine," *Am. Mineral.* 73, 727-740 (1988).
  11. **M. S., Ghiorso and R. O., Sack**, "Fe-Ti Oxide Geothermometry: Thermodynamic Formulation and the Estimation of Intensive Parameters in Silicic Magmas," *Contrib. Mineral. Petrol.* 108, 485-510 (1991a).
  12. **M. S., Ghiorso and R. O., Sack**, "Thermochemistry of the Oxide Minerals: Oxide Minerals: Petrologic and Magnetic Significance," *Rev. Mineral.* 25, 221-264 (1991b).
  13. **D. H., Green, T. J., Falloon, and W. R., Taylor**, "Mantle-Derived Magmas: Roles of Variable Source Peridotite and Variable C-O-H Fluid Compositions," in *Magmatic Processes: Physicochemical Principles* *Geochem. Soc. Spec. Publ.* 1, 139-154 (1987).
  14. **R., Halama, T., Vennemann, W., Siebel, and G., Markl**, "The Gronnedal-Ika Carbonatite-Syenite Complex, South Greenland: Carbonatite Formation by Liquid Immiscibility," *J. Petrol.* 46, 191-217 (2005).
  15. **T. J. B., Holland**, "Activities of Components in Omphacitic Solid Solutions. Application of Landau Theory to Mixtures," *Contrib. Mineral. Petrol.* 105, 446-453 (1990).
  16. **T., Holland and R., Powell**, "A Compensated Redlich-Kwong (CORK) Equation for Volumes and Fugacities of CO<sub>2</sub> and H<sub>2</sub>O in the Range 1 Bar to 50 Kbar and 100-1600°C," *Contrib. Mineral. Petrol.* 109, 265-273 (1991).
  17. **T. J. B., Holland and R., Powell**, "An Internally Consistent Thermodynamic Data Set for Phases of Petrological Interest," *J. Metamorphic Geol.* 16, 309-343 (1998).
  18. **S. V., Ikorsky and N. A., Shugurova**, "New Data on Age of Gases in Minerals from the Alkaline Rocks of the Khibiny Massif," *Geokhimiya* 12 (6), 943-947 (1974).
  19. **L. N., Kogarko**, *Genesis of Peralkaline Magmas* (Nauka, Moscow, 1977) [in Russian].
  20. **L. N., Kogarko, C., Kosztołanyi, and I. D., Ryabchikov**, "Geochemistry of Reduced Fluids of Alkaline Magmas," *Geokhimiya* 24 (12), 1688-1695 (1986).
  21. **E. E., Kostyleva-Labuntsova, B. E., Borutsky, M. N., Sokolova, et al.**, *Mineralogy of the Khibiny Massif. Minerals* (Nauka, Moscow, 1978) [in Russian].
  22. **U., Mann, M., Marks, and G., Markl**, "Influence of Oxygen Fugacity on Mineral Compositions in Peralkaline Melts: The Katzenbuckel Volcano, Southwest Germany," *Lithos* 91, 262-285 (2006).
  23. **G., Markl, M., Marks, G., Schwinn, and H., Sommer**, "Phase Equilibrium Constraints on Intensive Crystallization Parameters of the Ilimaussaq Complex, South Greenland," *J. Petrol.* 42, 2231-2257 (2001).
  24. **M., Marks and G., Markl**, "Fractionation and Assimilation Processes in the Alkaline Augite

- Syenite Unit of the Ilimaussaq Intrusion, South Greenland, As Deduced from Phase Equilibria," *J. Petrol.* 42, 1947-1969 (2001).
25. **M. A. W., Marks, J., Schilling, I. M., Coulson, et al.**, "The Alkaline-Peralkaline Tamazeght Complex, High Atlas Mountains, Morocco: Mineral Chemistry and Petrological Constraints for Derivation from a Compositionally Heterogeneous Mantle Source," *J. Petrol.* 49, 1097-1131 (2008).
  26. **V. A., Nivin**, "Gas Concentrations in Minerals with Reference to the Problem of the Genesis of Hydrocarbon Gases in Rocks of the Khibiny and Lovozero Massifs," *Geochem. Intern.* 40, 883-898 (2002).
  27. **V. A., Nivin, P. J., Treloar, N. G., Konopleva, and S. V., Ikorsky**, "A Review of the Occurrence, Form and Origin of C-Bearing Species in the Khibiny Alkaline Igneous Complex, Kola Peninsula, NW Russia," *Lithos* 85, 93-112 (2005).
  28. **H. S. C., O'Neill and V. J., Wall**, "The Olivine-Spinel Oxygen Geobarometer, the Nickel Precipitation Curve and the Oxygen Fugacity of the Upper Mantle," *J. Petrol.* 28, 1169-1192(1987).
  29. **E. F., Osborn**, "Role of Oxygen Pressure in the Crystallization and Differentiation of Basaltic Magma," *Am. J. Sci.* 257, 609-647 (1959).
  30. **A. L., Perchuk and L. Ya., Aranovich**, "Thermodynamic Model of the Solid Solution of the Jadeite-Diopside-Hedenbergite," *Geokhimiya* 29 (4), 539-547 (1991).
  31. **L. L., Perchuk, K. K., Podlessky, and L. Y., Aranovich**, "Thermodynamics of Some Framework Silicates and Their Equilibria: Application to Geothermobarometry," in *Progress in Metamorphic and Magmatic Petrology* (Univ. Press, Cambridge, 1991), pp. 131-164.
  32. **A., Petersilie**, "Carbonaceous Gases and Bitumen of Intrusive Massifs in the Central Part of the Kola Peninsula," *Dokl. Akad. Nauk SSSR* 122 (6), 1086-1089 (1958).
  33. **I. A., Petersilie and H., Sorensen**, "Hydrocarbon Gases and Bituminous Substances in Rocks from the Ilimaussaq Alkaline Intrusion, South Greenland," *Lithos* 3, 59-76 (1970).
  34. **J., Potter, A. H., Rankin, and P. J., Treloar**, "Abiogenic Fischer-Tropsch Synthesis of Hydrocarbons in Alkaline Igneous Rocks: Fluid Inclusion, Textural and Isotopic Evidence from the Lovozero Complex, N.W. Russia," *Lithos* 75, 311-330(2004).
  35. **D. C., Presnall**, "The Join Forsterite-Diopside-Iron Oxide and Its Bearing on the Crystallization of Basaltic and Ultramafic Magmas," *Am. J. Sci.* 264, 753-809 (1966).
  36. **I. D., Ryabchikov**, *Thermodynamic Analysis of the Behavior of Minor Elements during Crystallization of Silicate Melts* (Nauka, Moscow, 1965) [in Russian].
  37. **I. D., Ryabchikov and L. N., Kogarko**, "Redox Equilibria in Alkaline Lavas from Trindade Island, Brasil," *Intern. Geol. Rev.* 36, 173-183 (1994).
  38. **I. D., Ryabchikov, A. V., Ukhanov, and T., Ishii**, "Redox Equilibria in the Alkaline Rocks from Upper Mantle of the Yakutian Kimberlite Province," *Geokhimiya* 23 (5), 1110-1123 (1985).
  39. **I. D., Ryabchikov, I. P., Solovova, L. N., Kogarko, G. P., Brey, Th., Ntaflos, and S. G., Simakin**, "Thermodynamic Parameters of Generation of Meimechites and Alkaline Picrites in the Maimecha-Kotui Province: Evidence from Melt Inclusions," *Geokhimiya* 40 (11), 1139-1150 (2002) [*Geochem. Int.* 40 (11), 1031-1041 (2002)].
  40. **R. O., Sack and M. S., Ghiorso**, "An Internally Consistent Model for the Thermodynamic Properties of Fe-Mg-Titano-magnetite-Aluminate Spinels," *Contrib. Mineral. Petrol.* 106, 474-505 (1991).
  41. **S., Salvi and A., Williams-Jones**, "Alteration, HFSE Mineralization, and Hydrocarbon Formation in Peralkaline Igneous Systems: Insights from the Strange Lake Pluton, Canada," *Lithos* 91, 19-34 (2006).
  42. **K. I., Shmulovich**, *Carbon Dioxide in High-Temperature Mineral Formation* (Nauka, Moscow, 1988) [in Russian].
  43. **V., Sobolev, V. S., Kamenetsky, and N. N., Kononkova**, "New Data on Petrology of the Siberian Meimechites," *Geokhimiya* 29 (8), 1084-1095 (1991).
  44. **V. L., Vinograd**, "Thermodynamics of Mixing and Ordering in the Diopside-Jadeite System: I. A

- CVM Model," *Mineral. Magazine* 66, 513-536 (2002).
45. **D. R., Wones**, "Significance of the Assemblage Titanite + Magnetite + Quartz in Granitic Rocks," *Am. Mineral.* 74, 744\_749 (1989).
  46. **J., Wood, L. T., Bryndzya, and K. E., Johnson**, "Mantle Oxidation State and Its Relationship to Tectonic Environment and Fluid Speciation," *Science* 248, 337-345 (1990).
  47. **Xirouchakis and D. H., Lindsley**, "Equilibriums among Titanite, Hedenbergite, Fayalite, Quartz, Ilmenite, and Magnetite: Experiments and Internally Consistent Thermodynamic Data for Titanite," *Am. Mineral.* 83, 712-725 (1998).
  48. **Xirouchakis, and D. H., Lindsley, and D. J., Andersen**, "Assemblages with Titanite (CaTiOSiO<sub>4</sub>), Ca-Mg-Fe Olivine and Pyroxenes, Fe-Mg-Ti Oxides, and Quartz: Part I. Theory," *Am. Mineral.* 86, 247-253 (2001a).
  49. **Xirouchakis, D. H. Lindsley, and B. R., Frost**, "Assemblages with Titanite (CaTiOSiO<sub>4</sub>), Ca-Mg-Fe Olivine and Pyroxenes, Fe-Mg-Ti Oxides, and Quartz: Part II. Application," *Am. Mineral.* 86, 254-264 (2001b).
  50. **C, Zhang, Z., Duan, and Z., Zhang**, "Molecular Dynamics Simulation of the CH<sub>4</sub> and CH<sub>4</sub>-H<sub>2</sub>O Systems up to 10 GPa and 2573 K," *Geochim. Cosmochim. Acta* 71, 2036-2055 (2007).

# **Chemical Composition, Volatile Components, and Trace Elements in the Magmatic Melt of the Kurama Mining District, Middle Tien Shan: Evidence from the Investigation of Inclusions in Quartz**

V. B. Naumov<sup>a</sup>, V. A. Kovalenker<sup>b</sup>, and V. L. Rusinov<sup>b</sup>

<sup>a</sup> *Vernadsky Institute of Geochemistry and Analytical Chemistry, Russian Academy of Sciences, u. l. Kosygina 19, Moscow, 119991 Russia, e-mail: naumov@geokhi.ru*

<sup>b</sup> *Institute of Geology of Ore Deposits, Petrography, Mineralogy, and Geochemistry (IGEM), Russian Academy of Sciences, Staromonetny iper. 35, Moscow, 119017, Russia, e-mail: kva@igem.ru*

## **ABSTRACT**

Melt and fluid inclusions were investigated in six quartz phenocryst samples from the igneous rocks of the extrusive (ignimbrites and rhyolites) and subvolcanic (granite porphyries) facies of the Lashkerek Depression in the Kurama mining district, Middle Tien Shan. The method of inclusion homogenization was used, and glasses from more than 40 inclusions were analyzed on electron and ion microprobes. The chemical characteristics of these inclusions are typical of silicic magmatic melts. The average composition is the following (wt %): 72.4 SiO<sub>2</sub>, 0.06 TiO<sub>2</sub>, 13.3 Al<sub>2</sub>O<sub>3</sub>, 0.95 FeO, 0.03 MnO, 0.01 MgO, 0.46 CaO, 3.33 Na<sub>2</sub>O, 5.16 K<sub>2</sub>O, 0.32 F, and 0.21 Cl. Potassium strongly prevails over sodium in all of the inclusions (K<sub>2</sub>O/Na<sub>2</sub>O averages 1.60). The average total of components in melt inclusions from five samples is 95.3 wt %, which indicates a possible average water content in the melt of no less than 3–4 wt %. Water contents of 2.0 wt % and 6.6 wt % were determined in melt inclusions from two samples using an ion microprobe. The analyses of ore elements in the melt inclusions revealed high contents of Sn (up to 970 ppm), Th (19–62 ppm, 47 ppm on average), and U (9–26 ppm, 18 ppm on average), but very low Eu contents (0.01 ppm). Melt inclusions of two different compositions were detected in quartz from a granite porphyry sample: silicate and chloride, the latter being more abundant. In addition to Na and K chlorides, the salt inclusions usually contain one or several anisotropic crystals and an opaque phase. The homogenization temperatures of the salt inclusions are rather high, from 680 to 820°C. In addition to silicate inclusions with homogenization temperatures of 820–850°C, a primary fluid inclusion of aqueous solution with a concentration of 3.7 wt % NaCl eq. and a very high density of 0.93 g/cm<sup>3</sup> was found in quartz from the ignimbrite. High fluid pressure values of 6.5–8.3 kbar were calculated for the temperature of quartz formation. These estimates are comparable with values obtained by us previously for other regions of the world: 2.6–4.3 kbar for Italy, 3.7 kbar for Mongolia, 3.3–8.7 kbar for central Slovakia, and 3.3–9.6 kbar for eastern Slovakia. Unusual melt inclusions were investigated in quartz from another ignimbrite sample. In addition to a gas phase and transparent glass, they contain spherical Fe-oxide globules (81.2 wt % FeO) with high content of SiO<sub>2</sub> (9.9 wt %). The globules were dissolved in the silicate melt within a narrow temperature range of 1050–1100°C, and the complete homogenization of the inclusions was observed at temperatures of 1140°C or higher. The combined analysis of the results of the investigation of these inclusions allowed us to conclude that immiscible liquids were formed in the high-temperature silicic magma with the separation of iron oxide-dominated droplets.

## INTRODUCTION

The problem of the sources of ore components and fluids is still not fully understood, despite the considerable number of isotopic and inclusion studies that have been carried out worldwide in ore deposits of various genetic types. The

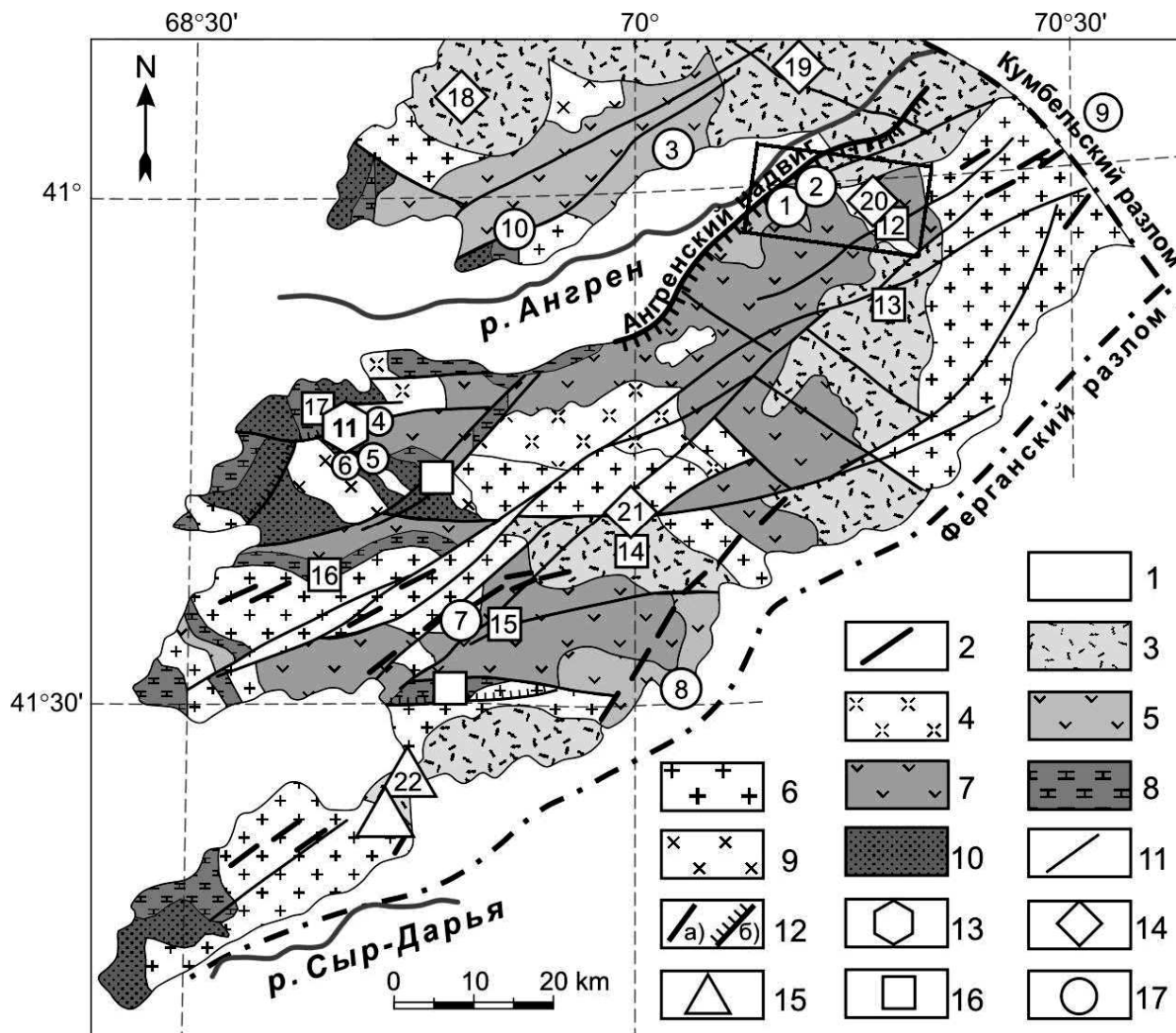


Fig. 1. Geological sketch map of the Kurama region [1].

(1) Quaternary deposits; (2) dike belts (diabases and felsites); (3) liparite volcanoplutonic association,  $C_3$ —P1; (4) granite porphyries,  $C_3$ ; (5) andesite—dacite volcanoplutonic association,  $C_{2-3}$ ; (6) granodiorites, granites, and diorites of the Karamazar type; (7) volcanic rocks,  $C_2$ ; (8) carbonate rocks,  $D_3$ —C1; (9) granodiorite and granite porphyries, O—S; (10) schists, hornfels, and spilites; (11) faults; (12a) regional faults; (12b) thrusts; and (13)—(17) deposit types and numbers: (13) Au—Ag, (14) Cu—Mo—Au; (15) Pb—Zn—fluorite, (16) U, and (17) W—Mo. Deposits: 1—Kochbulak, 2—Kairagach, 3—Kyzyl Alma, 4—Aktur-pak, 5—Kauldy, 6—Arabulak, 7—Shkol'noe, 8—Aprelevka, 9—Aktepe, 10—Akchasai, 11—Almalyk ore node (Kalmakyr, Sarycheku, and Dal'nee), 12—Naugarzan, 13—Lashkerek, 14—Kanimansur, 15—Kansai, 16—AltynTopkan, 17—Kurgash-inkan, 18—Chauli, 19—Alatan'ga, 20—Mailikatan, 21—Adrasman, and 22—Yangikan. The rectangle shows the region in which samples were collected for our study.

origin of relatively old deposits is especially controversial, because their long post

mineral history could involve many possible distortions of primary features characterizing ore formation proper. On the other hand, the Kurama mining district of Paleozoic age exemplify unique deposits with perfectly preserved characteristic features of Au—Cu porphyry and epithermal Au occurrences and no clear indications for their subsequent alterations (except for supergene ones). We investigated melt and fluid inclusions in quartz from the igneous rocks of both extrusive (ignimbrites and rhyolites) and subvolcanic (granite porphyries and rhyolite porphyries) facies occurring within the Lashkerek Depression. Their formation is related to the magmatic activity of the postbatholith stage of the development of this region. The igneous rocks are associated in space and time with the large epithermal deposits of the Kochbulak (Au—Ag—Te) and Lashkerek (Ag—Pb—Zn) ore fields, as well as numerous occurrences of Au, Ag, Cu, Pb, Zn, Bi, and Sn mineralization.

### **SHORT DESCRIPTION OF THE GEOLOGIC SETTING AND MAGMATISM OF THE KURAMA ORE DISTRICT**

The geologic setting of the Kurama mining district (Fig. 1) on the northern slope of the Kurama Range is controlled by its assignment to the structures of the eastern part of the extended Beltau—Kurama volcano-plutonic belt in the Middle Tien Shan. It is considered in geotectonic reconstructions as a continental margin volcanic belt of the Andean type, which was formed in the Middle Carboniferous—Permian. Intense magmatic processes occurred in this region throughout the whole Paleozoic, reaching a maximum at its end. Four stages of magmatic activity were distinguished in this region: prebatholithic, batholithic, small (porphyritic) intrusions, and dikes [2]. According to recent isotopic dating, most of the dikes were formed simultaneously with the complex of small intrusions and can be considered collectively as a single stage. The post-batholithic stage was related to the activity of porphyritic—epithermal ore-forming systems.

The general evolution of Paleozoic magmatism in the region shows a trend toward higher silica and alkali contents in the magmas [3]. With increasing degree of magmatic differentiation, the content of fluid components in the melts increased and reached a maximum in the magmas of the postbatholithic stage. The high content of fluid components resulted in the development of explosive volcanism and formation of tremendous amounts of ignimbrites, tuffs, and diatremes with the fluidization of enclosing volcanics. The rocks of this stage are of special interest for the interpretation of the magmatism of this region and its relation to ore mineralization.

The Kurama mining district is characterized by diverse metallogeny. It comprises numerous deposits of Au, Ag, Mo, W, Cu, Pb, Zn, U, other metals, and fluorite (captions to Fig. 1). The very high concentration of ore occurrences is related to the confinement of the region to the intersection of deep tectonic structures. Another unique feature of this region is that it is a rare example of

paleovolcanic areas with well preserved epithermal deposits of Late Paleozoic age [4, 5].

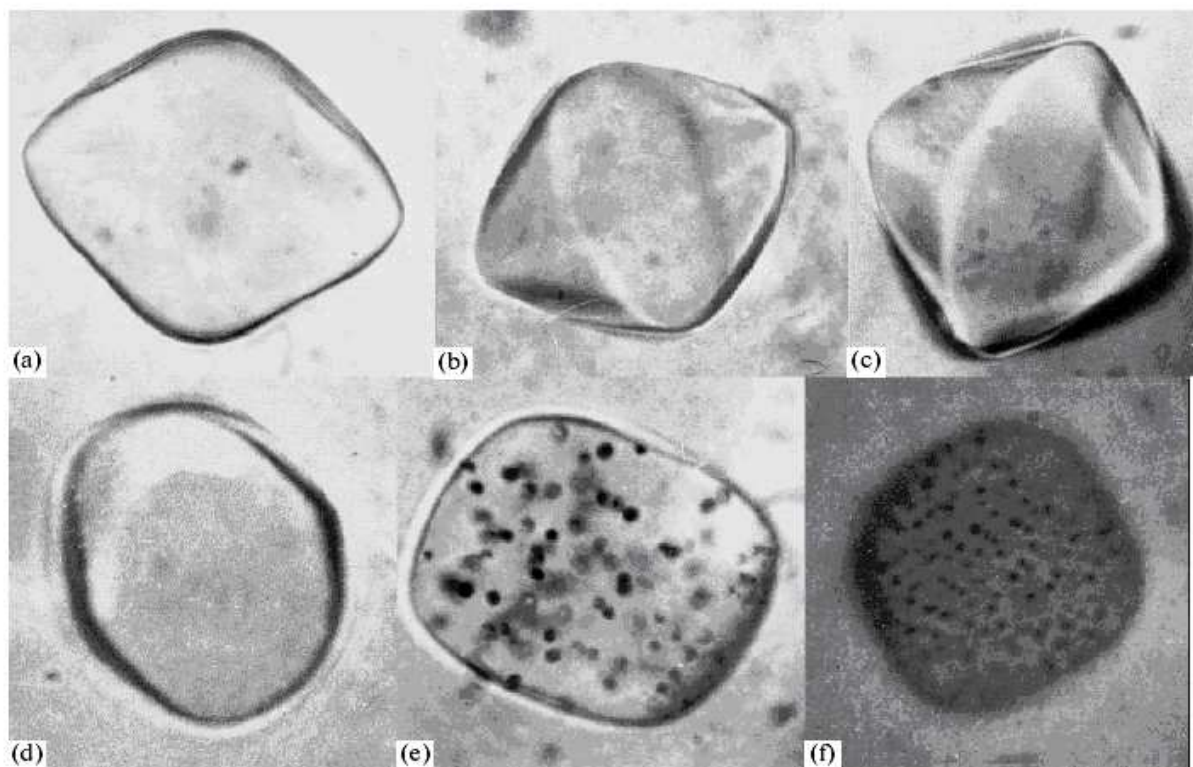


**Fig. 2. Melt inclusions in quartz phenocrysts from sample 1119.**

(a)—(d) Homogeneous inclusions of silicate melt; (e) and (f) heterogeneous inclusions, (e) unheated and (f) annealed at 580°C for 1 h and quenched.

After the formation of a volcanic andesite—dacite complex ( $C_{2-3}$ ) in this region, its rocks were intruded by stocks and dikes of porphyritic granitoids and sub-volcanic bodies of fluidal trachyliparites and ignimbrites ( $C_3$ —Pj). The Lashkerek massif is built up of fluidal trachyliparites and ignimbrites at the roof of a granitoid pluton as part of the larger Akshuran volcan-otectonic structure. The outer parts of the massif comprise outcrops of numerous dikes of quartz porphyries and felsites and pipelike bodies of explosive breccias.

## SAMPLES AND METHODS

Melt and fluid inclusions were investigated in igneous rock samples representing (1) the ignimbrites of the Lashkerek massif collected at the margin of the massif in the upper reaches of the Yangokla River (samples 28, 94, 98, and 1119) and (2) granite porphyries collected from two comagmatic dikes in the upper reaches of the Paraksai River (sample 217) and in the Mailikotan valley at the region of the Kamchik Pass (sample 682). Thus, the samples characterize both the extrusive (ignimbrites and rhyolites) and subvolcanic facies (granite porphyries). The rock samples are almost unaffected by secondary alteration, except for glass crystallization into a quartz—feldspar aggregate.

Table 1.

**Chemical compositions (wt %) of residual glasses, crystalline inclusions, and daughter phases in quartz-hosted melt inclusions from the silicic volcanics of the Kurama Province (Middle Tien Shan)**

Component	1(4)	2(3)	3(1)	4(2)	5(1)	6(10)
SiO <sub>2</sub>	73.19	72.07	46.97	40.61	44.74	9.93
TiO <sub>2</sub>	0.08	0.06	0.37	0.16	1.15	0.01
Al <sub>2</sub> O <sub>3</sub>	16.54	14.65	1.21	15.70	8.95	2.19
FeO	0.38	0.44	28.93	30.10	30.14	81.15
MnO	0.05	0.03	1.25	0.45	0.91	0.16
MgO	0.02	0.020	0.04	0.68	0.30	0.02
CaO	0.42	0.34	20.15	0.06	9.58	0.27
Na <sub>2</sub> O	2.92	1.48	1.12	0.13	2.15	0.34
K <sub>2</sub> O	6.86	5.18	0.09	9.42	1.15	0.36
F	0.10	0.23	0.00	1.52	—	—
Cl	0.13	0.14	0.01	0.48	0.52	0.01
<b>Total</b>	100.69	94.62	100.14	99.31	99.56	94.63

**Note:** (1) and (2) residual glasses from samples 682 and 94, respectively; (3) hedenbergite, sample 94; (4) siderophyllite, sample 682; (5) crystalline inclusion of amphibole (ferrohastingsite), sample 1119; and (6) opaque globules, the total includes 0.19 wt % ZnO (sample 28). FeO is total iron; the number of analyses is given in parentheses; here and in Tables 2—5, a dash means that the component was not determined.

The thermometric investigation of melt inclusions was carried out by the quench method [6] using a small electric furnace with a Pt heater, with which the temperature measurement accuracy was  $\pm 10^{\circ}\text{C}$ . Silicate glasses and daughter crystalline phases from inclusions were analyzed on Camebax Microbeam and Cameca SX-100 electron microprobes under the following conditions: an accelerating voltage of 15 kV, a beam current of 30 nA, and rastering over areas of 12 x 12, 5x5, and 2x2  $\mu\text{m}$  for glasses and 2x2  $\mu\text{m}$  for crystals. The analytical accuracy was 2% rel. for element contents  $>10$  wt %, 5% rel. for element contents 5—10 wt %, and 10% rel. for element contents  $<5$  wt %. The contents of water, fluorine, and trace elements in melt inclusions were determined by secondary ion mass spectrometry using an IMS-4f ion microprobe at the Institute of Microelectronics of the Russian Academy of Sciences (Yaroslavl) by the method described in detail in [7-9].

**INVESTIGATION OF MELT AND FLUID INCLUSIONS:  
RESULTS AND DISCUSSION**

Silicate melt inclusions were found in quartz from all of the samples. They consist of a single phase (silicate glass only, Figs. 2a—2d), two phases (glass and gas, Fig. 2e), or several phases with partly crystallized glass and daughter crystals (Fig. 3). Glass is absent in inclusions from sample 217, and their complete crystallization (Fig. 4a) suggests slower cooling of the respective area of the

granite porphyry dike. The inclusion size ranges from 5—10 to 264  $\mu\text{m}$  and is usually between 20 and 70  $\mu\text{m}$ . The gas phase accounts for 4.6—9.0 vol %.

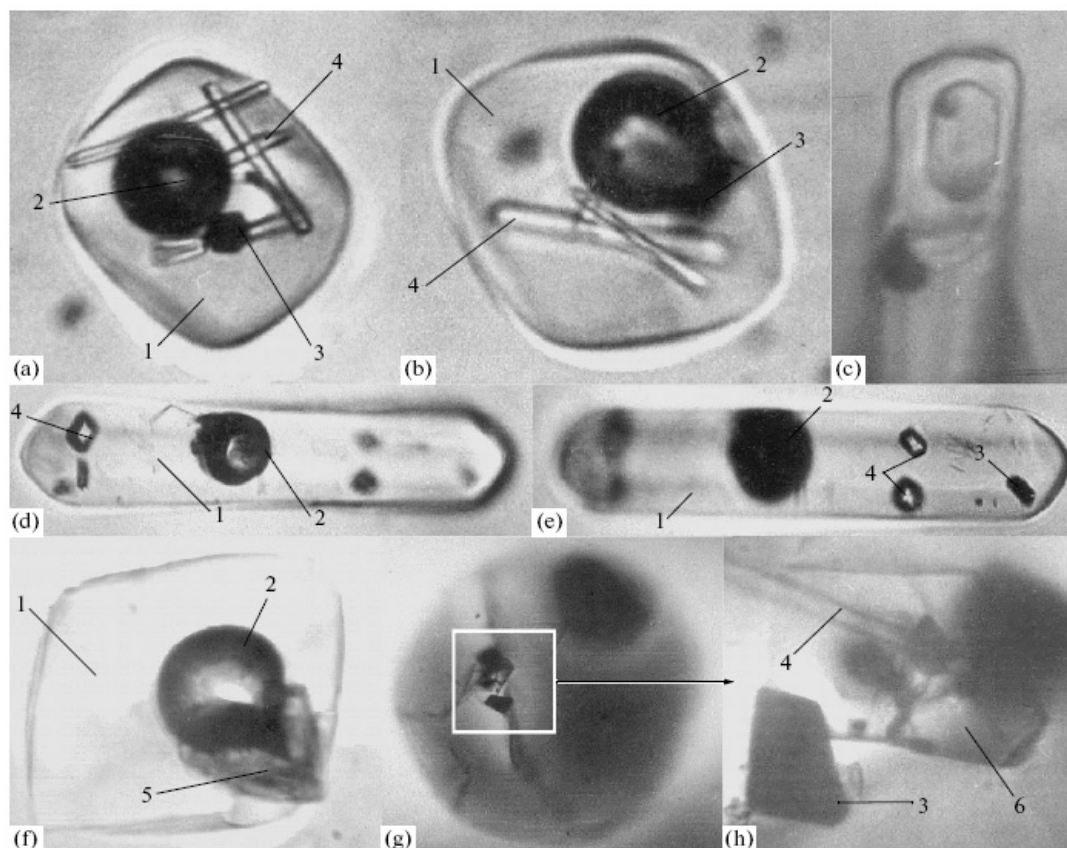


**Fig. 3. Melt inclusions in quartz phenocrysts from samples 94 and 682.**

(a), (b), (d), and (e) sample 94 and (c), (f), (g), and (h) sample 682; (c) apatite crystal with a melt inclusion; (d) and (e) melt inclusion with pyroxene and magnetite crystals focused on different parts of the inclusion. 1 is glass, 2 is a gas phase, 3 is magnetite, 4 is pyroxene, 5 is siderophyllite, and 6 is fluorite.

The results of the investigation are given in Tables 1—5. The high F content (0.10-0.23 wt %) in the residual glasses of melt inclusions (Table 1, analyses 1 and 2) indicates possible crystallization of magmatic fluorite. Previously, we identified fluorite using microprobe analysis in melt inclusions in quartz from the ongorhyolites of Mongolia [10] at an F content in the residual glass of 0.30—0.31 wt % and in anorthoclase from the trachytes of the Island of Pantelleria, Italy [11,12] at 0.1-0.16 wt% F in the glass. Indeed, a relatively large fluorite crystal (Figs. 3g, 3h) was observed together with a gas phase and pyroxene and magnetite crystals (Table 2, no. 1) in a large (264  $\mu\text{m}$  in diameter) melt inclusion from sample 682. The fluorite crystal is 32 x 44  $\mu\text{m}$  in size and accounts for 0.47 vol % of the inclusion. Its microprobe investigation showed the presence of only Ca, F, and Fe (0.10 wt %).

During heating-stage experiments, the first signs of glass melting were observed at 700°C when new gas bubbles appeared in the inclusions. Usually, the larger the inclusion, the greater the number of gas bubbles, which might be

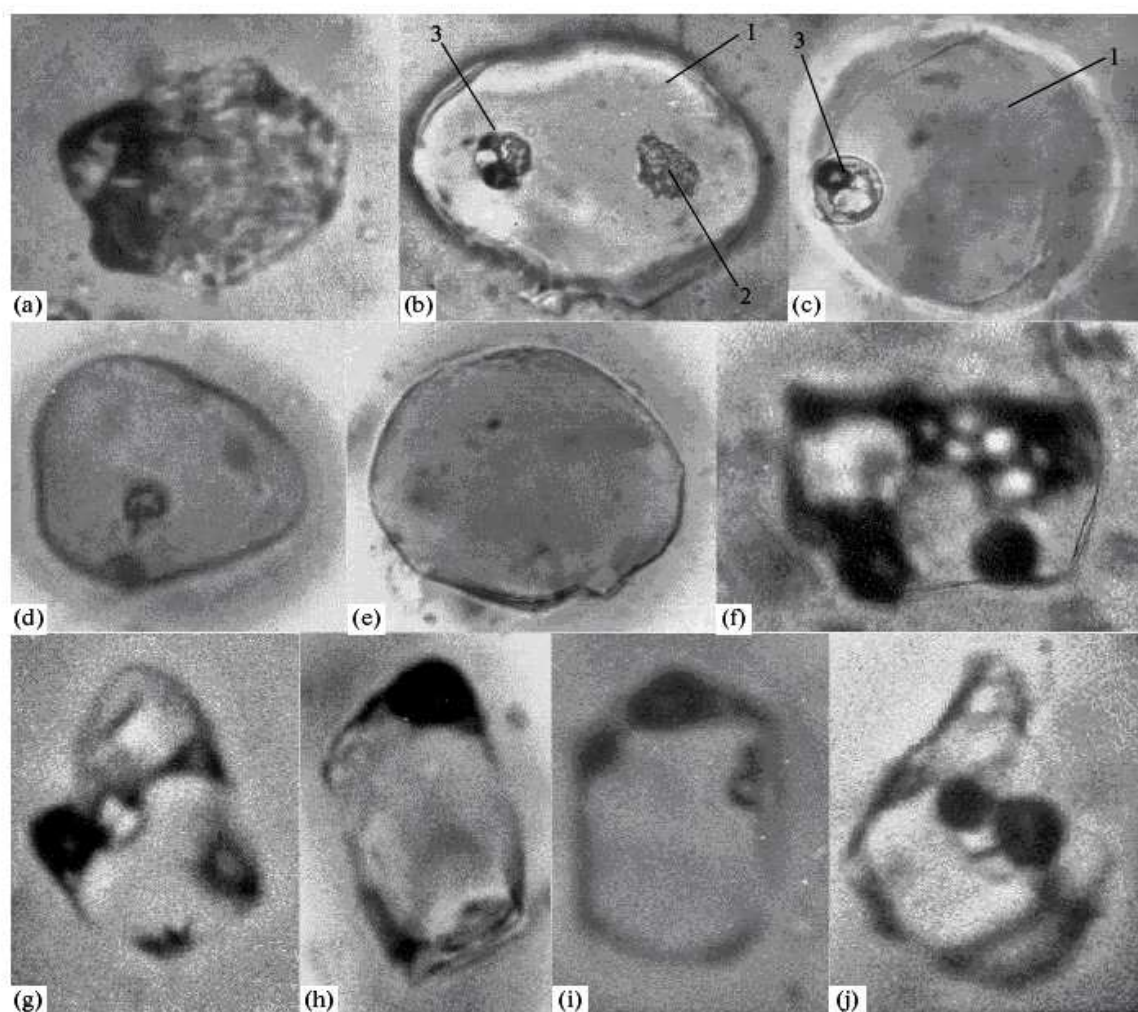


**Fig. 4. Melt inclusions in quartz phenocrysts from sample 217.**

(a)—(e) silicate melts and (f)—(j) chloride melts; (a) completely crystallized inclusion at 20°C; (b) quenched inclusion after annealing for 24 h at 780°C and 3.1 kbar external pressure; (c) quenched inclusion after heating up to 860°C; (d) quenched inclusion after heating up to 930°C; and (e) homogenized silicate melt inclusion after heating to 950°C. 1 is silicate glass, 2 is silicate minerals, and 3 is a salt globule consisting of an aqueous solution, a gas phase, and salt minerals.

several tens. A further temperature increase and annealing for several hours resulted in a decrease in sions was observed at different temperatures: 780—950°C in sample 217, 820-850°C in sample 1119, 1020-1050°C in samples 94 and 98, 1030-1080°C in sample 682, and 1140-1200°C in sample 28. The chemical compositions of homogenized melt inclusions and the average compositions of glasses for each sample are shown in Tables 3 and 4. Let us consider the characteristic features of melt inclusions in some samples.

Quartz from sample 217 contains melt inclusions of two different compositions [13], silicate (Figs. 4a— 4e; Table 3, inclusion nos. 14—20) and chloride salt (Figs. 4f— 4j), and the salt inclusions are more abundant. Most of the

Table 2.

**Chemical compositions (wt %) of magnetite from quartz-hosted melt inclusions in the silicic volcanics of the Kurama Province, Middle Tien Shan**

Component	1	2	3	4	5	6
SiO <sub>2</sub>	0.33	0.27	0.44	0.47	0.95	0.38
TiO <sub>2</sub>	3.72	3.51	3.57	3.55	3.96	1.64
Al <sub>2</sub> O <sub>3</sub>	1.42	1.30	2.07	2.13	1.67	2.38
FeO	91.39	90.07	89.20	89.91	86.97	88.92
MnO	0.70	0.74	0.67	0.66	0.70	0.23
MgO	0.01	0.07	0.07	0.04	0.01	0.04
CaO	—	—	0.22	0.21	0.00	—
ZnO	0.30	0.16	—	—	—	0.54
Total	97.87	96.12	96.24	96.97	94.26	94.13

Note: FeO is total iron. (1)—(4) sample 682, (5) sample 94, and (6) sample 28.

Table 3.

**Chemical compositions (wt %) of melt inclusions in quartz from the silicic volcanics of the Kurama Province, Middle Tien Shan**

Inclusion no.	Component											Total	K <sub>2</sub> O/ Na <sub>2</sub> O
	SiO <sub>2</sub>	TiO <sub>2</sub>	Al <sub>2</sub> O <sub>3</sub>	FeO	MnO	MgO	CaO	Na <sub>2</sub> O	K <sub>2</sub> O	F	Cl		
<i>Sample 682</i>													
1	70.87	0.11	11.23	1.05	0.01	0.01	0.63	3.08	5.99	0.19	0.14	93.31	1.94
2	73.43	0.07	13.51	1.04	0.03	0.02	0.55	3.00	5.49	0.29	0.14	97.57	1.83
3	73.73	0.12	13.29	0.76	0.01	0.02	0.50	3.34	5.43	0.17	0.06	97.43	1.63
4	72.29	0.10	12.32	1.35	0.02	0.04	0.72	3.78	6.35	0.20	0.15	97.32	1.68
5	73.43	0.05	13.74	1.18	0.01	0.04	0.63	3.28	5.54	0.15	0.18	98.23	1.69
6	70.69	0.04	14.88	0.44	0.07	0.00	0.37	3.20	4.81	0.23	0.15	94.88	1.51
7	72.32	0.07	14.76	0.37	0.02	0.00	0.41	2.09	4.82	0.23	0.14	95.23	2.31
8	72.36	0.06	14.28	0.48	0.02	0.00	0.22	3.00	6.46	0.15	0.07	97.10	2.15
9	73.73	0.05	13.31	1.29	0.01	0.02	0.66	4.29	5.11	0.20	0.16	98.83	1.19
x	72.54	0.07	13.48	0.88	0.02	0.02	0.52	3.23	5.56	0.20	0.13	96.66	1.77
<i>Sample 94</i>													
10	73.20	0.07	14.32	0.52	0.00	0.00	0.23	3.16	5.90	0.23	0.13	97.76	1.87
11	71.69	0.04	14.88	0.44	0.07	0.00	0.37	2.20	4.81	0.22	0.15	94.87	2.19
12	72.32	0.07	14.76	0.37	0.02	0.00	0.41	2.09	4.82	0.24	0.14	95.24	2.31
13	74.96	0.06	12.24	0.89	0.00	0.01	0.40	3.35	4.07	0.21	0.12	96.31	1.21
x	73.04	0.06	14.05	0.56	0.02	0.00	0.35	2.70	4.90	0.23	0.14	96.05	1.90
<i>Sample 217</i>													
14	74.45	0.04	12.33	1.15	-	0.00	0.40	3.20	4.47	0.39	0.53	96.96	1.4
15	73.46	0.08	11.41	1.01	0.03	0.00	0.12	4.03	3.97	-	0.22	94.33	0.99
16	72.17	0.06	12.61	1.00	0.12	0.02	0.37	2.09	4.12	0.40	0.46	93.42	1.97
17	76.65	0.05	12.95	0.93	0.10	0.03	0.18	2.23	3.43	-	0.34	96.89	1.54
18	73.62	0.07	14.01	1.36	0.09	0.02	0.38	1.88	4.42	0.93	0.33	97.11	2.35
19	73.69	0.05	10.46	1.96	-	0.01	0.62	3.26	3.57	0.44	0.13	94.19	1.10
20	74.77	0.03	10.52	0.91	0.04	0.00	0.19	3.06	3.61	-	0.43	93.56	1.18
x	74.12	0.05	12.04	1.19	0.08	0.01	0.32	2.82	3.94	0.54	0.35	95.14	1.50

Table 4.

**Chemical compositions (wt %) of melt inclusions in quartz from the silicic volcanics of the Kurama Province, Middle Tien Shan**

Inclusion no.	Component										Total	K <sub>2</sub> O/Na <sub>2</sub> O
	SiO <sub>2</sub>	TiO <sub>2</sub>	Al <sub>2</sub> O <sub>3</sub>	FeO	MnO	MgO	CaO	Na <sub>2</sub> O	K <sub>2</sub> O	Cl		
<i>Sample 1119</i>												
21	71,29	0,02	11,59	1,07	0,02	0,00	0,43	3,42	4,67	0,27	92,78	1,37
22	70,44	0,04	11,75	1,06	0,07	0,00	0,46	3,57	4,77	0,26	92,42	1,34
23	72,34	0,07	12,84	1,24	0,01	0,02	0,38	3,59	5,03	0,12	95,62	1,40
24	71,52	0,04	11,56	0,94	0,02	0,00	0,42	3,44	4,82	0,25	93,03	1,40
25	71,73	0,04	11,76	1,05	0,06	0,00	0,42	3,62	4,67	0,23	93,58	1,29
26	70,90	0,03	12,97	1,28	0,08	0,00	0,46	3,30	4,76	0,20	93,98	1,44
27	70,25	0,03	11,82	1,05	0,04	0,00	0,45	3,61	4,69	0,26	92,20	1,30
28	70,37	0,01	11,10	0,93	0,06	0,00	0,42	3,52	4,90	0,22	91,53	1,39
29	72,64	0,03	12,11	1,06	0,00	0,00	0,41	3,74	4,77	0,23	94,99	1,28
30	72,21	0,03	11,12	1,06	0,02	0,02	0,38	3,52	4,95	0,23	93,54	1,41
31	70,89	0,10	13,14	1,28	0,04	0,01	0,42	3,54	5,08	0,12	94,62	1,44
32	70,50	0,02	11,90	1,08	0,06	0,02	0,40	3,50	4,49	0,19	92,16	1,28
33	72,56	0,02	11,10	0,78	0,04	0,01	0,36	3,42	4,73	0,17	93,19	1,38
<i>x</i>	71,36	0,04	11,90	1,07	0,04	0,01	0,42	3,52	4,79	0,21	93,36	1,36
<i>Sample 98</i>												
34	73,26	0,02	11,15	1,09	0,01	0,00	0,47	4,07	5,12	0,14	95,33	1,26
35	73,20	0,05	11,11	1,04	0,02	0,01	0,47	3,87	5,10	0,13	95,01	1,32
36	73,06	0,12	11,07	1,10	0,00	0,00	0,48	3,77	5,10	0,12	94,80	1,35
<i>x</i>	73,33	0,06	11,11	1,08	0,01	0,00	0,47	3,90	5,11	0,13	95,05	1,31
<i>Sample 28</i>												
37	69,54	0,05	17,36	1,09	0,02	0,00	0,65	3,86	6,70	0,28	99,55	1,74
38	71,47	0,03	16,58	0,69	0,02	0,00	0,66	3,89	6,44	-	99,78	1,66
39	69,31	0,09	17,02	0,93	0,00	0,00	0,69	3,35	7,77	0,30	99,46	2,32
40	68,87	0,04	17,81	0,88	0,09	0,00	0,71	3,89	5,42	0,30	98,01	1,39
41	69,70	-	16,57	0,87	0,00	0,00	0,59	3,20	7,02	0,20	98,15	2,19
42	69,41	0,03	16,71	0,98	-	0,00	0,73	4,48	6,49	0,37	99,20	1,45
<i>x</i>	69,72	0,05	17,01	0,91	0,03	0,00	0,67	3,78	6,64	0,29	99,03	1,79

salt melt inclusions were confined to cross-cutting fractures, but we managed to find several areas in quartz grains, where the cogenetic character of both inclusion types could be clearly established. The silicate melt inclusions are completely crystallized; salt aggregates were observed in their fluid phase after heating to 700—900°C and quenching. The inclusions were homogenized at 780—950°C, and their subsequent quenching resulted in the formation of a homogenous glass. The analysis of homogeneous glasses (Table 3, nos. 14—20) showed that the acid silicate melts were enriched in K relative to Na (on average, K<sub>2</sub>O/Na<sub>2</sub>O = 1.50) and had high F (0.54 wt %) and Cl (0.35 wt %) contents. The deficit in analytical totals suggests that the melts probably contained 3—4 wt % water.

The salt melt inclusions are typically no larger than 10—15 μm in size and

Table 5.

**Chemical compositions of melt inclusions in quartz from the silicic volcanics of the Kurama Province, Middle Tien Shan**

Component	1	2	3	4	5	6	
			wt %				
SiO <sub>2</sub>	71.29	72.21	70.50	76.66	73.62	76.66	
TiO <sub>2</sub>	0.02	0.03	0.02	0.02	0.07	0.05	
Al <sub>2</sub> O <sub>3</sub>	11.59	11.12	11.90	11.10	14.01	12.95	
FeO	1.07	1.06	1.08	0.78	1.36	0.93	
MnO	0.02	0.02	0.06	0.04	0.09	0.10	
MgO	0.00	0.02	0.02	0.01	0.02	0.03	
CaO	0.43	0.38	0.430	0.36	0.38	0.18	
Na <sub>2</sub> O	3.42	3.52	3.50	3.42	1.88	2.23	
K <sub>2</sub> O	4.67	4.95	4.49	4.73	4.42	3.43	
P <sub>2</sub> O <sub>5</sub>	0.00	0.00	0.09	0.07	0.00	0.07	
Cl	0.27	0.23	0.19	0.17	0.33	0.34	
H <sub>2</sub> O	—	—	7.18	6.01	2.80	1.11	
<b>Total</b>	92.78	93.54	99.43	99.27	98.98	98.07	
			ppm				
Li	4.0	4.0	4.86	4.95	4.6	4.56	
Be	17	16	13.7	14.9	18	2.32	
B	92	88	80.9	93.1	24	3.00	
F	1610	1490	1520	1360	9260	—	
Cr	—	—	0.21	0.89	—	2.20	
Ga	25	24	—	—	28	—	
Rb	491	558	516	595	1060	267	
Sr	0.2	0.2	0.09	0.13	3.6	6.5	
Y	106	109	79.9	87.4	41	21.5	
Zr	194	176	142	165	140	102	
Nb	94	87	72.5	93.8	35	34.3	
Mo	6	7	—	—	5	—	
Sn	37	21	—	—	967	—	
Cs	51	49	—	—	169	—	
Ba	1.0	0.0	0.54	0.44	0.2	0.40	
La	15	16	17.3	14.1	17	8.82	
Ce	47	44	48.4	42.5	37	25.1	
Pr	6	7	—	—	7	—	
Nd	27	26	27.4	23.9	22	13.3	
Sm	9	11	10.3	9.35	7	4.3	
Eu	—	—	0.01	0.01	—	0.01	
Gd	—	—	11.3	11.1	—	4.23	
Tb	2.4	2.1	—	—	1.3	—	
Dy	18.4	17.6	13.0	13.9	7.5	4.89	
Ho	3.2	2.9	—	—	1.7	—	
Er	13.7	10.4	8.91	10.4	5	3.62	
Tm	1.9	2.1	—	—	0.8	—	
Yb	—	—	9.21	10.4	—	3.84	
Lu	1.4	1.3	—	—	0.6	—	
Hf	—	—	8.57	10.8	—	5.18	
Th	68	59	52.8	62.3	19	22.4	
U	21	20	19.9	25.7	9	12.1	

**Note:** (1)—(4) sample 1119, (5) and (6) sample 217. A dash means that the component was not determined. Analyses 1, 2, and 5 (F and trace elements) were obtained by R.L. Hervig at Arizona

University, Tempe, United States; and analyses 3, 4, and 6 (H<sub>2</sub>O, F, and trace elements) were obtained by S.G. Simakin at the Institute of Microelectronics, Russian Academy of Sciences, Yaroslavl, Russia.

dominated (80—90 vol %) by isotropic crystals of sodium and potassium chlorides. They usually contain one or several anisotropic crystals and an opaque phase accounting for approximately 2—7 vol %. The content of the fluid phase is no higher than 5—10 vol %. The qualitative microprobe analysis of two salt inclusions exposed on the surface showed that they are dominated by Na and Cl and contain K, Fe, and Mn, whereas Mg, Ti, Al, Ca, Cu, and F were not detected.

The homogenization temperatures of the salt melt inclusions proved to be rather high, from 680 to 820°C, and there are probably higher temperature inclusions. The quenching of homogenized inclusions for 1—2 s always caused their heterogenization and the separation of fluid, which is a characteristic difference from the silicate melt inclusions. Unfortunately, most of the salt inclusions were decrepitated before homogenization, especially at temperatures of ~ 570°C. It should be noted that lower temperature (550—110°C) inclusions were also found in this sample, but they are obviously secondary and dominated by a water phase.

The existence of chloride melts cogenetic with silicic silicate melts has been reported in several studies [14—21] after the pioneering papers of Roedder and Coombs [14] and Roedder [15]. These authors investigated melt and fluid inclusions in quartz from the granitic rocks of Ascensions Island and demonstrated the existence of immiscibility between chloride and silicate melts. Coexisting silicate and chloride melts in quartz were observed in thermometric experiments with the granitoids of the Mariktikan massif (Buryatia, Russia) [16]. This paper reported photomicrographs of such inclusions with two immiscible melts at 980°C. It was also noted that such inclusions were found only in the central part of the massif, where they occur in quartz crystals from miarolitic cavities and in rock-forming quartz of the granites near these cavities. Similar high-temperature silicate and chloride melts were investigated in quartz from the Mount Genis granite (southeastern Sardinia, Italy) [18] and in quartz from the pantellerites of the Island of Pantelleria, Italy [19]. Recently, such phenomena were described in the Industrial'noe tin deposit in northeastern Russia [20, 21]. The investigation of inclusions showed that during the crystallization of quartz in granites, globules of chloride melts were present in the magmatic silicate melt (73.2 wt % SiO<sub>2</sub>, 3.1 wt % Na<sub>2</sub>O, and 4.5 wt % K<sub>2</sub>O). The silicate melt (760- 1020°C) shows high Cl contents: up to 0.51 wt % at an average of 0.31 wt % (12 analyses). Using proton-induced X-ray emission (PIXE) analysis, the distribution and concentrations of a number of elements were determined in polyphase salt globules, which were found in quartz from the granites and in quartz from a mineralized miarolitic cavity in the granites. The analysis of quartz-hosted salt globules from the granites (eight analyses) and from the miarolitic cavity (29 analyses) revealed high average contents (wt %) of Cl (27.5-25.0), Fe (9.7-5.4), Mn (1.1-1.0), Cu (7.2), Zn (0.66-0.50), Pb (0.37-0.24), and such elements as (ppm) Rb (1850-810), As (2020), Sr

(1090), Br (990-470), and Sn (540). The presence of high-temperature chloride melts during the formation of Pt-bearing ultramafic series was demonstrated by Hanley et al. [22] on the basis of the investigation of inclusions in minerals.

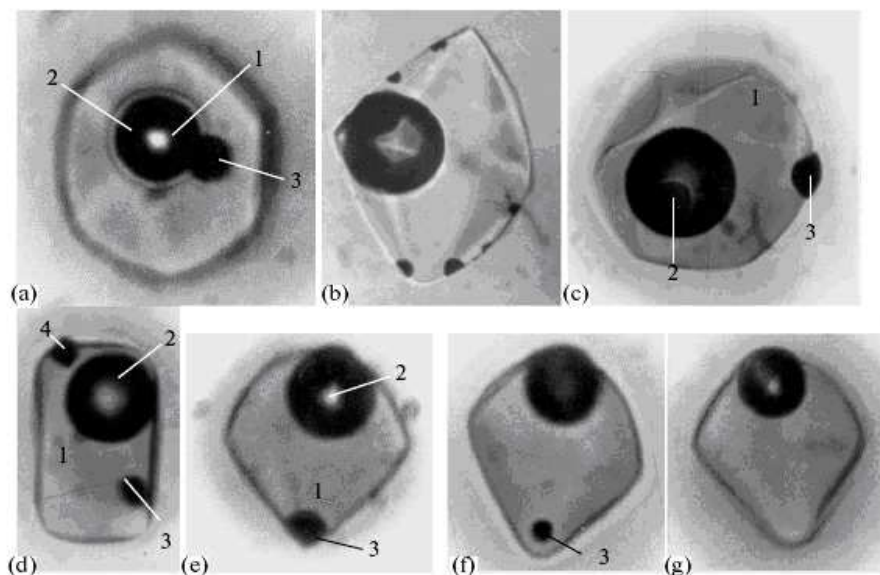


Fig. 5. Melt inclusions with opaque oxide globules (a—e) in quartz phenocrysts from sample 28.

(e) 20°C, (f) 1080°C, and (g) 1140°C. 1 is glass, 2 is a gas phase, 3 is an opaque oxide globule, and 4 is magnetite.

Unusual melt inclusions were observed in quartz from granite porphyry sample 1119 [23]. The sample is heterogeneous and contains brown areas stuffed with phenocrysts alternating with greenish gray glassy patches almost free of phenocrysts. The content of phenocrysts is, therefore, strongly variable, from 5—10 to 60—70 vol %. The phenocrysts are feldspars and quartz; they are strongly crushed, and most of them especially plagioclase, appear as angular fragments. Only some quartz grains preserved their initial outlines. The groundmass contains rounded voids, on the walls of which druses and individual crystals of feldspar and quartz were formed. These crystals are oriented toward the center of the void. The voids are probably relics of gas bubbles in melt, because they existed before the crystallization of some magmatic minerals in the rock groundmass.

The examination of polished sections of this sample revealed numerous single-phase glassy melt inclusions in quartz phenocrysts (Figs. 2a—2d). The inclusions range from 5—10 to 160—180  $\mu\text{m}$  across, and relatively large inclusions (30—70  $\mu\text{m}$ ) are most common. Usually, one phenocryst contains from one to five inclusions, although one phenocryst with 30 homogenous melt inclusions was also found. In some phenocrysts, homogeneous glass inclusions coexist with inclusions containing numerous gas bubbles (Fig. 2e). In addition to melt inclusions, an apatite crystal (8—10  $\mu\text{m}$  wide and 98  $\mu\text{m}$  long) and an amphibole crystal (analysis 5 in Table 1) were observed in the quartz. The amphibole composition is close to ferrohastingsite. There is no apparent difference in the characteristics of melt inclusions in quartz from the brown (with abundant

phenocrysts) and greenish gray zones (with rare phenocrysts) of the sample.

During heating-stage experiments, numerous gas bubbles appeared in all homogeneous melt inclusions in quartz phenocrysts (Fig. 2f). The inclusions became heterogeneous in 1.5—2.0 h at 500°C and 5—10 min at 550—600°C. Sometimes, tubular gas bubbles were observed. In such cases, it could be clearly seen at room temperature that the fluid consists of liquid (5—10 vol %) and gas (90-95 vol %) phases. A further increase in temperature resulted in the dissolution of many gas bubbles in the melt, the enlargement of the remaining bubbles, and, eventually, the complete homogenization of the inclusions at 820—850°C. During cooling, the inclusions became heterogeneous at 760-700°C.

The electron microprobe analysis of the homogenous glasses of melt inclusions performed by scanning over an area of 24 x 24  $\mu\text{m}$  showed that their composition is uniform (Table 4, inclusions 21—33) and persistently enriched in K relative to Na ( $\text{K}_2\text{O}/\text{Na}_2\text{O}$  averages 1.36). The average content of Cl in the melt is 0.21 wt %, and the content of F is lower, 0.14 wt % (two determinations). The low totals of microprobe analyses (93.36 wt %) may indicate a high water content in the melt (more than 6 wt %). The ion microprobe analysis of two melt inclusions supported this suggestion: the measured water contents are 7.2 and 6.0 wt % (Table 5, analysis nos. 3 and 4). In this connection, it is remarkable that the melt inclusions of silicic compositions (71.4 wt %  $\text{SiO}_2$ ) have remained completely glassy without any traces of devitrification for 280-290 Ma.

Numerous microfractures healed by late hydro-thermal solutions forming secondary fluid inclusions have been described very often during the investigation of quartz phenocrysts in rhyolites from various regions of the world. A distinguishing feature of sample 1119 is the absence of such fractures in all quartz phenocrysts. This observation suggests the absence of late hydro-thermal alteration of rocks in this region. In one quartz phenocryst, a primary fluid inclusion 57  $\mu\text{m}$  in size was observed at a distance of 100  $\mu\text{m}$  from a homogeneous melt inclusion 145  $\mu\text{m}$  in size. It consisted of two phases, liquid and gas. The motion of the gas bubble was observed in this inclusion at room temperature owing to variations in light intensity. During cooling-stage investigations, the liquid phase of this inclusion froze at  $-40^\circ\text{C}$ , and the gas bubble decreased in size. This indicates that the liquid phase is an aqueous solution, whose concentration can be estimated from the temperature of ice melting ( $-2.3^\circ\text{C}$ ) as 3.7 wt % NaCl eq. During heating, the homogenization of the fluid inclusion to a liquid phase was observed at  $165^\circ\text{C}$ , which suggests that the density of the aqueous solution was as high as  $0.93\text{ g/cm}^3$  at this temperature.

In order to calculate the solution density at the moment of inclusion entrapment, the thermal expansion and compressibility of quartz should be accounted for. These parameters are 4.4% and 1.9%, respectively, for the temperature range from 20 to  $850^\circ\text{C}$  and the pressure range from 1 atm to 7.5 kbar [24]; hence, the real density of the fluid at the moment of inclusion formation was  $0.91\text{ g/cm}^3$ . The calculation of fluid pressure for temperatures of 850 and  $700^\circ\text{C}$

yields 8.3 and 6.5 kbar, respectively. Such high pressure values are similar to our previous results [25—30] for the pantellerites of the Island of Pantelleria, Italy (2.6–4.3 kbar [25]), ongorhyolites of the Hetsu-Teg region of Mongolia (3.7 kbar [25]), rhyolites of the Stiavnica caldera in central Slovakia (3.3—8.7 kbar [26, 27]), rhyodacites from the Maly Kamenec region in eastern Slovakia (3.3—9.6 kbar [28]), and andesites of the Stiavnica caldera in central Slovakia (5.6—17 kbar [29, 30]). Primary dense aqueous fluids were also found in rhyolite magmatic melts from New Zealand and Chile [31].

Unusual melt inclusions (Figs. 5a—5f) consisting of a gas phase (10—14 vol %), a transparent colorless glass (85—90 vol %), and one or several opaque black globules (0.4—1.0 vol %) were observed in quartz phenocrysts from sample 28. Eleven melt inclusions with an opaque globule were found in one of the quartz phenocrysts. Despite the variable size of melt inclusions, the volume proportions of phases (gas, glass, and globule) were identical in all inclusions, which suggests that the melt was homogeneous at the moment of inclusion formation, and the gas and opaque phases were released after isolation within the host mineral. The inclusions range in size from 20 to 88  $\mu\text{m}$ , and the largest globule is 9  $\mu\text{m}$  in diameter. The microprobe analysis of the globules showed that they are chemically uniform (Table 1, analysis no. 6) and, in addition to dominant FeO ( $81.2 \pm 3.4\%$ ), they always contain SiO<sub>2</sub> ( $9.9 \pm 1.2\%$ ), Al<sub>2</sub>O<sub>3</sub> ( $2.2 \pm 0.6\%$ ), CaO, Na<sub>2</sub>O, and K<sub>2</sub>O. The relatively high content of ZnO (0.19 wt %) is noteworthy. A characteristic feature of the iron-oxide globules is high SiO<sub>2</sub> content (9.9 wt %), which distinguishes them from the magnetite composition, which is very poor in SiO<sub>2</sub> (0.38 wt %; Table 2, analysis no. 6). The low analytical total (ten determinations yielded an average of 94.6 wt %) is probably due to the fact that all iron was calculated as FeO, ignoring the probable occurrence of ferric iron. The residual glass of five inclusions shows high contents of SiO<sub>2</sub> ( $70.2 \pm 1.0$  wt %), Al<sub>2</sub>O<sub>3</sub> ( $17.2 \pm 0.5\%$ ), and Cl (0.29 wt %), low FeO ( $0.32 \pm 0.14$  wt %), and considerable prevalence of K<sub>2</sub>O ( $6.7 \pm 0.9\%$ ) over Na<sub>2</sub>O ( $3.7 \pm 0.3$  wt %). The high totals of components in the residual glass analyses ( $98.9 \pm 0.7$  wt %) suggest that only minor amounts of water could be dissolved in this melt.

When the quartz phenocrysts were heated in a microscopic stage, the opaque globules were dissolved (Figs. 5f, 5g) within a narrow temperature range of 1050—1100°C, which resulted in a significant increase in the iron content of the silicate melt from 0.32 in unheated residual glasses to 0.91 wt % in homogenized glasses (Table 4, inclusions 37—42). The complete homogenization of some inclusions was reached at 1140°C within 6 h, but, in most cases, even 20-h annealing at 1180°C did not lead to the complete dissolution of the gas phase in the silicate melt. The volume of the remaining gas phase suggests that the most probable homogenization temperatures for these inclusions are 1200–1250°C.

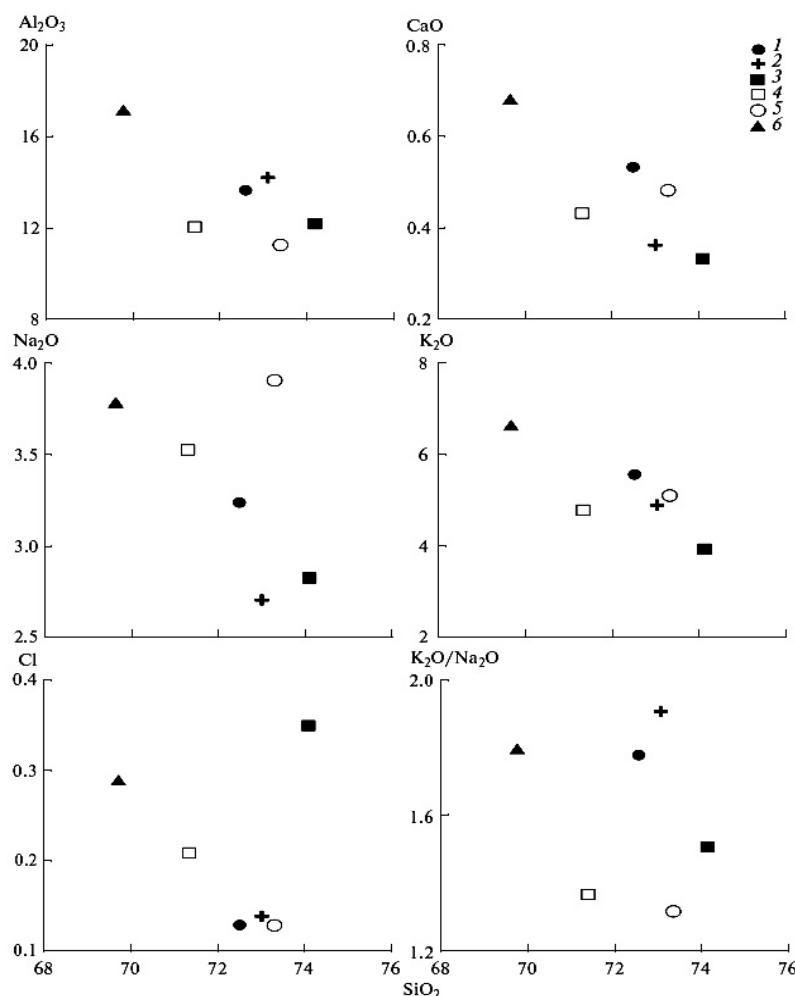


**Fig. 6. Average compositions of melt inclusions in quartz from the sample of volcanics from the Kurama mining district. Samples: (1) 682, (2) 94, (3) 217, (4) 1119, (5) 98, and (6) 28.**

Thus, summarizing the obtained results for inclusions from sample 28 (spherical shape of opaque globules, stable volume proportions of phases in melt inclusions of different size, sharp difference between the compositions of the matrix and globules, stable compositions of the globules with SiO<sub>2</sub> contents of up to 10 wt %, and the high temperatures and narrow interval of globule dissolution), it can be concluded [32] that liquid immiscibility phenomena occurred in the high-temperature silicic magma with the separation of iron oxide-dominated melt droplets.

Figure 6 shows the average compositions of quartz-hosted melt inclusions (Tables 3, 4) in the diagrams of SiO vs. Al<sub>2</sub>O<sub>3</sub>, CaO, Na<sub>2</sub>O, K<sub>2</sub>O, Cl, and K<sub>2</sub>O/Na<sub>2</sub>O. Despite the compositional variations for each sample, it can be concluded that, in general, these compositions are typical of silicic magmatic melts. The average composition is as follows (wt %): 72.4 SiO<sub>2</sub>, 0.06 TiO<sub>2</sub>, 13.3 Al<sub>2</sub>O<sub>3</sub>, 0.95 FeO, 0.03 MnO, 0.01 MgO, 0.46 CaO, 3.33 Na<sub>2</sub>O, 5.16 K<sub>2</sub>O, 0.32 F, and 0.21 Cl. All compositions show a strong prevalence of K<sub>2</sub>O over Na<sub>2</sub>O (K<sub>2</sub>O/Na<sub>2</sub>O averages 1.60). The total of components in melt inclusions from five samples averages 95.3 wt %, which suggests that the average water content in the

melt is probably no lower than 3—4 wt %. The ion microprobe analysis of melt inclusions yielded 1.2—2.8 wt % H<sub>2</sub>O for sample 217 and 6.0-7.2 wt % H<sub>2</sub>O for sample 1119 (Table 5). The analysis of trace elements in the melt inclusions (Table 5) revealed high Sn (up to 970 ppm), Rb (up to 1060 ppm), Th (19-62, averaging 47 ppm), and U (9—26 ppm, averaging 18 ppm), but very low Eu contents (0.01 ppm).

Finally, let us discuss some characteristic features of the Late Paleozoic magmatism in the region, which were revealed by our investigations and which, in our opinion, were favorable for the generation and development of ore-forming fluid—magma systems responsible for the formation of porphyritic and epithermal ore mineralization with a polymetallic (Au, Ag, Cu, Pb, Zn, Sn, Mo, Bi, and Te) geochemical signature. First, the high content of fluid components in the magma should be pointed out. It was favorable for the occurrence of liquid immiscibility and separation from the silicate magma of concentrated chloride brines (melts), which concentrated many metals involved in ore formation [33]. The high contents of fluid components in the magmas resulted in the wide occurrence of explosive volcanism during that period in the region with the formation of tremendous volumes of ignimbrites, tuffs, and diatremes accompanied by the fluidization of the volcanic country rocks. Since the main epithermal deposits of this region are confined to the areas where these rocks occur, they are of special interest for the interpretation of relationships between ore mineralization and magmatism. The second important conclusion is based on the finding that the melt of granite porphyry (sample 217) is very rich in Sn (967 ppm), F (9260 ppm), and Rb (1060 ppm) and contains significant amounts of Mo (5 ppm) (Table 5). These data are indicative of a distinct metallogenic signature of the magmatic melt with respect to Sn and Mo, its elevated K-dominated alkalinity ( $K_2O/Na_2O = 1.50$ ), and high F and Cl contents in it. It is remarkable that such a combination of peculiar compositional features was not detected in any of the other samples studied. Taking into account that Sn and Mo are typomorphic elements of the porphyritic—epithermal ore-bearing systems of the region [34], the obtained data suggest that F-rich porphyritic granites of elevated alkalinity similar to the granite porphyries from the upper reaches of the Paraksai River could initiate the activity of such systems and serve as sources of ore components for mineral-forming solutions.

### ACKNOWLEDGMENTS

This study was financially supported by the Russian Foundation for Basic Research (project nos. 07-05-00497 and 07-05-00517, 10-05-00209 and 10-05-00354) and within the Ore-Forming Systems of Base and Noble Metal Deposits: Geological, Mineralogical, and Geochemical Characteristics, Conditions of Development, and Factors of Productivity basis theme of the Institute of Geology of Ore Deposits, Petrography, Mineralogy, and Geochemistry, Russian Academy of Sciences.

### REFERENCES

1. **V. A. Kovalenker, Yu. G. Safonov, V. B. Naumov, and V. L. Rusinov**, "The Epithermal Gold-Telluride Kochbulak Deposit (Uzbekistan)," *Geol. Rudn. Mestorozhd.* 39 (2), 127-152 (1997) [*Geol. Ore Dep.* 39,107-128(1997)].
2. **Kh. T. Tulyaganov, E. A. Yudalevich, V. P. Korzhaev, et al.**, Map of the Magmatic Formation of the Uzbek USSR (FAN, Tashkent, 1984) [in Russian].
3. **S. S. Abramov, V. L. Rusinov, and V. A. Kovalenker**, "Petrological Model of the Formation of Complex of Porphyry Granitoids by the Example of the Kuramin Fluid-Magmatic System," *Petrologiya* 2 (4), 410-438 (1994).
4. **V. A. Kovalenker**, "Conditions of Formation and Factors of Large-Scale Gold Accumulation of Porphyric and Hydro thermal Deposits," in *Large and Superlarg Ore Deposits* (IGEM RAN, Moscow, 2006), Vol. 2, pp. 143-214 [in Russian].
5. **V. A. Kovalenker, O. P. Plotinskaya, V. Yu. Prokof ev, et al.**, "Mineralogy, Geochemistry, and Genesis of Gold—Sulfide—Selenide—Telluride Ores from the Kairagach Deposit (Uzbekistan)," *Geol. Rudn. Mestorozhd.* 45 (3), 195-227(2003) [*Geol. Ore Deposits.* 45, 171-200 (2003)].
6. **V. B. Naumov**, "Thermometrical Study of Melt Inclusions in Quartz Phenocrysts from Quartz Porphyries," *Geokhimiya*, No. 4, 494-498 (1969).
7. **V. Sobolev**, "Melt Inclusions in Minerals as a Source of Principle Petrological Information," *Petrologiya* 4 (3), 228-239 (1996) [*Petrology* 4, 209-220 (1996)].
8. **Nosova, L. V. Sazonova, V. V. Narkisova, and S. G. Simakin**, "Minor Elements in Clinopyroxene from Paleozoic Volcanics of the Tagil Island Arc in the Central Urals," *Geokhimiya*, No. 3, 254-268 (2002) [*Geochem. Int.* 3, 219-232 (2002)].
9. **M. V. Portnyagin, S. G. Simakin, and A. V. Sobolev**, "Fluorine in Primitive Magmas of the Troodos Ophio-lite Complex, Cyprus: Analytical Methods and Main Results," *Geokhimiya*, No. 7, 691-699 (2002) [*Geochem. Int.* 40, 625-632 (2002)].
10. **V. B. Naumov, V. I. Kovalenko, R. Clocchiatti, and I. L. Solovova**, "Conditions of Crystallization and Phase Composition of Melt Inclusions in Quartz of Ongorhyolites," *Geokhimiya*, No. 4, 451-464 (1984).
11. **P. Solovova, V. B. Naumov, V. I. Kovalenko, et al.**, "Magmatic Fluorite and Conditions of its Crystallization from Pantellerite Melt," *Dokl. Akad. Nauk SSSR* 297(6), 1449-1452(1987).
12. **V. B. Naumov, I. P. Solovova, V. I. Kovalenko, and A. V. Guzhova**, "Conditions of Crystallization and Features of Phase Composition of Melt Inclusions in the Anorthoclase of Agpaitic Trachytes of Pantelleria Island (Italy)," *Geokhimiya*, No. 2, 207-215 (1989).
13. **V. B. Naumov, I. P. Solovova, V. A. Kovalenker, et al.**, "Conditions of Crystallization and Composition of Silicate and Salt Melts of the Volcanoplutonic Complex of the Angren River Region (Middle Asia)," *Dokl. Akad. Nauk SSSR* 312 (5), 1227-1230(1990).
14. **E. Roedder and D. S. Coombs**, "Immiscibility in Granitic Melts, Indicated by Fluid Inclusions in Ejected Granitic Blocks from Ascension Island," *J. Petrol.* 8 (3), 417-451 (1967).
15. **E. Roedder**, "Laboratory Studies of Inclusions in Minerals from Granitic Blocks of Ascension Island and their Petrological Significance," in *Problems of Petrology and Genetic Mineralogy* (Nauka, Moscow, 1970), Vol. 2, pp. 247-258 [in Russian].
16. **F. G. Reif and E. D. Bazheev**, "Magmatogenic Chloride Solutions and Tungsten Mineralization," *Geokhimiya*, No. 1,63-70(1977).
17. **V. B. Naumov, V. I. Kovalenko, and L. G. Filimonova**, "Immiscibility of Silicate and Salt Melts based on Mineral Inclusion Data," in *Proceedings of Seminar on Geochemistry of Magmatic Rocks* (GEOKhI AN SSSR, Moscow, 1984), pp. 130-131 [in Russian].
18. **M. L. Frezzotti**, "Magmatic Immiscibility and Fluid Phase Evolution in the Mount Genis Granite (Southeastern Sardinia, Italy)," *Geochim. Cosmochim. Acta* 56,21-33(1992).
19. **J. B. Lowenstern**, "Chlorine, Fluid Immiscibility, and Degassing in Peralkaline Magmas from Pantelleria, Italy," *Am. Mineral.* 79 (3-4), 353-369 (1994).
20. **V.S. Kamenetsky, V. B. Naumov, P. Davidson, E. L. van Achterbergh, and C. G. Ryan**,

- "Immiscibility Between Silicate Magmas and Aqueous Fluids: a Melt Inclusion Pursuit Into the Magmatic-Hydrothermal Transition in the Omsukchan Granite (NE Russia)," *Chem. Geol.* 210(1-4), 73-90(2004).
21. **V. B. Naumov and V. S. Kamenetskii**, "Silicate and Salt Melts in the Genesis of the Industrial'noe Tin Deposit: Evidence from Inclusions in Minerals," *Geokhimiya*, No. 12, 1279-1289 (2006) [*Geochem. Int.* 44, 1181—1190(2006)].
  22. **J. J. Hanley, J. E. Mungall, T. Pettke, et al.**, "Fluid and Halide Melt Inclusions of Magmatic Origin in the Ultramafic and Lower Banded Series, Stillwater Complex, Montana, USA," *J. Petrol.* 49 (6), 1133-1160(2008).
  23. **V. B. Naumov, V. L. Rusinov, V. A. Kovalenker, and N. N. Kononkova**, "Melt Composition, Contents of Trace Elements, and Conditions of Crystallization of Quartz in the Ignimbrites of the Lashkerekskii Massif Based on Magmatic Inclusion Data," *Dokl. Akad. Nauk* 332 (1), 79–82 (1993).
  24. *A Reference Book of Physical Constants of the Rocks*, Ed. by **S. P. Clarke** (*Geol. Soc. Amer. Mem.* 97, 1966; Mir, 1969) [in Russian].
  25. **V. B. Naumov, I. P. Solovova, V. I. Kovalenko, and I. D. Ryabchikov**, "Composition and Concentration of Fluid Phase and Water Content in the Pantellerite and Ongonite Melts Based on Inclusion Data in Quartz," *Dokl. Akad. Nauk SSSR* 295 (2), 456–459 (1987).
  26. **V. B. Naumov, I. P. Solovova, V. A. Kovalenker, et al.**, "First Data on High Density Fluid Inclusions of the Magmatic Water in Phenocrysts from Rhyolites," *Dokl. Akad. Nauk SSSR* 318 (1), 187–190 (1991).
  27. **V. Naumov, V. Kovalenker, V. Rusinov, et al.**, "High Density Fluid Inclusions of Magmatic Water in Phenocrysts from Rhyolite of the Stiavnica Stratovolcano (Central Slovakia)," *Geol. Carpathica* 43 (2), 85–89 (1992).
  28. **V. B. Naumov, V. A. Kovalenker, V. L. Rusinov, and N. N. Kononkova**, "High Density Inclusions of the Magmatic Water in Phenocrysts from Afic Volcanics of the West Carpathian and Central Tien Shan," *Petrologiya*, No. 5, 480–494 (1994).
  29. **V. B. Naumov, I. P. Solovova, V. A. Kovalenker, et al.**, "Magmatic Water at Pressures of 15–17 kbar and its Concentration in the Melt: First Data on Inclusions in Plagioclases of Andesites," *Dokl. Akad. Nauk* 324 (3), 654–658 (1992).
  30. **V. B. Naumov, M. L. Tolstykh, V. A. Kovalenker, and N. N. Kononkova**, "Fluid Overpressure in Andesite Melts from Central Slovakia: Evidence from Inclusions in Minerals," *Petrologiya* 4 (3), 283–294 (1996) [*Petrology* 4, 265–276 (1996)].
  31. **P. Davidson and V. S. Kamenetsky**, "Primary Aqueous Fluids in Rhyolitic Magmas: Melt Inclusion Evidence for Pre- and Post-Trapping Exsolution," *Chem. Geol.* 237, C. 372–383 (2007).
  32. **V. B. Naumov, I. P. Solovova, V. A. Kovalenker, et al.**, "Immiscibility in Acidic Magmas: Evidence from Study of Melt Inclusions in Quartz Phenocrysts of Ignimbrites," *Geokhimiya*, No. 12, 1804–1808 (1991).
  33. **Bodnar R.J.** "Fluid Inclusion Evidence for a Magmatic Source for Metal in Porphyry Copper Deposits." In: Thompson E.J. F.H. (ed). *Magmas, Fluids and Ore Deposits*, Mineralogical Association of Canada, Short Course Series (1995). pp. 139–152.
  34. **V. A. Kovalenker, V. Yu. Prokof'ev, and O. Yu. Plotinskaya**, "Gold Porphyry–Epithermal Fluid-Magmatic System: Geological Characteristics and Metallogenic Significance," in *Magmatic, Metasomatic Formations and Related Mineralization. Proceedings of Scientific Conference, Tashkent, 2005* (FAN-TEKHNLOGIYA, Tashkent, 2005), pp. 148–151 [in Russian].

## **Black cluster microinclusions in the core of Yakutian diamonds: Implications for diamond nucleation**

A.M. Logvinova<sup>1</sup>, R. Wirth<sup>2</sup>

<sup>1</sup> *Institute of Geology and Mineralogy, Siberian Branch of Russian Academy of Science, Novosibirsk, Russia, logv@uiggm.nsc.ru;*

<sup>2</sup> *Helmholtz Centre Potsdam GFZ German Research Centre for Geosciences, Experimental Geochemistry and Mineral Physics, Potsdam, Germany.*

### **ABSTRACT**

The closely spaced black cluster microinclusions in the centre of the ten Yakutian diamonds (Komsomolskaya, Internatsionalnaya and Sytykanskaya kimberlite pipes) have been investigated by FIB/TEM method (electron diffraction, HRTEM, AEM, HAADF, EELS). They have been divided into three groups: 1) carbonate-silicate-oxide assemblages, represented by heterogeneous amorphous material, enriched in F, O, Fe, Mg, Al, Si, Ca, S, with a great number of nanocrystals over 10-15 nm in size and open pores that probably contained volatiles prior to the extraction of the foil. Among the crystalline phases are magnetite, omphacite (high Jd-component), sellaite, graphite, periclase and corundum established electron diffraction patterns and chemical composition. 2) Oriented graphite - sulfide intergrowths and sulfide inclusions, all of which are homogenous in composition and contain fluid bubbles. 3) multiple graphite inclusions, which trapped fluid/melt inclusions, which consist of a several phases (silicates, magnetite, silica, carbonates, sulfides and quenched material, enriched in F, K, Cl, Nb, Ba, Sr). The mineral assemblages located in the central zones of Yakutian diamonds indicate that they grew in a reduced environment [2], with oxygen fugacity controlled by a carbonate rich melt that was highly enriched in LIL (K, Ba, Sr) and HFSE (Nb, Ti) elements. This fluid also carried a carbonatitic component along with immiscible sulfide melts. The introduction of fluid into a reduced refractory environment may have been accompanied by a thermal pulse, and may have created the conditions necessary for the nucleation and growth of diamond. The complex character and composition of nanometer sized inclusions in diamond testify to the significant role of deep metasomatic processes in diamonds formation.

### **INTRODUCTION**

Syngenetic inclusions of minerals, melts, and fluids in natural diamonds suggest a complicated multicomponent diamond-producing environment, which is formed in the Earth's mantle. Despite many years of mineralogical studies of the matter entrapped by diamonds during their growth [1, 7, 19, 21, 24] the composition of the diamond-producing melt is still questionable. More sensitive and modern equipment, more careful matching of the available mineralogical data, and coordinated experiments provide a new level of investigation. The progress in understanding is obvious from the recent publication of new results dealing with media of diamond crystallization [11, 12, 16, 23, 28]. Important information comes from studying not only the bulk composition of the diamond crystallization medium but also the relationship between particular phases. Aggregates of

inclusions within the cores of diamond crystals provide the most valuable information because they are related to the earliest stages of diamond crystallization. Two types of such inclusions are recognized: cloudy and black cluster inclusions. Cloudy zones are populated by millions of nanometer-sized inclusions. These inclusions in cloudy diamonds from the Internatsionalnaya and Yubileinaya pipes (Yakutia) have been studied in detail by Logvinova et al. [16]. It has been shown that such inclusions are syngenetic polymineralic aggregates composed of silicates, oxides, carbonates, halides, bubbles of fluid, and amorphous residues, with Mg, Fe, K, Cl, Si, and Ca being predominant. Klein- BenDavid et al. [12] examined the phase relationships in Canadian cloudy diamonds. Black clusters are distinguished by a set of phases and are tight accumulations of graphite, sulfide, and fluid microinclusions. A significant study was that of Fesq et al. [5] who examined several hundred diamonds using neutron activation techniques. These authors revealed that most diamonds contain submicroscopic material, possibly in the form of a quenched or temperature re-equilibrated melt, from which the diamond formed. Furthermore, they believed that there was sufficient evidence to argue that H<sub>2</sub>O-CO<sub>2</sub> fluids as well as Fe-Ni-Co-Cu sulfides were present in these microinclusions. Bulanova et al. [2] investigated black clusters of heterogeneous material in the center of peridotitic diamond and identified native iron, wustite, and graphite. K, Ca, Mg, and Al were present in the areas consisting only of graphite. Using X-ray, electron diffraction, and qualitative electron microprobe techniques, J.W. Harris [8] identified this black material as graphite, pyrrhotite and pentlandite

New high-resolution imaging devices allowed us to determine the phase composition of central black aggregates as well as their dimensions and the relationships of particular phases represented by oxides, halides, graphite, sulfides, silicates, fluids phase, and polycrystalline nanometer-sized material. All these inclusions were entrapped at the earliest stages of diamond crystallization; therefore. They yield important information relevant for determining the composition of the melt/fluid from which the diamond was crystallized. We report here new data on the composition and phase relationships of black clusters from the diamond's core obtained by transmission electron microscopy (TEM).

## **SAMPLES AND METHODS**

We examined ten diamonds with aggregates of black material in the central zone of the crystal from three pipes of the Yakutian Diamond Province (Komsomolskaya, Internatsionalnaya and Sytykanskaya pipes). Seven samples are colorless crystals of octahedral habit, and three are yellow cubo-octahedral diamonds.

Preliminary identification of inclusions in the cluster zones was performed on a scanning electron microscope LEO-1430 VP equipped with an energy dispersion X-ray spectrometer. The diamond samples were examined by the method of transmission electron microscopy (TEM) using the techniques of electron

diffraction (SAED), high-resolution electron microscopy (HREM), electron energy loss spectroscopy (EELS), and analytical electron microscopy (AEM). This combination of methods provided information on the crystallography (at the level of the unit cell) and the chemical composition of phases as small as 5 nm. The phases were visualized by means of bright field (BF) images. Qualitative analysis for F and carbonate was performed by EELS. Interplanar distances,  $d_{hkl}$ , were determined by SAED and HREM.

TEM samples were prepared by ion thinning to films 100-200 Å wide using a focused ion beam (FIB) [25]. Infrared absorption spectra were obtained by means of a Bruker VERTEX 70 Fourier spectrometer with a HYPERION 2000 IR microscope. They showed the distribution patterns for nitrogen, hydrogen, carbonate, and silicate inclusions within the sample. Spectra with an aperture of 50 micrometers were recorded for diamonds in the range 7500-750  $\text{cm}^{-1}$  with a resolution of 2  $\text{cm}^{-1}$ .

## **RESULTS**

On the basis of their included mineral phases, all the samples were divided into three groups: crystals with silicate – carbonate – oxide inclusion assemblages; crystals with nanometer-sized inclusions of sulfides, found in intergrowths with graphite, and crystals with numerous nanometer-sized inclusions of graphite and fluid. The most typical samples are considered in detail in this paper.

### **1. IR**

Infrared absorption spectra were from all diamonds containing clusters of black inclusions in the central zone. Diamonds from the Komsomolskaya pipe are characterized by nitrogen that is present both in the low aggregated A and in higher aggregated B centers in virtually equal amounts, with the total content of nitrogen in the marginal zone (rim) exceeding that in the core (420 - 290 ppm). However, the degree of nitrogen aggregation throughout the crystal is nearly the same (46 – 54 %B). Infrared absorption characteristics support the presence of a significant content of hydrogen in the black cluster zone of all investigated Komsomolskaya diamonds (6,9 -7,2  $\text{cm}^{-1}$ ). In the rest of the studied diamonds nitrogen also occurs in two forms but the core is richer in nitrogen. Diamonds containing only graphite inclusions along with fluid entrapped in the process of growth display a drastic change in nitrogen aggregation degree from 16.8 to 42 %, manifest as significant increase in nitrogen amount in B aggregation.

### **2. TEM**

#### **2.1 Silicate-carbonate-oxide assemblages**

Three FIB foils were cut from different locations in the black central zone of the Komsomolskaya diamond. TEM investigation of all of these foils shows that this area consists of heterogeneous amorphous material with a great number of

nanocrystals over 10-15 nm in size and open pores that probably contained volatiles prior to the extraction of the foil (Fig. 1). Twenty mono - and polymineralic nanometer-sized inclusions found in the black cluster zone have

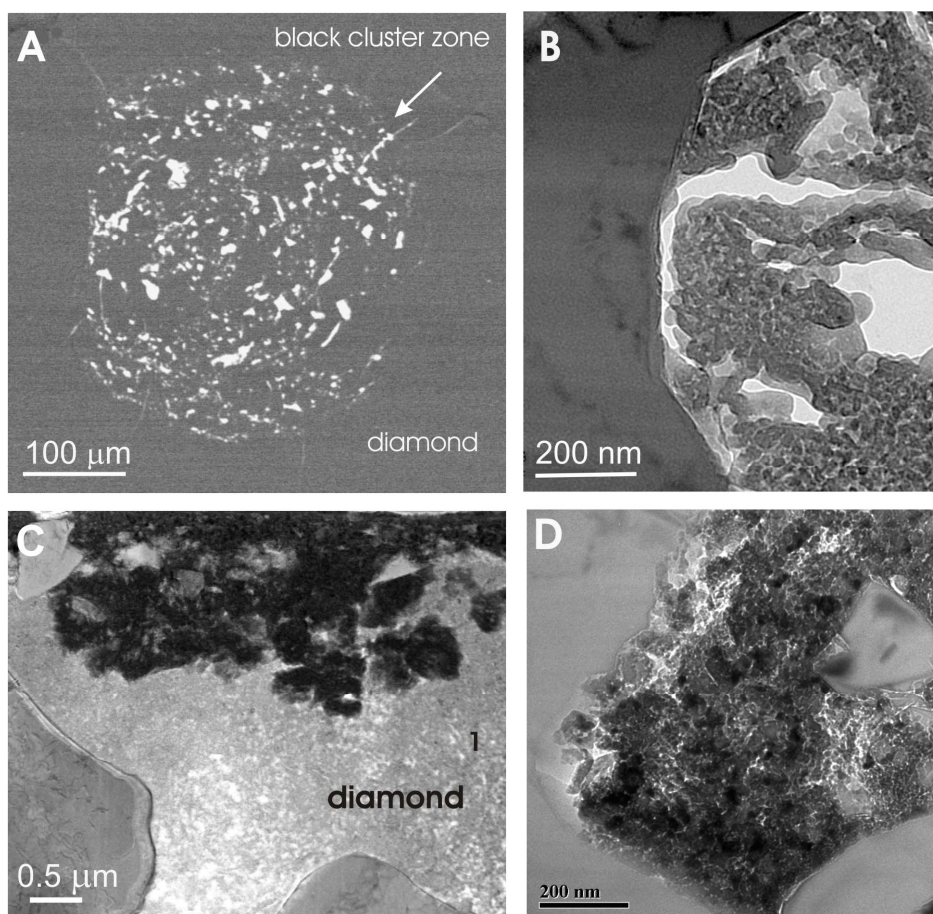


Fig. 1. (A): Backscattered electron (BSE) image of the black cluster zone in the centre of Komsomolskaya diamond; (B): TEM image of the diamond foil, showing the block-formed zone of diamond (I) contained the heterogeneous nanocrystalline inclusions, which are reflecting diamond-host habit (B, D), which are composed of Mg, Al, F, O-bearing phases (B) and magnetite nanocrystals (D).

been examined in this sample. Most of them are negatively faceted (Fig. 1 C, D), which permits their identification as syngenetic in relation to the diamond. The main phases were identified by microanalysis and electron diffraction. They are high-Al pyroxene, Ca-, Mg-, Fe - carbonate, Sr-enriched carbonate, graphite, magnetite and an unidentified high-Mg Al-bearing silicate (Fig. 2). Similar inclusions were found by Bulanova et al.(1998). An EPM analysis gave only the bulk composition, including  $\text{SiO}_2$ , high FeO content, MgO, CaO,  $\text{K}_2\text{O}$ , some Ba, P, Cl and in the areas of native iron and wustite, small contents of Si, Mg, and Al.

Quenched F, S, K, Cl – bearing phases has been found in this diamond. On the basis of EDX spectra, element maps, and electron diffraction data, we have identified magnetite, corundum and sellaite among the nanometre-sized phases within heterogeneous material. Magnetite is also present as crystals over 50 nm in

size. It should be noted that magnetite is one of the most common phase here. Sellaite is more difficult to confirm. To identify this phase we used an elemental map of the inclusions, which records a full spectrum pixel by pixel, allowing

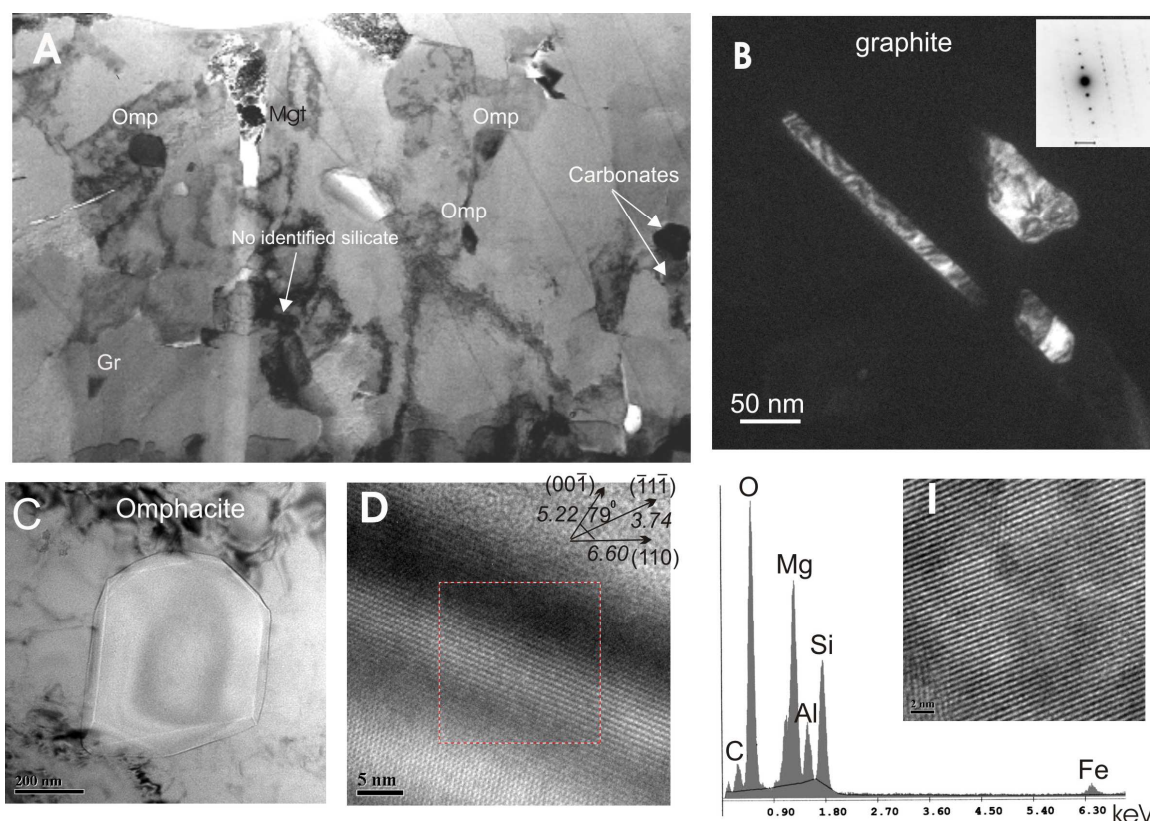
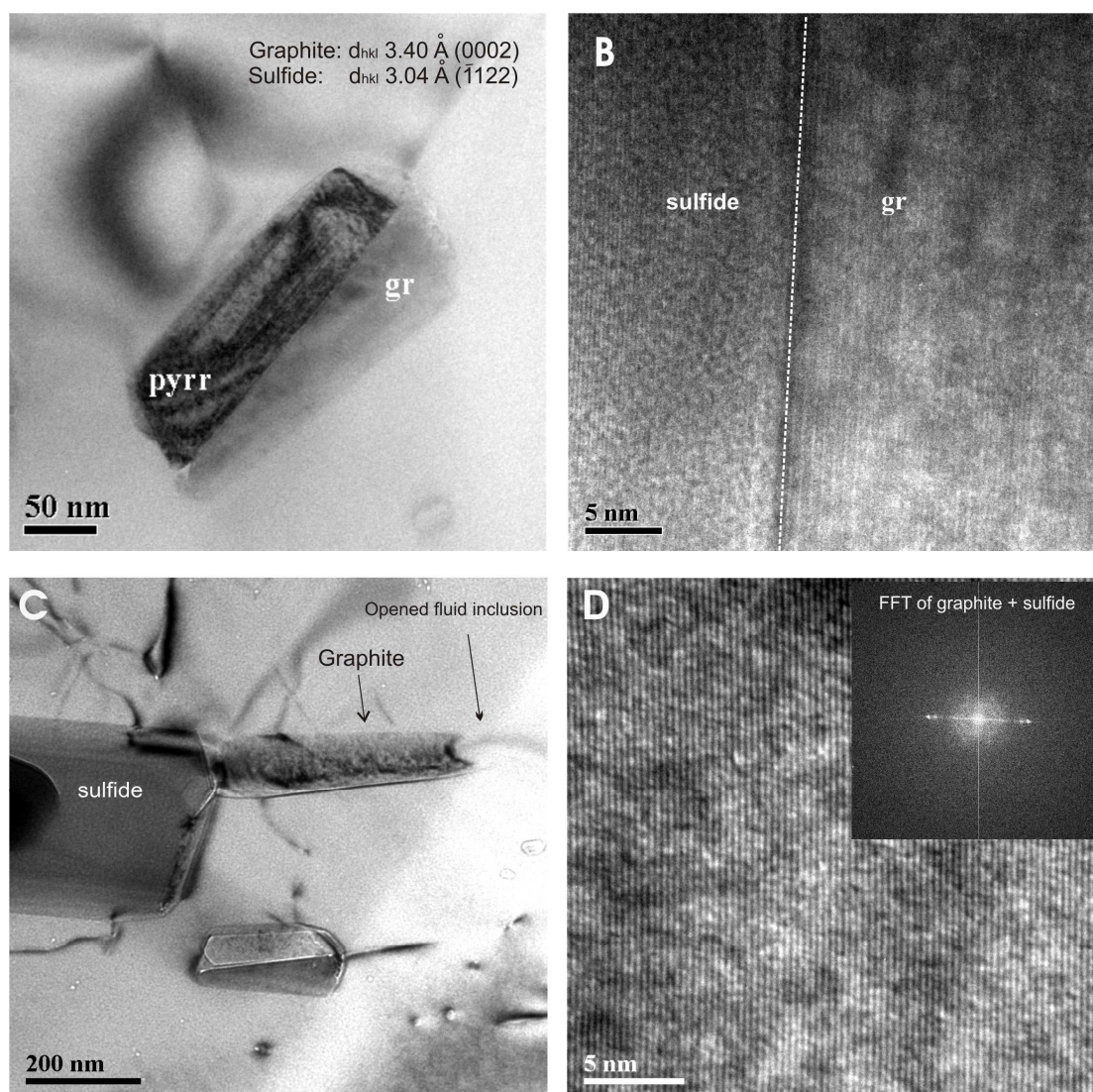


Fig. 2. TEM image of the diamond foil, showing crystalline phases inside black cluster zone (A): graphite (B); omphacite (C). (D): High resolution image of omphacite structure. (I): EDX spectra of high-Mg Al-bearing silicate phase (not identified). Ga intensity in the spectra is due to FIB preparation and Cu intensity is due to x-ray intensity from copper grid.

subsequent evaluation of the maps on a pixel by pixel basis. Such a procedure reveals that there are regions showing high F concentrations combined only with Mg. An electron energy-loss spectrum shows the fluorine K-edge and indicates the presence of fluorine in the composition of studied inclusion. Summarizing all of the data (AEM and EELS data, diffraction pattern and element map) we have determined this F-bearing phase as sellaite. This is the first observation of such a halide phase among the central inclusions in diamond. Amorphous carbon has been found in heterogeneous material. It was identified using electron energy-loss spectroscopy. In paragenesis with nanoinclusions we found several pyroxene-inclusions, which have an unusual composition compared with typical omphacites included in diamonds. It contains very high  $\text{Al}_2\text{O}_3$  (17,5-18,3 wt.%) along with high  $\text{SiO}_2$ , making it similar to the pyroxenes found in kyanite-bearing eclogite and grosspydrite xenoliths in Zagadochnaya kimberlite pipe [21].

## 2.2 Sulfide-graphite intergrowths

In Internatsionalnaya diamond we found oriented intergrowths of sulfide and graphite (Fig. 3), all of which are homogenous in their chemistry. These intergrowths also contain fluid bubbles. These mineral are accompanied by



**Fig. 3. (A,C): TEM bright field (BF) images of a sulfide – graphite intergrowths observed in the black cluster zone of Internatsionalnaya diamond. (B): Energy filtered TEM lattice fringe image of sulfide - graphite inclusion. Dotted line marks the boundary between two phases. (D): Energy filtered TEM lattice fringe image of graphite inclusion (diffraction pattern from fast Fourier transform FFT).**

pyrrhotite or monosulfide solid solution (Mss) – melt. All of them are reflecting the diamond habit and coexist with multiple omphacite-microinclusions. This is proof that the mineral association in this diamond is concerned to eclogitic type occurring in the deep lithosphere. EDX spectra of these sulfide inclusions show the high iron content (more than Ni) and relatively high Co content. Such compositions have not been observed in large sulfide inclusions extracted from diamonds [4, 27] or in micrometer-sized sulfide inclusions [2, 10]. From the homogenous chemical composition data and diffraction pattern we assume, that

these sulfide inclusions represent the first observation of monosulfide solid solution inclusions of eclogitic type.

### **2.3 Graphite inclusions**

In the central zone of three octahedral diamond crystals from Sytykanskaya and Internatsionalnaya pipes the main crystalline phases were found to be graphite, plus trapped fluid/ melt inclusions (silicates, sulfides, magnetite, carbonates and quenched material, enriched in K, Cl, F, Ba, Nb, Sr, Si, Mg, O). These fluid phases are present only in the areas consisting of graphite. Many dislocations are visible within and around the black cluster zone.

Fluid/melt inclusions are composed of multi-phase assemblages, which include solid phases as well as quenched material. High-Mg silicate-phase, sulfide, KCl, a Ba-rich phase, magnetite and silica have been identified using analytical electron microscopy. Similar nanometer-sized inclusions have been found in cloudy diamonds from Yakutian [16] and Canadian [9] kimberlitic bodies.

## **DISCUSSION AND CONCLUSION**

Information on the general chemical composition of the parental medium of diamond formation comes mostly from analytical studies of mineral, melt, and fluid inclusions in diamonds [2, 7, 9, 16, 17, 18, 22, 23, 24, and 28]. Syngenetic mineral inclusions in diamonds belong either to peridotite or eclogite parageneses or transitional a websterite-pyroxenite paragenesis. Studies of syngenetic inclusions within cloudy zones of diamonds from different parageneses shows that growing diamonds trapped not only minerals but also microscopic fragments of carbonatite melts. These melt from form on cooling, into crystalline associations of carbonates, silicates, phosphates, oxides, sulfides, chloride plus water and carbon dioxide. Thus the mineralogy of inclusions in diamonds and, therefore, the composition of their parental medium are heterogeneous and widely variable. The information obtained from inclusions serves as a basis for carrying out experiments aimed at establishing the composition of the crystallization medium and the physicochemical conditions of diamond formation. The commonest model is carbonatite (carbonate-silicate). Carbon sustaining the growth of diamonds seems to dissolve in the carbonate-silicate growth medium. The problem of its mantle source is of geochemical importance and has been discussed elsewhere [18, 19, and 26].

However, not only carbonate and carbonate-silicate melts but also multicomponent silicate compositions and melts of sulfides are highly efficient diamond-forming media [14, 15, and 20]. The abundance of syngenetic inclusions of sulfides associated with different silicates (chiefly olivine or omphacite depending on the type of matrix diamond paragenesis) suggests that a silicate-sulfide diamond-generating melt is also probable.

All the black cluster inclusions in Internatsionalnaya diamonds contain intergrowths of compositionally homogeneous sulfide, graphite, and fluid. The sulfides are enriched in Co (about 2 wt. %). This is the first report of such Co-rich inclusions in diamond. As omphacite is associated with these inclusions, we consider it the first finding of sulfide melt inclusions in diamond of eclogite paragenesis. Though in small amounts, sulfides are also present in cloudy central inclusions [16]. This type of polyphase nanometer-sized inclusion is dominated by a carbonate-silicate component.

It is very significant that hydrogen is present in these associations. Infrared absorption studies of diamonds show that hydrogen is typically present in the central zones of both peridotitic and eclogitic diamonds, but not in the intermediate or outer zones. In the central zones of Sytykanskaya and Internatsionalnaya diamonds, where multiple nanometer-sized inclusions of ordered graphite with fluid phases are found, a higher content of hydrogen is also recorded. Lambrecht et al. [13] suggested that graphite is the first phase to crystallize from the melt while hydrogen provides conditions (hydrogenation) for the further crystallization of diamond. Yet, the effect of hydrogen on diamond origin has not been studied in more detail. It is quite possible that either graphite was entrapped as a residual phase from the melt from which diamond was crystallized or graphite crystals could serve as seeds for diamond growth [2]. A similar view was given by Glinnemann et al. [6]. Based on their investigations on the oriented graphite single-crystal inclusions in diamond they assumed that the graphite crystal was formed first and served as a seed for the diamond.

Quite a different situation exists for the Komsomolskaya diamonds. Sulfides are also present in them but are subordinate and associated with magnetite. Crystals of ordered graphite are also recorded. The succession of crystallization can be inferred from the sizes of the crystallized mineral phases in the black cluster zone in Komsomolskaya diamond. The first phases to crystallize were Al-rich pyroxene and other silicates, carbonates, sulfides, and magnetite. The residual partially crystallized, melt contains nanometer-sized (about 10 nm) crystalline phases of magnetite, corundum, sellaite, and periclase. The components of the matter included into this diamond imply that the bulk composition of the parental medium for coated diamonds from the Komsomolskaya pipe is heterogeneous and can be generally described as the multicomponent system MgO-CaO-FeO-K<sub>2</sub>O-Al<sub>2</sub>O<sub>3</sub>-SiO<sub>2</sub>-CuS-FeS-KCl-MgF<sub>2</sub>-CO<sub>2</sub>-H<sub>2</sub>O-C, with the eclogite paragenesis being predominant in all associations of central inclusions of both cloudy and black cluster zones.

When considering genetic aspects of the melts, in two points are important: 1) The state of the growth medium from the time of trapping to complete sealing of the inclusion in diamond, with pressure and temperature corresponding to the conditions of diamond stability; 2) The history of the entrapped and sealed inclusion from time of trapping to the temperature of complete solidification of the inclusion.

In our case the growth medium consists of two diamond-forming solutions: carbonate-silicate (carbonatite) and sulfide. Data from experimental studies shows that carbon is dissolved in both types of melt melts [14]. Theirs diamond solubilities in carbonatite and sulfide melts are different and the degrees of supersaturation necessary for the spontaneous crystallization of diamond are also different. At relatively low carbon supersaturations which are unable to cause the formation of new diamond crystals but may support the growth of metastable diamond seeds already present in the growth environment, graphite can to be crystallized spontaneously, and even encapsulated fluid inclusions. In principle, we can not rule out that single crystals of thermodynamically unstable graphite grow in a sulfide melt that is highly concentrated, but not saturated in diamond. Another situation is also possible, when the entrapped sulfide melt contains dissolved carbon. Carbon remains dissolved in the sulfide melt until sulfide is liquid. But the inclusion parameters pass from the field of diamond stability to the graphite stability field. As carbon does not dissolve in solid sulfide, it has no choice but to separate into an independent phase of stable graphite. Most likely, it will be in the form of multiple intergrowths. Moreover, according to the phase diagram of Bundy et al. [3], graphite can exist as a metastable phase under the stable PT conditions of diamond.

The appearance of graphite-sulfide intergrowths can be explained as follows. If a liquid solution is oversaturated for graphite in the field of its stability, multiple spontaneous crystallization of graphite may occur and these small crystals may become centers that attract the carbon released during solidification of the sulfide solution-melt, thus producing oriented sulfide-graphite intergrowths. Sulfide melts are inert components in the growth of carbonate-silicate melt and hardly play any role in the formation of diamonds from the carbonate-silicate growth medium. Nevertheless, sulfide melts themselves are able to produce diamond because carbon in them dissolves under pressure. Unfortunately, this phenomenon has not been comprehensively studied yet.

The mineral assemblages located in the central zones of Yakutian diamonds indicate that they grew in a reduced environment, with oxygen fugacity controlled by a silicate rich melt, that was highly enriched in LIL (K, Ba, Sr) and HFSE (Nb, Ti) elements. This fluid also carried a carbonatitic component plus immiscible sulfide melts. The introduction of fluid into a reduced refractory environment may have been accompanied by a thermal pulse, and may have created the conditions necessary for the nucleation and growth of diamond. Our results on the complex character and composition of nanoinclusions in diamond testify the significant role of deep metasomatic processes in diamonds formation.

## REFERENCES

1. **Bulanova, G.P.** 1995. The formation of diamond. *Journal of Geochemical Exploration* 53, 1-23.

2. **Bulanova, G.P., Griffin, W.L., Ryan, C.G.** 1998. Nucleation environment of diamonds from Yakutian kimberlites. *Mineralogical Magazine* 62(3), 409-419.
3. **Bundy, F.P., Hall, H.T., Strong, H.M., Wentorf, R.H.** 1955, Man-made diamond. *Nature* 176, 51-54.
4. **Deines, P., Harris, J.W.** 1995. Sulfide inclusion chemistry and carbon isotopes of African diamonds. *Geochimica et Cosmochimica Acta* 59 (15), 3173-3188.
5. **Fesq, H.W., Bibby, D.M., Erasmus, C.S., Kable, E.J., Sellshop, J.P.** 1975. A comparative trace elements study of diamonds from Premier, Finsch and Jagersfontein mines, South Africa. *Phys. Chem. Earth, IX*, Ahrens, L. H. et al. (eds) Pergamon Press, 817-836.
6. **Glinnemann, J., Kusaka, K., Harris, J.W.** 2003. Oriented graphite single-crystal inclusions in diamond. *Z. Kristallogr.* 218, 733-739.
7. **Harris, J.W.** 1968. The recognition of diamond inclusions: Part I: Syngenetic inclusions. *Industr. Diamond Rev.* 28, 402-410.
8. **Harris, J.W.** 1972. Black material on mineral inclusions and in internal fracture planes in diamond. *Contr. Mineral. and Petrol.*, 35, 22-33.
9. **Klein-BenDavid, O., Izraeli, E., Hauri, E. and Navon, O.** 2007. Fluid inclusions in diamonds from the Diavik mine, Canada and the evolution of diamond forming fluids. *Geochim. Cosmochim. Acta.*, 71, 723-744.
10. **Klein-BenDavid, O., Logvinova, A.M., Izraeli, E.S., Sobolev, N.V., and Navon, O.** 2003. Sulfide melt inclusions in Yubileynaya (Yakutia) diamonds. 8th International Kimberlite Conference, Extended abstracts, FLA\_0111.
11. **Klein-BenDavid, O., Logvinova, A.M., Schrauder, M., Spetius, Z.V., Weiss, Y., Hauri, E.H., Kaminsky, F.V., Sobolev, N.V., Navon, O.** High-Mg carbonatitic microinclusions in some Yakutian diamonds – a new type of diamond-forming fluid // *Lithos*, 2009, v. 112, Suppl. 2, p. 648-659.
12. **Klein-BenDavid, O., Wirth, R., Navon, O.** 2006. TEM imaging and analysis of microinclusions in diamonds: a close look at diamond-growing fluids. *American Mineralogist* 91, 353-365.
13. **Lambrecht, W.R.L., Lee, C.H., Segall, B., Angus, J.C., Li, Z. and Sunkara, M.** 1993. Diamond nucleation by hydrogenation of the edges of graphitic precursors. *Nature* 264, 607-610.
14. **Litvin, Y.A.** 2007. High-pressure mineralogy of diamond genesis. *Geological Society of America, Special Paper*, 83-103.
15. **Litvin, Y.A., Shushkanova, A.V., Zharikov, V.A.** 2005. Immiscibility of sulfide-silicate melts in the mantle: Role in the syngensis of diamond and inclusions (based on experiments at 7.0 GPa. *Doklady Earth Sciences* 403, 719-722.
16. **Logvinova, A.M., Wirth, R., Fedorova, E.N., Sobolev, N.V.** 2008. Nanometre-sized mineral and fluid inclusions in cloudy Siberian diamonds: new insights on diamond formation. *Eur. J. Miner.* 20, 317-331.
17. **Meyer, H.O.A.** 1987. Inclusions in diamonds. In: Nixon, P.H. (Ed), *Mantle xenoliths*. John Wiley and Sons, Chichester, 501-522.
18. **Navon, O.** 1999: Formation of diamonds in the Earth's mantle. In J.Gurney, S. Richardson, and D.Bell, Eds., *proceedings of the 7<sup>th</sup> International kimberlite Conference*, p.584-604. Red Roof Designs, Cape Town.
19. **Navon, O., Hutcheon, I.D., Rossman, G.R., Wasserburg, G.J.** 1988: Mantle-derived fluids in diamond micro-inclusions. *Nature* 335, 784-789.
20. **Palyanov, Y.N., Borzdov, Yu.M., Khokhryakov, A.F., Kupriyanov, I.N., Sobolev, N.V.** 2006. Sulfide melts-graphite interaction at HPHT conditions: Implications for diamond genesis. *Earth Planet Sci. Lett.* 250, 269-280.

21. **Sobolev, N.V.** Deep-seated inclusions in kimberlites and the problem of Upper mantle the composition. F.R.Boyd, ed. American Geophysical Union, Washington DC. Translation from Russian, Moscow, Nauka Press, 1974.
22. **Sobolev, N.V., Logvinova, A.M., Zedgenizov, D.A., Yefimova, E.S., Seryotkin, Y.V., Floss, K., Taylor, L.A.** 2004. Mineral inclusions in microdiamonds and macrodiamonds from Yakutian kimberlites: a comparative study. *Lithos* 77, 225-242.
23. **Stachel, T., Harris, J.W.** 2008. The origin of cratonic diamonds – Constrains from mineral inclusions. *Ore Geology Reviews*, 34, 5-32.
24. **Taylor, L.A. and Anand, M.** 2004: Diamonds: Time capsules from the Siberian Mantle. *Chemie der Erde*, 64, 1-74.
25. **Wirth, R.** 2004. Focused Ion Beam (FIB): a novel technology for advanced application of micro- and nanoanalysis in geosciences and applied mineralogy. *Eur. J. Mineral.* 16, 863-876.
26. **Wyllie, P.J. and Ryabchikov, I.D.** 2000: Volatile components, magmas, and critical fluids in upwelling mantle. *Journal of Petrology*, 41, 1195-1206.
27. **Yefimova, E.S., Sobolev, N.V., Pospelova, L.N.** 1983. Sulfide inclusions in diamonds and peculiarities of their paragenesis, *ZVMO, CXII* (3), 300-310.
28. **Zedgenizov, D.A., Kagi, H., Shatsky, V.S., Sobolev, N.V.** 2004. Carbonatitic melts in cuboid diamonds from Udachnaya kimberlite pipe (Yakutia): evidence from vibrational spectroscopy. *Mineral. Mag.*, 68, 61-73.

# Chemical Composition, Volatile Components, and Trace Elements in Melts of the Karymskii Volcanic Center, Kamchatka, and Golovnina Volcano, Kunashir Island: Evidence from Inclusions in Minerals

V. B. Naumov<sup>a</sup>, M. L. Tolstykh<sup>a</sup>, E. N. Grib<sup>b</sup>, V. L. Leonov<sup>b</sup>, and  
N. N. Kononkova<sup>a</sup>

<sup>a</sup> Vernadsky Institute of Geochemistry and Analytical Chemistry, Russian Academy of Sciences, ul. Kosygina 19, Moscow, 119991 Russia, e-mail: naumov@geokhi.ru

<sup>b</sup> Institute of Volcanology and Seismology, Far East Division, Russian Academy of Sciences, bul'v. Piipa 9, Petropavlosk-Kamchatskii, 683006 Russia, e-mail: gen@ksnet.ru

## ABSTRACT

Melt inclusions were examined in phenocrysts in basalt, andesite, dacite, and rhyodacite from the Karymskii volcanic center in Kamchatka and dacite from Golovnina volcano in Kunashir Island, Kuriles. The inclusions were examined by homogenization and by analyzing glasses in more than 80 inclusions on an electron microscope and ion microprobe. The SiO<sub>2</sub> concentrations in the melt inclusions in plagioclase phenocrysts from basalts from the Karymskii volcanic center vary from 47.4 to 57.1 wt %, these values for inclusions in plagioclase phenocrysts from andesites are 55.7-67.1 wt %, in plagioclase phenocrysts from the dacites and rhyodacites are 65.9-73.1 wt %, and those in quartz in the rhyodacites are 72.2-75.7 wt %. The SiO<sub>2</sub> concentrations in melt inclusions in quartz from dacites from Golovnina volcano range from 70.2 to 77.0 wt %. The basaltic melts are characterized by usual concentrations of major components (wt %): TiO<sub>2</sub> = 0.7-1.3, FeO = 6.8-11.4, MgO = 2.3-6.1, CaO = 6.7-10.8, and K<sub>2</sub>O = 0.4-1.7; but these rocks are notably enriched in Na<sub>2</sub>O (2.9-7.4 wt % at an average of 5.1 wt %, with the highest Na<sub>2</sub>O concentration detected in the most basic melts: SiO<sub>2</sub> = 47.4-52.0 wt %). The concentrations of volatiles in the basic melts are 1.6 wt % for H<sub>2</sub>O, 0.14 wt % for S, 0.09 wt % for Cl, and 50 ppm for F. The andesite melts are characterized by high concentrations (wt %) of FeO (6.5 on average), CaO (5.2), and Cl (0.26) at usual concentrations of Na<sub>2</sub>O (4.5), K<sub>2</sub>O (2.1), and S (0.07). High water concentrations were determined in the dacite and rhyodacite melts: from 0.9 to 7.3 wt % (average of 15 analyses equals 4.5 wt %). The Cl concentration in these melts is 0.15 wt %, and those of F and S are 0.06 and 0.01 wt %, respectively. Melt inclusions in quartz from the dacites of Golovnina volcano are also rich in water: they contain from 5.0 to 6.7 wt % (average 5.6 wt %). The comparison of melt compositions from the Karymskii volcanic center and previously studied melts from Bezmyannyi and Shiveluch volcanoes revealed their significant differences. The former are more basic, are enriched in Ti, Fe, Mg, Ca, Na, and P but significantly depleted in K. The melts of the Karymskii volcanic center are most probably less differentiated than the melts of Bezmyannyi and Shiveluch volcanoes. The concentrations of water and 20 trace elements were measured in the glasses of 22 melt inclusions in plagioclase and quartz from our samples. Unusually high values were obtained for Li concentrations (along with high Na concentrations) in the basaltic melts from the Karymskii volcanic center: from 118 to 1750 ppm, whereas the dacite and rhyolite melts contain 25 ppm Li on average. The rhyolite melts of Golovnina volcano are much poorer in Li: 1.4 ppm on average. The melts of the Karymskii volcanic center are characterized by relative minima at Nb and Ti and maxima at B and K, as is typical of arc magmas.

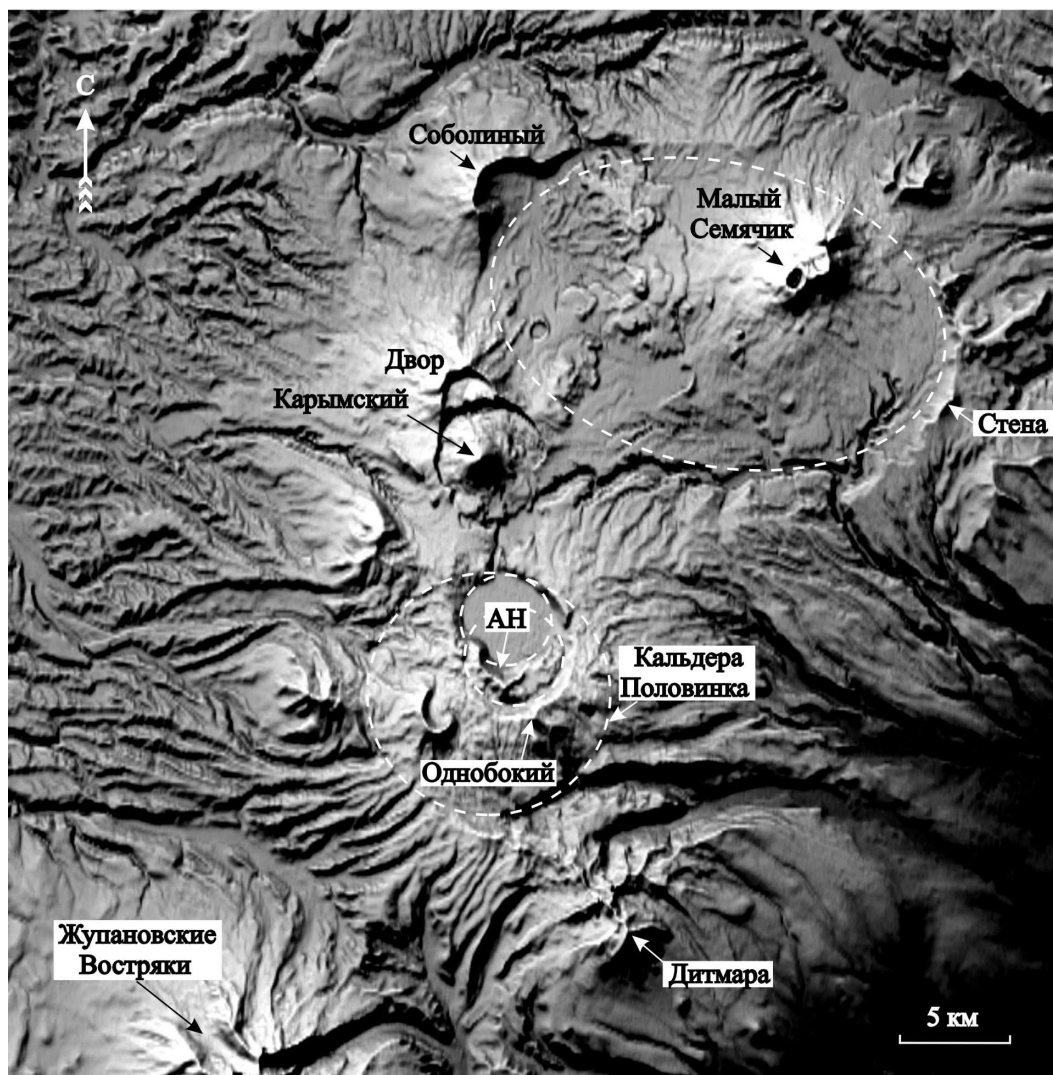


Fig. 1. Satellite image of the central part of the Karymskii volcanic center. Dashed lines outline calderas, AN is the volcano and caldera of Akademii Nauk (the caldera houses Lake Karymskoe). The oval in the northern part of the image outlines the Stena-Sobolinaya caldera system.

## INTRODUCTION

The Karymskii volcanic center in the southwestern flank of the central part of the Eastern Volcanic Belt in Kamchatka has sizes of 55×65 km and is slightly elongated northeastward, along the strike of the volcanic belt. The Karymskii volcanic center has a complicated structure (Fig. 1) and consists of numerous volcanic edifices of differentiated composition and a series of caldera structures, which dynamically evolved starting in the Pliocene [27, 12, 9, 18, 2 and others). The development of the calderas (Stena, Sobolinaya, and Polovinka calderas) began in the Middle Pleistocene 180–150 ka BP [28] and was associated with powerful eruptions of pyroclastic material of intermediate and acid composition ~280 km<sup>3</sup> in volume, which corresponds to ~100 km<sup>3</sup> when recalculated into magma [7, 8]. After the origin of the middle Pleistocene calderas, volcanic activity

was restricted exclusively to them. During this time span in the initial Late Pleistocene, such volcanoes were formed as Odnobokii, Dvor, Pra-Semy-achik, and Pra-Karymskii. Their lavas were of predominantly basalt, basaltic andesite, and andesite composition. The volume of the products erupted during that period was estimated at 80 km<sup>3</sup> [28]. Younger calderas developed later on some of the volcanoes (Odnobokaya and Malyi Semyachik), then new volcanoes (Akademii Nauk and Malyi Semyachik) started to form within these calderas in the Late Pleistocene, and eventually new calderas were produced (Akademii Nauk and Karymskaya). Volcanism in the Late Pleistocene-Holocene produced compositionally more diverse products of various facies types.

The inner structure, tectonics, eruption dynamics, the petrography of the magmatic rocks, and their possible genetic links were discussed in numerous publications. However, data on the chemical composition of the magmatic melts that formed the Karymskii center and on their volatile and trace components are still scarce. However, the genesis of the rocks and more general problems of the regional magmatic history cannot be studied comprehensively enough without this information. Because of this, our research was centered on the detailed study of melt inclusions in minerals from compositionally diverse rocks (from basalts to rhyo-dacites) to elucidate the chemical composition of the magmatic melts and the possible genetic relations between magmatic rocks of various silicity. The first data of these studies were published in [25]. In order to compare our results on the chemical composition of melts of the Karymskii volcanic center, we also studied inclusions in quartz crystals from dacites of Golovnina volcano in Kunashir Island.

## **BRIEF PETROGRAPHIC CHARACTERIZATION OF THE KARYMSKII VOLCANIC CENTER**

The Karymskii volcanic center started to attract close attention of researchers after eruptions in it in 1996. These eruptions were characterized by simultaneous activity at two sites, so that the melts simultaneously poured at the surface had an intermediate and basic composition. The eruption process can be subdivided into three stages. During the first of them (on January 2-3, 1996), two volcanic centers spaced 6 km apart erupted: the summit crater of Karymskii volcano and the northern segment of Lake Karymskoe, which is the Akademii Nauk caldera [2]. The main crater was characterized by a continuous ascent of a gas-ash column to a height of 500-1200 m. The dark trail of the ascending column extended southward for up to 50-70 km, and tephra continuously fell from it. At the same time, subaquatic eruptions of basalt occurred in Lake Karymskoe from the eruption center at a distance of 500 m from its shore [9]. Powerful discrete

Table 1.

**Chemical composition (wt %) of rocks and groundmass glasses in rocks from the Karymskii volcanic center**

Component	K-2	K-4	K-63	K-41	K-35	K-31	K-23	K-2a	K-4a	K-63a
SiO <sub>2</sub>	52.00	62.45	62.05	64.80	65.41	66.32	69.00	66.59	74.80	75.28
TiO <sub>2</sub>	0.73	0.92	0.88	0.72	0.56	0.38	0.43	0.50	1.06	0.83
Al <sub>2</sub> O <sub>3</sub>	19.21	16.27	16.60	16.00	16.39	14.99	14.35	12.62	12.62	12.46
Fe <sub>2</sub> O <sub>3</sub>	-	-	-	1.79	2.77	1.19	1.26	-	-	-
FeO	8.30*	6.58*	6.95*	3.45	2.27	2.27	1.94	1.78*	3.59*	3.14*
MnO	0.14	0.15	0.12	0.18	0.16	0.03	0.16	0.06	0.10	0.11
MgO	5.34	2.01	2.0	1.62	0.940	0.94	0.94	0.23	0.18	0.49
CaO	10.47	5.38	5.39	3.90	4.41	3.28	1.76	4.65	0.92	0.94
Na <sub>2</sub> O	2.80	4.52	4.08	3.72	4.12	3.91	3.66	5.76	1.88	1.77
K <sub>2</sub> O	0.58	1.57	1.58	1.86	1.48	1.98	2.46	1.64	3.50	3.44
P <sub>2</sub> O <sub>5</sub>	0.14	0.26	0.25	0.03	0.19	0.09	0.06	-	-	-
LOI	-	-	-	2.40	1.48	4.10	3.80	-	-	-
<b>Total</b>	<b>99.71</b>	<b>100.11</b>	<b>99.8210</b>	<b>100.47</b>	<b>100.4</b>	<b>99.48</b>	<b>99.82</b>	<b>100.73</b>	<b>98.65</b>	<b>98.46</b>

**Note:** Here and in Tables 2-5, sample K-2 is basalt of the 1996 eruption, Novogodnii peninsula, Akademii Nauk caldera; samples K-4 and K-63 are andesites from lava flows of the 1996 and 1997 eruption from the summit crater of Karymskii volcano; sample K-41 is dacite from the eastern wall of the Odnobokaya caldera; sample K-35 is tuff of dacitic composition from the western wall of the Polovinka caldera; sample K-31 is pumice of dacitic composition from the left-hand bank of the Karymskaya River eastern wall of the Karymskaya caldera; sample K-23 in pumice of rhyodacitic composition from the eastern slope of Akademii Nauk volcano; and samples K-2a, K-4a, and K-63a are groundmass glasses of the respective samples. \* is total iron.

Table 2.

**Representative analyses (w%) of plagioclase in rocks from the Karymskii volcanic center**

Component	K-41	K-2	K-2	K-4	K-63	K-41	K-41	K-31	K-23	K-35
SiO <sub>2</sub>	45.00	44.79	47.64	47.58	52.85	53.39	58.266	58.26	60.40	62.15
Al <sub>2</sub> O <sub>3</sub>	33.02	34.35	33.66	31.65	30.47	28.03	24.99	24.74	23.54	21.59
FeO	0.55	0.62	0.59	0.75	0.66	0.440	0.35	0.44	0.33	0.07
CaO	19.29	18.09	17.10	13.1	14.51	13.13	9.92	9.65	7.36	5.31
Na <sub>2</sub> O	0.82	0.99	1.56	2.65	3.36	4.25	6.15	5.83	7.42	8.22
K <sub>2</sub> O	0.01	0.03	0.01	0.08	0.11	0.10	0.20	0.25	0.36	0.93
<b>Total</b>	<b>98.69</b>	<b>98.87</b>	<b>100.56</b>	<b>100.12</b>	<b>98.04</b>	<b>99.30</b>	<b>99.27</b>	<b>99.17</b>	<b>99.41</b>	<b>98.27</b>
An	92.7	90.8	85.8	78.1	70.0	62.7	46.6	47.1	34.7	24.5
Ab	7.2	9.0	14.1	21.5	29.4	36.7	52.3	51.5	63.3	69.9
Or	0.1	0.2	0.1	0.4	0.6	0.6	1.1	1.4	2.0	5.2

Table 3.

## Representative analyses (w%) of pyroxenes in rocks from the Karymskii volcanic center

Component	K-2	K-63	K-63	K-4	K-41	K-41	K-35	K-35	K-23	K-31
SiO <sub>2</sub>	53.58	52.35	52.08	50.76	52.53	52.53	51.97	52.97	53.12	52.48
TiO <sub>2</sub>	0.49	0.34	0.53	0.63	0.21	0.16	0.10	0.13	0.10	0.26
Al <sub>2</sub> O <sub>3</sub>	1.33	1.11	1.54	1.88	1.26	0.87	0.35	0.74	0.40	0.89
FeO	19.55	20.37	10.94	10.40	11.6321	11.63	21.39	8.96	22.95	10.62
MnO	0.44	0.71	0.49	0.49	0.59	0.44	1.49	0.58	1.48	0.40
MgO	20.80	23.24	14.75	13.89	23.74	13.63	22.92	14.11	21.30	13.83
CaO	2.24	1.92	19.78	20.98	1.69	20.36	1.11	21.88	1.02	20.44
Na <sub>2</sub> O	0.13	0.00	0.35	0.31	0.00	0.150	0.00	0.15	0.00	0.29
<b>Total</b>	98.56	100.04	100.46	99.34	100.53	99.82	99.33	99.52	100.37	99.21
Fs	32.9	31.7	17.5	16.8	30.4	18.8	33.6	14.4	36.9	17.3
En	62.3	64.5	42.0	39.9	66.2	39.2	64.2	40.5	61.0	40.1
Wo	4.8	3.8	40.5	43.3	3.4	42.0	2.2	45.1	2.1	42.6

phreatomagmatic explosions occurred one after another with time intervals of 10-15 min, and vapor-gas ejecta with ash rose to a height of a few kilometers. The most powerful explosions ejected numerous bombs, and the waves induced in the lake reached a height of 10 m. During the first stage of the eruption, Novogodnii Peninsula (0.7 km<sup>2</sup> in area) was formed in Lake Karymskoe.

Table 4.

## Representative analyses (w%) of ore minerals in rocks from the Karymskii volcanic center

Component	K-2	K-63	K-4	K-4	K-41	K-41	K-35	K-31	K-31	K-23
FeO	52.25	78.09	78.05	92.90	52.04	85.63	55.31	55.52	86.26	85.60
TiO <sub>2</sub>	40.13	11.80	12.87	3.17	43.61	10.15	40.72	40.52	9.25	8.89
Al <sub>2</sub> O <sub>3</sub>	0.43	3.26	3.35	1.30	0.43	2.14	0.05	0.33	1.59	1.54
MnO	0.29	0.45	0.42	0.45	0.090	0.48	0.74	0.09	0.04	0.61
MgO	3.18	2.69	2.691	2.101	2.86	1.69	2.10	1.86	1.40	0.58
CaO	0.04	0.13	0.06	0.06	-	-	-	-	-	-
SiO <sub>2</sub>	0.03	0.18	0.06	0.19	-	-	-	-	-	-
<b>Total</b>	96.35	96.60	96.72	99.18	99.64	100.09	97.22	98.32	98.55	97.22

The second stage of the eruption on January 4-12, 1996, was characterized by eruptive activity only at the summit crater of Karymskii volcano, with a much lower frequency of the explosions. The height of the ejecta was 500-900 m, and ash trails extended for 50-60 km, mostly in the western and eastern directions. During the third stage (from January 13, 1996, until present), a series of lava flows was erupted from the main crater of Karymskii volcano. The length of the thickest of them reached 1.5 km, and the height of its frontal part was 25 m. The lava eruptions were associated with explosions. The vapor-gas ejecta loaded with ash rose to heights from 100 to 500-600 m and produced eruption clouds. During the most powerful explosions (250 m and more), their lower parts persistently included bombs 1-2 m in diameter, occasionally up to 4-5 m [18].

We examined three samples selected from among products of the 1996-1997 eruption, whose composition is reported in Table 1. The first sample (K-2) is a basaltic volcanic bomb from Novogodnii Peninsula. It is a black porous vitreous rock with numerous plagioclase phenocrysts 0.3-3 mm in size. The composition of the phenocrysts varies from  $An_{94-80}$  in cores to  $An_{75-62}$  in marginal parts. The composition of plagioclase with abundant melt inclusions is shown in Table 2. The olivine ( $Fo_{83-72}$ ) and pyroxenes (orthopyroxene and clinopyroxene, Table 3) occur more rarely. The accessory minerals of the basalt are apatite and an ore mineral. The former was found as crystalline inclusions and the latter as both crystalline inclusions and microlites (Table 4).

The other two samples (K-4 and K-63, Tables 1-4) are andesite from lava flows from the summit crater of Karymskii volcano. The samples were taken in a hot state on September 22, 1996, and August 19, 1997, respectively. These are weakly porous dark gray rocks with 30-35 vol % phenocrysts. Their major rock-forming mineral is plagioclase, which accounts for ~85% of all phenocrysts. The plagioclase occurs as grains of various sizes, with none of them (even large phenocrysts) showing resorption zones. The composition of the plagioclase ranges from  $An_{85}$  to  $An_{52}$ . The mafic minerals are orthopyroxene, clinopyroxene, and rare olivine, which displays reaction relations with the pyroxenes. The groundmass consists of glass and microlites of plagioclase, pyroxene, and an ore mineral.

Karymskii volcano is spatially restricted to the central part of the Karymskii caldera, which was produced by a catastrophic explosive eruption of Præ-Karymskii volcano at 7600-7700 years BP [28]. The pyroclastic deposits related to its origin consist of pumice tuffs of dacite composition (sample K-31, Tables 1-4). Pumice fragments of beige color have psephitic to agglomerated sizes, are submerged in finegrained material, and sometimes compose strata with numerous pumice lapilli. The other samples examined in the course of this research were from pyroclastic deposits from the southern sector of the Karymskii volcanic center consisting of three calderas telescopically nested in one another. The Polovinka caldera is the oldest. The bulk of its pyroclastic deposits (close to 42 km<sup>3</sup>) consists of agglomerated ash-pumice tuffs of rhyodacite and dacite composition (sample K-35, Tables 1-4). Later, Odnobokii volcano was formed in the Polovinka caldera, and the lavas of this volcano completely filled the caldera. The evolutionary history of the volcano involved two episodes of catastrophic explosive eruptions with a period of volcanic activity in between. These processes formed the Odnobokaya caldera at 110-80 ka [28, 5,6]. The pyroclastic flows consist mostly of ash-pumice tuffs and are zonal, with their composition systematically varying from rhyodacite in the bottom of the flows to dacite in their upper parts. The pumice tuffs (sample K-41, Tables 1-4) consist of angular pumice fragments of psephitic and agglomerate size submerged in finer grained material.

The pumices are dense, finely porous and have beige or gray color. They contain 10-20 vol % crystalline phase.

In the Late Pleistocene, Akademii Nauk volcano was formed near the southern boundary of the Odnobokaya caldera. The pyroclastic deposits of an explosive eruption of this volcano consist of agglomerate pumice tuffs of rhyodacite composition (sample K-23, Tables 1-4) and cover the southern slopes of the volcano. The tuffs are white, their pumice fragments are no larger than 5-10 cm, and their porosity is approximately 30-50%. The upper portions of the stratigraphic sequences are rewashed, which suggests that the tuffs were deposited in a lake. There is still no consensus about the genesis of the Akademii Nauk caldera in its modern form because it does not contain significant volumes of pyroclastic deposits related to its origin. It is thought that the caldera was formed in the Late Pleistocene-Early Holocene as a consequence of basaltic eruption in the zone of the submeridional fault in the northern part of Lake Karymskoe. This eruption was similar to the event in 1996. Basalt injections into the bottom part of the upper crustal chamber resulted in the mobilization of acid melt in it and a nearly synchronous eruption at Akademii Nauk volcano, its destruction, and the collapse of the walls of the already existing Odnobokaya caldera. The thorough investigation of the pyroclastic deposits related to calderas in the southern sector of the Karymskii volcanic center has demonstrated that basaltic tephra strata (sometimes in association with weakly compacted tuffs) are quite common in them starting in the terminal Middle Pleistocene deposits. This suggests that the events analogous to the 1996 eruption also occurred in this area previously [5, 6]. The basaltic tephra of the Late Pleistocene and Holocene eruptions composes terraces along the northern shore of Lake Karymskoe that fills the Akademii Nauk caldera.

Phenocrysts in the pyroclastic deposits are plagioclase, orthopyroxene, clinopyroxene, and ore minerals, whose compositions often reflect the unequilibrated state of the melt during its crystallization. The early products in each caldera contain hornblende, and the earliest agglomerated tuffs of the Polovinka caldera contain quartz and biotite. A distinctive feature of the pyroclastic deposits of the Odnobokaya caldera is the presence of holocrystalline clusters (perhaps, cumulates). The pumice agglomerated tuffs of the first stage contain these clusters composed of plagioclase, clinopyroxene, and titanomagnetite that form poikilophitic intergrowth textures. This association sometimes also contains high-Al hornblende. The second-stage tuffs and ignimbrites typically contain olivine-anorthite nodules and their crystalline fragments, which are very unevenly distributed in the rocks. The agglomerated tuffs of andesite composition bear olivine microphenocrysts with skeletal growth structures.

Plagioclase dominates in all types of the pyroclastic deposits. Its phenocrysts range from 0.6 to 1.5 mm in size and occasionally reach 2-3 mm. The composition of the plagioclase is determined mostly by the composition of the pyroclastic deposits. For example, the rhyodacite pumice tuffs are dominated by oligoclase-andesine ( $An_{28-42}$ ), and the predominant plagioclase of the dacitic tuffs is andesine

(An<sub>42-52</sub>). Some of the phenocrysts contain corroded calcic cores (An<sub>52-55</sub>, more rarely An<sub>75-85</sub>). The plagioclase contains melt inclusions, apatite, and, more rarely, magnetite and ilmenite. The holocrystalline aggregates are dominated by bytownite-anorthite (An<sub>68-94</sub>). The basaltic tephra contains plagioclase phenocryst of bytownite composition (An<sub>85-90</sub>) with crystalline inclusions of clinopyroxene and melt inclusions. The marginal zones of these plagioclase grains are characterized by a progressive decrease in the anorthite concentration and corresponds to An<sub>68-66</sub>.

The mafic minerals of all of the pyroclastic deposits are dominated by orthopyroxene and clinopyroxene. They were found in the form of phenocrysts (0.6-1.5 mm), microphenocrysts (100-300 µm), as polymineralic aggregates, and, more rarely, as crystalline inclusions in other minerals. The pyroxenes contain crystalline inclusions of magnetite, ilmenite, apatite, and rare plagioclase, along with melt inclusions. Amphibole occurs in the early products of each caldera in the southern sector of the Karymskii volcanic center. These minerals occur as black elongated columnar crystals from 1.5 to 2.5 mm long. The crystals are euhedral and are not altered. Hornblende in the rhyodacite pumice deposits of the Odnobokaya caldera and Akademii Nauk volcano are compositionally similar and correspond to moderately aluminous (6.0-8.0 wt % Al<sub>2</sub>O<sub>3</sub>) ordinary hornblende. The phenocrysts contain crystalline inclusions of titanomagnetite, ilmenite, apatite, and occasional plagioclase (An<sub>42-48</sub>), as well as melt inclusions. The pumice tuffs of the Odnobokaya caldera sometimes contain aluminous amphibole (9-11, occasionally up to 12-13 wt % Al<sub>2</sub>O<sub>3</sub>). Biotite is the only mafic mineral in the most evolved rocks, namely, in the tuffs and ignimbrites ejected early during the development of the Polovinka caldera.

The ore minerals are titanomagnetite and ilmenite, whose contents vary from a few fractions of a percent to 1.5-2.0%. Their contents are the lowest in the pyroclastics of rhyodacite composition and are much higher in the dacitic rocks. They occur as crystalline inclusions in pyroxene and amphibole phenocrysts (and, more rarely, also in plagioclase and quartz) and as polymineralic aggregates. The sizes of the phenocrysts vary from 100 to 300 µm, and those of the crystalline inclusions are from a few micrometers to 100-150 µm.

In addition to the samples listed in Table 1, we also studied large quartz crystals from a buried pyroclastic flow found at the western wall of the complex of southern calderas of the Karymskii volcanic center. In an artificial exposure in a pyroclastic flow related to the Polovinka caldera, these deposits include a buried layer of coarse-grained sand, which is, in turn, overlain by younger ignimbrite. The quartz and plagioclase crystal-lapilli from this layer are 2-3 mm in size, and melt inclusions in them can be discerned even under a binocular magnifier.

As was mentioned above, for comparison we also examined melt inclusions in quartz crystals from Golovnina volcano. This volcano is situated in the southern

part of Kunashir Island and has a caldera and central extrusion dome of Holocene age [4, 3]. The dacites of this volcano are porphyritic and contain phenocrysts of plagioclase ( $An_{72-43}$ ) and orthopyroxene and large quartz crystals.

## INCLUSIONS IN MINERALS

Melt inclusions were prepared for studying and analyzed on a Camebax Microbeam microprobe using the technique that we previously applied to study andesites from some volcanoes in the Kuriles and Kamchatka [24] and trachybasalts from eastern Tuva volcanic highland [15]. The concentrations of  $H_2O$ , F, and trace elements in the melt inclusions were determined by secondary-ion mass spectrometry on an IMS-4f ion microprobe at the Institute of Microelectronics, Russian Academy of Sciences, in Yaroslavl by the method described in detail in [22, 17, 21].

We have examined more than 70 melt inclusions in plagioclase and quartz from various rocks of the Karymskii volcanic center and a few inclusions in quartz from dacites of Golovnina volcano. Our data on the chemical composition of the glasses of the melt inclusions are presented in Tables 5-7. The  $SiO_2$  concentrations in inclusions in plagioclase phenocrysts from basalt from the Karymskii volcanic center vary from 47.4 to 57.1 wt %, inclusions in plagioclase phenocrysts from the andesites contain 55.7-67.1 wt %  $SiO_2$ , inclusions in plagioclase phenocrysts from the dacites and rhyodacites contain 66.1-72.5 wt %  $SiO_2$  (Table 5), and quartz phenocrysts from the rhyodacites contain inclusions with 72.2-75.7 wt %  $SiO_2$  (Table 7). The  $SiO_2$  contents in quartz from the dacites of Golovnina volcano vary from 70.2 to 77.0 wt % (Table 7).

The basaltic melts (Table 5) contain usual concentrations (wt %) of  $TiO_2$  (0.7-1.3), FeO (6.8-11.4), MgO (2.3-6.1), and CaO (6.7-10.8) but are significantly enriched in  $Na_2O$  (2.9-7.4 wt % at an average of 5.1 %), with the highest  $Na_2O$  concentrations detected in the most basic melts ( $SiO_2 = 47.4-52.0$  wt %). The  $K_2O$  concentrations range from 0.4 to 1.7 wt %. The only exception was one melt inclusion that contained much more  $K_2O$  (5.95 wt %) than  $Na_2O$  (2.64 wt %). Note that this  $K_2O$ -rich inclusion contains very little Cl (0.01 wt %), whereas the other 19 inclusions in sample K-2 are much richer in Cl (0.06-0.12 wt % at an average of 0.09 wt %). This feature of potassic melts in terms of Cl concentration was noted earlier in the melts of volcanics from the Medvezh'ya caldera in Iturup Island, southern Kuriles [26] and in acid melts of the Verkhneuralsk mining average, in 17 inclusions). Two inclusions were determined to contain as much as 0.7 and 2.4 wt %  $H_2O$  (Table 6).

The  $SiO_2$  concentrations in the glasses of melt inclusions in the andesite sample vary from 55.7 to 67.1 wt %, i.e., is 9 wt % on average higher than in the glasses in melt inclusions in the basalt sample (Table 5). The melts in plagioclase from the andesite are characterized by high concentrations of FeO (9.0-4.1 wt %,

Table 5.

**Chemical composition (wt %) of glasses in melt inclusions in plagioclase from rocks from the Karymskii volcanic center**

Inclusion no.	Component												Total	T, °C	An
	SiO <sub>2</sub>	TiO <sub>2</sub>	Al <sub>2</sub> O <sub>3</sub>	FeO	MnO	MgO	CaO	Na <sub>2</sub> O	K <sub>2</sub> O	P <sub>2</sub> O <sub>5</sub>	Cl	S			
Sample K-2															
1	47.44	0.73	19.67	6.83	0.13	5.19	10.82	7.40	0.44	0.09	0.07	0.14	98.95	1140	93
2	49.47	1.08	16.09	8.66	0.12	6.10	10.00	5.96	1.13	0.24	0.12	0.19	99.16	1140	81
3	50.71	0.99	18.93	8.01	0.19	3.20	9.93	4.64	0.73	0.25	0.07	0.13	97.79	20	88
4	50.92	1.05	15.69	8.77	0.22	4.95	9.08	6.90	1.24	0.18	0.10	0.16	99.26	20	84
5	50.98	0.79	19.05	7.86	0.16	4.30	9.69	6.21	0.66	0.15	0.10	0.16	100.11	1120	89
6	51.27	0.91	17.36	8.12	0.22	3.65	8.90	5.33	1.07	0.16	0.06	0.15	97.20	1140	84
7	51.47	0.95	17.76	9.03	0.21	4.70	9.05	6.38	0.66	0.16	0.08	0.10	100.55	1120	92
8	51.84	0.87	19.83	7.24	0.13	3.75	9.28	5.91	0.74	0.16	0.07	–	99.82	1100	85
9	52.04	1.02	16.45	8.45	0.12	5.26	8.38	7.07	1.40	–	–	0.22	100.41	1130	91
10	53.55	1.08	18.71	7.83	0.23	3.06	9.82	4.02	0.92	0.19	0.09	0.19	99.69	1100	89
11	53.87	1.01	18.35	7.71	0.14	3.55	7.61	5.56	0.94	0.22	0.09	–	99.09	1100	88
12	53.90	1.30	13.93	11.39	0.23	4.76	7.03	3.88	1.25	0.24	0.11	0.11	98.13	20	84
13	54.11	0.85	16.42	8.90	0.21	4.63	8.16	4.43	1.66	0.14	0.07	0.17	99.58	1120	86
14	54.68	1.00	17.30	7.70	0.15	3.68	8.12	6.05	0.91	0.13	0.08	0.14	99.94	1140	87
15	54.87	0.83	14.41	8.98	0.14	6.59	8.21	4.60	0.68	0.24	0.09	0.10	99.74	1140	86
16	55.44	1.19	16.23	8.96	0.15	3.92	6.66	5.15	1.44	0.19	0.11	0.15	99.59	1100	83
17	55.44	0.86	17.67	5.45	0.09	3.72	8.15	2.64	5.95	0.11	0.01	0.03	100.12	1140	82
18	55.47	1.03	17.62	8.08	0.21	3.63	7.24	3.09	1.11	0.17	0.11	–	97.76	20	83
19	55.62	0.91	18.59	6.85	0.16	3.61	7.90	4.84	1.04	0.21	0.09	0.10	99.92	1120	83
20	57.14	0.88	17.97	7.29	0.17	3.50	7.46	2.87	1.10	0.15	0.11	0.10	98.74	1120	83
Sample K-63															
21	56.89	2.25	13.60	8.98	0.26	2.43	6.17	5.66	1.80	–	0.38	0.12	98.54	1110	84
22	57.26	1.71	15.76	7.82	0.26	2.15	6.33	5.22	1.79	1.16	0.30	0.15	99.91	1110	84
23	58.21	1.70	15.15	7.84	0.20	1.97	6.44	4.95	1.74	1.23	0.30	0.13	99.86	1110	84
24	59.26	1.33	16.34	6.73	0.23	1.62	6.00	5.22	1.75	0.89	0.29	0.06	99.72	1110	60
25	59.45	1.47	16.58	6.29	0.18	1.63	5.53	5.83	1.84	0.36	0.29	0.05	99.50	1120	78
26	59.55	2.11	16.03	6.89	0.25	1.67	5.52	5.28	1.81	0.46	0.29	0.09	99.95	1110	60
27	60.39	1.60	14.86	8.16	0.23	1.99	5.47	4.74	1.77	0.28	0.30	0.13	99.92	1110	84
28	60.64	1.29	16.42	5.94	0.15	1.67	5.35	5.60	1.67	0.39	0.25	0.07	99.44	1120	78
29	60.71	1.69	15.48	7.02	0.24	1.68	5.68	4.42	1.77	0.59	0.33	0.06	99.67	1120	70
30	61.30	1.35	14.12	6.87	0.26	2.27	5.40	5.02	1.89	1.16	0.33	0.09	100.06	1110	84
31	62.45	1.22	15.49	6.23	0.21	1.57	5.32	3.88	2.12	0.46	0.29	0.06	99.30	1120	70
32	63.02	1.58	15.62	5.70	0.25	1.20	4.57	3.84	1.94	0.45	0.21	–	98.38	1120	78
33	63.64	0.98	16.88	4.31	0.16	1.02	3.77	4.84	3.10	0.59	0.31	0.07	99.67	1120	58
34	64.57	1.14	12.30	5.45	0.20	1.36	3.23	4.86	2.85	0.47	0.21	0.04	96.68	1120	52
35	67.10	0.90	13.85	5.66	0.21	1.28	3.55	4.22	2.21	0.33	0.20	0.08	99.59	1120	59
Sample K-4															
36	55.70	1.27	15.87	8.15	0.14	2.74	6.45	5.82	1.37	0.32	0.27	0.10	98.20	1100	80
37	56.67	1.47	15.36	8.54	0.46	2.70	6.81	5.71	1.68	0.36	0.26	0.07	100.09	1100	78
38	58.33	1.40	15.09	7.54	0.21	2.15	6.60	5.94	1.89	0.45	0.35	0.09	100.04	1100	78
39	61.68	1.47	14.20	7.75	0.21	2.00	5.34	4.65	1.96	0.33	0.26	0.06	99.91	1110	65
40	62.26	1.52	14.44	7.41	0.24	1.87	5.02	4.29	1.93	0.36	0.28	0.05	99.67	1110	65

Table 5. (Contd.)

Inclusion no.	Component												Total	T, °C	An
	SiO <sub>2</sub>	TiO <sub>2</sub>	Al <sub>2</sub> O <sub>3</sub>	FeO	MnO	MgO	CaO	Na <sub>2</sub> O	K <sub>2</sub> O	P <sub>2</sub> O <sub>5</sub>	Cl	S			
41	63.01	1.52	14.48	7.69	0.22	1.77	5.30	3.24	1.88	0.45	0.26	0.08	99.90	1110	69
42	64.13	0.92	15.38	5.60	0.17	1.57	5.07	4.06	2.29	0.32	0.21	0.08	99.80	1110	64
43	64.30	0.69	16.30	4.08	0.12	1.05	4.97	4.96	3.07	0.18	0.14	0.07	99.93	1110	58
44	64.70	1.39	14.06	6.03	0.20	1.48	4.40	3.98	2.77	0.53	0.19	0.06	99.79	1110	58
45	64.73	0.83	15.46	4.72	0.14	1.07	4.97	4.96	2.00	0.22	0.15	0.07	99.32	1110	59
46	65.21	1.02	14.64	4.48	0.20	1.06	3.66	4.18	2.03	0.24	0.17	0.08	96.97	1100	53
47	65.46	1.04	15.70	4.65	0.11	1.26	4.47	4.12	2.05	0.36	0.18	0.08	99.48	1100	53
48	65.75	0.94	14.13	4.93	0.18	1.18	3.62	3.65	2.54	0.37	0.16	0.06	97.51	1100	55
49	65.78	0.96	15.05	5.33	0.20	1.39	4.39	3.65	2.55	0.41	0.15	0.07	99.93	1100	53
Sample K-41															
50	47.27	0.67	18.93	6.34	0.16	5.56	10.56	7.07	0.25	0.15	0.04	0.09	97.09	1150	93
51	50.69	0.74	16.42	7.99	0.15	5.80	9.22	6.62	0.47	0.11	0.03	0.12	98.36	1150	93
52	65.93	0.37	13.77	2.02	0.12	0.63	2.29	3.64	2.55	0.09	0.17	0.01	91.59	20	49
53	66.05	0.40	13.80	2.21	0.00	0.59	2.10	4.54	2.40	0.12	0.19	0.01	92.41	20	47
54	66.76	0.32	13.89	2.31	0.11	0.64	2.23	4.40	2.46	0.00	0.15	0.00	93.27	20	63
55	68.24	0.46	14.00	2.59	0.14	0.66	2.26	4.20	2.56	0.06	0.19	0.01	95.37	20	63
56	68.32	0.21	13.93	2.32	0.11	0.64	2.15	4.48	2.46	0.08	0.19	0.01	94.90	20	47
57	69.95	0.47	13.73	2.94	0.03	0.89	2.23	4.44	2.47	0.10	0.19	0.02	97.46	20	63
Sample K-35															
58	71.76	0.21	13.16	0.94	0.03	0.27	0.83	4.97	3.32	0.00	0.20	0.01	95.70	1150	25
Sample K-31															
59	70.78	0.23	12.25	1.59	0.08	0.31	1.49	4.18	3.33	0.06	0.22	0.01	94.53	20	43
60	71.74	0.30	12.45	1.58	0.06	0.37	1.40	4.25	3.43	0.09	0.24	0.01	95.92	20	43
61	71.85	0.29	12.36	1.38	0.06	0.26	1.25	4.21	3.15	0.03	0.17	0.00	95.01	20	43
62	72.09	0.35	12.48	1.57	0.03	0.33	1.41	2.99	3.26	0.01	0.19	0.01	94.72	20	47
63	72.13	0.32	11.67	1.44	0.08	0.30	1.28	3.89	3.19	0.01	0.19	0.00	94.50	20	41
64	72.18	0.28	12.42	1.67	0.01	0.34	1.30	3.80	3.29	0.02	0.18	0.02	95.51	20	41
65	72.35	0.27	12.09	1.39	0.10	0.25	1.27	3.86	3.26	0.04	0.16	0.00	95.04	20	41
Sample K-23															
66	72.42	0.18	12.40	1.16	0.07	0.24	1.20	3.60	3.06	0.01	0.20	0.01	94.55	20	35
67	72.54	0.18	11.93	1.13	0.00	0.21	1.20	3.63	3.05	0.00	0.20	0.02	94.09	20	35
68	73.09	0.28	12.50	1.20	0.09	0.27	1.28	2.80	2.91	0.06	0.19	0.01	94.68	20	35

6.5 wt % on average) and CaO (5.2 wt % on average) at usual concentrations of Na<sub>2</sub>O (4.5 wt %) and K<sub>2</sub>O (2.1 wt %). The Cl concentration in the andesite melt is much higher than in the basalt melt (up to 0.26 wt % on average), and the S concentration is lower (up to 0.07 wt % on average).

The glasses of melt inclusions in plagioclase (An<sub>63-25</sub>) from the dacite and rhyodacite samples are characterized by usual concentrations (wt %) of SiO<sub>2</sub> (65.9-73.1), FeO (1.1-2.9), MgO (0.2-0.9), Na<sub>2</sub>O (2.8-5.0), and K<sub>2</sub>O (2.4-3.4). The Cl concentration of these melts is as high (0.19 wt % on average) as in the andesite melts, but the S concentration is much lower: 0.01 wt %. Ion microprobe analyses

Table 6.

**Concentrations of water (wt %) and trace elements (ppm) in melt inclusions in plagioclase from rocks from the Karymskii volcanic center, Kamchatka**

Comp nent	Inclusion no. in Table 5											
	50	3	4	53	54	56	60	61	62	65	67	58
H <sub>2</sub> O	0.69	2.44	-	7.27	4.64	4.97	5.14	5.87	3.12	4.96	6.65	4.75
Li	1750	284	118	25.2	22.3	23.2	14.8	14.6	16.0	15.8	22.2	73.7
Be	0.19	0.69	0.56	1.07	1.25	1.34	1.13	1.18	0.95	1.04	1.11	0.95
B	5.98	7.90	6.32	36.0	26.9	14.9	32.6	32.7	32.0	35.1	41.6	58.4
F	6.79	142	6.32	533	508	814	801	569	948	587	324	14.0
Cr	-	36.3	70.6	-	-	-	-	-	-	-	-	0.81
Rb	-	12.0	30.0	-	-	-	-	-	-	-	-	91.8
Sr	531	418	449	255	285	363	107	105	188	102	107	57.2
Y	8.90	15.2	19.3	19.8	16.1	9.19	18.6	21.5	22.4	22.9	16.9	8.15
Zr	17.5	55.9	64.1	134	107	58.2	183	177	204	209	140	57.2
Nb	0.42	1.88	1.87	2.89	2.53	1.46	4.05	4.31	6.30	4.96	3.71	3.69
Ba	88.1	187	236	413	481	461	629	629	734	685	606	1070
La	1.81	4.88	7.17	8.19	8.07	7.44	10.8	11.3	12.8	11.6	10.3	12.4
Ce	3.35	12.8	17.7	23.8	20.1	24.0	27.6	28.6	29.8	30.2	24.0	21.5
Nd	4.28	8.87	13.0	10.9	10.0	7.08	12.2	13.01	14.4	13.4	10.6	7.54
Sm	0.87	2.37	3.41	3.42	2.56	2.57	3.11	3.50	3.42	3.78	2.71	1.32
Eu	0.42	0.86	1.27	0.57	0.91	0.72	0.68	0.99	0.70	0.72	0.76	0.31
Gd	1.13	2.84	3.35	3.80	2.51	2.99	2.24	4.41	3.17	3.77	2.51	0.64
Dy	1.15	2.53	3.56	3.76	2.71	2.70	2.85	3.63	3.36	4.15	2.52	1.24
Er	0.77	1.83	2.59	2.87	2.08	2.09	2.17	2.68	2.61	3.08	2.00	1.04
Yb	0.79	2.03	2.35	2.86	2.00	1.80	1.25	2.97	2.2	3.32	2.26	1.25
Hf	-	1.69	2.17	-	-	-	-	-	-	-	-	1.78
Th	0.14	0.90	0.59	1.63	12.42	0.80	2.32	2.11	2.42	2.44	2.76	3.76
U	0.05	0.47	0.36	1.11	0.85	0.54	1.52	1.49	1.78	1.88	1.66	2.17
Th/U	2.80	1.91	1.64	1.47	1.67	1.48	1.53	1.42	1.36	1.30	1.66	1.73
La/Yb	2.29	2.40	3.05	2.86	3.804	4.13	4.12	3.80	4.71	3.49	4.56	9.92

of nine melt inclusions allowed us to determine the water concentrations during the crystallization of the plagioclase (Table 6). These concentrations turned out to be very high: from 3.1 to 7.3 wt % at an average of 5.5 wt %. It should be noted that dacite sample K-41 contained a plagioclase phenocryst ( $An_{93}$ ) with melt inclusions of composition analogous to those of inclusions in basalt sample K-2. They were also determined (Table 5) to bear high concentrations (wt %) of Na<sub>2</sub>O (6.6-7.1), MgO (5.6-5.8), and FeO (6.3-8.0) at low concentrations of K<sub>2</sub>O (0.2-0.5). It is pertinent to recall that sample K-2 is basalt erupted in 1996 at Novogodnii peninsula in the Akademii Nauk caldera, and sample K-41 was taken from the eastern wall of the Odnobokaya caldera (Fig. 1).

Table 7.

Chemical composition (wt %) of melt inclusions in (1-6) quartz from a buried pyroclastic flow in the Karymskii volcanic center, Kamchatka, and (7-10) quartz in dacites from Golovnina volcano, Kunashir Island

Component	1	2	3	4	5	6	7	8	9	10
SiO <sub>2</sub>	72.15	72.83	73.28	74.02	74.91	72.127	70.18	72.12	74.05	77.02
TiO <sub>2</sub>	0.24	0.1	0.12	0.09	0.11	0.1	0.24	0.19	0.16	0.16
Al <sub>2</sub> O <sub>3</sub>	12.82	12.51	12.98	12.44	12.95	12.83	10.95	11.78	11.02	9.29
FeO	1.30	0.51	0.57	0.54	1.25	0.67	1.57	1.25	1.18	0.90
MnO	0.04	0.06	0.07	0.13	0.15	0.11	0.040	0.15	0.08	0.04
MgO	0.27	0.12	0.16	0.06	0.24	0.210	0.27	0.21	0.20	0.19
CaO	1.23	0.66	0.88	0.62	1.19	0.68	1.43	1.35	1.04	0.98
Na <sub>2</sub> O	3.89	3.32	3.60	3.72	4.03	4.794	5.81	4.79	4.46	4.10
K <sub>2</sub> O	2.82	3.82	3.74	3.92	3.12	4.12	1.78	1.83	1.84	1.69
p <sub>2</sub> o <sub>5</sub>	0.02	0.04	0.020	0.06	0.01	0.04	0.02	0.02	0.04	0.10
Cl	0.14	0.1	0.140	0.1	0.15	0.140	0.28	0.26	0.26	0.19
H <sub>2</sub> O	4.89	4.88	4.20	3.41	0.90	1.64	6.68	5.73	4.98	5.10
<b>Total</b>	<b>99.81</b>	<b>98.97</b>	<b>99.70</b>	<b>99.12</b>	<b>99.21</b>	<b>99.21</b>	<b>99.21</b>	<b>99.68</b>	<b>99.31</b>	<b>99.76</b>
Li	18.2	13.6	21.0	18.9	16.9	24.0	0.16	0.59	0.27	4.42
Be	1.04	0.94	0.76	0.94	0.99	0.93	0.70	0.58	0.58	0.49
B	30.0	55.4	37.1	54.6	43.5	57.5	105	110	100	70.9
F	605	269	223	274	644	163	539	925	765	401
Cr	2.26	0.74	1.13	0.73	2.38	1.09	1.130	2.00	2.50	1.46
Rb	-	-	-	-	-	-	25.7	39.3	43.4	23.8
Sr	123	50.6	113	54.9	121	59.1	74.0	68.2	56.5	45.2
Y	15.8	11.5	7.20	9.62	26.6	8.65	37.8	29.8	27.8	20.6
Zr	163	64.0	63.2	59.9	237	56.5	148	121	111	95.3
Nb	3.22	5.44	2.90	4.14	4.19	3.85	1.35	1.44	1.46	1.10
Ba	563	843	782	933	556	778	464	575	554	323
La	11.6	14.7	9.82	12.5	14.7	10.7	8.02	9.12	8.29	5.87
Ce	28.0	22.2	19.2	25.0	36.8	20.9	21.9	20.4	21.1	13.6
Nd	13.9	10.3	7.24	8.91	21.1	8.912	12.7	12.5	12.3	8.25
Sm	2.87	1.52	1.40	2.15	5.12	1.48	3.84	3.43	3.27	2.25
Eu	0.77	0.74	0.47	0.81	1.12	0.21	0.43	0.61	0.81	0.49
Gd	2.78	1.45	1.08	1.60	5.19	1.82	4.89	5.01	4.76	2.14
Dy	2.64	1.44	1.09	1.57	4.31	1.44	5.35	4.83	4.52	2.96
Er	1.69	1.27	0.92	1.34	3.13	1.02	4.47	3.89	3.48	2.32
Yb	1.91	1.35	0.95	1.53	3.19	1.20	5.45	4.29	9.35	2.84
Hf	4.28	2.21	1.85	1.96	5.26	1.63	4.94	4.79	4.75	3.08
Th	1.99	4.66	2.54	4.52	2.28	3.53	2.77	2.49	2.34	1.84
U	1.38	2.90	1.73	2.77	1.48	2.19	1.27	1.31	1.17	0.82
Th/U	1.44	1.61	1.55	1.63	1.54	1.61	2.18	1.90	2.00	2.24
La/Yb	6.07	10.9	10.3	8.17	4.61	8.92	1.47	2.12	0.89	2.07

Note: Oxides are given in wt %, trace elements are in ppm.

Table 8.

Average La and Yb concentrations (ppm) and the La/Yb ratio of melt inclusions in minerals of volcanic rocks from Kuriles and Kamchatka

Volcano	Rock	Mineral	n	La	Yb	La/Yb
<b>Kurile Islands</b>						
<b>Golovnina, Kunashir Island</b>	dacite	quartz	4	7.8	5.5	1.4
<b>Kudryavyi, Iturup Island</b>	basaltic	plagioclase	2	4.9	4.0	1.2
<b>Men'shoi Brat, Iturup</b>	basaltic	plagioclase	2	9.4	5.3	1.8
<b>Cjikurachki, Paramushir</b>	basalt	olivine	19	6.9	2.8	2.5
<b>Kamchatka</b>						
<b>Karymskii</b>	basalt	plagioclase	3	4.6	1.7	2.7
	dacite	plagioclase	9	10.3	2.4	4.3
<b>rr</b>	rhyodacite	quartz	6	12.3	1.7	7.2
<b>Klyuchevskoi**</b>	basalt	olivine	78	5.1	1.9	2.7
<b>Avachinskii***</b>	avachite	olivine	5	6.9	1.5	4.6
<b>Avachinskii</b>	andesite	plagioclase	2	7.3	1.2	6.1
<b>Bezemyannyi</b>	andesite	plagioclase	3	11.8	1.5	7.9
<b>Dikii Greben'</b>	dacite	plagioclase	2	11.8	1.4	8.4
<b>Shiveluch</b>	andesite	plagioclase	7	9.1	0.7	13.0

Note: \* Data from [10], \*\* data from (Mironov and Portnyagin, in press), \*\*\* data from [21]; *n* is the number of analyses.

The SiO<sub>2</sub> contents in the glasses of melt inclusions in quartz from the buried pyroclastic flow (Table 7) are even lower: from 72.2 to 75.7 wt %. These acid melts bear usual concentrations (wt %) of TiO<sub>2</sub> (0.09-0.31), FeO (0.5-1.3), MgO (0.06-0.27), CaO (0.6-1.2), Na<sub>2</sub>O (3.3-4.0), K<sub>2</sub>O (2.8-4.1), and Cl (0.10-0.15). The water concentration in the melt varied from 0.9 to 4.9 wt % (at an average of 3.3 wt % of six analyses).

In order to compare them with the compositions of acid melts from the Karymskii volcanic center, we examined melt inclusions in quartz from dacite from Golovnina volcano. These inclusions (Fig. 2) are large, up to 100-140µm and are either partly recrystallized (Figs. 2a, 2b) or contain only glass and small gas bubbles (Fig. 2c). The complete homogenization temperatures of these inclusions are 820-850°C, and the inclusions usually homogenized for no more than 5-10 min. The melts heterogenized with the separation of numerous gas bubbles (Fig. 2d) at temperatures of 700-780°C for 15-30 s, which testifies that the melt has a low viscosity. This behavior of the inclusions in our thermal experiments definitely indicates that the melt contained much water, which also follows from ion microprobe analyses of the inclusions (5.0-6.7 wt % H<sub>2</sub>O at an average of 5.6 wt % of six analyses; Table 7). Compared to the acid melts of the Karymskii volcanic center, these melts are richer in Na<sub>2</sub>O (4.1-5.8 wt %) and Cl (0.19-0.28 wt %) but poorer in K<sub>2</sub>O (1.7-1.8 wt %).

## DISCUSSION

Microprobe analysis of glasses in inclusions reveals very interesting compositional features of the melts of the Karymskii volcanic center. When plotted in a  $\text{SiO}_2$  vs.  $(\text{Na}_2\text{O} + \text{K}_2\text{O})$  diagram, most of the melts correspond to alkaline varieties from tephrite to trachyte, although some melts have lower alkalinity (Fig. 3). The rocks (Table 1) do not, however, contain elevated concentrations of alkalis. Another noteworthy feature is that the compositional trend in the diagram is nearly parallel to the abscissa, i.e., an increase in the silicity of the melts is not associated with an increase in the sum of alkalis, whereas crystallization differentiation should have resulted a simultaneous increase in both silica and alkalis.

The evolution of the melt is illustrated more comprehensively in Fig. 4. The behavior of various major components can be provisionally classified into the following three types:

1. The concentrations of  $\text{Al}_2\text{O}_3$ ,  $\text{MgO}$ , and  $\text{CaO}$  systematically decrease with increasing  $\text{SiO}_2$ , and the concentration of  $\text{K}_2\text{O}$  simultaneously increases. The trends have no bends and are typical of crystallization differentiation processes.

2. The concentrations of  $\text{TiO}_2$  and  $\text{FeO}$  systematically decrease with increasing  $\text{SiO}_2$  only until  $\text{SiO}_2 > 57$  wt % because of the precipitation of ore components in the course of crystallization differentiation. In more basic melts, which were found in inclusions in plagioclase from sample K-2 (basalt of the 1996 eruption at the Akademii Nauk caldera), the  $\text{TiO}_2$  concentration even slightly increases (from 0.7 to 1.3 wt %). Much higher  $\text{TiO}_2$  concentrations were detected in inclusions in plagioclase from samples K-4 and K-63 (andesite of the 1996 and 1997 eruptions of Karymskii volcano).  $\text{TiO}_2$  concentrations higher than 1.3 wt % were found in 17 melt inclusions. The  $\text{FeO}$  concentration remains practically unchanging (7-9 wt %) at  $\text{SiO}_2 < 57$  wt % (sample K-2, Fig. 4).

The most unexpected behavior shows  $\text{Na}_2\text{O}$ , whose content decreases with increasing silicity, and the plot (Fig. 4) displays two compositional trends. In one of them, the  $\text{Na}_2\text{O}$  concentration varies from 7.5 to 3 wt % within a relatively narrow range of  $\text{SiO}_2$  (47-57 wt %), whereas the other trend has a gentler slope, with  $\text{Na}_2\text{O}$  varying from 6 to 3 wt % at  $\text{SiO}_2$  changing from 57 to 73 wt %. The former trend was obtained for basalt (sample K-2), and the latter is for andesite (samples K-4 and K-63) and dacite (samples K-41 and K-31).

The basaltic melts of the Karymskii volcanic center ( $\text{SiO}_2 = 47-57$  wt %) are characterized, along with high  $\text{Na}_2\text{O}$  concentrations, also by high  $\text{Na}_2\text{O}/\text{K}_2\text{O}$  ratios, which is equal to 8.0 on average (average of 23 analyses). Equally high  $\text{Na}_2\text{O}$  concentrations and similar  $\text{Na}_2\text{O}/\text{K}_2\text{O}$  ratios were previously detected in xenoliths from Mongolia and Yemen [11, 1). Glasses in peridotite xenoliths from alkaline basalts from Mongolia [11] contain 51.8-57.0 wt %  $\text{SiO}_2$  and 6.8-10.6 wt %  $\text{Na}_2\text{O}$  and have  $\text{Na}_2\text{O}/\text{K}_2\text{O} = 4.5-17.2$  at an average of 8.6 (19

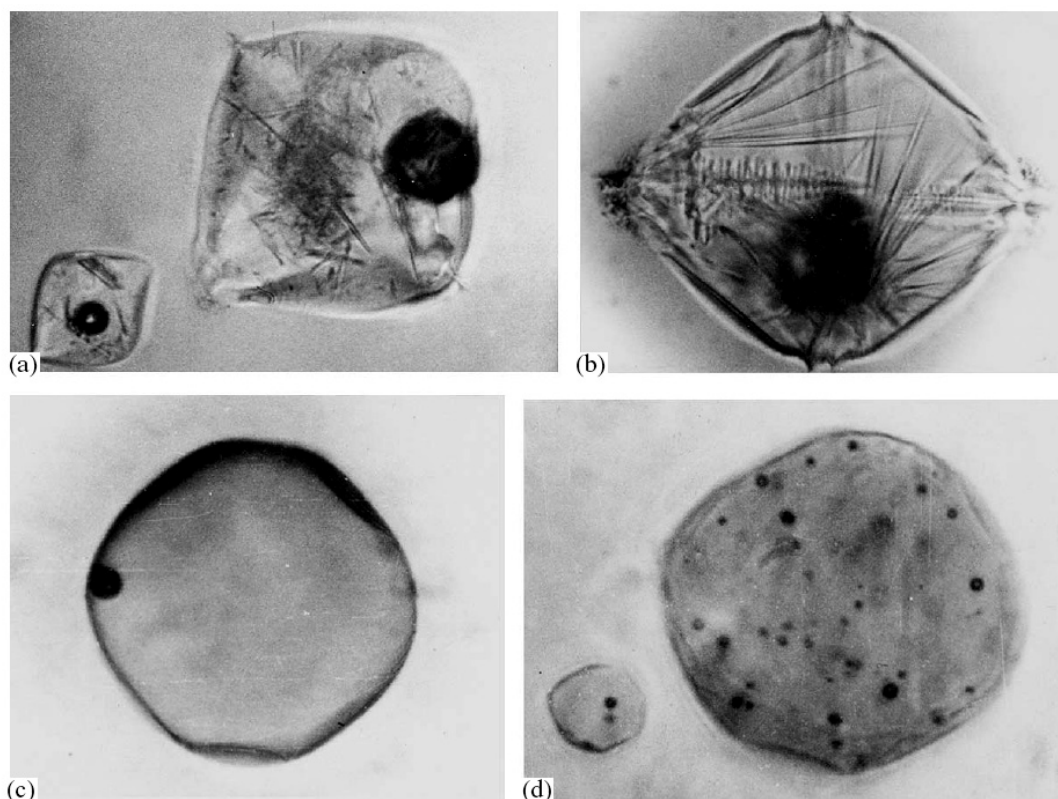


**Fig. 2. Melt inclusions in quartz from dacite of Golovkina volcano. Sizes of inclusions: (a, c) 100  $\mu\text{m}$ ; (b, d) 50  $\mu\text{m}$ .**

analyses). The glasses found in spinel lherzolites from Yemen [1] contain 50.0-55.8 wt %  $\text{SiO}_2$  and 5.9-8.9 wt %  $\text{Na}_2\text{O}$  at  $\text{Na}_2\text{O}/\text{K}_2\text{O} = 7.5-14.1$  (average 9.7 of 15 analyses). The authors of these publications considered the genesis of such melts problematic and thought it could have been affected by mantle metasomatism under the effect of sodic mantle fluid.

The comparison of the compositional fields of the melts (Fig. 5) from various volcanoes (Karymskii volcanic center, Bezmyannyi, and Shiveluch) demonstrates that the volcanics of the Karymskii volcanic center show the broadest spectrum of melt compositions (including basic varieties enriched in Fe, Mg, and Ti). At the same time, the compositional trends of these melts are pronounced much more clearly in the variation diagrams, and the paired correlations of major components are stronger than those of the products of Bezmyannyi and Shiveluch volcanoes.

The distributions of incompatible elements in the basaltic and dacite-rhyolitic melts of the Karymskii volcanic center and in the rhyolitic melts of Golovkina volcano (Fig. 6) suggest an arc provenance of all of these melts. Inasmuch as the most strongly incompatible elements practically do not fractionate one relative

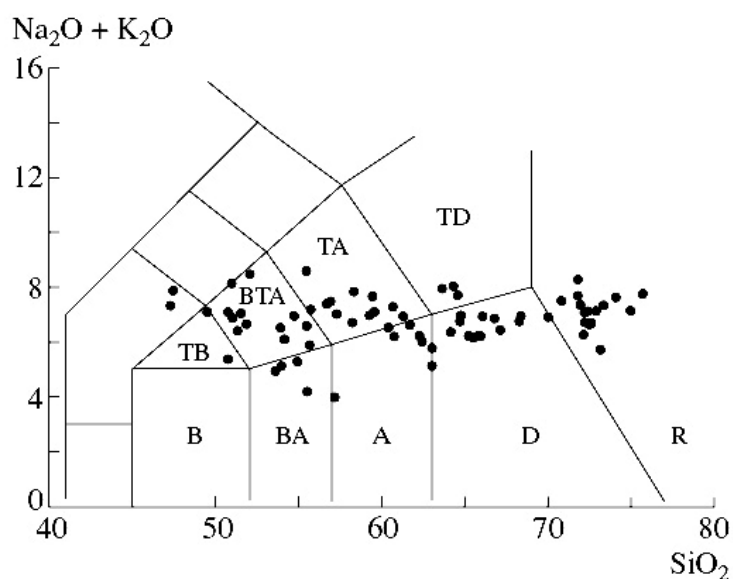


**Fig. 3.**  $\text{SiO}_2$ - $(\text{Na}_2\text{O} + \text{K}_2\text{O})$  classification diagram (Le Bas et al., 1986) for the composition of melt inclusions. Rocks: B—basalt, TB—trachybasalt, BA—basaltic andesite, BTA—basaltic trachyandesite, A—andesite; TA—trachyandesite, D—dacite, TD—trachydacite, R—rhyolite.

another during crystallization, their bulk concentrations can provide information on the magmatic source of the volcanic center. The arc

characteristics of the melts of the Karymskii volcanic center include, for example, Nb minima and high B a/Th ratios relative to those in MORB. These features are characteristic of both the most primitive and the most differentiated melts. This points to a state of the mantle source, which was probably metasomatized by a fluid component enriched in LREE and relatively depleted in Nb. The magmatic source of the Karymskii volcanic center shows some distinctive features, first of all, relative enrichment in Li, which is pronounced particularly conspicuously in comparison with the melts of Golovnina volcano. Note that the enrichment in Li relative to HREE and Y compared to MORB is typical of many basic arc magmas (Portnyagin et al., 2007). However, the absolute concentrations of this element usually do not exceed 5-6 ppm, whereas the basic melts of the Karymskii volcanic center contain 19 to 290 times more Li, and the acid melts contain 2-12 times more this element. The difference for acid arc melts is even more significant (Fig. 6). Note that Li-rich melts are also noted for elevated Na concentrations (up to 7.5 wt %). These values are generally atypical of basic melts.

It is interesting that, according to the analyses reported in [19], some inclusions in olivine from Karymskii volcano correspond to basic melts with an average  $\text{Na}_2\text{O}$  concentration of 2.9 wt % and 5.23 ppm Li. The concentrations of incompatible elements reported by these researchers and ourselves were analyzed on the same equipment and with the use of the same standards, which rules out analytical errors. Thus, the relatively primitive melts of the Karymskii volcanic center (basic melts depleted in incompatible elements, including LREE) or some of them differ from most analogous basic magmas elsewhere in having elevated concentrations of Na and Li. The reasons for this enrichment remain uncertain. As one of the possible explanation variants, it could have been melt contamination with crustal minerals, for example, zeolites of the natrolite group, which were formed in the source from the material of ancient basalts of the volcanic center. The absence of information on these minerals makes it hard to draw any more specific conclusions.

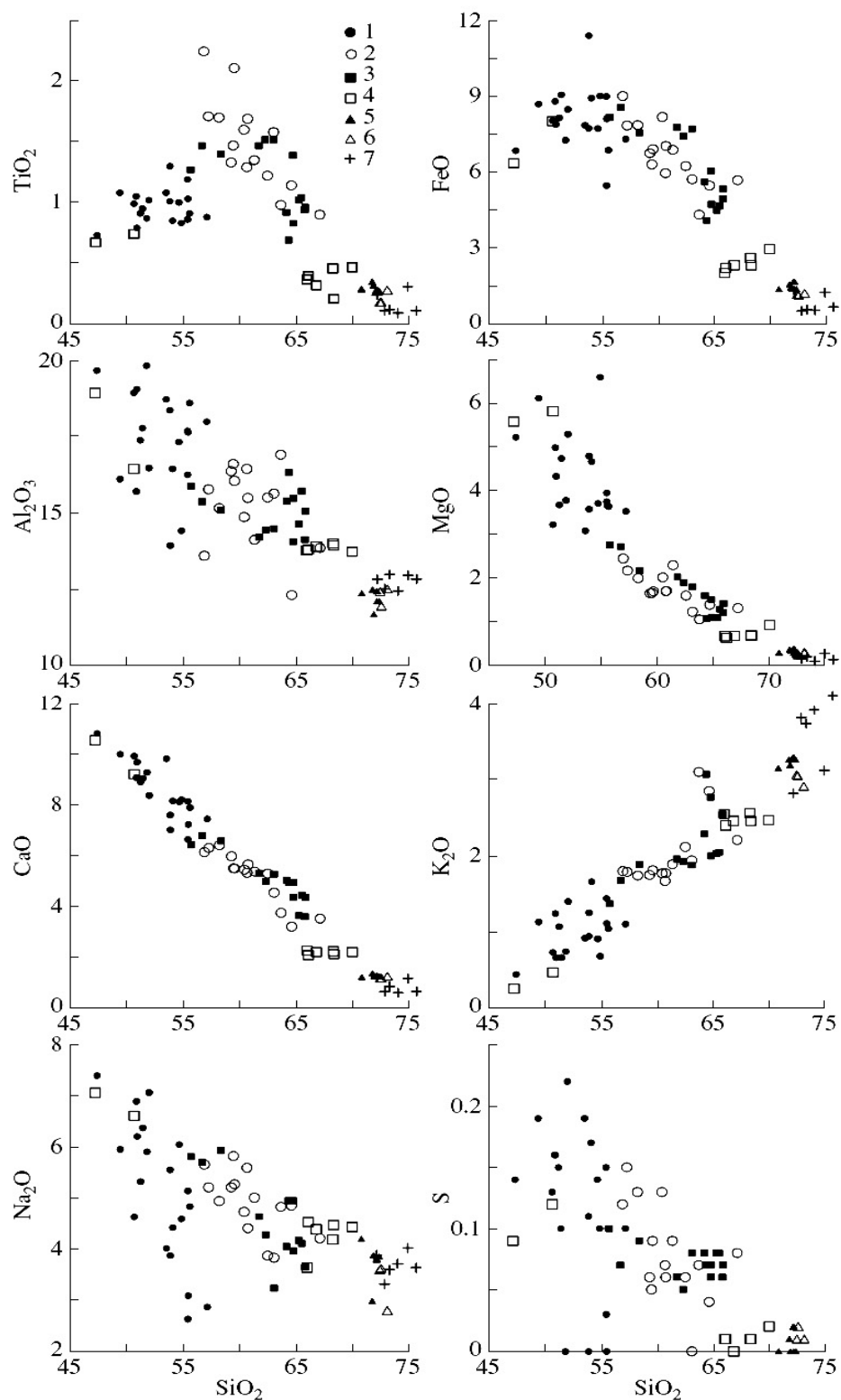


**Fig. 4. Variation diagrams SiO<sub>2</sub>–major element and SiO<sub>2</sub>–S (wt %) for the compositions of melt inclusions in (1–6) plagioclase and (7) quartz from the Karymskii volcanic center.**

Samples: (1) K-2; (2) K-63; (3) K-4; (4) K-41; (5) K-31; (6) K-23.

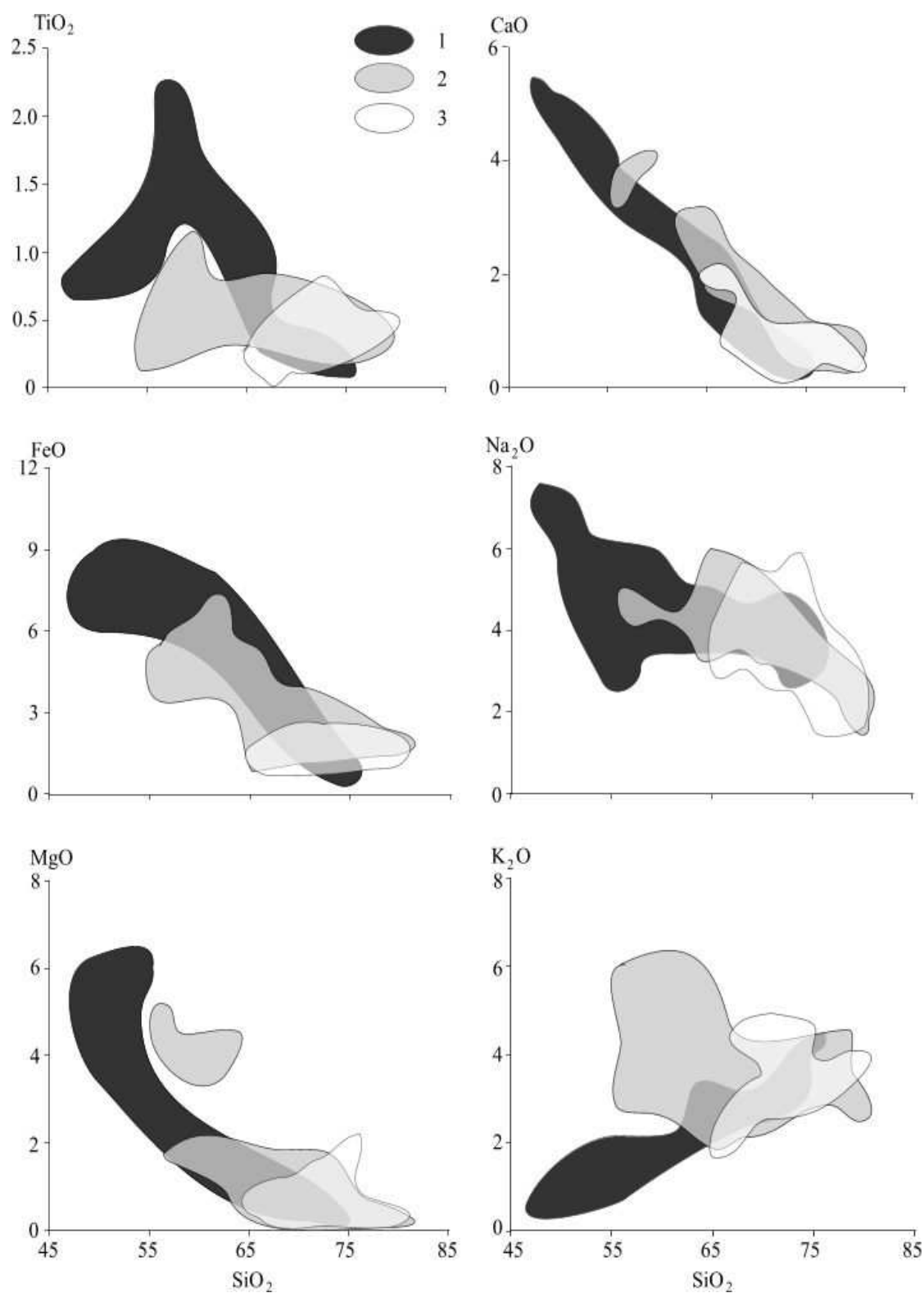


**Fig. 5. Comparison of the composition (wt %) of melt inclusions in phenocrysts in volcanic rocks from (1) the Karymskii volcanic center, (2) Bezmyannyi, and (3) Shiveluch volcanoes.**

Number of analyses of inclusions: Karymskii volcanic center—73, Bezmyannyi volcano—47, Shiveluch volcano—38.

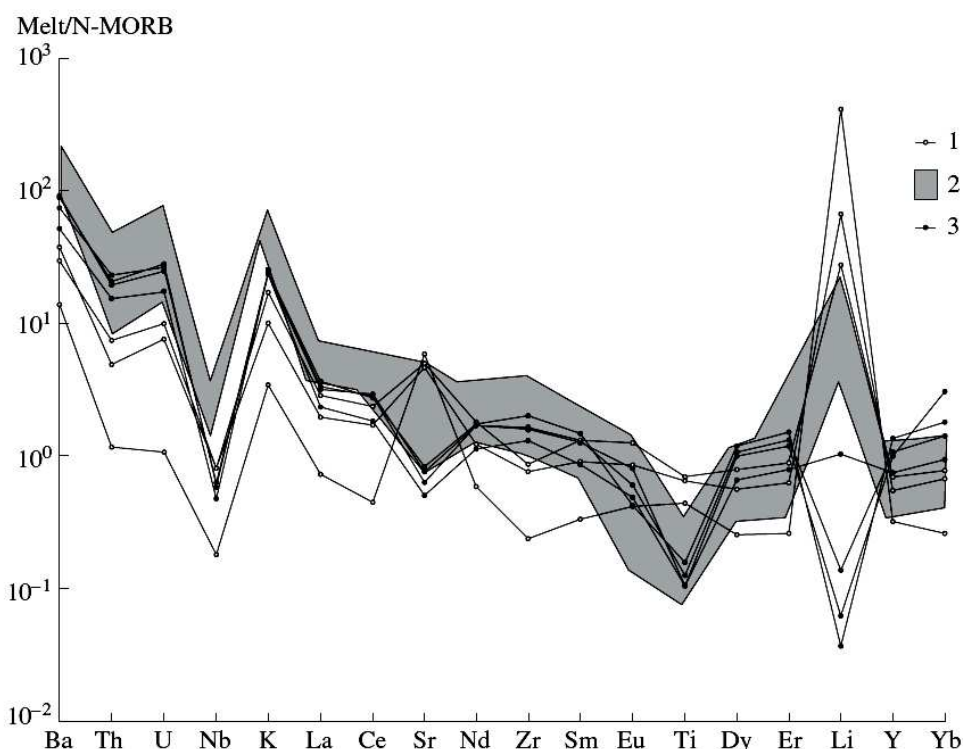


**Fig. 6. N-MORB (Sun and McDonough, 1989) normalized trace-element composition of the melt inclusions.**

(1, 2) Karymskii volcanic center: (1) basaltic melts, (2) rhyodacitic melts; (3) rhyolitic melts of Golovnina volcano.

Note that one of the samples in which the melt inclusions with high Na and Li concentrations were found was taken from a wall of the ancient caldera, and the other two samples were collected during the 1996 eruption. This led us to conclude that either the assimilation processes of crustal material were multiple over a long time period or the residence time of phenocrysts that crystallized from the melt was very long in shallow sitting chambers.

It is also difficult to reproduce the process because all minerals containing appreciable Li concentrations are either secondary (zeolites) or crystallize from differentiated melts late in the crystallization process of magmatic bodies (pegmatite minerals). Thus, as follows from available mineralogical data, the melt could enrich in these elements only near the surface via the reworking of crustal material.

A secondary nature of the Li- and Na-enriched phase can be ruled out: first, the inclusions are primary (as follows from their morphology); second, the rocks were not affected by secondary alterations because all of them were collected when still hot during the 1996 eruption; and, third, the features listed above are also inherited by more acid (i.e., more differentiated) melts of the volcanic center. Thus,

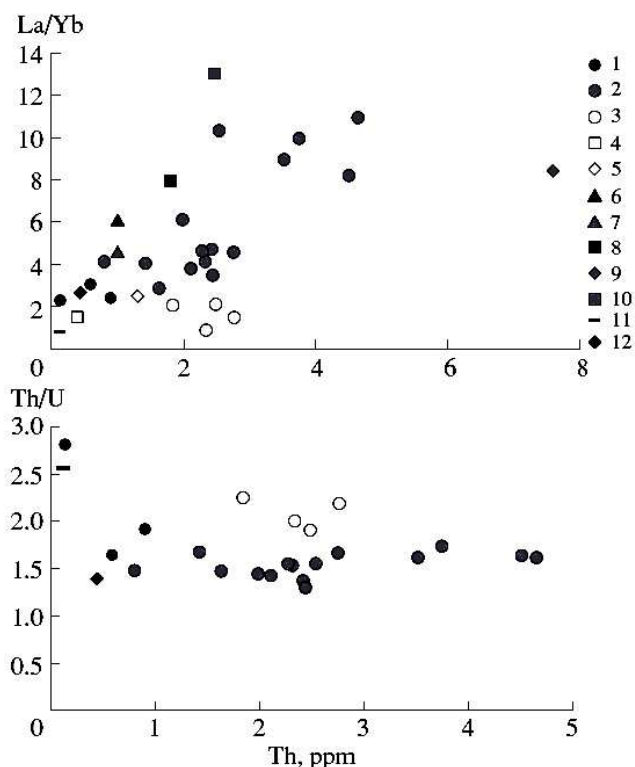


**Fig. 7. Th-La/Yb and Th-Th/U diagrams for melt inclusions in minerals from volcanic rocks of Kamchatka and the Kurile Islands.**

(1, 2) Karymskii volcanic center: (1) basalts, (2) andesites and dacites; (3) Golovnina volcano, Kunashir Island; (4) Medvezh'ya caldera, Iturup Island [13]; (5) Chikurachki volcano, Paramushir Island [10]; (6, 7) Avachinskii volcano: (6) according to [24], (7) according to [19]; (8) Bezymyannyi volcano; (9) Dikii Greben' volcano; (10) Shiveluch volcano; (11) N-MORB [23]; (12) Kly-uchevskoi volcano [19].

relative enrichment in Li is characteristic of all melts of the Karymskii volcanic center.

Li behavior in melts of the Karymskii volcanic center should be considered anomalous, because this element should enrich melts in compliance with the classic differentiation scheme. In our situation, more acid melts have lower Li concentrations than more basic varieties. Because of this, we cannot rule out the mixing of basic melts with high Li concentrations with acid melts and the resultant enrichment of the latter in Li. Figure 7 shows the La/Yb-Th and Th/U-Th relations for various volcanics from the Kurile-Kamchatka island arc and depleted MORB. As can be seen, the La/Yb ratio of the melts suggests their different degrees of differentiation. The melts of Golovnina volcano have La/Yb = 1.4, which is very close to the values of MORB (Table 8, Fig. 7). In this diagram (Fig. 7), other melts similar to MORB are from Kudryavyi and Men'shoi Brat volcanoes in Iturup Island, Kuriles, and the basaltic melts of the Karymskii volcanic center and Klyuchevskoi volcano in Kamchatka. The andesite-dacite melts of Karymskii and Avachinskii volcanoes (inclusions in olivine and plagioclase) plot slightly farther away from N-MORB. The melts of the southern sector of the Karymskii volcanic center, Bezymyannyi, Dikii Greben', and Shiveluch volcanoes are differentiated even more strongly.

The Th/U ratio in melts from the Karymskii volcanic center (Fig. 7) almost does not vary for all of the compositions and lies within the range of 1.3-1.9. At the same time, a basaltic melt with a remarkably higher Th/U ratio (equal to 2.8) was found. This melt is characterized by the highest Li concentration (1750 ppm) and a very high concentration of Na<sub>2</sub>O (7.1 wt %) and the lowest content of K<sub>2</sub>O (0.25 wt %). Acid melts from Golovnina volcano have Th/U ratios from 1.9 to 2.2.

Interpreting the analyses, it can be concluded that the Karymskii volcanic center was produced as a result of the fairly complicated evolution of the melts. The most primitive of them exhibit anomalously high concentrations of Na and Li.

The genesis of these unusual melts should be further elucidated. The possible sources of the Li-Na complex could be zeolites of the natrolite group or Li micas. In any event, the melts should have been contaminated with crustal material. It is necessary to determine the composition of rock-forming melts in inclusions in mafic minerals: pyroxenes, olivine, and amphiboles and to examine the trace-element composition of the secondary minerals that developed in the Karymskii volcanic center.

## CONCLUSIONS

1. We have examined more than 80 melt inclusions in phenocrysts from basalt, andesites, dacites, and rhyodacites from the Karymskii volcanic center, Kamchatka, and dacites from Golovnina volcano, Kunashir Island, Kuriles. The SiO<sub>2</sub> concentrations in melt inclusions in phenocrysts from the Karymskii volcanic center range from 47 to 57 wt % in plagioclase phenocrysts from basalts, from 56 to 67 wt % in plagioclase phenocrysts in andesites, from 66 to 73 wt % in plagioclase phenocrysts from dacites and rhyodacites, and from 72 to 76 wt % in quartz phenocrysts from dacites and rhyodacites. The SiO<sub>2</sub> concentration in melt inclusions in quartz from dacites of Golovnina volcano varies from 70 to 77 wt %.

2. It was determined that basaltic melts of the Karymskii volcanic center are significantly enriched in Na (Na<sub>2</sub>O = 2.9-7.4 wt % at an average of 5.1 wt % of 23 analyses), with the highest Na<sub>2</sub>O concentrations found in the most basic melts (SiO<sub>2</sub> = 47-52 wt %). These melts are characterized by very high Na<sub>2</sub>O/K<sub>2</sub>O ratios equal to 8.0 on average.

3. Concentrations of volatile components were determined in the basaltic melts of the Karymskii volcanic center (1.6 wt % H<sub>2</sub>O, 0.14 wt % S, 0.09 wt % Cl, and 50 ppm F) and in dacitic and rhyodacitic melts (0.9-7.3 wt % H<sub>2</sub>O at an average of 4.5 wt % of 15 analyses; 0.15 wt % Cl; 600 ppm F; and 100 ppm S). The H<sub>2</sub>O concentrations in melt inclusions in quartz from dacites of Golovnina volcano are higher (5.0-6.7 wt % at an average of 5.6 wt %), the Cl concentrations are also high (0.19-0.28 wt %), and the F concentrations are 660 ppm.

4. The comparison of the composition of melts from the Karymskii volcanic center with those of the previously examined melts of Bezmyannyi and Shiveluch volcanoes revealed their significant differences. The former are more basic and are enriched in Ti, Fe, Mg, Ca, Na, and P but are notably depleted in K. The melts of the Karymskii volcanic center are likely less differentiated than the melts of Bezmyannyi and Shiveluch volcanoes.

5. Concentrations of 20 trace elements were measured on an ion microprobe in the glasses of 22 melt inclusions in plagioclase and quartz. An unusual feature is the very high Li concentrations (along with high concentrations of Na) in the basaltic melts of the Karymskii volcanic center (118-1750 ppm), whereas the dacitic and rhyolitic melts contain 25 ppm Li on average. The rhyolitic melts of Golovnina volcano contain much less Li: 1.4 ppm on average. The La/Yb, Th-La/Yb, and Th-Th/U relations of the melts suggest their different degrees of differentiation.

The melts of the Karymskii volcanic center are characterized by relative Nb and Ti minima and Ba and K maxima, as is typical of arc magmas.

## ACKNOWLEDGMENTS

The authors thank A. A. Kadik (Vernadsky Institute of Geochemistry and Analytical Chemistry, Russian Academy of Sciences) for quartz phenocrysts from dacite from Golovnina volcano provided for this research and A.V. Sobolev (Vernadsky Institute of Geochemistry and Analytical Chemistry, Russian Academy of Sciences) and V. V. Yarmolyuk (Institute of the Geology of Ore Deposits, Petrography, Mineralogy, and Geochemistry, Russian Academy of Sciences) for constructive criticism of the text. This study was financially supported by the Russian Foundation for Basic Research (projects 04-05-65123, 05-05-64730, and 07-05-00497), Project 06-III-A-08-329 of the Far East Division, Russian Academy of Sciences, Program for the Support of Leading Research Schools (project 2006-RI-112.0/001/008), and a program of the Division of Earth Sciences of the Russian Academy of Sciences.

## REFERENCES

1. **G. Chazot, M. Menzies, and B. Harte**, "Silicate Glasses in Spinel Lherzolites from Yemen: Origin and Chemical Composition," *Chem. Geol.*, 159-179 (1996).
2. **S. A. Fedotov**, "Study and Mechanism of the 1996 Akademii Nauk Caldera and Karymsky Volcano Eruptions in Kamchatka," *Vulkanol. Seismol.*, No. 5, 3-37 (1997).
3. **T. I. Frolova, I. A. Burikova, A. V. Gushchin, et al.**, *Origin of the Island Arc Series (Nedra, Moscow, 1985)* [in Russian].
4. **G. S. Gorshkov**, *Volcanism of the Kuril Island Arc* (Nauka, Moscow, 1967), pp. 178-180 [in Russian].
5. **E. N. Grib and V. L. Leonov**, "Evolution of the Caldera Magmatic Chambers in the Southern Sector of the Karymsky Volcanic Center. Part 1. Geology, Structure, and Composition of Pyroclastic Flows," *Vulkanol. Seismol.*, No. 4, 21-40 (2004a).
6. **E. N. Grib and V. L. Leonov**, "Evolution of the Caldera Magmatic Chambers in the Southern Sector of the Karymsky Volcanic Center. Part 2. PTF-Crystallization Conditions of Ignimbrite-Forming Melts, Magmatic Evolution," *Vulkanol. Seismol.*, No. 5, 23-37 (2004b).
7. **E. N. Grib and V. L. Leonov**, "Different Evolution Trends of the Upper Crustal Magmatic Chambers of the Caldera Complexes of Eastern Kamchatka. Part 1. Structure of Pyroclastic Flows: Comparative Mineralogy," *Vulkanol. Seismol.*, No. 4, 3-17 (2001a).
8. **E. N. Grib and V. L. Leonov**, "Different Evolution Trends of Upper Crustal Magmatic Chambers of the Caldera Complexes of Eastern Kamchatka. Part 2. Physicochemical Crystallization Conditions of the Ignimbrite-Forming Melts," *Vulkanol. Seismol.*, No. 4, 18-28 (2001b).
9. **E. N. Grib**, "Petrology of the Products of Akademii Nauk Caldera Eruption on January 2-3, 1996," *Vulkanol. Seismol.*, No. 5, 71-96 (1997).
10. **A. A. Gurenko, A. B. Belousov, R. B. Trumbull, and A.V. Sobolev**, "Explosive Basaltic Volcanism of the Chikurachki Volcano (Kurile Arc, Russia): Insights on Pre-Eruptive Magmatic Conditions and Volatile Budget Revealed from Phenocryst-Hosted Melt Inclusions and Groundmass Glasses," *J. Volcanol. Geotherm. Res.* 147, 203-232 (2005).
11. **D. A. Ionov, A. W. Hofmann, and N. Shimizu**, "Metasomatism-Induced Melting in Mantle Xenoliths from Mongolia," *J. Petrol.* 35, 753-785 (1994).

12. **B. V. Ivanov**, 1962-1956 Karymsky Volcano Eruption and the Karymsky Volcanic Group (Nauka, Moscow, 1970) [in Russian].
13. **V. I. Kovalenko, V. B. Naumov, M. L. Tolstykh, et al.**, "Composition and Sources of Magmas in Medvezh'ya Caldera (Iturup Island, Southern Kuriles) from a Study of Melt Inclusions," *Geokhimiya*, No. 5, 467-487 (2004) [*Geochem. Int.* 42, 393-413 (2004)].
14. **M. J. Le Bas, R. V. Maitre, A. Streckeisen, and B. A. Zannettin**, "A Chemical Classification of Volcanic Rocks Based on the Total Alkali-Silica Diagram," *J. Petrol.* 27, 745-750 (1986).
15. **V. B. Naumov, M. V. Portnyagin, M. L. Tolstykh, and V. V. Yarmolyuk**, "Composition of Magmatic Melts from the Southern Baikal Volcanic Region: A Study of Inclusions in Olivine from Trachybasalts," *Geokhimiya*, No. 3, 243-253 (2003) [*Geochem. Int.* 41, 213-223 (2003)].
16. **V. B. Naumov, V. S. Karpukhina, E. N. Baranov, and N. N. Kononkova**, "Melt Compositions, Contents of Volatile Components and Trace Elements, and Temperatures of Quartz Crystallization in Silicic Volcanic Rocks of the Verkhneural'sk Ore District (Southern Urals)," *Geokhimiya*, No. 4, 339-351 (1999) [*Geochem. Int.* 37, 289-301 (1999)].
17. **A. Nosova, L. V. Sazonova, V. V. Narkisova, and S. G. Simakin**, "Minor Elements in Clinopyroxene from Paleozoic Volcanics of the Tagil Island Arc in the Central Urals," *Geokhimiya*, No. 3, 254-268 (2002) [*Geochem. Int.* 40, 219-232 (2002)].
18. **A. Yu. Ozerov**, "Dynamics of the 1996 Karymsky Volcano Eruption and composition of Its Products," *Vestnik DVO RAN*, No. 3, 86-93 (1997).
19. **M. Portnyagin, K. Hoernle, P. Plechov, et al.**, "Constraints on Mantle Melting and Composition and Nature of Slab Components in Volcanic Arcs from Volatiles (H<sub>2</sub>O, S, Cl, F) and Trace Elements in Melt Inclusions from the Kamchatka Arc," *Earth Planet. Sci. Lett.* 255, 53-69 (2007).
20. **M. V. Portnyagin, N. L. Mironov, S. V. Matveev, and P. Yu. Plechov**, "Petrology of Avachites, High-Magnesian Basalts of Avachinsky Volcano, Kamchatka: II. Melt Inclusions in Olivine," *Petrologiya* 13, 358-388 (2005) [*Petrology* 13, 322-351 (2005)].
21. **M. V. Portnyagin, S. G. Simakin, and A. V. Sobolev**, "Fluorine in Primitive Magmas of the Troodos Ophiolite Complex, Cyprus: Analytical Methods and Main Results," *Geokhimiya*, No. 7, 691-699 (2002) [*Geochem. Int.* 40, 625-632 (2002)].
22. **A. V. Sobolev**, "Melt Inclusions in Minerals as a Source of Principle Petrological Information," *Petrologiya* 4, 228-239 (1996) [*Petrology* 4, 209-220 (1996)].
23. **S.-S. Sun and W. F. McDonough**, "Chemical and Isotopic Systematics of Oceanic Basalts: Implications for Mantle Composition and Processes," in *Magmatism in the Ocean Basins*, Ed. by A. D. Saunders and M. J. Norry, *Geol. Soc. London Spec. Publ.* 42, 313-345 (1989).
24. **M. L. Tolstykh, V. B. Naumov, A. D. Babanskii, et al.**, "Chemical Composition, Volatile Components, and Trace Elements in Andesitic Magmas of the Kurile Kamchatka Region," *Petrologiya* 11, 451-471 (2003) [*Petrology* 11, 407-425 (2003)].
25. **M. L. Tolstykh, V. B. Naumov, A. Yu. Ozerov, and N. N. Kononkova**, "Composition of Magmas of the 1996 Eruption at the Karymskii Volcanic Center, Kamchatka: Evidence from Melt Inclusions," *Geochem. Int.* 39 (5), 447-458 (2001).
26. **M. L. Tolstykh, V. B. Naumov, and N. N. Kononkova**, "Three Types of Melt in the Basaltic Andesite from the Medvezh'ya Caldera, Iturup, Southern Kuril Islands" *Geokhimiya*, No. 4, 391-397 (1997) [*Geochem. Int.* 35, 339-345 (1997)].
27. **V. I. Vlodayets**, "Volcanoes of the Karymsky Group," *Tr. Kamchat. Vulkanost.*, No. 3, 3-48 (1947).
28. **Volcanic Center: Structure, Dynamics, and Composition (Karymsky Structure)**, Ed. by Yu. P. Masurenkov (Nauka, Moscow, 1980) [in Russian]

# Garnet Orthopyroxenites from the Udachnaya Kimberlite Pipe (Yakutia); Features of Their Composition and Origin

Pokhilenko L.N.<sup>1</sup>, Pokhilenko N.P.<sup>1</sup>, Vladykin N.V.<sup>2</sup>

<sup>1</sup>V.S. Sobolev Institute of geology and mineralogy, 3 Koptyuga ave., Novosibirsk, Russia

<sup>2</sup>A.P. Vinogradov Institute of geochemistry, 1a Favorskogo st., Irkutsk, Russia

## ABSTRACT

Mineral composition of three deep-seated xenoliths of garnet pyroxenites from the Udachnaya kimberlite pipe has been studied. Subtle methods of study including scanning electron microscopy made it possible to reveal minerals from different thermal and oxidative settings at the micro level. The rims around the garnet mainly consist of aluminous ortho-, clinopyroxenes and spinel. Phlogopite, sodalite, potassium feldspar and apatite were also found in the rim of UV92/03 sample. Phlogopite and spinel from the rim differ in composition from the similar minerals of orthopyroxene matrix and interstices between opx blocks. Orthopyroxenes from the garnet rim show a variety of aluminous compositions. The rim clinopyroxenes demonstrate narrower compositional range. Olivine is represented by different morphological segregations of different composition. High Mg# and Si# olivine and high Mg# clinopyroxene intergrowth was found in one of the micro cracks of UV46/92 sample. Sulfides including K-sulfides (djerfisherite, rasvumit) among them are abundant in UV92/03 sample. Sodalite and sylvite in the fresh sample UV92/03 are a direct evidence of chlorine participation in the processes of deep metasomatism. Slightly varying mineral composition of the studied rocks is explained by heterogeneity of the initial matter, different degree of partial melting and metasomatic treatment.

**Key words:** *orthopyroxenite, garnet rim, metasomatism, partial melting.*

## INTRODUCTION

The samples of xenoliths of megacryst series reflect complex evolution history of the deep-seated mantle substance. The investigation of xenoliths, made by Pokhilenko et al. [12], Solov'eva et al. [14], Dawson [6] and other authors, allowed them to model the processes, which occurred in low horizons of the lithosphere.

We have compared three megacryst garnet pyroxenites including UV92/03, described by Pokhilenko [11] in detail. The study of composition and interrelations of their minerals makes it possible to trace the rock transformations during their multi-stage formation and to draw the conclusion that mantle metasomatism has played a key role in that process at least immediately in the period prior to kimberlite formation.

## TEXTURE, MINERAL COMPOSITION OF XENOLITHES AND CHEMICAL COMPOSITION OF MINERALS

Three garnet pyroxenite samples have been studied. The deformed orthopyroxene megacrystals constitute the bulk of the rock volume.

Table 1.

Mineral compositions of the xenoliths UV92/03, UV46/92, U-36.

sample	Main minerals	Minerals from the garnet rim	Minerals from the opx-matrix, interstices, micro-cracks
UV92/03	Orthopyroxene, garnet, phlogopite	Al-orthopyroxene, Al-clinopyroxene, Al-spinel, phlogopite, sodalite, apatite, potassium feldspar	Graphite, olivine, phlogopite, clinopyroxene, sodalite, potassium feldspar, apatite, Cr-Ti-spinelide, Ca-carbonate, sylvite, Fe-Ni and K-sulfides
UV46/92	Orthopyroxene, garnet	Al-pyroxenes, Al-spinel, potassium feldspar, phlogopite placed around the garnet rim	Olivine, clinopyroxene, phlogopite, Cr-Ti-spinelide, apatite, Ca-carbonate
U-36	Orthopyroxene, garnet, phlogopite	Al-pyroxenes, Al-spinel, phlogopite placed around the garnet rim	Olivine, clinopyroxene, phlogopite, Cr-Ti-spinelide

Garnet occurs as oriented vermicular intergrowths, chains of small grains between opx blocks and isometric grains beyond orthopyroxene. Garnet isolations are surrounded by reaction rims, which mainly consist of nonequilibrium pyroxenes with varying degree of alumina and highly alumina spinel. Table 1 demonstrates total mineral compositions of the xenoliths.

Despite the fact that they are similar in appearance, they slightly differ in mineral composition and chemical composition of the constituent minerals.

### Orthopyroxene.

Table 2 demonstrates the orthopyroxene compositions. By and large the opx matrix compositions of three samples are similar and correspond to the ordinary stoichiometric composition of mantle opx. U-36 and UV46/92 matrixes are heterogeneous and contain more ferrous areas (spots) with slightly elevated  $\text{Cr}_2\text{O}_3$ ,  $\text{Al}_2\text{O}_3$  and CaO as compared to the matrix. UV46/92 matrix contains rare thin cpx lamella (7-8microns). High CaO content in the opx rim of UV92/03 (2,31 wt%) is typical of the high-alumina composition (closed to garnet), high calcium content is also noted for the intermediate composition ( $\text{SiO}_2=50,45$  wt%,  $\text{Al}_2\text{O}_3=9,12$  wt%). The same parameter in UV46/92 is maximal for the intermediate compositions ( $\text{SiO}_2=49,74-52,48$  wt%;  $\text{Al}_2\text{O}_3=8,95-6,52$  wt%) and CaO average values (1,11 wt%) were noted in the high-alumina compositions..

For clarity the opx compositions were plotted on the diagrams Mg#-Ca#

(Fig.1) and Mg#-(Al+Cr-Na) (Fig.2).

Table 2.

The compositions of the matrix and spot orthopyroxenes and the compositions of high-alumina opx from the rim of garnet xenoliths UV92/03, UV46/92 and U-36. Mg# =Mg/(Mg+Fe)\*100; Ca# =Ca/(Ca+Mg)\*100; Al#=Al+Cr-Na

wt.%	Opx matrix			opx «spot»		Opx from the garnet rim				
	UV92/03	UV46/92	U-36	UV46/92	U-36	UV92/03	UV92/03	UV92/03	UV46/92	UV46/92
SiO <sub>2</sub>	58,18	58,55	58,26	56,88	56,68	43,70	51,95	54,58	44,03	52,48
TiO <sub>2</sub>	0,02	0,00	0,00	0,15	0,00	0,04	0,02	0,04	0,03	0,04
Al <sub>2</sub> O <sub>3</sub>	0,48	0,28	0,36	1,09	0,87	15,17	7,28	3,65	15,34	6,52
Cr <sub>2</sub> O <sub>3</sub>	0,34	0,20	0,18	0,78	0,86	5,04	1,74	0,82	6,22	1,61
MnO	0,08	0,09	0,00	0,14	0,18	0,26	0,36	0,24	0,47	0,49
FeO	4,49	4,40	4,66	5,83	6,06	7,32	7,51	6,02	8,29	7,15
MgO	35,76	35,66	36,10	32,99	33,54	25,53	29,18	32,28	24,58	28,93
CaO	0,24	0,32	0,37	0,92	0,90	2,31	1,40	1,22	1,11	2,34
Na <sub>2</sub> O	0,15	0,02	0,00	0,16	0,15	0,00	0,14	0,13	0,00	0,17
K <sub>2</sub> O	0,00	0,00	0,00	0,00	0,00	0,01	0,01	0,30	0,00	0,00
Total	99,74	99,52	99,93	98,94	99,24	99,35	99,58	99,28	100,07	99,73
Mg#	93,42	94,3	93,25	90,98	90,68	82,2	87,18	89,61	82,65	87,56
Ca#	0,49	0,65	0,73	1,97	1,89	6,11	3,32	2,64	3,13	5,49
Al#	0,019	0,016	0,019	0,049	0,056	0,785	0,341	0,164	0,822	0,304

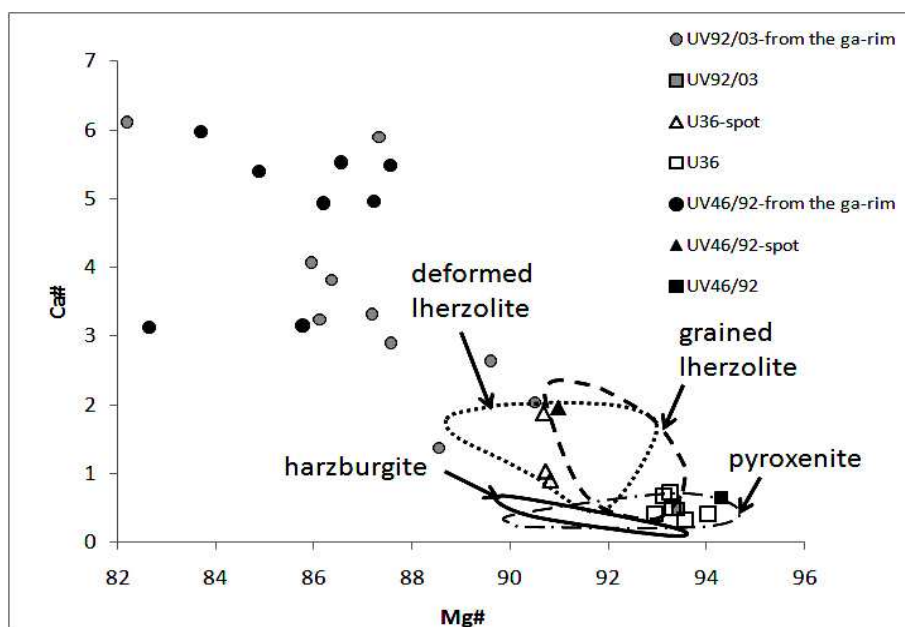


Fig. 1. Opx Mg#-Ca# diagram of the studied xenoliths. Opx compositions of basic and ultrabasic parageneses of the Udachnaya pipe: pyroxenites, harzburgites, grained and deformed lherzolites.

Fig. 1 demonstrates the matrix compositions of three studied opx, which are high Mg# opx and fall into the pyroxenite area. Ca and Fe enriched spots in the opx matrixes fall into the area of deformed peridotites.

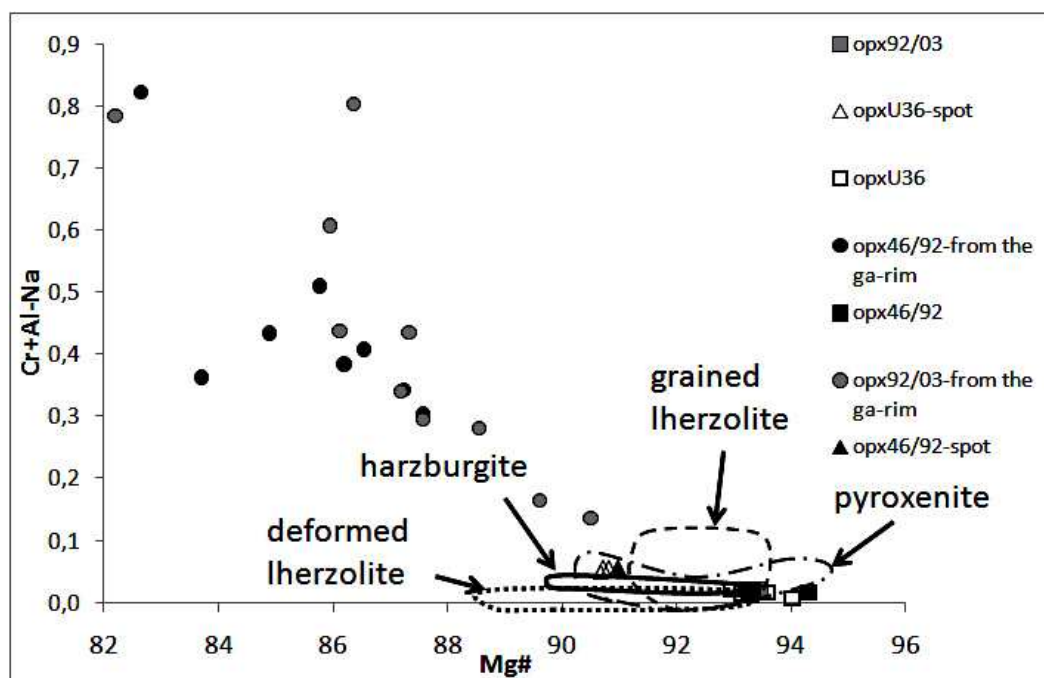


Fig. 2. Mg# - (Cr+Al-Na) diagram of the orthopyroxenes of the studied xenoliths. The composition fields of pyroxenes of basic and ultrabasic parageneses from the Udachnaya pipe: pyroxenites, harzburgites, grained and deformed lherzolites.

The compositions of non-stoichiometric non-equilibrium opx from the garnet rim have no analogs among the known mantle rocks. High calcium content manifests itself in the presence of diopsides or Ca-Tschermak minerals typical for clinopyroxenes.

Fig. 2 supports this fact and clearly demonstrates that Al in opx from the garnet rim is found not only in VI coordination in jadeite component ( $\text{NaAlSi}_2\text{O}_6$ ) but in IV (Si position) in Tschermak component ( $\text{CaAl}_2\text{SiO}_6$ ).

### Garnet.

The garnet compositions are given in Table 3 and standard diagram  $\text{Cr}_2\text{O}_3$ -CaO. According to Fig. 3, the garnets of the studied orthopyroxenites fit the compositions of different mantle parageneses: UV92/03 – harzburgite-dunite (69,3% pyrope, 7% knorringite component), U-36 – lherzolite (70,7% pyrope, 4,2% knorringite component) UV46/92 – wehrlites (65,9% pyrope, 15,6% uvarovite component).

Garnet UV92/03 is in the harzburgite-dunite field on the diagram Mg# -CaO and doesn't fall into any of the peridotite fields of Yakutian pipes on the diagram Mg# - $\text{Cr}_2\text{O}_3$ . Garnet UV46/92 lies close to the lherzolite fields. Garnet U-36 (the upper diagram Mg# - CaO) falls into the field of the deformed lherzolites and

wt.%	UV92/03	U-36	UV46/92
SiO <sub>2</sub>	41,30	41,95	41,66
TiO <sub>2</sub>	0,05	0,00	0,00
Al <sub>2</sub> O <sub>3</sub>	19,51	20,00	18,88
Cr <sub>2</sub> O <sub>3</sub>	5,40	4,14	6,28
MnO	0,27	0,45	0,38
FeO	7,15	7,68	7,33
MgO	21,62	20,74	18,91
CaO	3,82	4,16	6,56
Na <sub>2</sub> O	0,05	0,00	0,02
K <sub>2</sub> O	0,00	0,00	0,01
Total	99,16	99,11	100,01
Mg#	84,35	82,79	82,13

Table 3

The compositions of garnet xenoliths  
 UV92/03,UV46/92,U-36.Mg#= $Mg/(Mg+Fe)*100$

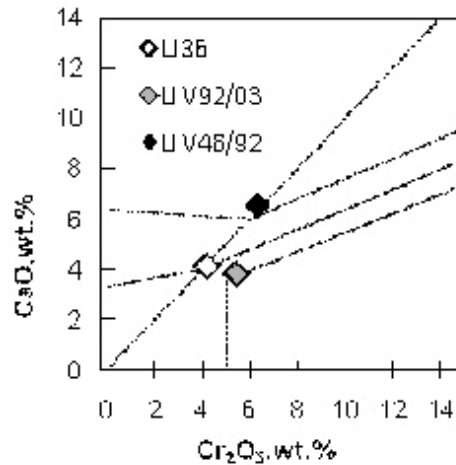


Fig. 3. Diagram Cr<sub>2</sub>O<sub>3</sub>-CaO. Dotted contours correspond to the classification boundaries [13].

lies in the field of the deformed lherzolites just near the grained lherzolite boundary on the diagram Mg# - Cr<sub>2</sub>O<sub>3</sub>. Structurally this sample doesn't show any signs of deformation or cataclasm: no flow structures, recrystallized sugar-like bulk mass etc.

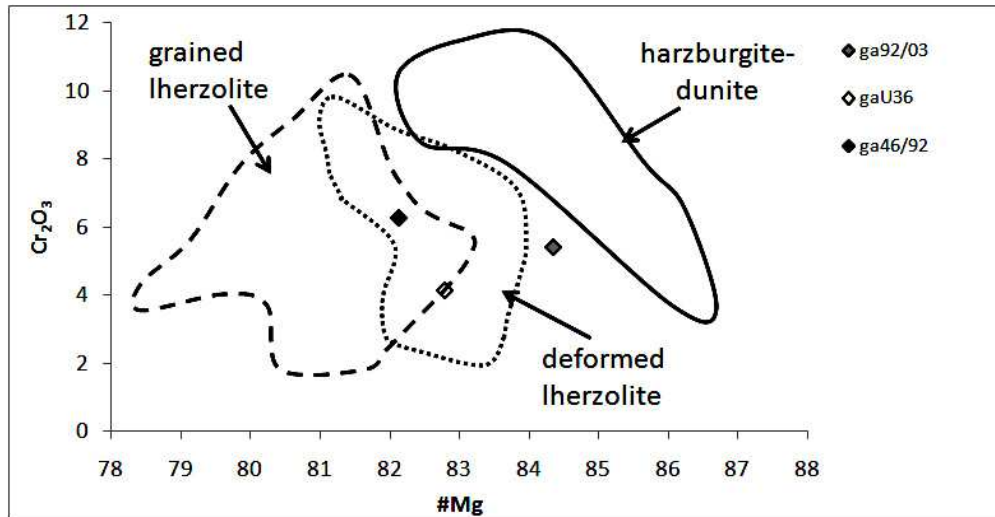


Fig. 4. Mg# -CaO diagram of the garnets of the studied xenoliths. The composition fields of garnets of ultrabasic parageneses of the Udachnaya pipe: harzburgite-dunites, grained and deformed lherzolites. Pyroxenite garnets are less Mg# (49-78) and are not plotted on the diagram.

**Clinopyroxene.**

The studied samples contain different amounts of clinopyroxene. Very rare

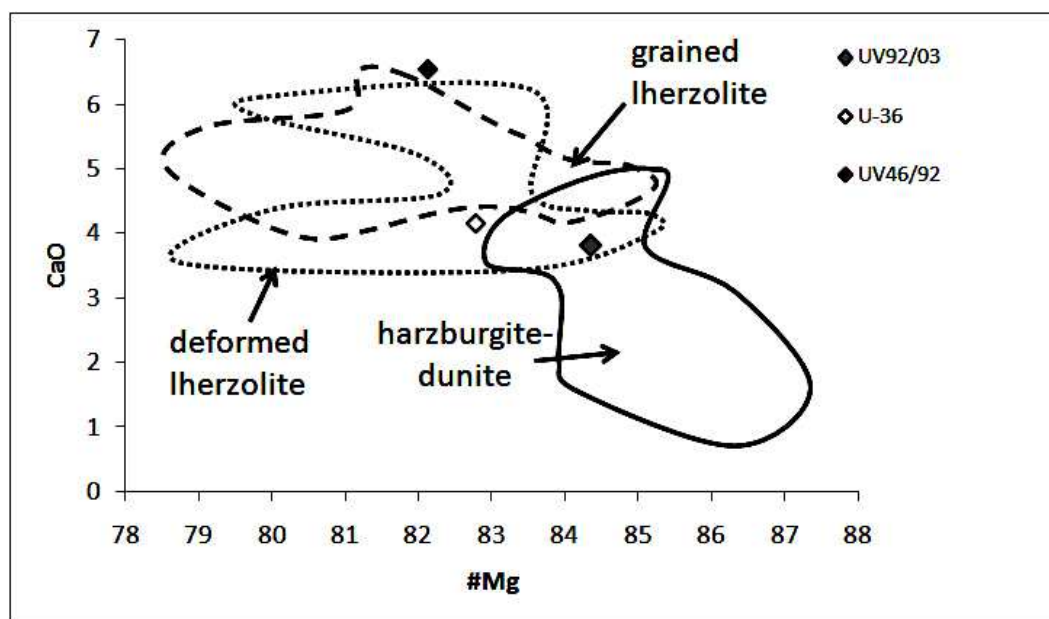


Fig. 5. Diagram Mg# -Cr<sub>2</sub>O<sub>3</sub> of the garnets of the studied xenoliths. The composition fields of garnets of ultrabasic parageneses of the Udachnaya pipe: harzburgite-dunites, grained and deformed lherzolites. Pyroxenite garnets are less magnesia (Mg# 49-78) and not plotted on the diagram.

Table 4.

Compositions of the clinopyroxenes from UV92/03, UV46/92, U-36.  
Mg# = Mg/(Mg+Fe)\*100; Ca# = Ca/(Ca+Mg)\*100; Al# = Al+Cr-Na

wt. %	Cpx from the garnet rim					Cpx from the interstices & cracks				
	U-36	U-36	UV46/92	UV92/03	UV92/03	U-36	U-36	UV46/92	UV92/03	UV92/03
SiO <sub>2</sub>	49,04	51,73	49,15	48,85	51,32	53,73	55,04	54,04	52,32	54,28
TiO <sub>2</sub>	0,14	0,39	0,39	0,06	0,07	0,29	0,28	0,73	0,24	0,11
Al <sub>2</sub> O <sub>3</sub>	10,65	7,68	7,07	8,25	7,97	6,10	3,52	2,34	5,22	2,02
Cr <sub>2</sub> O <sub>3</sub>	3,27	1,68	2,54	3,00	1,72	0,22	0,63	1,74	0,86	1,31
MnO	0,41	0,40	0,27	0,27	0,23	0,34	0,44	0,16	0,18	0,11
FeO	4,62	4,71	3,98	4,49	3,97	3,98	4,19	3,80	3,63	2,92
MgO	15,36	17,03	15,82	16,10	15,92	17,63	19,97	18,35	16,60	17,60
CaO	15,84	14,95	19,16	17,51	17,24	16,35	14,71	17,32	18,98	19,63
Na <sub>2</sub> O	0,54	0,75	0,82	0,58	0,88	0,98	0,73	0,96	1,08	1,07
K <sub>2</sub> O	0,14	0,00	0,01	0,02	0,26	0,00	0,00	0,01	0,04	0,16
Total	100,01	99,30	99,20	99,13	99,56	99,62	99,50	99,47	99,14	99,21
Mg#	85,57	86,57	87,63	86,46	87,73	88,75	89,46	89,58	89,08	91,49
Ca#	42,57	38,69	46,56	43,89	43,78	40,01	34,62	40,42	45,12	44,51
Al#	0,51	0,32	0,32	0,4	0,33	0,20	0,12	0,08	0,17	0,05

clinopyroxene grains (fractions of mm) are observed in U-36. Rare grains (as big

as 70-80 microns) are observed in UV46/92 at the garnet rim boundary and in the micro cracks with olivine and apatite. In UV92/03 it occurs in the cracks with phlogopite, apatite, calcium carbonate, chromite and sulfides. Clinopyroxene with

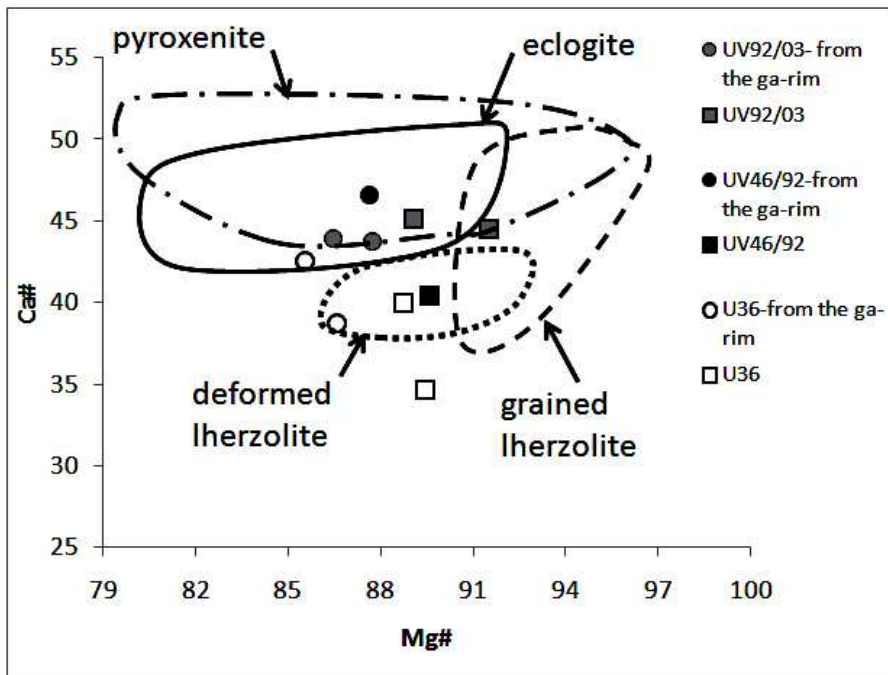


Fig. 6. Diagram Mg# -Ca# of the clinopyroxenes of the studied xenoliths. The composition fields of pyroxenes of basic and ultrabasic parageneses of the Udachnaya pipe: pyroxenites, eclogites, grained and deformed lherzolites.

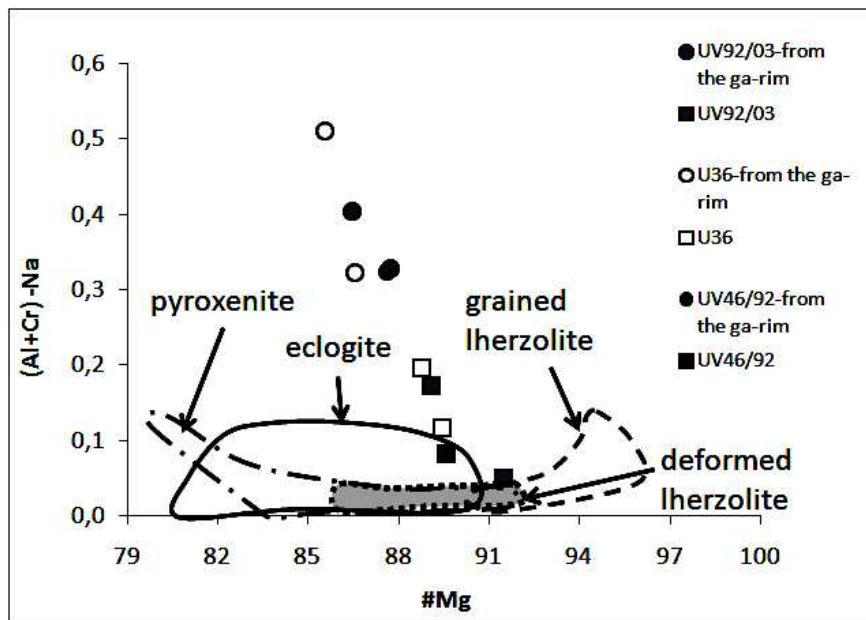


Fig 7. Diagram Mg# -(Cr+Al-Na) of the clinopyroxenes of the studied xenoliths. The composition fields of pyroxenes of basic and ultrabasic parageneses of the Udachnaya pipe: pyroxenites, eclogites, grained and deformed lherzolites.

different aluminum content was observed in all studied xenoliths among the minerals of the rim around the garnet. Table 4 shows the compositions of some clinopyroxenes.

Fig. 6 demonstrates that clinopyroxenes from interstices and cracks, like less magnesian clinopyroxenes from the rims around the garnet, fall into the fields of different mantle rocks. This fact may point both to the varying degree and time of the source orthopyroxenite enrichment, different P-T conditions and multistage process and reactions, that have taken place at the periphery of garnet grains at the late stages of the rock formation.

Fig. 7 clearly demonstrates that clinopyroxenes from the interstices and cracks mostly fall into the fields of compositions of classic mantle rock parageneses: UV46/92 and U-36 – eclogite field, UV92/03 – intersection of pyroxenite and lherzolite fields. Some compositions, which correspond to pyroxenite clinopyroxenites in the aluminum content, appear to be significantly more magnesian and have no analog among the pyroxenes of the mantle parageneses of the Yakutian pipes like clinopyroxenes from the rim around the garnet.

### *Olivine.*

In the sample UV46/92 olivine occur in micro cracks (10mkm) with bulges (up to 30 microns) filled with clinopyroxene and apatite along with olivine. It also occurs in wider cracks (100-120 microns) together with clinopyroxene, phlogopite and calcium carbonate. Olivine with high Mg and elevated Si is found in one of these cracks (Fig. 8). The area (0,5x0,5 mm) made of cryptocrystalline olivine (grains up to 15 microns) and symplectitic spinel and clinopyroxene intergrowths is found in UV92/03. The intergrowths of more ferruginous olivine and clinopyroxene were also found in microcracks (10-12 mkm). Olivine was observed in U-36 as single grains up to 100microns with phlogopite, spinel, orthopyroxene and clinopyroxene. Olivine compositions are given in Table 5.

Table 5.

#### **Compositions of olivine from the xenoliths UV92/03, UV46/92, U-36.**

**Fo – forsterite component  $Mg/(Mg+Fe)*100$**

wt.%	U-36	U-36	UV46/92	UV46/92	UV92/03	UV92/03
<b>SiO<sub>2</sub></b>	39,96	40,07	41,04	42,74	41,52	40,69
<b>Cr<sub>2</sub>O<sub>3</sub></b>	0,00	0,00	0,38	0,02	0,02	0,13
<b>MnO</b>	0,34	0,52	0,23	0,08	0,05	0,24
<b>FeO</b>	10,83	11,39	9,20	5,01	7,06	9,25
<b>MgO</b>	48,20	47,47	48,88	52,15	50,79	49,02
<b>CaO</b>	0,21	0,17	0,16	0,08	0,01	0,16
<b>NiO</b>			0,154	0,061	0,59	0,15
<b>Total</b>	99,53	99,61	100,04	100,14	100,03	99,63
<b>Fo</b>	88,80	88,13	90,45	94,88	92,76	90,42

U-36 contains least magnesium-rich olivines. In Fig. 8 their compositions fall (or fall close) into the extremes of the field of the deformed lherzolites. UV46/92 and UV92/03 compositions also lie in this field but at the intersection with the field of the grained lherzolites; UV92/03 composition falls into the most magnesian part of the deformed lherzolite field at the boundary of grained lherzolite and harzburgite-dunite fields. Highly magnesian olivine UV46/92 found in the crack has no analogs among the olivines of the Udachnaya pipe mantle rocks.

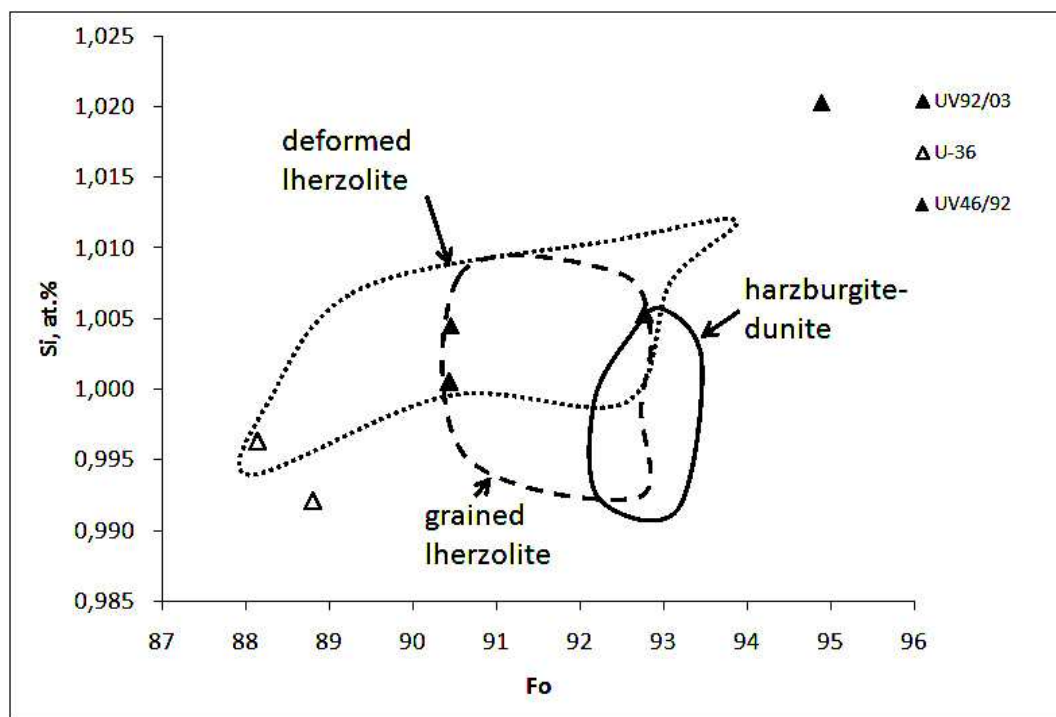


Fig. 8. Mg and Si content of olivines of the studied xenoliths. The composition fields of olivines of basic and ultrabasic parageneses of the Udachnaya pipe: harzburgite-dunites, grained and deformed lherzolites.

### *Phlogopite.*

Phlogopite compositions are given in Table 6.

Figures 9-11 demonstrate that phlogopites UV46/92 and UV92/03, which occur among the minerals around the garnet rim and outline this rim, are less magnesian than phlogopites from the orthopyroxene matrix and large cracks. U-36 phlogopites occurring between opx blocks are more ferruginous than phlogopites outlining the rim, though their compositions differ less than phlogopite of two other xenoliths in all components. By and large phlogopites from the rim and adjacent to it are similar in Mg# content (83,4-58,2, Table 6), all of them are enriched in Ti, Al, Cr (Fig. 9,11), what is indicative of the similarity of their formation processes. All U-36 phlogopites are enriched in K and phlogopites from the rim UV46/92 and UV92/03 are depleted in this component.

Table 6.

Compositions of phlogopites from the xenoliths UV92/03, UV46/92, U-36: 1-2 - phlogopite plates sited between the orthopyroxene blocks, 3-5 – phlogopite, which outlines the garnet rim; UV92/03: 6 – phlogopite from large cracks (500mkm), 7 – phlogopite plates from the orthopyroxene matrix, 8 – phlogopite from the garnet rim; UV46/92: 9 – phlogopite, which outlines the garnet rim, 10-11 – large plates, which outline the garnet rim.

wt. %	1	2	3	4	5	6	7	8	9	10	11
SiO <sub>2</sub>	39,96	39,28	<b>39,93</b>	<b>39,86</b>	<b>39,07</b>	44,43	42,85	<b>39,94</b>	<b>40,12</b>	40,85	40,23
TiO <sub>2</sub>	2,35	2,34	<b>2,46</b>	<b>2,42</b>	<b>2,40</b>	0,12	0,10	<b>1,45</b>	<b>2,34</b>	1,52	2,09
Al <sub>2</sub> O <sub>3</sub>	13,84	15,55	<b>13,92</b>	<b>13,07</b>	<b>14,43</b>	10,02	12,41	<b>15,32</b>	<b>13,98</b>	12,10	12,99
Cr <sub>2</sub> O <sub>3</sub>	1,90	1,95	<b>2,24</b>	<b>1,88</b>	<b>2,06</b>	0,05	0,75	<b>2,33</b>	<b>2,08</b>	1,26	1,54
MnO	0,00	0,00	<b>0,00</b>	<b>0,00</b>	<b>0,15</b>	0,03	0,02	<b>0,04</b>	<b>0,03</b>	0,06	0,03
FeO	5,11	4,72	<b>4,33</b>	<b>4,50</b>	<b>4,39</b>	3,18	2,81	<b>3,95</b>	<b>3,98</b>	3,54	3,72
MgO	21,95	21,81	<b>22,16</b>	<b>22,50</b>	<b>22,01</b>	27,37	25,43	<b>22,66</b>	<b>20,76</b>	23,71	23,74
CaO	0,00	0,00	<b>0,00</b>	<b>0,10</b>	<b>0,00</b>	0,01	0,01	<b>0,03</b>	<b>0,03</b>	0,01	0,02
Na <sub>2</sub> O	0,45	0,44	<b>0,31</b>	<b>0,30</b>	<b>0,42</b>	0,10	0,16	<b>0,41</b>	<b>0,30</b>	0,16	0,20
K <sub>2</sub> O	11,28	11,51	<b>11,51</b>	<b>11,84</b>	<b>11,75</b>	10,58	10,24	<b>9,69</b>	<b>9,12</b>	9,10	9,69
Total	96,83	97,59	<b>96,85</b>	<b>96,48</b>	<b>96,68</b>	96,68	95,23	<b>96,23</b>	<b>92,74</b>	92,30	94,25
Mg#	81,11	82,21	<b>83,64</b>	<b>83,35</b>	<b>83,38</b>	89,59	90,07	<b>85,15</b>	<b>83,92</b>	87,00	86,47

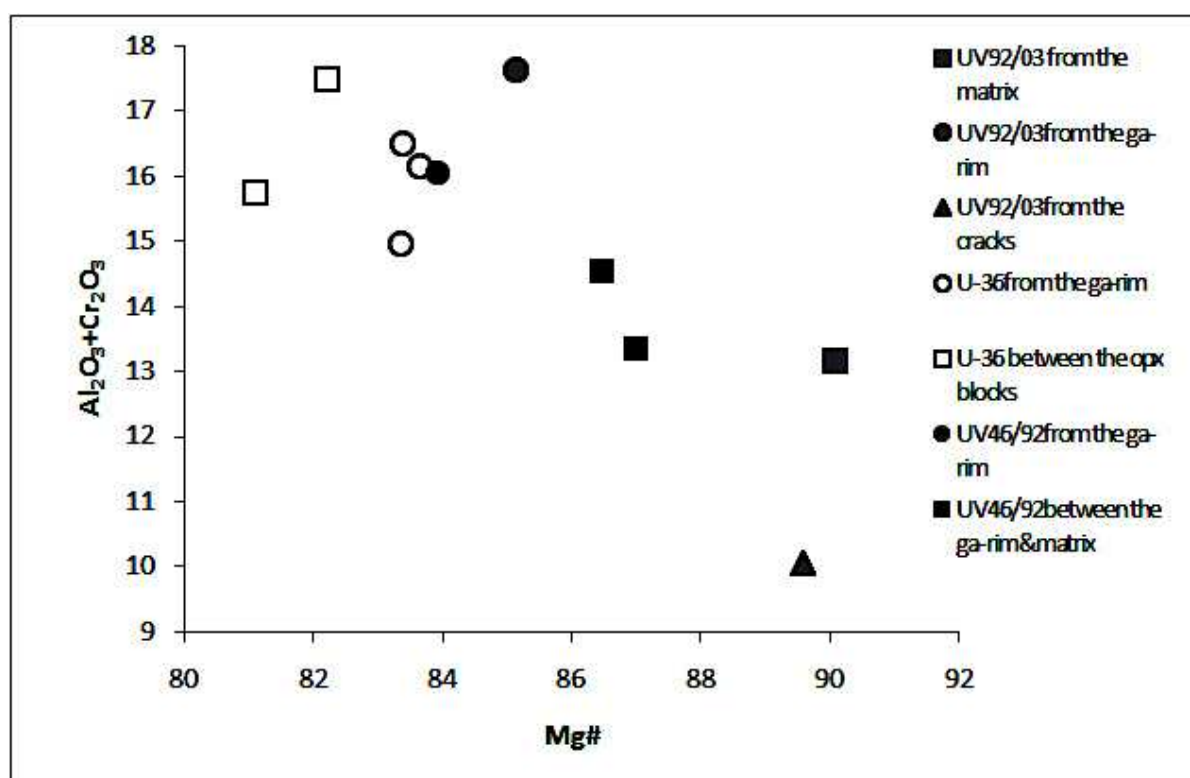


Fig. 9. Diagram Mg#-Al<sub>2</sub>O<sub>3</sub> for phlogopites of the studied xenoliths.

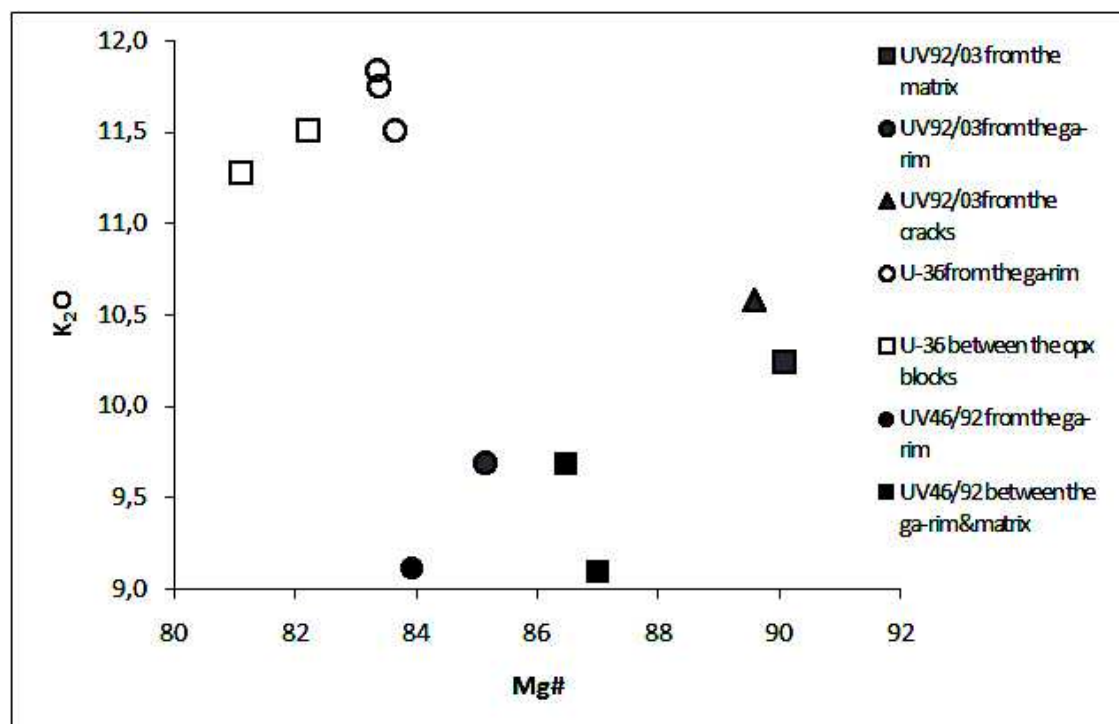


Fig. 10. Diagram Mg#-K<sub>2</sub>O for phlogopites of the studied xenoliths.

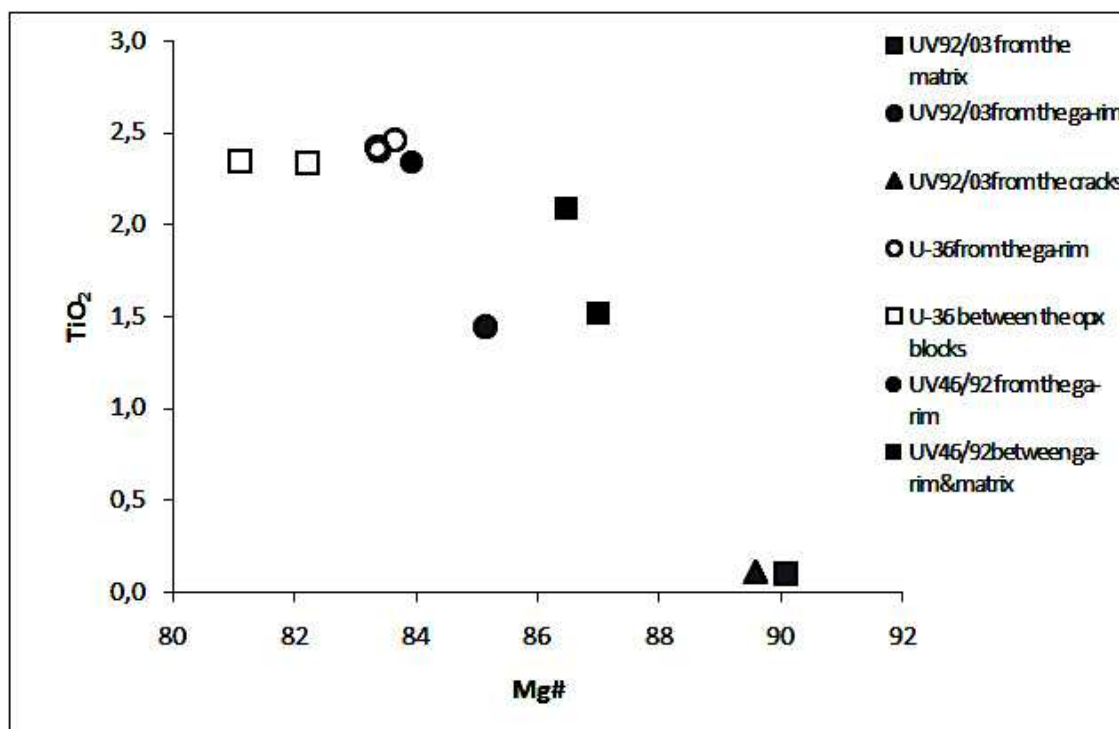


Fig. 11. Diagram Mg#-TiO<sub>2</sub> for phlogopites of the studied xenoliths.

### *Spinelides.*

Isometric, zonal as a rule, often of square, triangular or star section spinelide grains occur in the garnet rim of three studied xenoliths along with high-alumina

orthopyroxene and clinopyroxene. Spinelides with elevated TiO<sub>2</sub> content (Fig. 13) were observed at the orthopyroxene grain boundaries or in the cracks filled with potassium feldspar and phlogopite. Spinelide-clinopyroxene micro symplectites

Table 7.

Compositions of spinelides from the xenoliths UV92/03, UV46/92, U-36.  
Mg# = Mg/(Mg+Fe<sup>2+</sup>)\*100; Cr# = Cr/(Cr+Al+Fe<sup>3+</sup>)\*100

	centre	rim	sp1	sp2	centre	rim	sp3	sp4	centre	rim	sp5
wt. %	uv92/03	uv92/03	uv92/03	uv92/03	u-36	u-36	u-36	u-36	uv46/92	uv46/92	uv46/92
TiO <sub>2</sub>	0,54	0,34	0,28	2,77	1,08	0,44	2,81	2,12	0,91	0,36	3,33
Al <sub>2</sub> O <sub>3</sub>	28,81	38,70	47,51	14,42	40,88	49,59	18,84	24,63	24,94	50,29	9,50
Cr <sub>2</sub> O <sub>3</sub>	40,19	30,09	17,92	43,64	20,15	13,74	38,24	29,50	41,16	16,42	50,62
FeO	13,26	12,08	13,24	22,82	20,20	16,38	24,98	27,11	18,48	13,69	23,05
MnO	0,10	0,10	0,16	0,31	0,35	0,00	0,31	0,00	0,30	0,26	0,26
MgO	16,59	17,98	19,98	14,94	17,29	19,60	13,93	15,80	13,39	19,35	12,24
NiO	0,41	0,38		0,14					0,106	0,060	0,155
Total	99,91	99,66	99,12	99,04	99,94	99,75	99,11	99,16	99,29	100,43	99,15
Mg#	73,07	75,83	80,15	69,41	71,73	77,63	63,68	69,43	61,09	76,88	58,80
Cr#	46,93	33,52	19,18	56,78	22,48	14,57	49,17	36,07	50,32	17,30	69,34

were found in the fine crystalline olivine mass of UV92/03 sample. Compositions of zoned spinels from the garnet rim and Cr-Ti-spinelides from the interstices are given in Table 7.

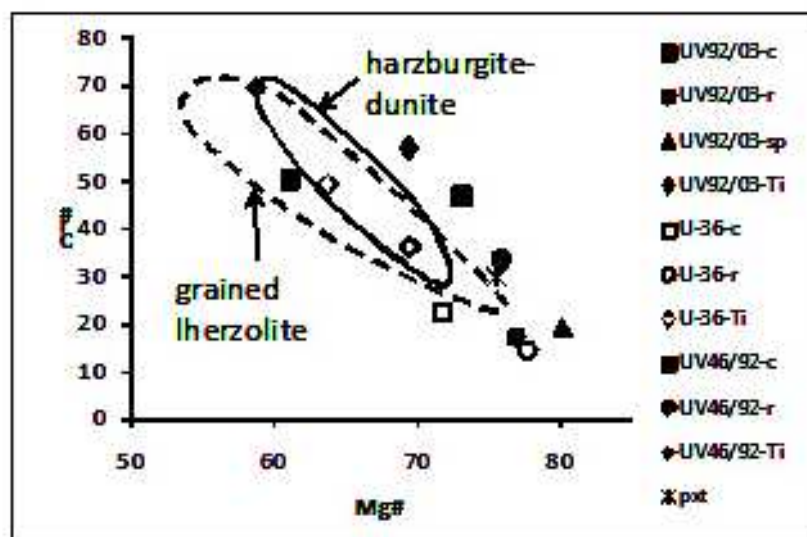


Fig. 12. Diagram Mg# Cr# for spinelides of the studied xenoliths. The composition fields of spinelides of basic and ultrabasic parageneses of the Udachnaya pipe: harzburgite-dunites, grained lherzolites and composition of the spinel from pyroxenite of the Obnazhennaya pipe. The compositions of central (c) and marginal (r) parts of spinelides are connected by tie lines.

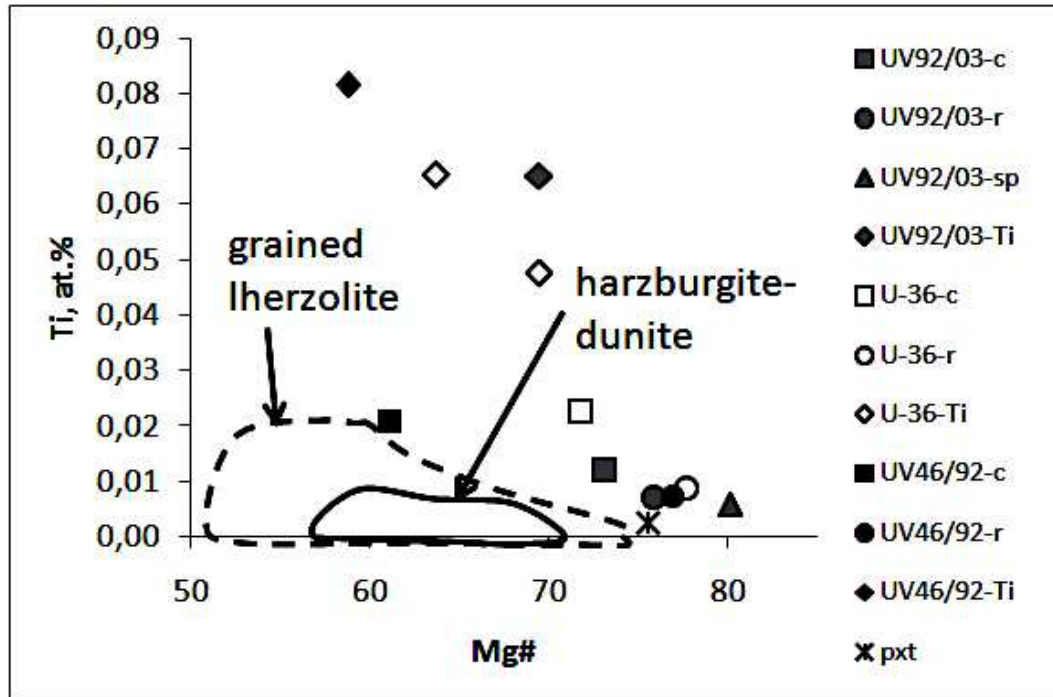


Fig. 13. Diagram Mg# -Ti for spinelides of the studied xenoliths. Diagram Mg# Cr# for spinelides of the studied xenoliths. Composition fields of spinelides of basic and ultrabasic parageneses of the Udachnaya pipe: harzburgite-dunites, grained lherzolites and composition of the spinel from pyroxenite of the Obnazhennaya pipe. The compositions of central (c) and marginal (r) parts of spinelides are connected by tie lines.

According to Mg# -Cr#, the majority of Ti-spinelides and composition of the central part of strongly zonal spinelide from UV/46/92 garnet rim fall into the fields of the mantle rock of ultrabasic parageneses. The margin of zonal spinelide from UV/92/03 garnet rim and spinelide from the Obnazhennaya pipe pyroxenite are similar in composition. U-36 spinelides are the least chromium spinelides. Spinelide margins from the garnet rim are less chromium and ferruginous as compared to their central parts.

### PT-PARAMETERS OF EQUILIBRIUM OF THE STUDIED XENOLITHS

Unfortunately it is impossible to determine exact PT-parameters of the initial orthopyroxenes because of the complexity of the reconstruction of their initial compositions. The samples are heterogeneous in garnet distribution and contain high amount of accessory minerals. Probably the approximate calculations allowed rough determinations to be made of lower temperature of the orthopyroxene formation. Garnet enstatite equilibrium parameters were determined from orthopyroxene-garnet pair.

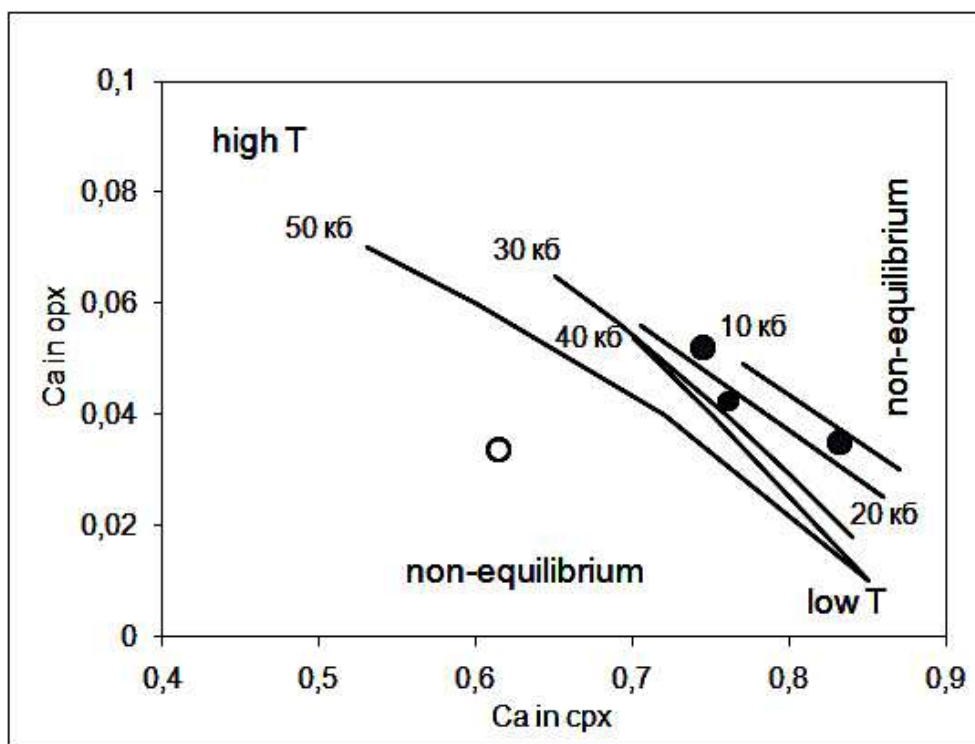


Fig. 14. Equilibrium clino- and orthopyroxenes from the garnet rim on the diagram Ca in opx – Ca in coexisting cpx.

Lines show the compositional trends of equilibrium pyroxene compositions. The trends were experimentally obtained in the natural system by Bray at 900-1400°C and 1-6 GPa [3,5]. Gray circles – UV92/03, black circles – UV46/92, empty circle – non-equilibrium pyroxene pair from U-36 garnet rim.

Probable equilibrium pairs among aluminous pyroxenes from the garnet rim have been determined using the scheme of Bray for lherzolite four-mineral parageneses considering the presence of later olivine, clino- and orthopyroxenes. Temperature and pressure were calculated by the known geothermobarometers (Table 8).

Table 8.

Equilibrium parameters of the key stages of formation of the studied xenoliths: BK – Brey, Kohler, 1990 [4], Ha – Harley, 1984 [7], WB – Wood, Banno, 1973 [15], BM – Bertrand, Mercier, 1985 [2], NT – Nimis, Taylor, 2000 [10], MG – MacGregor, 1974 [9]

UV92/03 U-36 UV46/92	1405 1370 1380	T, °C by BK, opx	50 50 50	fixed P, kb	1425 1405 1445	T, °C by BM, opx	50 50 50	fixed P, kb	1-2 fig.15
UV92/03 U-36 UV46/92	915 953 1002	T, °C by Ha, ga+opx	46 47 47	P, kb by Ha, ga+opx					3 fig.15
UV92/03 UV92/03 UV46/92	1155 1165 1060	average T by BK, WB,BM, cpx+opx	19 17 27	average P by MG(opx), NT(cpx), BM(cpx+opx)					5 fig.15

## DISCUSSION

The studied xenoliths are crystallization products of the melt of sub-lithosphere mantle of maximal partial melting (70%), which corresponds in composition to primitive mantle substance (Fig. 15-1).

Slightly different compositions of the studied rocks can be first related to the initial substance inhomogeneity and second – different degree of partial melting. If you look at the garnet compositions – harzburgite for UV92/03, lherzolite for U-36 and wehrlites for UV46/92, it would seem reasonable to assume that initial melt fractions of UV46/92 and U-36 were less deep and more enriched in the low melting components than the melt from which UV92/03 crystallized. Although it is possible that UV46/92 has experienced wehrlitization later [8].

Reasoning from the high degree of melting and compositions of initial pyroxenes (before they have lost garnet molecule) it can be assumed that their crystallization temperature were about 1400-1600°C [1]. During cooling the resulting highly aluminous enstatite has lost garnet as energetically unfavorable phase by the known reaction:



This process occurred as temperature decreased but was still high. The pair consisting of recrystallized, free of alumina enstatite and released pyrope gives PT parameter of completion of the first phase of complex evolution of this type of rocks (Fig. 15 -2,3). On further cooling and sufficient CaO amount in the system the cpx precipitation (fallout) from the opx matrix should be expected. This process is fixed in its infancy as rare thin (up to 10mkm) oriented cpx plates in one of the opx areas of UV46/92. U-36 contains rare cpx grains. UV92/03 has been initially depleted and contains only later cpx, probably related to metasomatic treatment of the rock.

Further transformations of the studied rocks were related to their secondary enrichment in the deep mantle horizons, which was caused by the general preparatory of substrate to kimberlite formation. At that time hot melts containing aggressive fluids accumulated in the mantle areas adjacent to our rocks. This phase is related to large phlogopite grains in UV92/03, micro cracks in opx matrix filled with high Mg# olivine, Cr-Ti spinelide, high temperature (low-Ca) cpx in UV46/92, the area in UV92/03 opx made of cryptocrystalline olivine intergrowths, chrome-spinel, high temperature cpx and the beginning of the formation of reaction rims around garnet, which are mainly made of ortho-, clinopyroxenes of different aluminum content and enlarged and zonal spinel at the rim periphery. UV92/03 garnet rim also contains phlogopite enriched in Ti, Al, Cr as compared to the matrix phlogopite. UV46/92 phlogopite, which edges the rim, is also enriched in these components. This fact can points to discrete or stepwise nature of metasomatic effect. The complex metasomatic stage was followed by Ti, K, Cr introduction for U-36 rock as demonstrated by the compositions of phlogopites

located between opx blocks and edged garnet rims (Fig. 9-11). Similarity of their compositions may be a demonstration of simultaneous growth or at least similar growth conditions. As indicated above, minerals of garnet rim seldom fall into any field of basic and ultrabasic mantle rocks because they were formed in different conditions under the action of active metasomatic agents probably as PT medium parameters changed (Fig. 15-4).

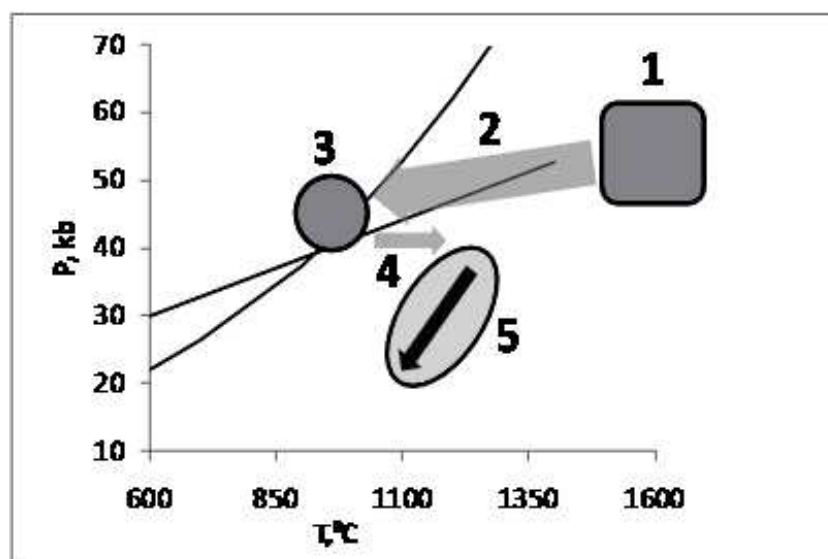


Fig. 15. Model of formation of mantle xenoliths UV92/03, UV46/92, U-36.

1 – expected initial melt, 2 – crystallization of initial highly aluminous megacryst orthopyroxenite, garnet loss, 3 – intermediate equilibrium – garnet enstatites, 4 – heating and rock enrichment in melts and fluids accumulated during the kimberlite formation, the beginning of the garnet rim formation, 5 – capture of the rock by kimberlite and lifting to the surface, growth, enlargement and further formation of the rim minerals around the garnet.

During the capture of the studied rocks by alkali enriched kimberlite melt and transport to the surface they underwent further transformations. Probably the transportation didn't occur immediately but with short stop somewhere at the crust boundary. Potassium feldspar, cryptocrystalline phlogopite of different composition (enriched in K and Si), which contains apatite and clinopyroxene and sometimes calcium carbonate in the cracks point to the fact. UV92/03 was recovered from the block of fresh kimberlite, which didn't subject to serpentinization and other changes. Variety of alkaline minerals supports this fact. Thus sodalite (Na-enrichment) occurs in the garnet rim at this stage and sylvite was found in the interstitial space between opx blocks, large phlogopite grain and garnet rim. Small grains of K-containing sulfides (first microns) djerfisherite and rasvumite were noted in the micro cracks. UV92/03 garnet rim contains a wider in aluminum content range of pyroxenes and in this case compositions vary within the small areas (20-50mkm). This suggests an extreme nonequilibrium and high process rate (Fig. 15-5).

## REFERENCES

1. **Becker, H.** Petrological constraints on the cooling history of high-temperature garnet peridotite massifs in lower Austria. 1997. *Contrib Mineral Petrol* 128: 272±286.
2. **Bertrand, P., Mercier, J.C.-C.** The mutual solubility of coexisting ortho- and clinopyroxene: toward the absolute geothermometer for the natural system? // 1985, *Earth Planet. Sci. Lett.* 76: 122±152.
3. **Brey, G.P.** Fictive conductive geotherms beneath the Kaap- vaal craton (abstract). 1991. In: *5th Int Kimberlite Conf Brazil Ex- tended Abstr.* CPRM Spec Publ 2/91, Brasilia, pp 23±25.
4. **Brey, GP, Kohler, T** Geothermobarometry in four-phase lherzolites. II. New thermobarometers and practical assessment of existing thermobarometers. 1990. *J Petrol* 31: 1353±1378.
5. **Brey GP, Kohler T, Nickel KG** Geothermobarometry in four-phase lherzolites. I. Experimental Results from 10 to 60 kbar. 1990. *J Petrol* 31: 1313±1352.
6. **Dawson, J.B.** A fertile harzburgite–garnet lherzolite transition: possible inferences for the roles of strain and metasomatism in upper mantle peridotites. 1990. *Lithos* 77: 553±569.
7. **Harley, S.L.** An experimental study of the partitioning of Fe and Mg between garnet and orthopyroxene. 1984. *Contrib Mineral Petrol* 86: 359±373.
8. **Kogarko, L.N.** Role of deep-seated fluids in genesis of mantle heterogeneities and alkaline magmatism //2005. *Geol. and Geoph.*, 46 (12): 1234±1245 (in Russian).
9. **MacGregor, I.D.** The system MgO-Al<sub>2</sub>O<sub>3</sub>-SiO<sub>2</sub>: solubility of Al<sub>2</sub>O<sub>3</sub> in enstatite for spinel and garnet peridotite compositions. //1974. *American Mineralogist* 59: 110±119.
10. **Nimis, P., Taylor, W.** Single clinopyroxene thermobarometry for garnet peridotites. Part I. Calibration and testing of a Cr-in-Cpx barometer and an enstatite-in-Cpx thermometer //2000. *Contrib. Mineral. Petrol.* 139 (5): 541±554.
11. **Pokhilenko, L.N.** On mineralogy of deep-seated xenoliths – sample UV92/03: rock transformation // *Deep seated magmatism, its sources and plums*, 2009. Irkutsk, 99-117, (in Russian).
12. **Pokhilenko, N.P., Sobolev N.V., Boyd F.R., Pearson G.D., Shimizu N.** Megacrystalline pyrope peridotites in the lithosphere of the Siberian platform: mineralogy, geochemical peculiarities and origin //2003. *Geol. and Geoph.*, 34 (1): 71±84 (in Russian).
13. **Sobolev, N.V., Pokhilenko N.P., Lavrent'ev Yu.G., Usova L.V.** The role of chromium in the garnets from kimberlites // The problems of petrology of the Earth Crust and the Upper Mantle. Institute of geol. and geophys., SB AS USSR, issue 403, 1978. Novosibirsk, Nauka, Siberian branch, p. 145-168.
14. **Solov'eva, L.V., Kostrovitsky S.I., Ukhanov A.V., Suvorova L.F., Alyмова N.V.** Megacrystalline orthopyroxenite with graphite from Udachnaya pipe, Yakutia // 2002. *Doklady ANR*, 385 (2): 231±235 (in Russian).
15. **Wood, B.J., Banno, S.** Garnet-ortopyroxene and ortopyroxene-clinopyroxene relationships in simple and complex systems //1973. *Contrib. Mineral. Petrol.* 42: 100±124.

## **The alkaline ultrabasic magmatism of the Onega peninsula Nenoksa fields - reflection (display) of the plume and subduction processes in Belomorsky region (Arkhangelsk diamond province)**

S.M. Sablukov <sup>1</sup>, Belov A.V. <sup>2</sup> and Sablukova L.I.

<sup>1</sup> «RUSGEO», Ltd., Moscow, Russia, e-mail: [sablukoff@rambler.ru](mailto:sablukoff@rambler.ru)

<sup>2</sup> «Arkhangelsk diamond» Co. Ltd, Arkhangelsk, Russia

### **ABSTRACT**

The Joint-Stock Company «Arkhangelsk diamonds» in 2008-2009 discovered 3 new pipes (An-G448, An-G056 and An-G429) in the western part of the Nenoksa field, the Onega peninsula. The geological structure and the composition of these pipes show, that the magmatism of the Nenoksa field is more diverse, than was earlier considered. The western part of the field is different in the geology as well. When the pipes originated this site contained the Cambrian-Ordovician sediments, eroded prior to the intrusion of other pipes of the field. New pipes in places show a complex multiphase texture; in addition to common volcanic rocks the pipes showed for the first time the body of sintered tuffsite of kimmilitites. The An-G056 and An-G429 pipes demonstrate the increased degree of ultrabasicity, lack of clinopyroxene phenocrysts, presence of tetraferriphlogopite and macrocrysts of “olivine of the first generation” (an essential feature of the rocks from the kimberlite series), high concentrations of intratelluric inclusions (chrome-spinellids, clinopyroxene, amphibole-pargasite, olivine, pleonaste), as well as features of the asthenosphere influence on the mantle source of rocks (influence of the mantle plume). The rocks from An-G056 and An-G429 pipes belong to the non-pyroxene feldspathoid olivine melilitites and in terms of the composition they are similar to “kimmilitites” of Chidvia and Verkhotina of the alumina series of the Zimnyi Bereg region. The pipes of the Nenoksa field are of the same age, similar in the geologic texture and composition to the pipes of the Terskyi Bereg and Zimnyi Bereg and fall into a general pattern of zoning of the Early Hercynian volcanism of the Belomorsky region. The central part of the Belomorsky region includes abundant diamondiferous and weakly-diamondiferous kimberlites, while the peripheral part contains non-diamondiferous melilitites, foidites and basalts. The Early Hercynian pipes of the Terskyi field, Nenoksa field and Zimnyi Bereg region are located on the northern and eastern margins of the Belomorsky maximum dg, which is connected with the Devonian mantle diapir, or «plume». The pipes do not contain typical minerals-satellites of diamond of the ultrabasic paragenesis, however they include abundant deep minerals from eclogites, including diamond-bearing, and eclogites of the group I "C", being indicators of subduction processes at the level of the diamondiferous mantle. These features point out a deep character of magmatic occurrences in the region, the diamond potential of which can be of purely eclogite (subduction) nature. The discovered An-G056 (and An-G429) pipes indicate new possible bedrock diamond potential of the Nenoksa field, the Onega peninsula, and the Belomorsky region as a whole.

### **INTRODUCTION**

The Arkhangelsk diamond-bearing province [27] unites various alkaline-ultrabasic Devonian volcanic complexes, occurring mainly along the coast of the

White Sea: on Zimnyi Bereg, Letnyi Bereg of the Onega peninsula, the Terskyi Bereg of the Kola Peninsula, and also on Middle Timan (Fig. 1). The maximal

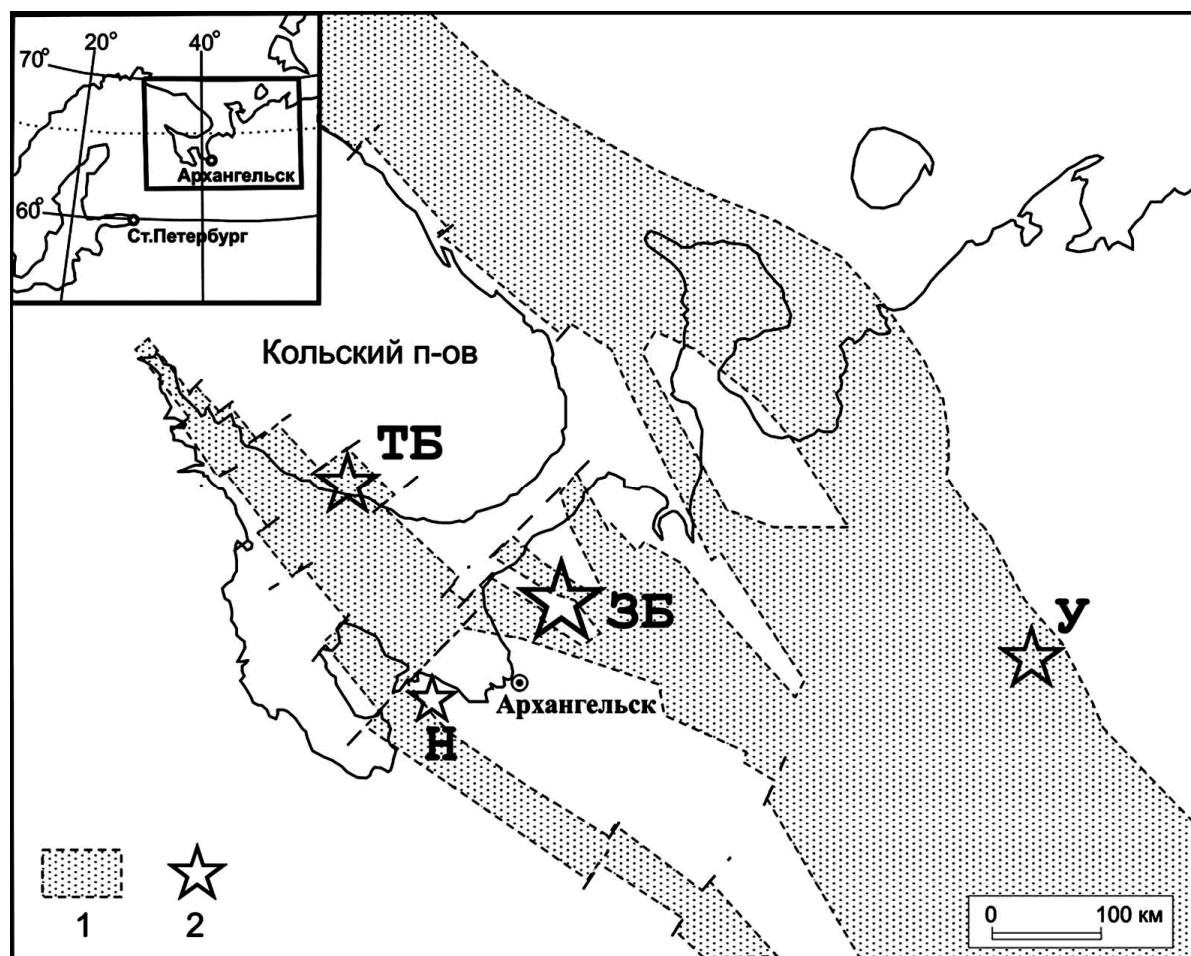


Fig.1. Areas of the kimberlitic and related volcanism, North of the Russian Platform.

1 – Riphean paleorift system; 2 – areas of the Early Hercynian volcanism: ZB – Zimnyi Bereg, TB – Terskyi Bereg, Kola Peninsula, N – Nenoksa region, Onega Peninsula, U – Umba region, Middle Timan.

activity and a diversity of the Late Devonian kimberlites and associated magmatism are found in the Belomorsky region. About 150 magmatic occurrences have been discovered here. They mainly include volcanic pipes, dykes and sills. The detailed studies of the Late Devonian kimberlite fields (Zimnyi Bereg – 70 bodies and Terskyi Bereg of the Kola Peninsula (about 50 bodies) showed that the magmatism of these fields is extremely diverse. These fields contain volcanic rocks of different composition - from diamond-bearing kimberlites of different type, kimpicrites, and kimmelilitites (terminology [19]) up to alkaline picrite, non-pyroxene, olivine melilitites and melilitites showing features of diamond potential or without such features (a similar series of rocks is found for three Middle Devonian pipes of the Umba field of the Middle Timan [36,22,30,42]). These diverse volcanic rocks are regularly located: the distribution of many compositional parameters of rocks (mineralogical, petrochemical, geochemical,

isotope) over the fields has zonal character, possesses elements of symmetry of the central or linear type and indicates a various degree of the astenosphere influence on areas of magma generation in different zones of these fields [28,31]. At the same time in another site of the Belomorsky region – Nenoksa filed of the Onega peninsula (about 40 bodies) we found the pattern of monotonous distribution of the numerous magmatic occurrences of similar type, composed of feldspathoid olivine melilitites [9,35,23,30,17]. Only the Ust-Syus'ma pipe on the northwest of the Nenoksa filed, one of the bodies of which contained the non-pyroxene feldspathoid olivine melilitites, suggested a greater variety of volcanic rocks and the existence of elements of zoning in the Nenoksa field [28]. The company «Arkhangelsk diamonds» (Joint-Stock Company) discovered in 2008-2009 three new pipes in the western part of the Nenoksa field; the features in the composition of these pipes verify a great variety of volcanic rocks in this field, and the zoning of their distribution within both the field and within the Belomorsky region as a whole. Additional studies of volcanic occurrences of the Nenoksa field, the Onega peninsula are required as little attention was given to these studies for the last 20 years.

### **SITES AND METHOD OF INVESTIGATIONS**

44 pipes have been discovered in the Nenoksa field up to now (July, 2010); 19 pipes were studied by us, among them 7 pipes were thoroughly studied, 12 pipes were not thoroughly studied (only separate sites of the core and separate samples). During the investigations (1983-2010) authors studied 904 m of the core from 16 bore holes, 48 m of 22 prospect-holes and ditches, more than 350 samples, more than 100 transparent thin sections. We have done the following analyses of rocks: silicate - 92 analyses, neutron-activation - 28 analyses, ICP-MS - 19 analyses, X-ray powder diffraction - 11 analyses, mineralogical - 23 analyses. We performed the following isotope analyses of rocks: Rb-Sr - 4 determinations, Sm-Nd - 4 determinations, Pb-Pb - 3 determinations. The composition of minerals is studied by X-ray microprobe (351 analyses); the surface of minerals was studied via the scanning electronic microscope (54 images). The age of rocks was defined by means of spore-pollen analysis (1 analysis.) and paleofloristic analysis (6 analyses).

### **THE COMPOSITION OF PIPES OF THE NENOKSA FILED, DISCOVERED PRIOR TO 2008**

The first magmatic occurrences of the Arkhangelsk diamond-bearing province were discovered in the Onega peninsula. In the period from 1936 to 2000 about 40 pipes were discovered in the Nenoksa field (Fig.2). They are composed of different structural varieties of the feldspathoid olivine melilitites [35, 9]. The pipes are characterized by isometric or weakly elongated shape (Fig. 3) and large size (from 200\*200 up to 600\*800m); on the surface they are revealed by contrast magnetic

anomalies (200-1400 nTl). The pipes cut the Upper Vendian aleurolites and argillites and are overlapped by the Quaternary sediments of various thicknesses (from 0-1 m up to 90 m). The age of the intrusion of the Nenoksa field is determined from carbonized plant remnants and spore-pollen analysis as the Late Devonian, corresponding to the Early Hercynian stage of the tectonic-magmatic activation of the region [23, 24, 26].

An internal structure of the pipes is one and the same type and is very similar to the structure of volcanic pipes of Al-series from the Zimnyi Bereg [25, 26]. Only crater facies of pipes were penetrated in the Nenoksa field, the crater parts were distinguished by us only on the Kholmistaya and An-25 pipes. It may indicate a more significant erosion shear of pipes of the Nenoksa field as compared with the pipes of the Zimnyi Bereg. Crater facies of pipes form subvertical bodies (columns) of two types: 1) tuffisites and xenotuffisites; 2) eruptive volcanogenic-fragmentary rocks. Rocks of the lava type (3<sup>rd</sup> type) are rare. The bodies composed of tuffisites demonstrate a very homogeneous texture. Tuffisites (intrusive tuffs) are characterized by greenish-grey color, breccia lithoclastic psephitic -fine-psephitic texture and massive structure. Tuffisites contain lithoclasts of feldspathoid olivine melilitites and carbonate-clay (with zeolites) fine-crystalline cementing matrix. Xenotuffisites are marked by the increased concentrations of xenoliths cut by the Vendian terrigenous rocks (10-30%). The bodies composed of eruptive rocks show a very non-uniform, coarsely zonal texture. They contain various volcanic-clastic rocks: reddish-brown, in cases greenish -grey xenotuffites, xenotufosandstones, breccias of sedimentary rocks with a different share of melilitites lithoclasts (5-30 %), xenoliths of sedimentary rocks (5-60 %) and sandy-clayey cementing matrix (20-80 %). Rocks having elements of the pisolite structure are rare. The bodies composed of effusive rock types (lavas of melilitites) occur rare. Like tuffisites they show a homogenous structure.

The pipes of the Nenoksa field include various structural-genetic varieties of the feldspathoid melilitites, olivine melilitites, in rare cases non-pyroxene olivine melilitites. The texture of rocks of lithoclasts is middle-fine-porphyry. The rock-forming minerals involve products of the crystallization of the magmatic melt: phenocrysts of diopside-augite, olivine, rarely amphibole and minerals of the groundmass (melilite microlites, magnetite and apoglass aggregate. The xenomorphic olivine macrocrysts (“olivine of the first generation”) characteristic of kimberlites, are not found in the rocks.

In terms of geochemical features the rocks of the Nenoksa field are typical alkaline-ultrabasic rocks of melilitite type [15, 20] with a moderate silica content (42,19/36,16-52,23 % SiO<sub>2</sub> (an average/interval of values)). They are characterized by very high concentrations of alumina (11,52/9,14-13,28 % Al<sub>2</sub>O<sub>3</sub>), the increased concentrations of titan (0,76/0,56-1,03 % TiO<sub>2</sub>) and iron (8,67/6,54-11,15 % FeOtot), high contents of alkalis (2,9/0,90-5,08 % Na<sub>2</sub>O; 1,02/0,31-2,40 K<sub>2</sub>O; 3,92/2,00-6,45 % Na<sub>2</sub>O+K<sub>2</sub>O) at constant prevalence of sodium over

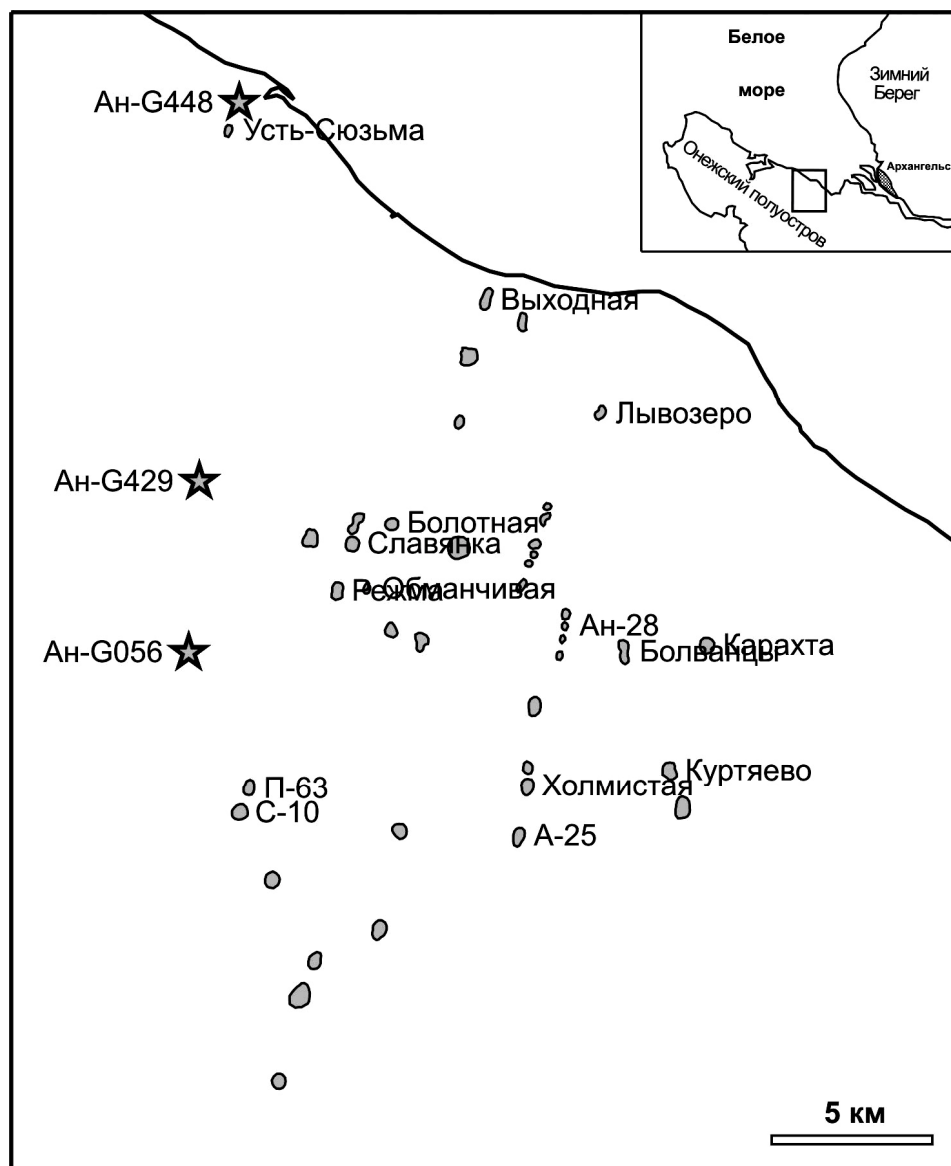


Fig.2. Location of melilitite pipes in the Nenoksa field, Onega Peninsula.

Asterisks show pipes, discovered in 2008-2009.

potassium ( $\text{Na}_2\text{O}/\text{K}_2\text{O}=4,8$ ). These rocks also demonstrate variable (and increased) magnesium content ( $\text{Kmg} = 72/65-82$ ), high content of scandium (23,4/16-31 ppm) and low concentrations of nickel (189/75-330 ppm), chrome (222/43-426 ppm) and cobalt (40/29-55 ppm). The most vivid feature of the Nenoksa rocks is a very low concentration of all incoherent elements (except for strontium and barium): Ti (see above), Ta (0,6 ppm), Nb (9,8 ppm), Zr (77 ppm), Hf (2,5 ppm), U (0,9 ppm),

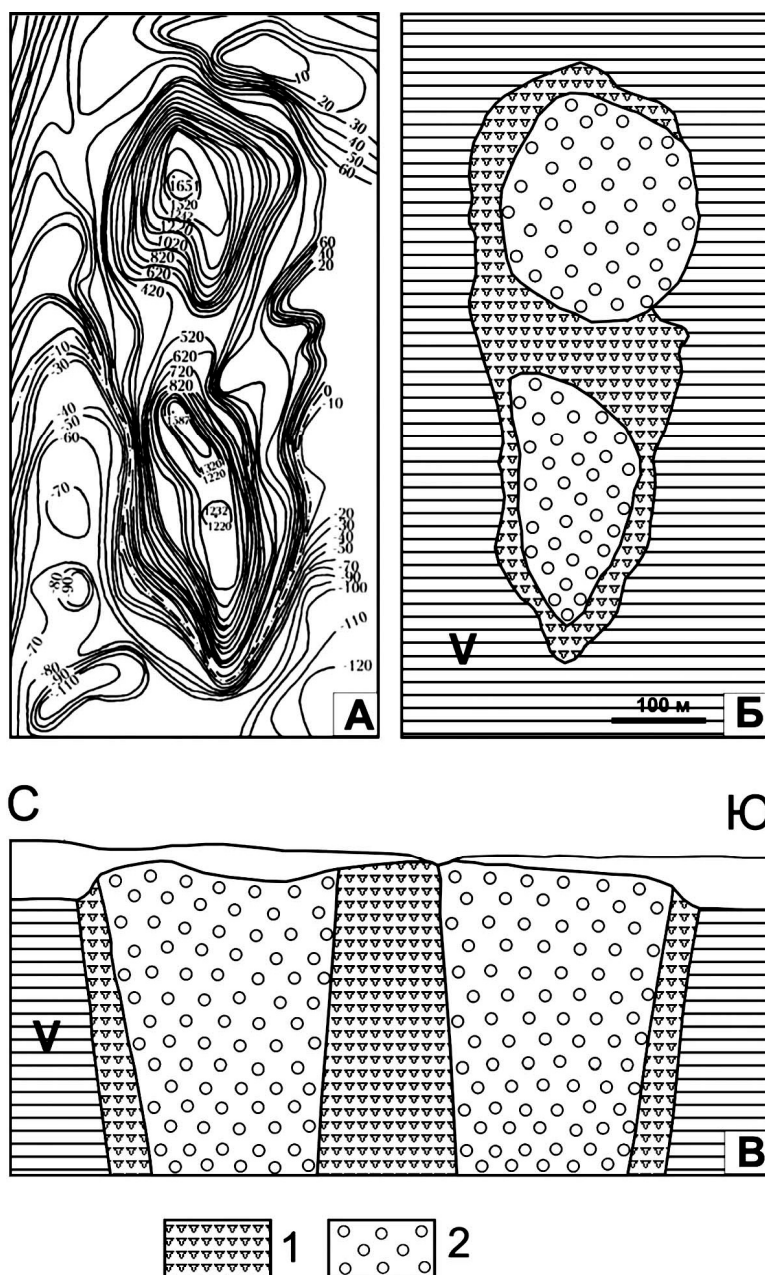


Fig.3. Bolvantsy pipe.

A - scheme of isolines of the magnetic field  $dT_{an}$ .; B – schematic geologic plan; C – schematic geologic section North-South. Varieties (intrusion phases) of volcanic rocks: 1 - xenotuffite; 2 – tuffisite.

Th (1,3 ppm), light rare-earth element (sum of REE = 70 ppm) and lanthanum / ytterbium ratio ((La/Yb) N = 6,4).

From Sr-Nd-Pb isotope characteristics it is evident that the source for melts of Nenoksa melilitites was the ancient enriched lithosphere mantle ( $eSr = +52$ ;  $eNd = -11$ ,  $T_{Nd} (Dm) = 2280$  Ma;  $^{206}Pb/^{204}Pb=18,122$ ;  $^{207}Pb/^{204}Pb=15,582$ ). The astenosphere influence on the mantle substratum of melilitites is not clear.

Amongst deep minerals the Nenoksa melilitites contain only low-titanium moderately-chromium chrome-spinellids of B and C2 depth facies [34], as well

high alumina chrome-diopside or chrome-bearing diopside of B facies [34]). Pyrope and picroilmenite have not been found in the rocks.

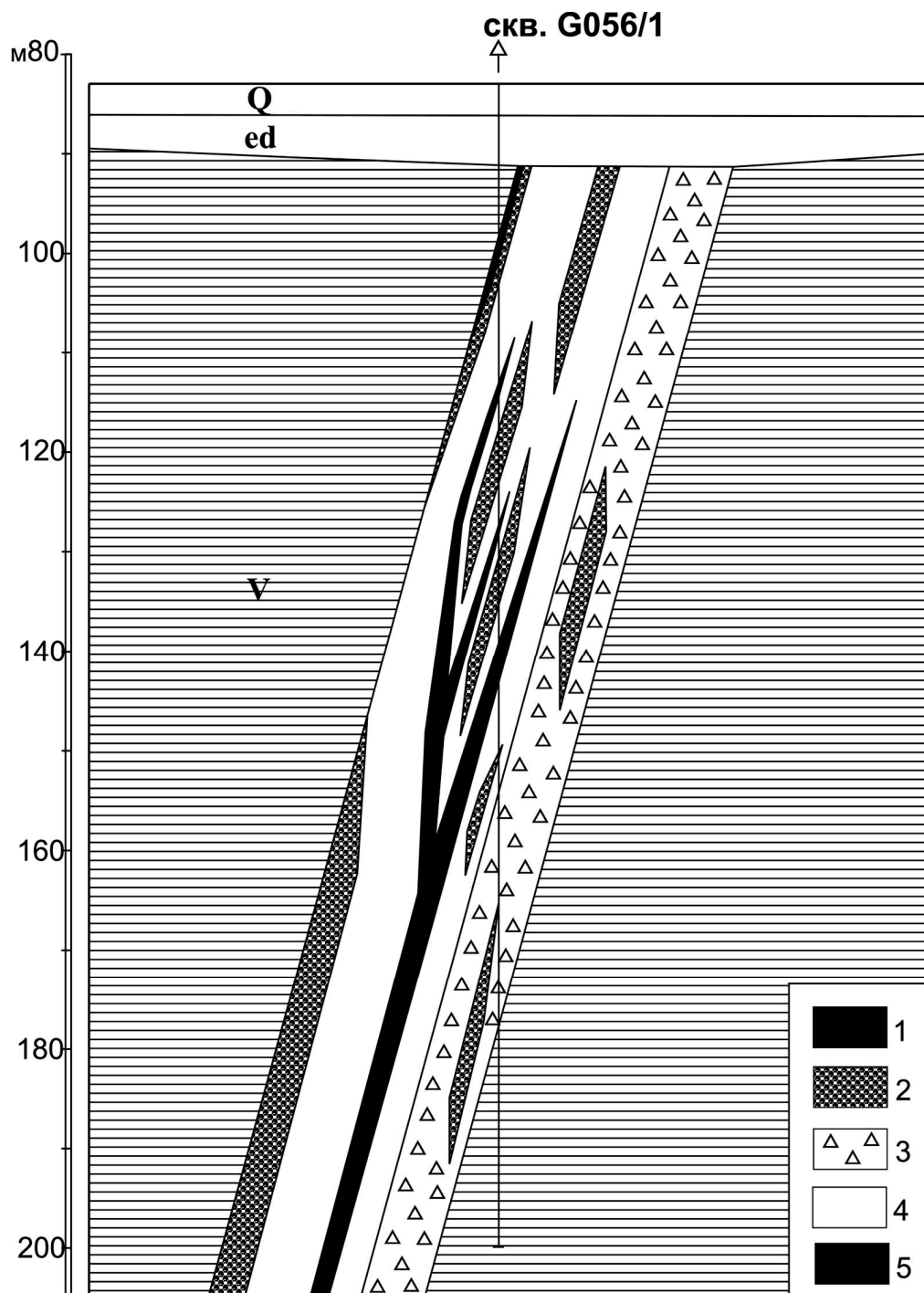


Fig.4. Schematic geologic section of the An-G056 pipe (with the overlapped sediments).

Varieties (intrusion phases) of volcanic rocks: 1 –aphyric lava; 2 – sintering tuffisite; 3 – xenotuffisite; 4 – tuffisite; 5 – middle-fine-porphry lava.

By age, features of the geological structure, petrographic, mineralogical, geochemical, Sr-Nd-Pb isotope characteristics, modeled age of the source (TNd

(Dm)) the feldspathoid olivine melilitites from the Nenoksa field are very similar to the Al-series rocks of the Zimnyi Bereg-non-pyroxene olivine melilitites of the pipes of the Izhma group (Izhma, Vesennyyaya, Letnyaya, Ozernaya) and Suksoma, but as opposed to these rocks they contain clinopyroxene phenocrysts and demonstrate the increased alumina content. The melilitites from the Nenoksa field are very different from the rocks of the Terskyi Bereg pipes primarily by geochemical and Sr-Nd-Pb isotope characteristics. As a whole, the Nenoksa melilitites form an own series of rocks, which occupies the extreme most «basaltoid» part of the general trend of Al-series kimberlites and continues the trend of Al-series kimberlite rocks from the Zimnyi Bereg.

### **FEATURES OF THE STRUCTURE AND COMPOSITION OF NEW PIPES FROM THE NENOKSA FIELD (2008-2009)**

The company «Arkhangelsk diamonds» (Joint-Stock Company) in 2008-2009 discovered three new pipes (An-G448, An-G056 and An-G429) in the western part of the Nenoksa field, some features in the structure and composition of these pipes distinguish them from 40 (!) pipes discovered earlier. As compared with the size of the pipes discovered earlier (200-800 m) the size of these new pipes is not big: from 20-25 m (An-G448, An-G056) up to 70-100 m (An-G429). The intensity of magnetic anomalies is one order lower for new pipes (25-50 nTl), as opposed to the pipes discovered earlier (200-1400 nTl). Two pipes (An-G448 and An-G429) have a simple single-phase structure and are composed of a column of red-brown xenotuffisites and xenotuffites, correspondingly, while the body of An-G056 pipe forms a volcanic complex of the complicated geology. The body of An-G056 pipe contains steeply inclined volcanic elongated pipe. Despite a small size the An-G056 pipe has a very complex internal texture (Fig. 4).

The An-G-056 pipe is composed of gray, greenish-gray volcanic rocks of the melilitites group of 5 phases of intrusion, forming 5 subvertical internally homogeneous bodies (or the preserved fragments of bodies) of different structural-genetic type: effusive rocks of the lava type and pyroclastic rocks.

- 1st phase - the aphyric, fine-crystalline lava;
- 2nd phase – sintering average-fragmentary, vitro-lithoclastic tuffisite;
- 3rd phase –middle-fragmentary, lithoclastic xenotuffites;
- 4th phase –middle-fragmentary, lithoclastic tuffisite;
- 5th phase - middle-fine-porphyry lava

The rocks of different intrusion phases occur as subvertical “columns” and (or) blocks; fragments and blocks of rocks of one intrusion phase in another one (fragments of sintering tuffisites and lavas in tuffisites and xenotuffisites) are found. A very specific feature of the pipe is the presence of sintering tuffisite of melilitites with a characteristic “fork-like” and crock-like structure of the fine-ashy vitroclastic cementing matrix, which is a new variety of rocks found in kimberlite pipes and associated rocks for the first time (Fig. 5). Such multiphase pipes with a complex structure have not been found in the Nenoksa field before. If we don't

take into account the composition of the magmatic material and size of the pipes, then as regard to the features of the geologic structure and structural-genetic types of rocks, abundance, pattern and succession of intrusion phases the An-G056 pipe is very similar to the Nyurba kimberlite pipe of the Nakyn field, Yakutia [32].

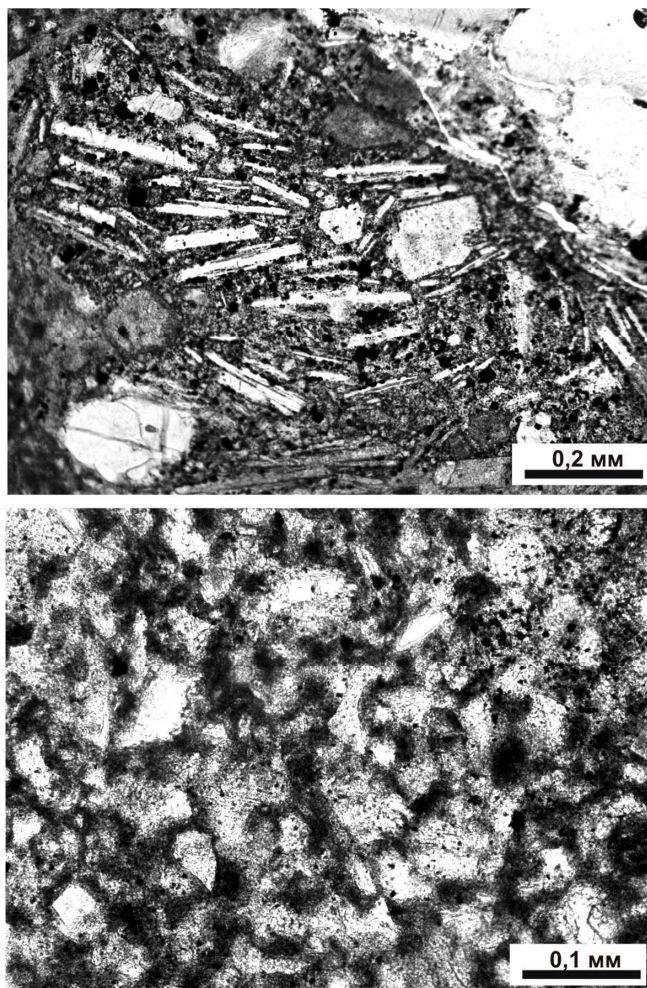


**Fig.5. An-G056 pipe, 2<sup>nd</sup> intrusion phase, sintering tuffisite of feldspathoid olivine melilitites.**

The rock contains different-size fragments of melilitites and cementing matrix of the aleurolite vitroclastic texture. On the top – melilitite lithoclast, composed of olivine-2 phenocrysts, microlites of melilitite, feldspathoid, magnetite and apoglass aggregate. At the bottom –cementing matrix, composed of fragments of volcanic glass of characteristic “fork-like” and crock-like shape. Transmitting light, Nicole II.

The magmatic material of all rock varieties from the An-G056 pipe includes strongly altered fine-medium-porphyry non-pyroxene feldspathoid olivine melilitites with idiomorphic olivine phenocrysts -2 (2-8 mm in size) in the matrix, containing apoglass aggregate with microlites of olivine-3, nepheline, melilite and magnetite. A specific feature of rocks from An-G056 pipe is the presence of large (5 - 15 mm) pseudomorphs of “olivine of the first generation”, macrocrysts, characteristic of rocks of the kimberlite series, as well as abundant large (0,5-2 mm) chrome-shpinellid separations as separate grains (octahedra ) as well as

intergrowths with olivine. Clinopyroxene phenocrysts are not found. However, one can find intratelluric inclusions, containing intergrowths of clinopyroxene, olivine and chrome-spinellid (and/or plenaste) in different ratio. The groundmass contains rare separations of tetraferriphlogopite, which is typical of Al-series kimberlite rocks of the Zimnyi Bereg (and kimberlites and kimmelilitites), but in the pipes of melilitites from the Nenoksa field it has not been found before. A similar petrographic composition is common to the rocks from the An-G429 pipe. As a whole the studied rocks from An-G056 and An-G429 pipes are similar to the rocks from other pipes of the Nenoksa field. However, the absence of clinopyroxene phenocrysts, occurrence of olivine macrocrysts and rare tetraferriphlogopite grains typical of kimberlites as well as abundant chrome-spinellid separations and intratelluric olivine-clinopyroxene intergrowths distinguish the rocks of these pipes among other pipes of the Nenoksa field and somehow makes them similar to kimmelilitites, being a transitional type of rocks between kimberlites and melilitites. At the same time like the Ust-Syuz'ma pipe the An -G448 pipe located close to it is composed of non-pyroxene feldspathoid olivine melilitites showing no signs of occurrence of the substratum from the depth.

As regard to geochemical features the rocks from An-G448 pipe as a whole are similar to melilitites from the pipes studied earlier, while the rocks from An-G056 hold a specific position (rocks of An-G429 pipe have intermediate geochemical characteristics). Geochemical characteristics of rocks of the An-G056 pipe correspond to those of alkaline ultrabasic rocks of melilitite group. As regard to the sum of alkalis, the rocks from the pipe belong to alkaline-subalkaline series ( $\text{Na}_2\text{O} + \text{K}_2\text{O} = 1,20-3,67\%$ ), but in terms of K/Na ratio the rocks can be regarded as potassium-sodium ( $\text{Na}_2\text{O}/\text{K}_2\text{O} = 0,83-4,48$ ). They are characterized by very low silica content ( $30,63-33,46\%$   $\text{SiO}_2$ ), rather low concentration of alumina ( $7,85-9,00\%$   $\text{Al}_2\text{O}_3$ ), increased magnesium content ( $\text{Kmg}=73,4-81,3$ ), moderated to increased (for melilitites) concentrations of the "ultrabasic" coherent elements: Ni, Co, Cr (up to 203, 50,6 and 452 ppm, accordingly), that well agrees with high olivine and chrome-spinellid concentrations. The concentrations of iron, vanadium and scandium vary from average to increased ( $7,92-10,28\%$   $131-208$  ppm and  $17,4-33,8$  ppm, accordingly), that is typical of melilitites from other pipes of the Nenoksa field.

The rocks of the An-G056 pipe demonstrate as a whole very low contents of incoherent elements. The concentrations of P ( $0,49-0,81\%$   $\text{P}_2\text{O}_5$ ), Rb ( $11,4-23,6$  ppm), Cs ( $0,03-0,97$  ppm) are low up to average, the contents of Sr ( $357-465$  ppm), Ba ( $155-606$   $\mu\text{g/g}$ ) vary from average to increased, concentrations of Zr ( $37-76$  ppm) and Hf ( $0,99-2,04$  ppm) are moderately low. The majority of elements in the rocks of An-G056 pipe show very small concentrations: Th ( $0,80-2,23$  ppm), U ( $0,14-0,46$  ppm) and especially Nb ( $6,91-8,57$  ppm) and Ta ( $0,33-0,48$  ppm) and LREE (sum REE =  $35,2-54,9$  ppm, (La/Yb) N =  $2,8-5,4$ ). The chondrite-normalized REE

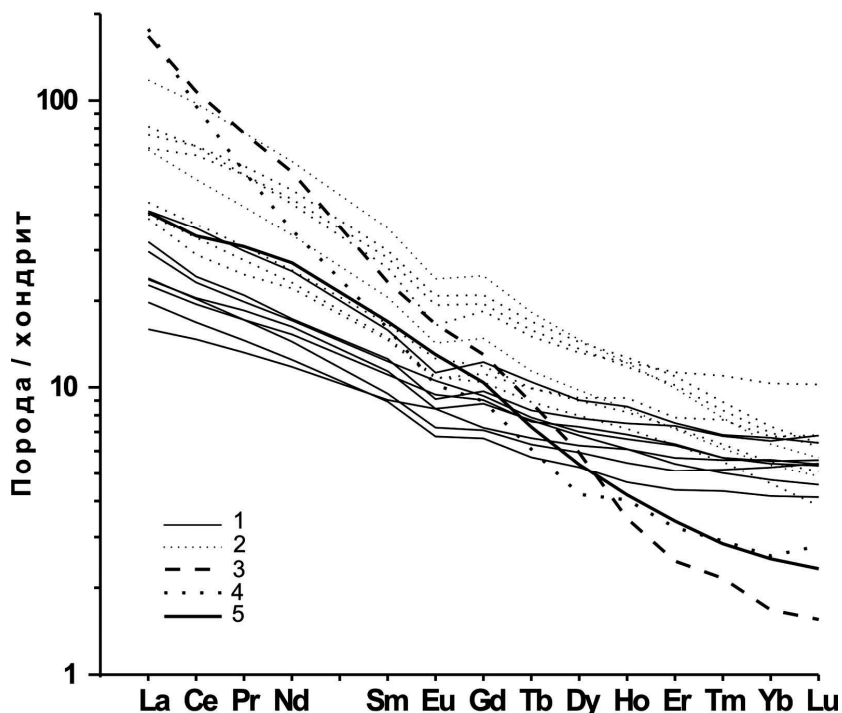


Fig. 6 . Chondrite-normalized [40] REE distribution in melilitites of the Nenoksa pipes.

1 – kimmilitites of the An-G-056 pipe; 2 – melilitites from other pipes of the Nenoksa field; 3 – Fe-Ti series kimberlites, Zimnyi Bereg (group 1); 4 – Al-series kimberlites, Zimnyi Bereg (group 2); 5 – kimberlites of the Nyurba pipe (Nakyn field, Yakutia).

distribution pattern for various rock types is characterized by a flat positive inclination both in the field of heavy, and light lanthanoids, and a clear Eu minimum. In terms of REE distribution the studied rocks are similar to melilitites from other pipes of the Nenoksa field and are different from kimberlites of the Zimnyi Bereg. It should be noted, that as regard to the distribution of light REE the rocks from An-G056 pipes are similar to kimberlites of the Nyurba pipe of the Nakyn field, [32], but the increased concentrations of heavy REE significantly distinguish the rocks of An-G056 pipes from kimberlite rocks of different types.

By main geochemical characteristics the rocks from the An-G056 pipe are similar to the feldspathoid olivine melilitites of other pipes of the Nenoksa field; however they are markedly different in the increased basicity: low contents of  $\text{SiO}_2$  and  $\text{Al}_2\text{O}_3$ , high magnesium content, increased Cr and Ni concentrations and the lower concentrations of the majority of incoherent elements. In terms of some geochemical parameters (high magnesium content, increased chrome content) the rocks of An-G056 pipe become similar to «kimmilitites- a transitional type of rocks between kimberlites and melilitites.

The mineralogical data indicate that rocks from the An-G056 pipe are almost completely altered, autometasomatically mudded, only magnetite and apatite have been preserved among primary-magmatic minerals. Among deep minerals only low-titanium moderate-chrome chrome-spinellid of B and C2 depth facies [34], as well as high-alumina chrome-diopside of B facies [34] have been found in the

rocks. By the morphology and composition they are protomagmatic but not the mantle minerals.

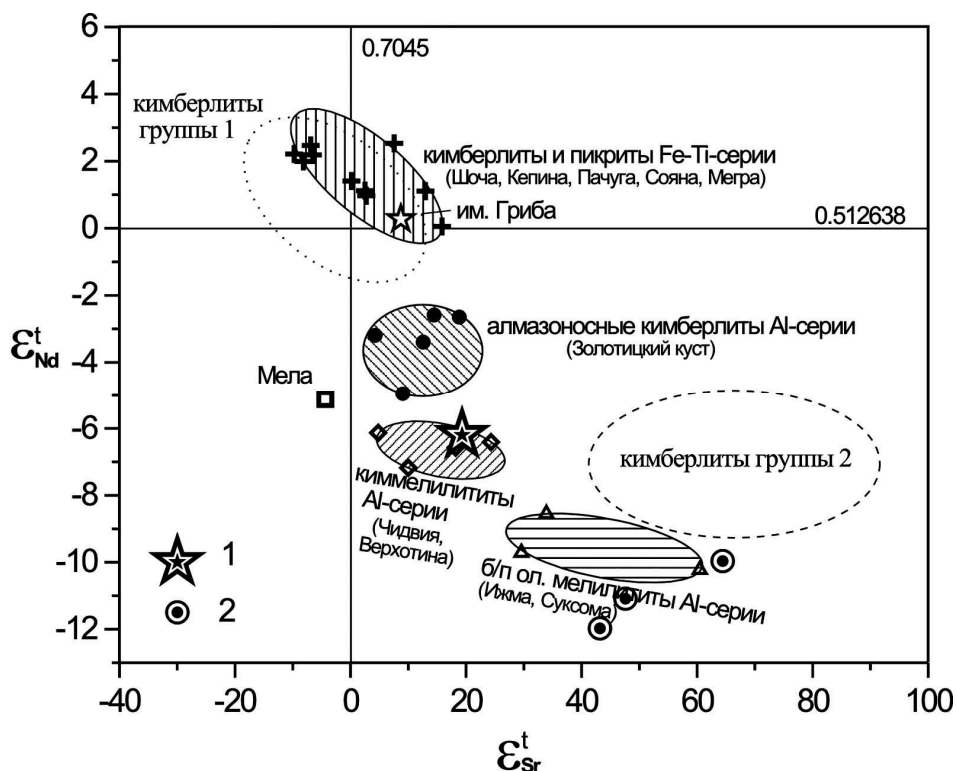


Fig. 7.  $\epsilon_{\text{Sr}}^t$ - $\epsilon_{\text{Nd}}^t$  diagram for melilitites of the An-G056 pipe, other pipes of the Nenoksa field and different types of volcanic rocks of the kimberlite series, Zimnyi Berg [31].

All data are corrected for the age of intrusion as 370 Ma.

Unlike others pipes of the Nenoksa field, the rocks of An-G056 (and An-G429 as well) pipes demonstrate high concentrations of intratelluric minerals and inclusions (olivine+clinopyroxene+/-amphibole+/-chrome-spinellid; olivine+pleonaste+/-clinopyroxene). Deep minerals of the ultrabasic paragenesis typical of kimberlites (pyrope, picroilmenite chrome-diopside, chrome-spinellid) have not been found in the rocks of the pipe. However, the pipe contains deep minerals of eclogite paragenesis: pyrope-almandine, corresponding to garnets from diamond-bearing eclogites of I «A», I «B» and I «C» groups as well as non-diamondiferous eclogites of II «B» and II «C» groups [41,43], individual grains of pale pinkish-violet corundum.

The source of melilitite melt of pipes from the Nenoksa field studied by us earlier was the ancient isotope-enriched lithosphere mantle (EM II) with the following parameters:  $\epsilon_{\text{Sr}}^t$  from + 43 up to + 64 and  $\epsilon_{\text{Nd}}^t$  from -10 up to -12, with modeled age  $T_{\text{Nd}}(\text{DM}) = 2168\text{-}2365$  Ma, and with a probable participation of the ancient lower crust substratum of the subduction origin. Moreover, the features of the asthenosphere influence on mantle substratum are not available. The rocks from the An-G056 pipe demonstrate moderately increased positive  $\epsilon_{\text{Sr}}^t$  (+19,3), and moderately low negative value  $\epsilon_{\text{Nd}}^t$  (-6,2) that significantly differ them from

melilitites of pipes studied earlier. The source of melilitite melt of An-G057 was also the ancient isotope-enriched lithosphere mantle (EM II) with the same modeled age ( $T_{Nd}(DM) = 2268$  Ma) and a probable-participation of the ancient lower crust substance of the subduction origin. However, the asthenosphere influence on the mantle source of rocks from the An-G056 pipe is evident as its Nd-Sr-isotope characteristics are similar to parameters BSE (asthenosphere source) (Fig. 7).

The distribution pattern of Nd-isotope characteristics of volcanic rocks, mainly  $\epsilon Nd$ , over the area of the Zimnyi Bereg shows a natural pattern with elements of symmetry of the central (centripetal) type. Values  $\epsilon Nd$  increase from those common to the ancient enriched lithosphere mantle in the Izhma and Suksoma melilitites in the marginal part of the region ( $\epsilon Nd$  from -8,6 up to -10,2,  $T_{Nd}(Dm) = 2110$  Ma), to the values, characteristic of weakly enriched mantle in Chidvia and Verkhotina kimmellitites ( $\epsilon Nd$  from -6,1 up to -7,2), and further - up to diamond-bearing Al-series kimberlites of the Zolotitskyi group of pipes in the intermediate zone of the region ( $\epsilon Nd$  from -2,6 up to -4,9), and, at last, reach values common to the weakly depleted mantle and BSE values in the central part of the region, (in the zone of occurrence of Fe-Ti-series kimberlite rocks ( $\epsilon Nd$  from +0,1 up to +2,5)). Such a pattern of changes in Nd-isotope characteristics for volcanic rocks from the margin towards the center of the region can result from a gradual increase of the influence of the asthenosphere diapir (intrusion), on the lithosphere mantle substratum. That diapir intruded in the Middle-Late Devonian in the central part of the Zimnyi Bereg. As regard to Nd-Sr isotope characteristics melilitites of Nenoksa pipes studied earlier are completely similar to the Izhma and Suksoma melilitites in the marginal part of the Zimnyi Bereg area ( $\epsilon Nd = -10$  --  $-12$  and  $-8,6$  --  $-10,2$ ;  $\epsilon Sr = +43$  -  $+64$  and  $+30$  -  $+61$ ;  $T_{Nd}(Dm) = 2280$  and  $2110$  Ma, accordingly). At the same time by Nd-Sr-isotope characteristics and the type of the mantle source the melilitites from An-G056 pipe significantly differ from Izhma and Suksoma melilitites and on the contrary are similar to Al-series Chidvia and Verkhotina kimmellitites in the intermediate zone of the Zimnyi Bereg region ( $\epsilon Nd = -6,2$  and  $-6,1$  --  $-7,2$ ;  $\epsilon Sr = +19,3$  and  $+5$  -  $+24$ ) (Fig. 7). An unusual feature of new type of pipes, discovered on the west of the Nenoksa field, is the occurrence of xenoliths of diverse rocks from eroded formation in the An-G429 pipe. They include the Upper Vendian-Lower Cambrian argillites with charring remnants of tubules of tubemakers «sabellidites» (*Sabellidites cambriensis*); the clay, glauconite-containing sandstones and Low Paleozoic ferriferous gravelites (Upper Cambrian – Lower Ordovician); as well as Late Devonian numerous charred vegetative remnants (archaeopteryx plant *Callixylon* sp.).

## DISCUSSION

The detailed studies in 2008-2009 in the middle part of the Onega peninsula led to the discovery of three new pipes on the western margin of the Nenoksa field. The geological structure and composition of them differ from those in pipes of

olivine melilitites and indicates a more differentiated (various) magmatism in the Nenoksa field. By some features the rocks of these pipes are similar to «kimmelilitites» - the rocks of transitive type between melilitites and kimberlites. It allows estimating the diamond potential of the Onega peninsula more precisely.

The Lower Vendian eroded deposits (argillites) and Upper Cambrian-Middle Ordovician sediments (argillites and sandstones with glaukonite, ferriferous gravelites of oolite and beanlike ferriferous ores) existed in the western part of the Nenoksa field when the volcanic pipes intruded. However, the Cambrian-Ordovician sediments didn't exist in the central part of the Nenoksa field, when the volcanic pipes intruded. It is connected with a different level of the erosion shear, with rather different age of pipe intrusion within the Late Devonian (a possible interval up to 14 Ma), as well as features of paleogeography and paleotectonics of the region in the Cambrian-Late Devonian. By the composition the pipes of the western part of the Nenoksa field (An-G056 and An-G-429 pipes) noticeably differ from the other pipes of the field. The characteristics which make them different from typical melilitites and similar to «kimmelilitites», include:

1) Complex multiphase (5-phase!) structure and a complete autometasomatic argilization of rocks transformed in a homogeneous montmorillonite - saponite aggregate;

2) Increased magnesium content of rocks, moderately high Cr, Ni and lower SiO<sub>2</sub> and Al<sub>2</sub>O<sub>3</sub> contents;

3) Olivine composition of phenocrysts, absence of clinopyroxene phenocrysts, occurrence of tetraferriphlogopite separations, abundant large chrome-spinellid separations as well as macrocrysts of "olivine of the first generation" (a necessary feature of kimberlite rocks);

4) High concentrations of minerals of the crystallization protomagmatic stage (chrome-spinellids, clinopyroxene, amphibole, olivine) and intratelluric inclusions (olivine+clinopyroxene+/-amphibole+/-chrome-spinellid; olivine+pleonaste+/-clinopyroxene);

5) Presence of minerals-satellites of diamond of the eclogite paragenesis (pyrope-almandine from diamond-bearing eclogites of I "A", I "B" and I "C" groups and non-diamondiferous eclogites of II "B" and II "C" groups [41, 43], pale pinkish-violet corundum).

In addition, as opposed to other pipes of the Nenoksa field, the asthenosphere influence on the mantle source in An-G056 pipe is apparent in its Nd-Sr isotope characteristics similar to BSE (asthenosphere source). The melilitites of the Nenoksa pipes studied earlier by many (including isotope) characteristics are similar to the non-diamondiferous Izhma and Suksoma melilitites in the marginal part of the Zimnyi Bereg region while the rocks of the An-G056 pipe by the majority of characteristics of the composition and type of mantle source differ from the Izhma and Suksoma melilitites and on the other hand are similar to Chidvia and Verkhovina kimmelilitites of Al-series (with features of diamond potential) in the intermediate zone of the Zimnyi Bereg Region. As regard to the composition of

rocks, real occurrence of diamonds in the An-G056 is improbable. Only mineralogical features of volcanic rocks of the pipe specify their diamond potential (most likely even hypothetical) of these pipes. These features indicate a deep character of magmatic occurrences of the region, the diamond potential of which can have eclogite (subduction) nature. Revealing of new sites in the Nenoksa field differing in composition is of great significance. The rocks of An-G056 pipe, correspond to the non-pyroxene feldspathoid olivine melilitites, however by the combination of the compositional features (petrographic, mineralogical, geochemical, isotope) they become similar to “kimmelitites” of Al-series, demonstrating the features of the protomagmatic deep (mantle) substratum, that distinguish the rocks of this pipe from other Nenoksa pipes. The An-G056 pipe can be a new site, allowing finding the specific features and even elements in the symmetry of monotonous distribution of numerous similar magmatic occurrence of the Nenoksa field.

As researches [28] indicate, the North of Russian platform as a whole demonstrates a close spatial—temporal and genetic association of the kimberlitic (including diamond-bearing) volcanism with melilititic volcanism. It results in a close location of volcanic occurrences with significantly different features, including the diamond potential. It is common to the Devonian magmatism of all sites of the Arkhangelsk diamond-bearing province: Zimnyi Bereg, Letnyi Bereg of the Onega peninsula, Terskyi Bereg of the Kola peninsula, as well as Middle Timan. The distribution of many parameters in the composition of rocks all over the areas possesses elements of symmetry [7,26] so the linear type of symmetry is characteristic of the distribution of coherent elements all over the Zimnyi Bereg region. In this region from the east towards the west one can observe a change in types of rocks from typical basalts, through non-pyroxene olivine melilitites poorly diamond-bearing kimberlites of Fe-Ti-series, kimpicrites and kimmelitites to diamond-bearing kimberlites of the Griba pipe and the Lomonosov deposit. Thus, from the east to the west we can observe an increase in the degree of basicity and total magnesium content of rocks, the concentration of the substratum from the depth and total diamond potential of rocks. A similar lateral zoning in the location of explosion pipes by the composition and depth of occurrence of the magmatic center is characteristic of the Terskyi volcanic field of the Kola peninsula, however the trend of change in the composition of rocks from explosion pipes is opposite as compared with the Zimnyi Bereg: the increase in the degree of ultrabasicity is evident from the west towards the east. There is a change of rocks in the following succession: alkaline picrites (foidites) – melilitites – olivine melilitites - non-pyroxene olivine melilitites («kimmelitites») – poorly diamond-bearing kimberlites. The comparison of zoning in the Terskyi field and Zimnyi Bereg region can suggest a common regular petrologic zoning of alkaline-ultrabasic volcanism of the Belomorsky Region (Fig. 8). This zoning can be characterized by plane type of symmetry (with a plane of symmetry of the White Sea) or elements

of symmetry of the central type (with the center of symmetry in the southwest termination of the White sea gulf).

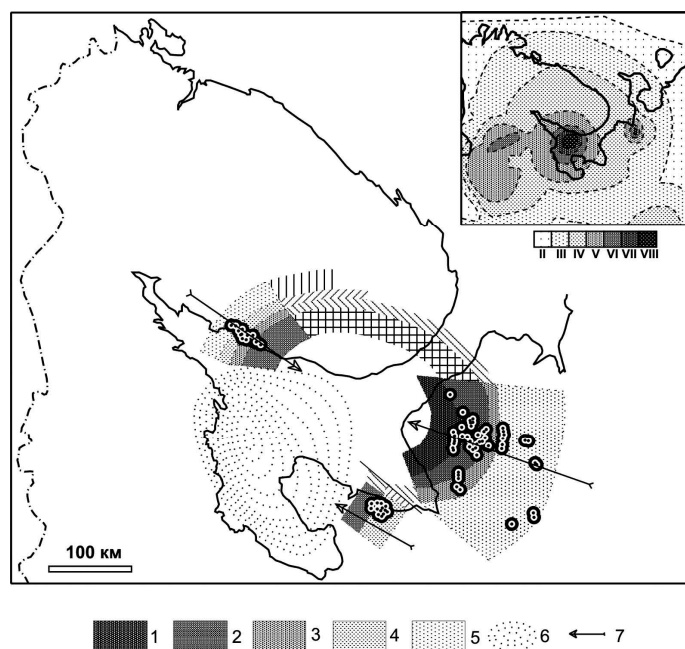


**Fig.8. Scheme of the petrologic zoning of the early Hercynian volcanism. Belomorsky region (from [29] with additions).**

Zones of the Early Hercynian volcanic rocks occurrence: 1 – diamond-bearing kimberlites; 2 – weakly-diamondiferous kimberlites, kimmilitites, kimpicrites; 3 – non-pyroxene olivine melilitites; 4 – olivine melilitites; 5 – basalts and foidites, 6 – Belomorsky gravitational maximum dg; 7 – direction of the increase in the degree of ultrabasicity of volcanic rocks. Inlet at the top – fragment of the map of macroseismic field of the Russian platform [2] with the distribution of isoseist from II to VIII magnitude.

Together with other explosion melilitite pipes the An-G056 and An-G429 pipes found in 2008-2209 in the western part of the Nenoksa field, Onega peninsula the rocks of which by the composition are similar to kimmilitites form elements of petrologic zoning, demonstrating the same pattern and the same increase in the degree of ultrabasicity of rocks (east-west like the pipes of the Zimnyi Bereg. The pipes of the Nenoksa field are similar in age, geologic structure and composition to the pipes of the Terskyi Bereg and Zimnyi Bereg and fall into a general zoning pattern of the Early Hercynian volcanism in the Belomorsky region. Diamond-bearing and poorly diamond-bearing kimberlites occur in the central part of the Belomorsky region, while non-diamondiferous melilitites, foidites and basalts are found on the periphery. The Early Hercynian pipes of the Terskyi filed, Nenoksa field and the Zimnyi Bereg region are located in the northern and eastern margins of the Belomorsky gravitational dg maximum, associated with the Devonian mantle diapir or “plume”. The features of the petrologic zoning of the Early Hercynian volcanism are most likely related to features in the geometry and formation of the Belomorsky mantle plume.

It should be noted, that the Belomorsky dg maximum almost precisely coincides with a rather contrast maximum of intensity of earthquakes (isoseists up to VII-VIII magnitude) in a macroseismic field of the Russian platform [2] - is quoted from [38], that is actually coincides with the epicenters of recent earthquakes. Therefore, the existence of the Devonian Belomorsky mantle diapir (plume) till now is revealed through the intensive tectonic activity of the region.

## CONCLUSION

The pipes discovered in the western part of the Nenoksa field, Onega peninsula in 2008-2009 the rocks of which are similar in composition to kimmilitites together with other pipes of melilitites of the Nenoksa field form the elements of the petrologic zoning demonstrating the same pattern and increase in the degree of ultrabasicity of rocks (east-west), like Zimnyi Bereg pipes.

The pipes of the Nenoksa field are similar in age, geology and composition to the pipes of the Terskyi Bereg and Zimnyi Bereg and fall into a general pattern of the zoning of the Early Hercynian volcanism of the Belomorsky region. The diamond-bearing and weakly diamond-bearing kimberlites occur in the central part of the Belomorsky Region while diamond-free melilitites, foidites and basalts are found in the peripheral part. The early Hercynian pipes of the Terskyi field, Nenoksa field and Zimnyi Bereg Region are located in the northern and eastern margins (slope) of the Belomorsky g maximum associated with the mantle diapir or "plume".

The rocks of the An-G056 pipe demonstrate deep minerals of the eclogite paragenesis - a garnet and corundum from various eclogite rocks (groups I "A", I "B", I "C", II "B", II "C"), including those from diamond-bearing eclogites and eclogites of the group I "C" - indicators of the subduction process at the level of the diamond-bearing mantle. These features specify deep character of magmatic occurrences of the area, probable diamond potential of which can have purely eclogite (subduction) nature.

A variety of the composition of diamond-bearing magmatic rocks becomes larger from year to year, and we do not know yet, what composition has to be common to the volcanic rocks, the magmatic centers of which were localized only in deep parts of subduction zones and whether these volcanic rocks can be potentially diamond-bearing (and industrially diamond-bearing). We hope, that discovery of three new pipes indicate new, still not opened possibilities of the bed-rocks diamond potential of the Nenoksa field, the Onega peninsula, and the Belomorsky region as a whole.

## REFERENCES

1. **Above N.V., Rosanova N.A.** Greywacke of the Nenoksa region // Geological results of deep drilling in the Arkhangelsk Region, issue. 8, 1940, Arkhangelsk, p. 47-54.
2. **Anan'in I.V.** The associations of the seismicity of the Russian platform with modern tectonic movements. // Modern movements of the Earth's crust., 1968. № 3.

3. **Vardanyants L.A.** Geological map of the Precambrian basement (scale 1:5000000). An explanatory note. Gosgeoltekhizdat, 1960.
4. **Verichev E.M., Volkova N.A., Piskun L.V., Sivertseva I.A., Stankovsky A.F.** The Ordovician acritarchs in the north of the Russian plate. // *Izvestiya AN SSSR, Geology. series*, 1990, N 7, p.152-155.
5. **Verichev E.M., Sablukov S.M., Sablukova L.I., Zhuravlyov D.Z.** New type aof diamond-bearing kimberlites of the Zimnyi Bereg // *Doklady of Russian Academy of Sciences*, 1999. v.368, N 2. p. 226-229.
6. **Vyruchaev V.A.** Thermomagnetic characteristics of breccias from the Onega peninsula. // *Geology and minerals of the North of Russian platform*. 1987. p. 112-122.
7. **Garanin V.K.** Mineralogical zoning of kimberlites // *Geology and prospecting*, 1991 № 9, p.38-49.
8. **Grib V.P., Stankovsky A.F., Verichev E.M., Dobeiko I.P., Konstantinov Yu.G., Sobolev V.K.** The first finding of the prior to Middle Carbonaceous eruptive breccia in the north of the Russian plate. // *TsNIIGRI Proceedings*, 1981, issue.156, p.112-113.
9. **Danilov M.A, Mal'kov B.A.** Explosion pipes of the Onega peninsula // *Geology and minerals of Northeast RSFSR. Syktyvkar*, 1973.
10. **Danilov M.A.** Features of the structure of the Earth's crust on the Onega peninsula in connection with forecasting of kimberlitic volcanism in the North of Russian platform // *Tectonics of Arctic regions. Issue 1*, 1975.
11. **Du-Toit A.L.** *Geology of Southern Africa.*, Publishing House Foreign Literature, Moscow, 1957.
12. **Kalinkin M.M., Arzamastsev A.A., Polyakov I.V.** Kimberlites and related rocks of the Kola Region // *Petrology*, 1993, v. 1, # 2, pp. 205-214.
13. **Kaminsky F.V., Klyuev Yu.A., Konstantinovskiy A.A, Piotrovskiy S.V., Sochneva E.G., Yuzhakov V.M.** Features of the diamond potential of alkaline basaltoids, North of the Russian Platform. // *Doklady AN USSR*, 1975, V.222, # 4, pp. 939-941.
14. **Kaminsky F.V.** Alkaline-basaltoid breccias of the Onega peninsula // *Izv. AN USSR. Geology*, 1976, # 7, p .50-59.
15. **Bogatikov O.A., Gon'shakova V.I., Efremova S.V. et al.,** Classification and the nomenclature of magmatic rocks. M. Nedra. 1981.160 p.
16. **Kol'tsov N.F.** Features of volcanic activity on the Onega peninsula // *Pripoda.1937. № 7*
17. **Konstantinov Yu.G.** Explosion pipes of the Bolvantsy // In: *Sketches on geology and minerals of the Arkhangelsk area. Arkhangelsk: Pomorsk State University*, 2000. pp. 45-51.
18. **Maleev E.F.** *Volcanics.* Moscow. Nedra. 1980.240 p.
19. **Milashev V.A.** Kimberlite provinces // *NIIGA Proceedings. V.176. L. Nedra*, 1974, 236 p.
20. **The Petrographic code.** Magmatic, metamorphic, metasomatic, impact formations. The third edition. *Izd. VSEGEI*. 2009.194 p.
21. **Ruzhtskiy V.O..** On explosion pipes on the Russian Platform // *Doklady AN USSR*, 1963, V.152, N2, p. 404-407.
22. **Sablukov S.M., Dudar L.P., Dovzhikova E.G., Fishman M.V.** Phases of formation and age of kimberlite pipes of Middle Timan // *TsNIIGRI Proceedings*, issue 182, 1983, p. 64-74.
23. **Sablukov S.M.** On the problem of phases of formation and age of explosion pipes of the Onega peninsula. // *Doklady ANUSSR*, 1984, V.277, N 1, p.168-170.
24. **Sablukov S.M.** On age of explosion pipes of the ultrabasic rocks// *TsNIIGRI Proceedings*, Issue.218, 1987, p.24-27.
25. **Sablukov S.M** About petrochemical series of kimberlite rocks. // *Reports of AN SSSR*, 1990, V.313, N 4, p.935-939.
26. **Sablukov S.M.** Volcanism of the Zimnyi Bereg and petrologic criteria of diamond potential of kimberlites: Thesis, Sciences. M.: TSNIGRI. 1995. 24 pp.
27. **Sablukov S.M.** .Arkhangelsk diamond-bearing province // *Sketches on geology and minerals of the Arkhangelsk area. Arkhangelsk: Pomor State University*, 2000. p. 75-84.

28. **Sablukov S.M.** Petrologic zoning of kimberlite sites of the Arkhangelsk diamond-bearing provinces // *Diamonds and diamond potential of the Timan-Ural region*. Syktyvkar, Geoprint, 2001. p. 127-129.
29. **Sablukov S.M., Sablukova L.I., Verichev E.M.** Type of mantle substratum of the Zimnyi Bereg region in connection with formation of kimberlites with rounded and table-cut diamonds // *Deep magmatism, magmatic sources and plumes*, .2002. Irkutsk, p. 134-149.
30. **Sablukov S.M., Sablukova L.I.** System of the early Hercynian magmatism in the north of the Russian platform as a basis for diagnostics of rocks and estimation of their diamond potential // *Efficiency of forecasting and prospecting of deposits of diamonds: past, present and future*. 2004 «ALROSA». VSEGEI p. 288-291.
31. **Sablukov S.M., Sablukova L.I.** Degree of the asthenosphere influence as one of defining factors of kimberlite rocks diversity // *Deep magmatism, its sources and plumes*. 2006, Irkutsk, p. 175-190.
32. **Sablukov S.M., Sablukova L.I., Stegnitskiy Yu.B., Karpenko M.A., Spivakov S.V.** Volcanic rocks of the Nyurba pipe: reflection of the state of the upper mantle of the region from Riphean to the Carbonaceous // *Deep magmatism, its sources and plumes* .2008, Irkutsk, p. 131-164.
33. **Sinitsyn A.V., Stankovsky A.F., Danilov M.A.** Kimberlite-like eruptive Nenoksa breccia and diamond potential in the north of Russian Platform // *State and perspectives of expansion of source of raw materials of Northwest Russia*, Nedra, 1973, p. 292-301.
34. **Sobolev V.S., Dobretsov N.L., Sobolev N.V.** Classification of deep xenoliths and types of the upper mantle // *geology and Geophysics*. 1972.№12. p.37-42.
35. **Stankovsky A.F., Danilov M.A., Grib V.P., Sinitsyn A.V.** Pipes of explosion Onega Peninsula // *Сов.геология*, 1973, N 8, с.69-79.
36. **Stankovsky A.F., Verichev E.M., Grib V.P., Skripnichenko V.A., Sobolev V.K.** new type of the magmatism in the Vendian in the north of the Russian plate // *Doklady AN SSSR*, 1979, v.247, N 6, p. 1456-1460.
37. **Shutov B.S., Smirnov Yu.D., Lukyanova L.I., Mikhailovskaya L.N.** Brief mineralogical-petrographic characteristics of Middle Timan kimberlites // *ZVMO*, 1983, v.4, p.436-443.
38. **Yudakhin F.N., Schukin Y.K., Makarov V.I.** Deep a structure and modern geodynamic processes in the lithosphere of the east-European platform. Yekaterinburg, 2003. 300 pp.
39. **Beard A.D., Downes H., Htegner E., Sablukov S.M., Vetrin V.R., Balogh K.** Mineralogy and geochemistry of Devonian ultramafic minor intrusions of the southern Kola peninsula: implications for the petrogenesis of kimberlites and melilitites. 1998. *Contrib. Mineral. Petrol.* 130: p.288-303.
40. **Boynton W.V.** Geochemistry of the rare earth elements: meteorite studies. In: Henderson P. (ed.), *Rare earth element geochemistry*. Elsevier, 1984, pp. 63-114.
41. **Coleman R.G., Lee, D.E., Beatty, L.B. and Brannock, W.W.** 1965. Eclogites and eclogites: their differences and similarities. *Bull. Geol. Soc. Amer.* 76, 3, 483-508
42. **Sablukov S.M.** (1995) Petrochemical series of kimberlite rocks of Arkhangelsk Province // 6th IKC, Russia, Novosibirsk, Extended Abstracts, pp. 481-483.
43. **Schulze, D.J.** A classification scheme for mantle-derived garnets in kimberlite: a tool for investigating the mantle and exploring for diamonds. In: Jones, A.G., Carlson, R.W. and Grutter, H. (Eds.), *A Tale of Two Cratons: The Slave-Kaapvaal Workshop*. Lithos, 2003. v. 71 (2-4), p. 195-213.

## Deep seated xenoliths from the Phlogopite-bearing brown breccia of Udachnaya pipe.

Ashchepkov I.V.<sup>1</sup>, Ntaflos T.<sup>2</sup>, Vladykin N.V.<sup>3</sup>, Ionov D.A.<sup>4</sup>, Kuligin S.S.<sup>1</sup>, Malygina L.V.<sup>1</sup>, Mityukhin S.I.<sup>5</sup>, Palessky S.V.<sup>1</sup>, Khmelnikova O.S.<sup>1</sup>

<sup>1</sup> *Institute of Geology and Mineralogy, SD RAS Novosibirsk 630090, Russia;*

<sup>2</sup> *University of Vienna, Austria;*

<sup>3</sup> *Institute of Geochemistry SD RAS, Favorsky str. 1a, Irkutsk;*

<sup>4</sup> *Université J. Monnet & Umr-Cnrs 6524, 23 P. Michelon, 42023 Saint-Etienne, France;*

<sup>5</sup> *66403 Central Science and Research Geology And Prospecting Institute Of The Stock Company "ALROSA", Chernyshevsky Str, 7, Mirny, 678170 Russian Federation.*

### ABSTRACT.

The brown breccia from the bottom of the Udachnaya kimberlite quarry contain the most deep and fresh mantle xenoliths in the pipes captured from the levels of about 80 kbar and representing 5 separate capturing intervals. Detail study in thin section of the large set (>200) of xenoliths from these kimberlite face allowed to reconstruct the mantle section to this level. In the lowermost part of the mantle sections prevail dunite – eclogite lenses together with the porphyroclastic peridotites of harzburgitic compositions essentially fertilized by Ti - rich melts which produced Cr-rich associations (to 14 Cr<sub>2</sub>O<sub>3</sub>% in garnets). Deep seated metasomatites Ilmenite – clinopyroxene pyroxenites (eclogites) and sheared peridotites are developed within 75-55 kbar intervals. The levels upper 40-55 kbars are correspondent to 2 lenses of peridotites with growing up Fe# and high developing of the pyroxenites due to several stages of melt percolation leaving the trends of different Fe#, CaO content in the clinopyroxenes and garnets.

Interaction of the protokimberlite melt with the deeper level was responsible for peridotite heating and shearing and wide scale interaction producing the remelting of the deep eclogites, and possibly creation of some population of the diamonds. The phlogopite metasomatism accompanies this interaction.

The high precision Ol data obtained on Cameca100SX for 64 xenoliths show grouping in to several groups. The higher in Ca -Ti in Ol is porphyroclastic peridotites or sheared peridotites. The lower Ca but high Ni values are typical for the coarse garnet peridotites the lower in Ni for the Sp varieties.

Phlogopite metasomatism is developed in the whole section of the mantle column beneath the pipe. Melt related phlogopites from the spinel facies probably are related to the ancient stages of the melt percolation like those found in the peridotite xenoliths from Alakite field or to the basaltic stages preceding kimberlite magmatism. The deeper levels probably are correspondent to the deep seated melts close to kimberlite II which produced the Ti-Ca enrichment not long before the eruption and accompany last stages of shearing. The deep seated phlogopite breccia were formed at the deep level of the mantle column due to the H<sub>2</sub>O rich fluid interaction with the mantle peridotites.

**Key words.** *Mantle, olivine, high precision geochemistry, thermobarometry, peridotites, eclogites. Layering, trace elements.*

## **INTRODUCTION.**

Deep seated xenoliths from Udachnaya were described in several publications [1, 4, 9, 20, 29, 30, 31, 36, 41, 47, 48, 49, 51, 52, 54, 55, 56, 58-65, 68] Peridotites and pyroxenite xenoliths were not so detailed in description as the eclogites and pyroxenites [8, 34, 45-47, 58-62]. Here are reported the investigation the collection which was collected in the deepest level of the Udachnaya quarry near 550 m depth. The peridotite xenoliths form the most fresh brown breccia which contain largest and most fresh xenoliths. We studied more than 200 peridotite xenoliths which vary in sizes from 0.7 m to several cm at first with the EPMA for the detail thermobarometry mostly in thin section to see the variations of the structures and minerals and found several assemblages in some xenoliths which possibly refer to the intermediate stops during the upwelling of the material to the surface. Xenoliths from this pipe are the most fresh kimberlite xenoliths among the known in the World. These circumstances allow recognize the details in of the intergranular material and secondary association in the rims around the garnets and on some pyroxenes.

## **SAMPLES.**

Studied samples show mainly ellipsoid configurations which show the shortest direction across the perpendicular to the foliation plain thus the sheared peridotites which area commonly more elongated the granular garnet peridotites and coarse granular Sp lherzolites. The largest in sized xenoliths belong to the sheared or porphyroclastic varieties which sometimes rich up to 0.7 m. though this is prevailing type also among the small xenolith. The pyroxenites are more rounded in section though they are often elongated usually and rich sizes about 10-15 cm. Eclogites which less than 5% are of different types they are characterized sometimes angular sections and not so flat surfaces.

## **PETROGRAPHIC DESCRIPTION.**

Several main petrographic varieties were recognized among the studied collection. At first the most widely distributed are sheared peridotites which are of several varieties. The most wide spread are those containing large relic garnets and fine grained aggregates of olivine the irregular shaped or pen like aggregates of Cpx and Opx. Sometimes Opx is also relic and show the corrosion by the Ol fine grained aggregates or the rims o the fine Cpx. Sometimes Cpx is distributes more rare than Opx. In some unusual variety the *ллойки* garnets which is pink or red and is surrounding by the 1-2 mm rims of the orange garnets. The detail of the thin sections shows that the deformations have two or more stages because there several populations of the deformed aggregates which are cut by the more fine grained material. Sometimes in the intergranular space possible to determine grains of phlogopites which look as equilibrated with the olivines they are common in the helophytic rims which are judging by the equilibrium with the fine grained

material are of mantle origin. Porphyroclastic varieties are compiled by the course grained material mostly by olivine and the Ol grains which are of two kinds. One is represented by the common recrystallized fine grained olivine aggregates and the second one by the veins or veinlets of Cpx, Opx and sometimes garnets showing the signs of fertilization. Rare garnet wehrlites and harzburgites with green garnets also show the porphyroclastic structures. Common granular garnet peridotites also vary in structures. Some show large grains of garnets and Opx and more fine olivines but in another huge olivine grains are surrounding by the subordinate grains of pyroxenes and garnets. The nearly equal grain structures also occur in the rare garnet peridotites. Spinel peridotites mostly are very coarse grained. Some Sp peridotites are fine grained or mean grained. The most large grain size reveal dunites which are of two types: garnet or chromite bearing, more rarely contain very light Opx.

### **METASOMATIC ASSOCIATIONS**

The symplectites of Cpx, Opx, Spinel and very often Phl are common in SP such rocks. The Fe - rich metasomatites with the honey-colored olivine with the intergranular amphiboles and rare phlogopites are occurring also [61]. The rare Phl veins with the Amph, picroilmenites, rutile, apatite, Ti-bearing spinel and apatites and modal intergranular phl metasomatism are discovered in garnet – bearing xenolith. The amount of the Phl bearing rocks is about 1/3 or more among the brown breccia xenoliths which is higher than reported by the F.Boyd (1/20) [8]. Phl are mostly intergranular and occurs as a rims on the garnets sometimes together with the secondary minerals. Most of phlogopites are intergranular and form thin films with the secondary clinopyroxenes and sometimes spinels. Nevertheless the structurally equilibrated phlogopites associated with pyroxenes occur in the deformed and porphyroclastic peridotites also. Phl is relatively rare mineral in the pyroxenites.

Richterite Amph is found in the garnet facies peridotites as the rims and pockets on and in the Opx.

The rare and unusual inclusion of the Phl bearing deep seated breccia is represented by the fine grained material of the debris or microxenoliths essentially olivine aggregates cemented by the phlogopites and clinopyroxene, amphibole-chromite and magmatic olivines aggregates. The later shows the structures of the typical sheared peridotites or more coarse grained but without the pyroxenes and garnet, only minor spinels are found. The chromites as olivines show two morphological varieties. The first ones reveal xenocrystic shapes and zonation visible in thin section in color and the second are elongated or idiomorphic beautifully shaped cuts of crystals. The intergranular material is represented by Cpx, Fe – enriched phlogopites the two type of amphiboles (richterite and pargasite) alkaline feldspar, apatite barite and stroncianite and sulfides. Rock contain also self crystallized 7% Cr<sub>2</sub>O<sub>3</sub>) and (10-11% Cr<sub>2</sub>O<sub>3</sub>). and xenocrysts of picroilmenites.

## METHODS

Collection was analyzed by EPMA and ICP MS. Several analyses were made using Jeol Superprobe in IGM SD RAS with the similar conditions. For the comparison one mount with 20 associations was analyzed using Camebax Micro machine and methods established by Lavrentiev Yu and colleagues [32, 33] in UGMS SO RAN. The detection limit about 2% for most of elements was calculated for the most of the elements for the measurements made in Jeol Superprobe. A bit lower (~1%) was found for the Camebax Micro. Most part were studied in thin section in Vienna University on Cameca100SX. All analyses were made against mineral standards with wavelength-dispersive spectrometers; acceleration voltage and beam current were 15 kV and 20 nA, respectively, and standard correction procedures were applied.

For the high precision analyses of the olivine the acceleration voltage 20 kV and beam current 30 nA and 12 minutes of the measurements of counts was used. The precision is varying from 8 to 15 ppm for several components (Ca, Al, Cr, Ni, Mn, Zn).

Abundances of approximately 30 trace elements were determined in situ in selected minerals and glasses by laser ablation inductively coupled plasma mass spectrometry (LA-ICP-MS). Analytic Centre of IGM on a Finnigan Element ICPMS with a UV Laser Probe using international reference standards NIST 612 SRM and NIST 614 SRM.

## VARIATIONS OF THE MAJOR COMPONENTS.

*Clinopyroxenes.* The variations of the major elements of the garnets from the studied collections are represented on the (Fig 1) in comparison with the previous published data. The set of the peridotites show high scale variation in FeO 1 - 5% and other components. The most Fe-low are referred to the coarse SP harzburgites and rare porphyroclastic peridotites with the coarse olivine. The variations of the other components are rather high 1 - 4 % for Al<sub>2</sub>O<sub>3</sub> and 0.5-2 for Cr<sub>2</sub>O<sub>3</sub> and Na<sub>2</sub>O. Common Garnet lherzolites [62] show the variations between 1.5 - 2.5 FeO and smaller variations in Na, Al, Ti then sheared varieties. Essential rising for this components are found for the Cpx from sheared peridotites having FeO near 2.7 - 4 %. Essential enrichment in TiO<sub>2</sub> were found for the most of the Phl bearing associations. Eclogites are characterized by the broad variations in FeO and high Al, Na contents.

*Garnets* from studied peridotites show higher variations in Cr<sub>2</sub>O<sub>3</sub> then determined before [34, 66] going to 13.5% for green garnets (Fig. 2) which refer to pyroxenites field. The most of figurative points including harzburgites are lying within the lherzolite field. But green wehrlite garnets are enriched in CaO as other pyroxenites while Cr - rich harzburgite shows the lherzolitic signatures, demonstrating the origin due to fertilization as well as high concentration of TiO<sub>2</sub>.

Rare dunites and harzburgites reveal sub calcic compositions close to those for the diamond inclusions [66]. The compositions of the Phl bearing associations also mainly show the enrichment in  $TiO_2$ .

**Clinopyroxenes from Udachnaya pipe**

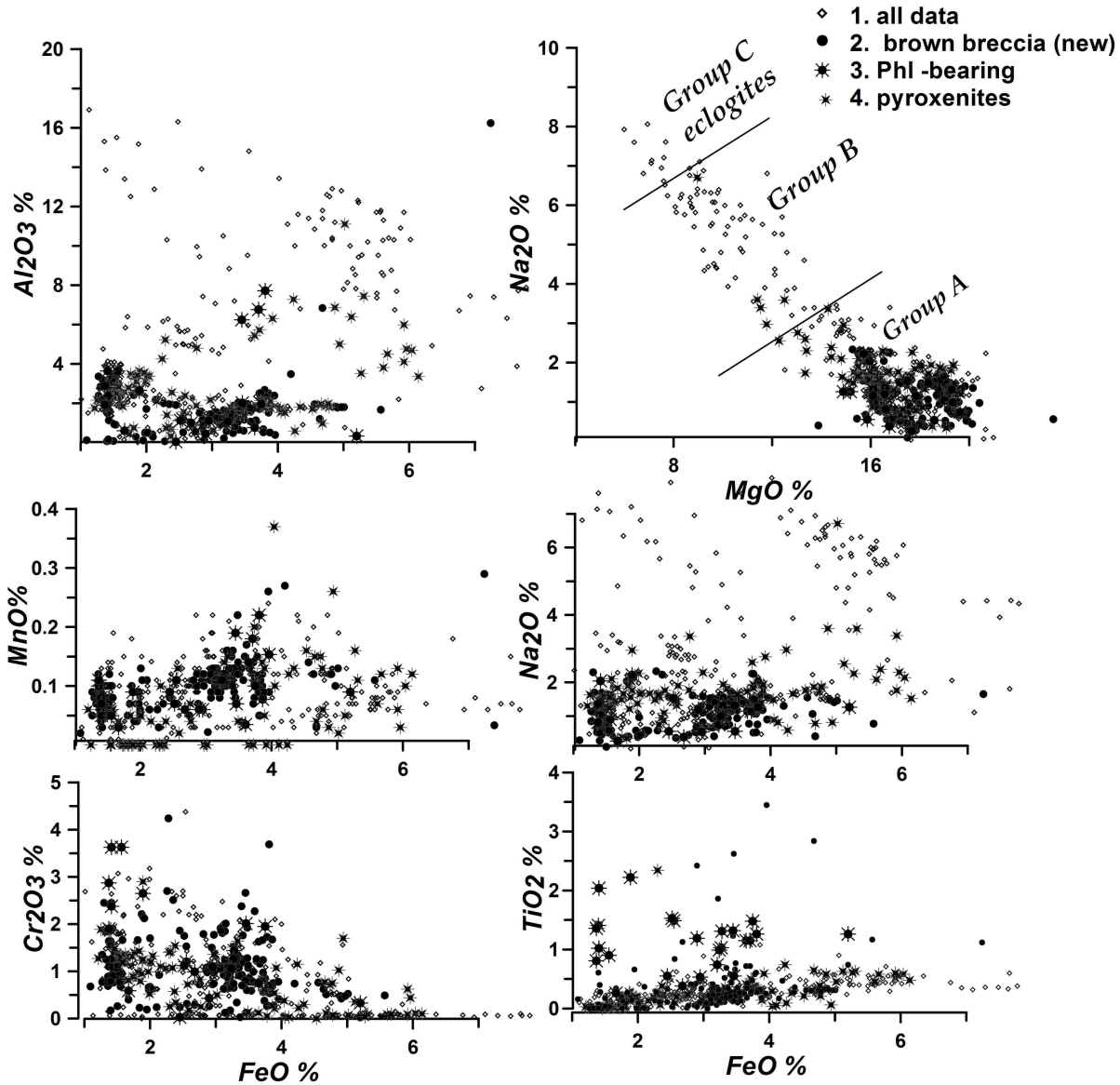


Fig.1. Variations of major element compositions from the clinopyroxenes of brown kimberlite breccia in comparison with other published associations from Udachnaya pipe.

1. previous data. 2.new data. 3. Phl bearing associations. 4. pyroxenites.

*Chromites.* This mineral show variations from 10 to 60 %  $Cr_2O_3$ , varieties with  $> 40$   $Cr_2O_3$  are enriched in  $TiO_2$  and  $FeO$ . This is more typical for the pyroxenites. Chr in associations with the phlogopites are enriched in  $TiO_2$  also (Fig. 3).

*Phlogopites.* The compositions of the phlogopites are ranging in FeO from 2 to 6.5% (Fig. 4). The Phl from polymict breccia are varying from 5 to 8.5%. The later are low in Cr<sub>2</sub>O<sub>3</sub> but higher in Na<sub>2</sub>O in general.

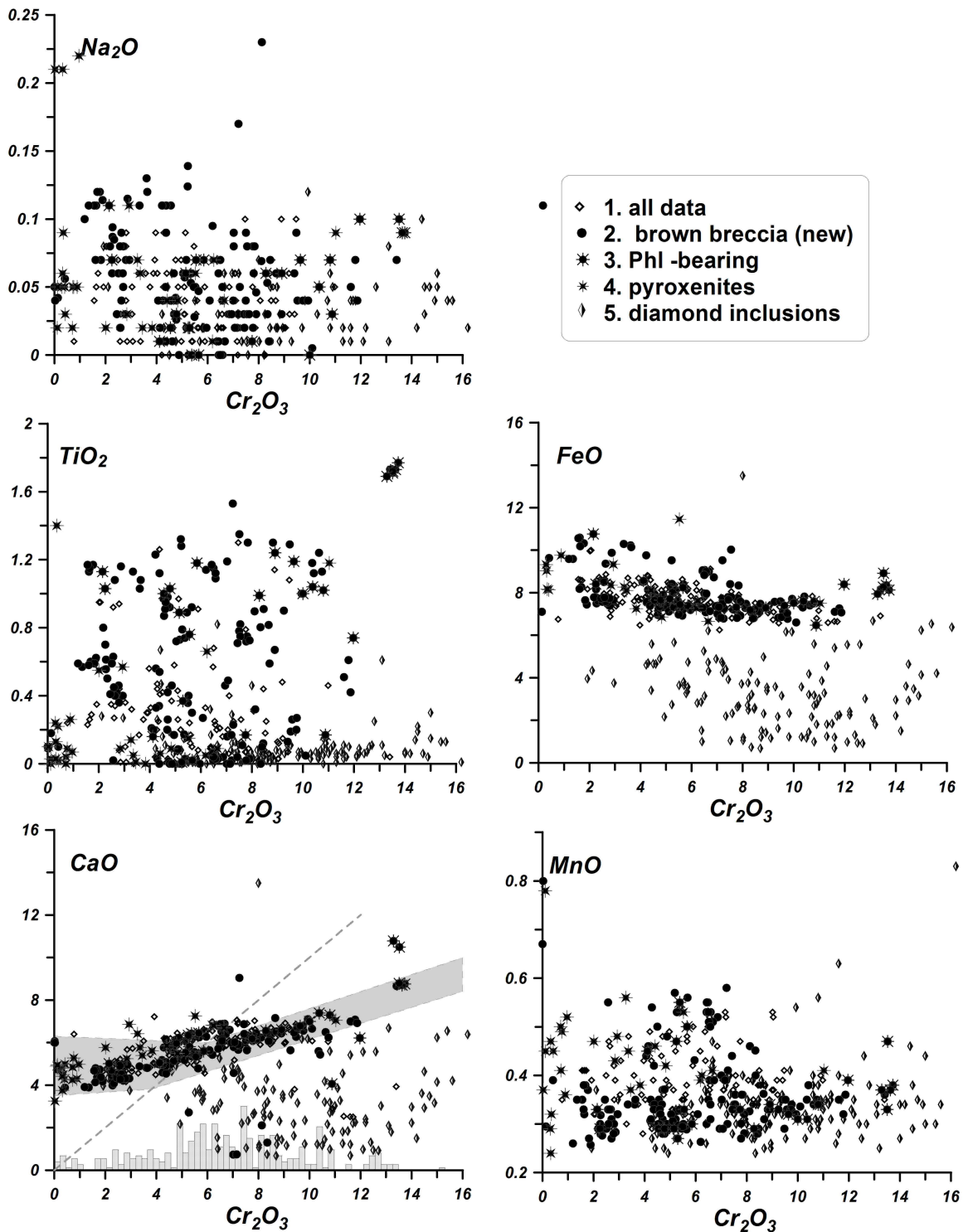
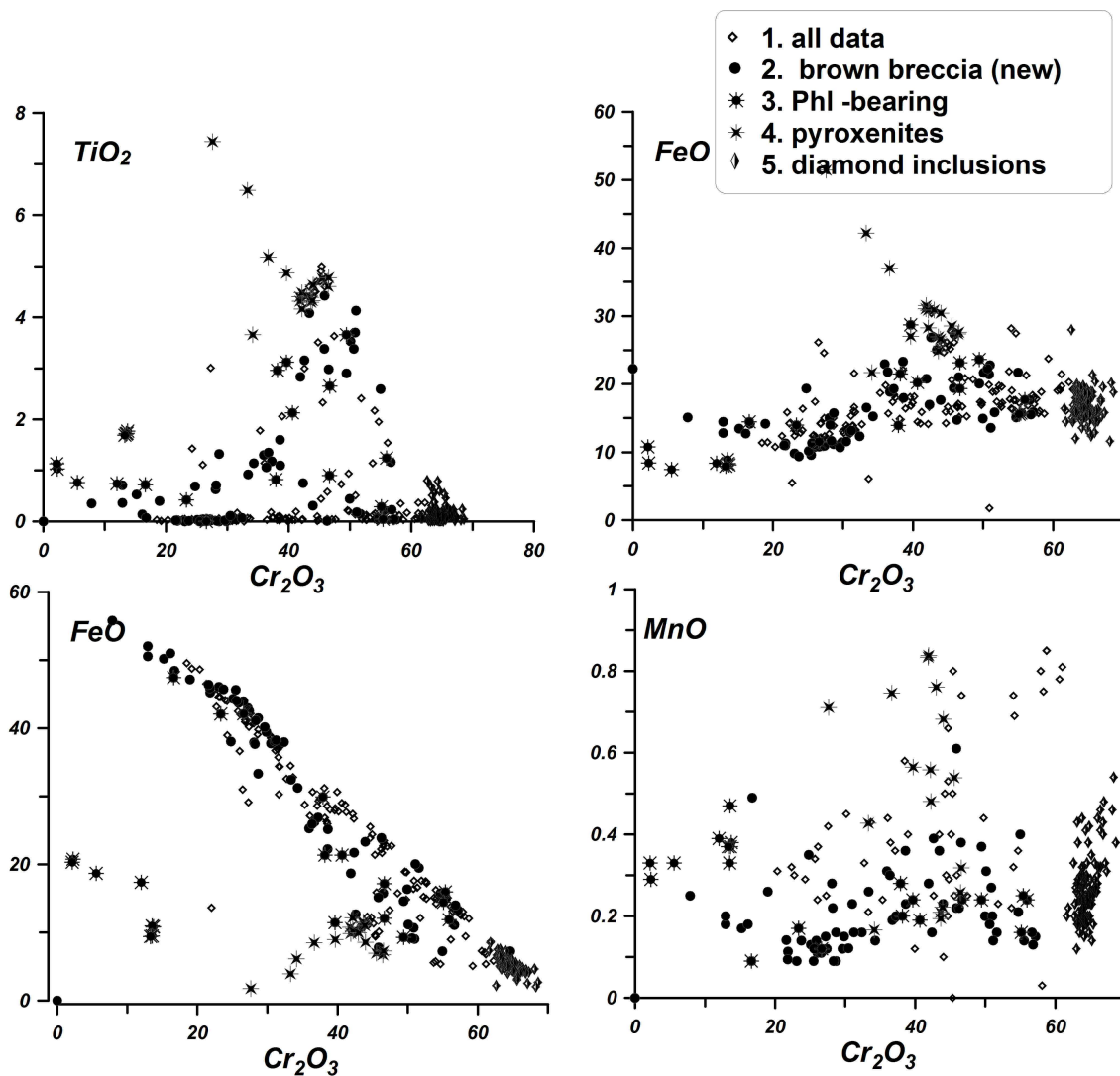


Fig.2. Variations of major element compositions of the garnets from brown kimberlite breccia in comparison with other published associations from Udachnaya pipe.

Sign the same and diamond inclusions. 5. diamond inclusions.

*High precisions data of olivines*

The precision data for olivines [56] were analyzed from 64 associations. Their compositions are dividing according to the petrographic features. The most HT Ca – rich associations are some porphyroclastic peridotites (Fig. 5). They are low in Ti but rather high in Cr. Olivine s from sheared peridotites show the Ca content near 400 ppm. All of them are enriched in Ti, Cr and Al. The course grained Sp peridotites have low Ca content which is in general correlating with the temperatures are higher in Ni but lower in Cr. Between the coarse garnet and spinel coarse grained garnet are higher in Ni.



**Fig.3 Variations of major element compositions of the garnets from brown kimberlite brecciaing comparison with other published associations from Udachnaya pipe.**

Sign are the same. 4. deep seated Phl bearing breccia.

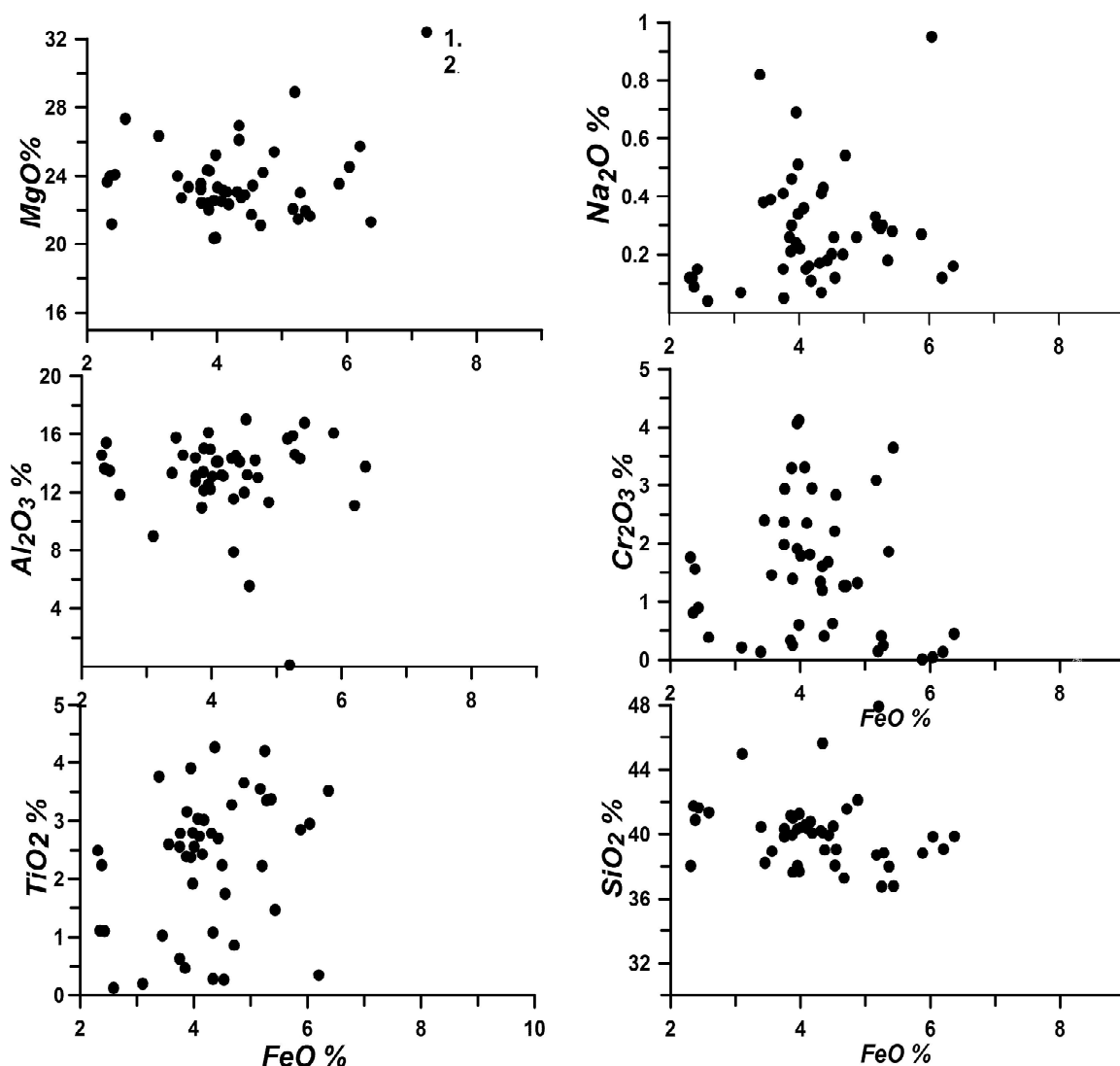


Fig.4 Variations of major element compositions of the phlogopites from brown kimberlite brecciaing comparison with those from the Phl in xenoliths from deep seated polymict breccia from Udachnaya pipe.

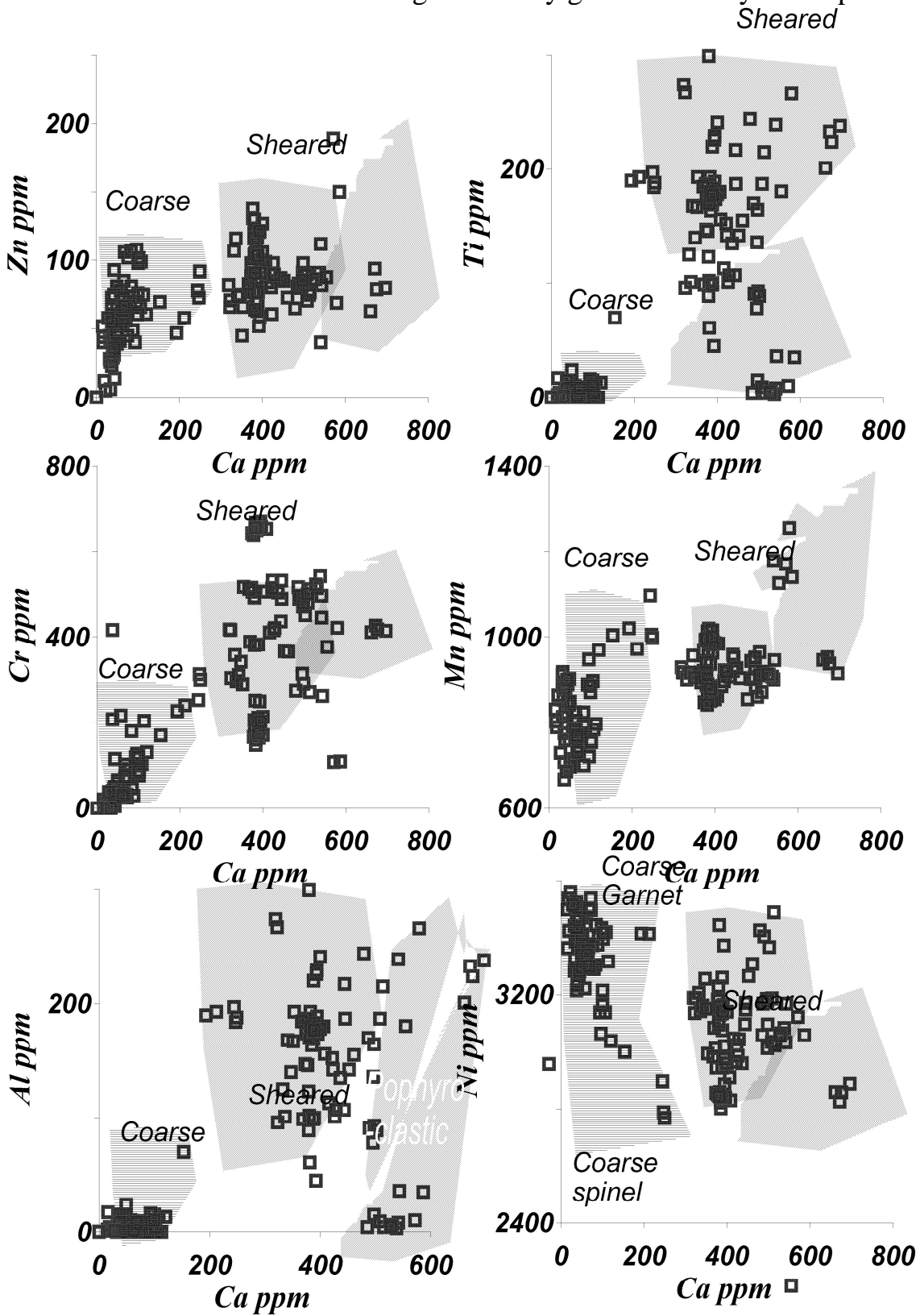
1. Phlogopites from xenoliths. 2. Phl form deep seated Phl bearing breccia.

## THERMOBAROMETRY.

### Thermobarometry of olivine.

High precision compositions of the olivines obtained by the LAM ICP MS are used to compile the new monomineral thermometers [12]. We checked all of them and reveal that the best one is those using the Cr-Al exchange though Ca and Al thermometry are also close (Fig6.B). Using this thermometry and common Opx barometry it possible to obtain nearly the same geotherm [4]. De Hoog and

colleagues [12] reported that these thermometric equations in inverse form may be used as barometers. Nevertheless in general they give essentially lower pressure



D.'

Fig.5. Minor element variations in olivine obtained with the high precision olivine measurements.

that Opx based methods [9,33]. Ca-Ol-Cpx barometry [27] for olivine also give not a regular geotherm when using this equation together with the Ol thermometers [12]. Nevertheless the single olivine trace element thermobarometer is promising and seems to be may be developed using the combination in equation several components.

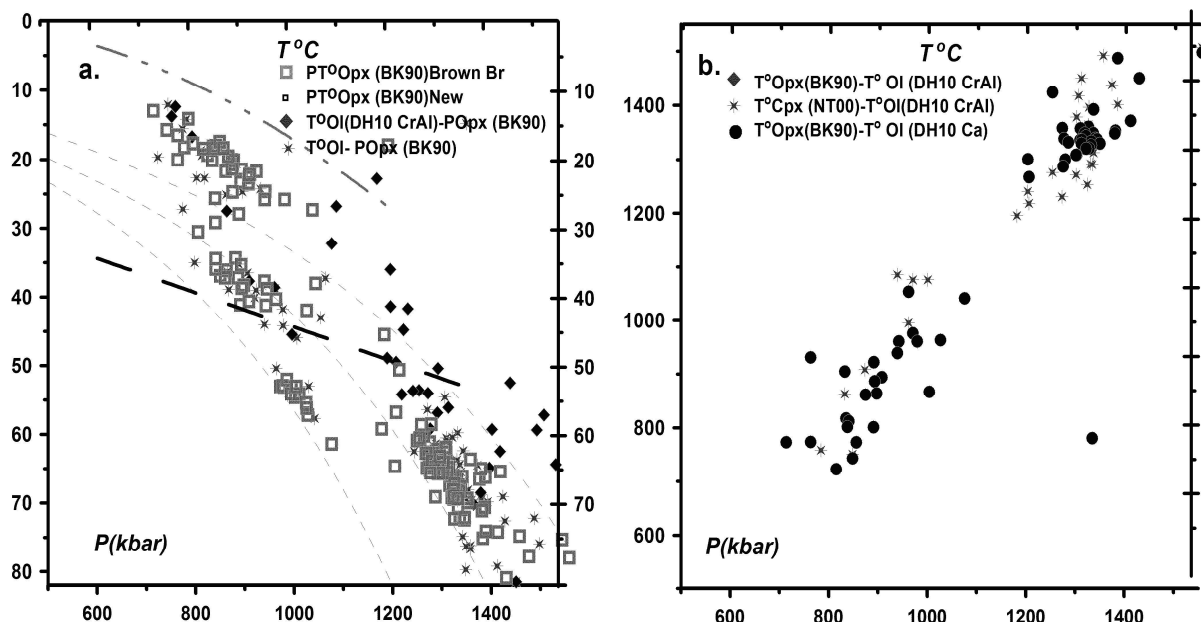
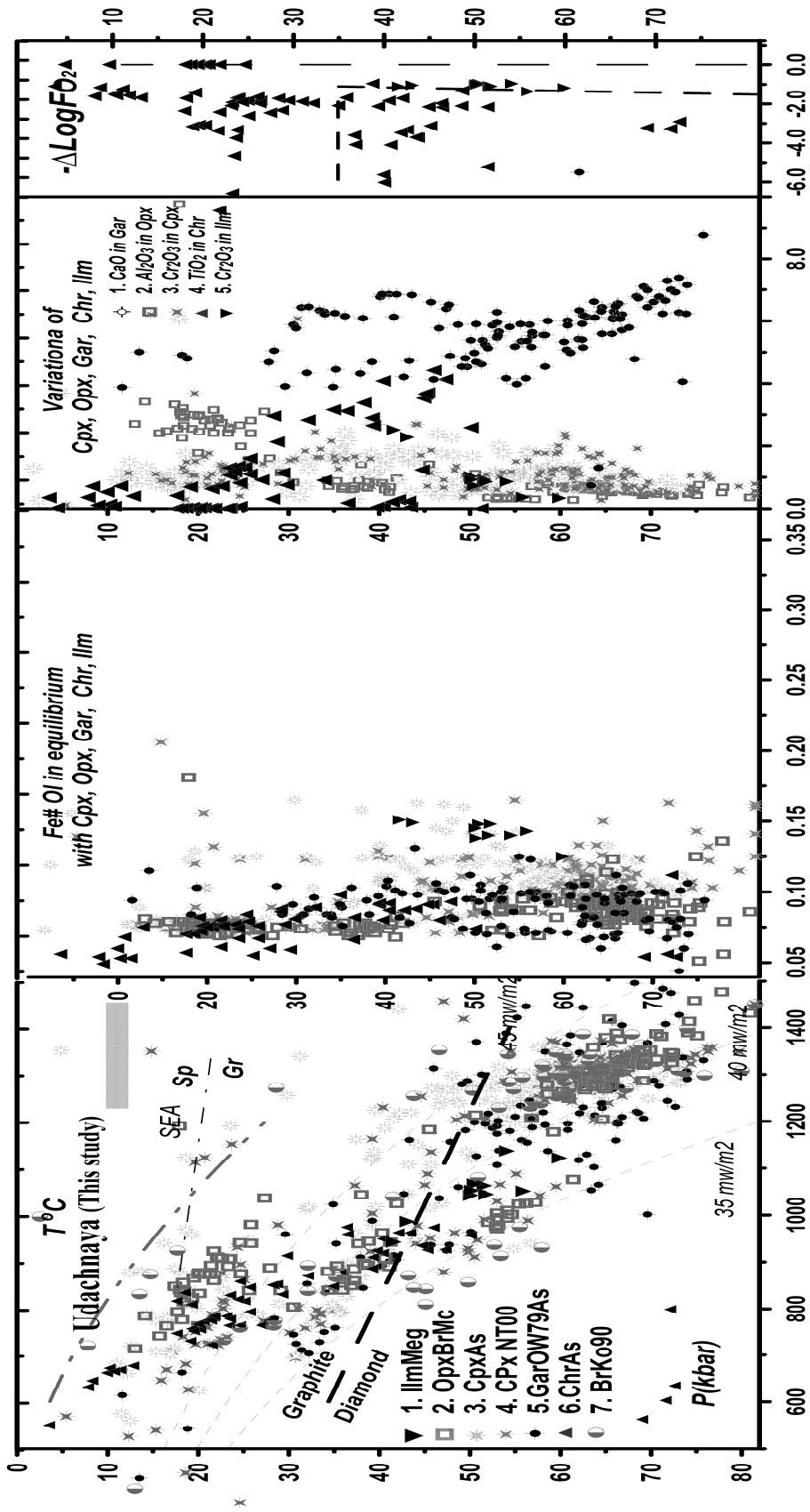


Fig.6. PT conditions for the new data for peridotites from the brown brown kimberlite breccia from Udachnaya pipe. A. PT Correlations of the Ol – based  $T^{\circ}$  according to [12]. Signs see Fig.7 .B. High precision analyses and Opx  $T^{\circ}$  Correlations of the temperatures

### Common Px-Gar thermobarometry.

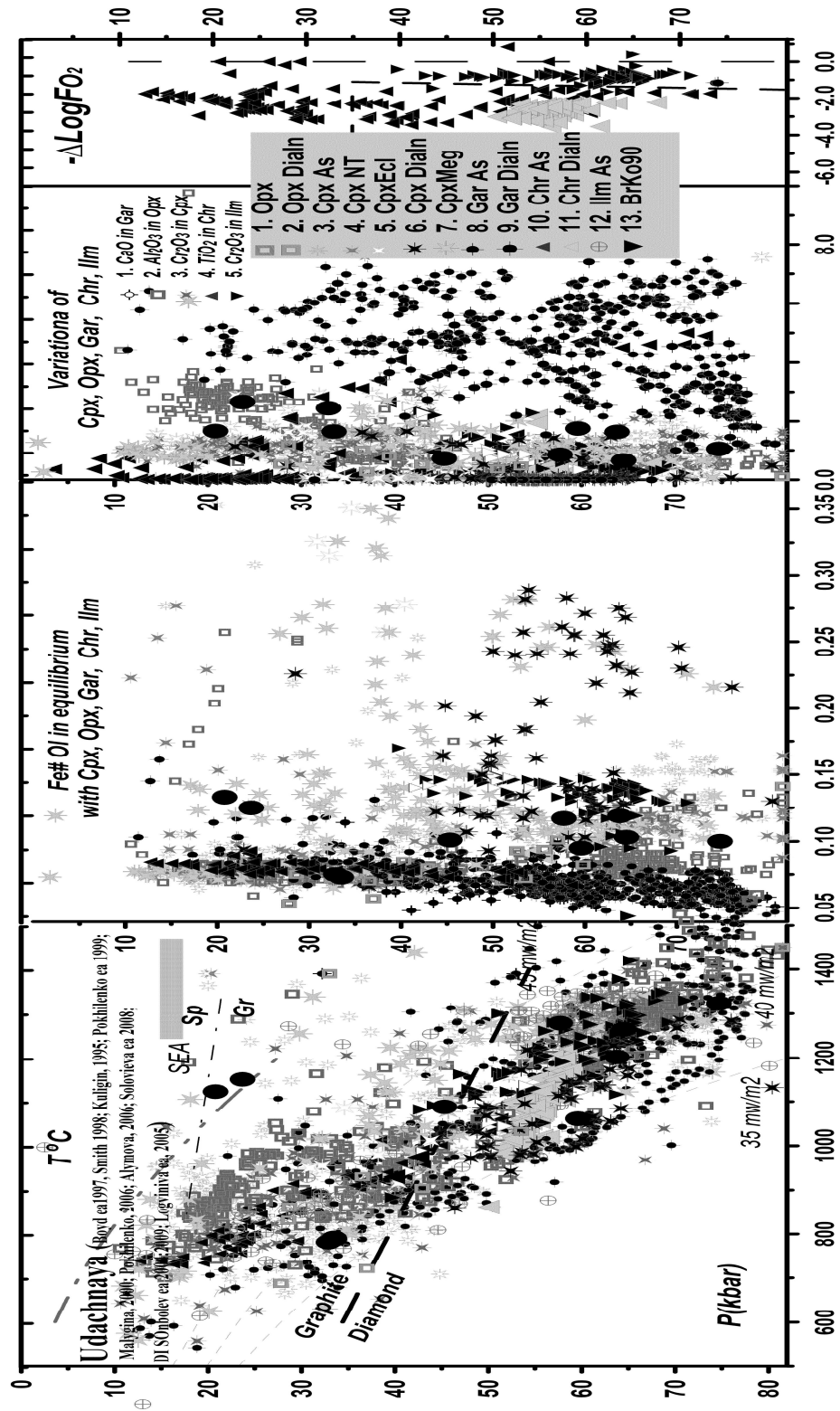
Opx based thermobarometry [9,33] gives the PT plot which is in general very similar plot to those obtained with the previous data sets together for the peridotites [4], pyroxenites [28-30, 43-46,], diamond bearing rocks and inclusions [32, 45, 53, 58]. The difference is that convective branch which now is more extending reaching 80 kbars and possibly more steep [6, 7, 8]. Lower part of the diagram is dividing into the several arrays with the slightly different PT gradients. The Cpx thermobarometry give [4, 37] also abundant PT points correspondent to the base of the subcratonic lithospheric mantle (SCLM). But the cold branch still exist to 80 kbars marked mainly by the – rich garnets and cold eclogitic PT estimates. This level is heterogeneous and is represented by the rocks showing the irregular heating. There is a relic low temperature (LT) gradients (34-36 mvm-2) mainly found from 60 to 30 bars and in opposite relic points bellow 65 kbar. This data are supported also by the CPx and garnet thermobarometry [4]. The common and most abundant PT points are correspondent to the 40 mvm-2 geotherm which was published before [8,36] obtained with [13,33] or [37] methods. The convective

Fig.7. PT conditions for the new data for peridotites from the brown breccia and phl bearing associations (Stars) Signs see Fig 8



**Fig.8. PT conditions for the new data for all previous data set of deep seated inclusions from Udachnaya pipe.**

Signs: 1. Opx T°C [13]- P(kbar) [33], 2. The same for diamond inclusions 3. Cpx: T°C [4]- P(kbar) [4]; 4. TP [37], 5. ToC [37]- P(kbar) [4] for eclogites; 6. the same for diamond inclusions; 7. the same for pyroxenites Gar (mono)- 8. ToC [40]-P(kbar) [4] , 9. -the same for diamond inclusions, 10. Chromite ToC [41]- P(kbar) [4]; 11. the same for diamond inclusions; 12. Ilmenite [65]- P(kbar) [4]. 13. ToC[14] -P(kbar); [9].



branch determined in the 60-65 kbar for sheared peridotites most of methods is situated between 40 and 45 mvm-2 geotherms and also refer to PT estimates for the chromite diamond inclusions and for Ilm clinopyroxenites. Estimated by the all the monomineral barometric method together [4, 9, 37] advective branch is crossing 45 mvm-2 conductive geotherm with sub adiabatic inclination is rising upward from the 60-65 to 35 kbars. It now received the support with G.Brey and P.Kohler [9] method using the more detail data from the analyses in thin sections. Cpx thermobarometry [4, 37] shows that some primary and most of secondary Cpx generation trace this advective branch. The middle part of the diagram is correspondent to the so called pyroxenite layer which is irregularly heated. Upper part of the mantle is column from 30 – 10 kbar is correspondent to the geotherm near 60 mvm-2 and is the layer of the basalt generation. Thus all three traps for the mantle melts [64] in the mantle beneath the Udachnaya are represented by the HT associations.

### **Trace element chemistry of the minerals.**

The trace elements patterns for the minerals from the deep seated xenoliths are highly varying and differ for peridotites, pyroxenites and eclogites.

Clinopyroxenes from peridotites show mainly highly inclined  $(La/Yb)_n$  patterns with the small hump which is shifted to the left part of the REE patterns [Fig.9]. The TRE are complex and varying [20]. Most of the diagrams show the Zr dips and sometimes with Hf. They show also small or pronounced depressions in Nb and Ta. But small peaks in U exist for the most of the samples. Essential peak in Pb may be result of the pollution on our analyses because it did not exist among the similar xenoliths from the another set of the analyses [20]. Cpx patterns from, the pyroxenites are nearly uniform in the REE close to the derivation from the source enriched melts close to primitive mantle associations with the melting degrees close to 1% . Only two show the very low HREE due to the presence of high amounts of garnets in the source. But the TRE diagrams show they were depleted in most HFSE mainly in Zr due to the phosphates derivations. Rutile and ilmenite may regulate the other components. Pb show the parent melts differentiation and derivation of the sulfides.

Eclogite Cpx differ in TRE diagrams even by the level which is lower for those with the signs of the primary subduction origin showing Eu, U , Sr peaks. The others show high level of the TRE and highly inclined REE patterns, TRE with fluctuation in Ta and elevated LILE. They may be differentiates from plum melts probably protokimberlite or derived from magma contaminated in metasomatic association.

Peridotitic garnet patterns are more regular in our collection comparing to [20] though some of them reveal S- shaped or even U shaped REE patterns which are typical for the depleted compositions with lower TRE content. They all reveal deep Sr minima and Zr and Hf dips as well as for Ba, Th but fluctuating Nb and Ta [Fig.9].

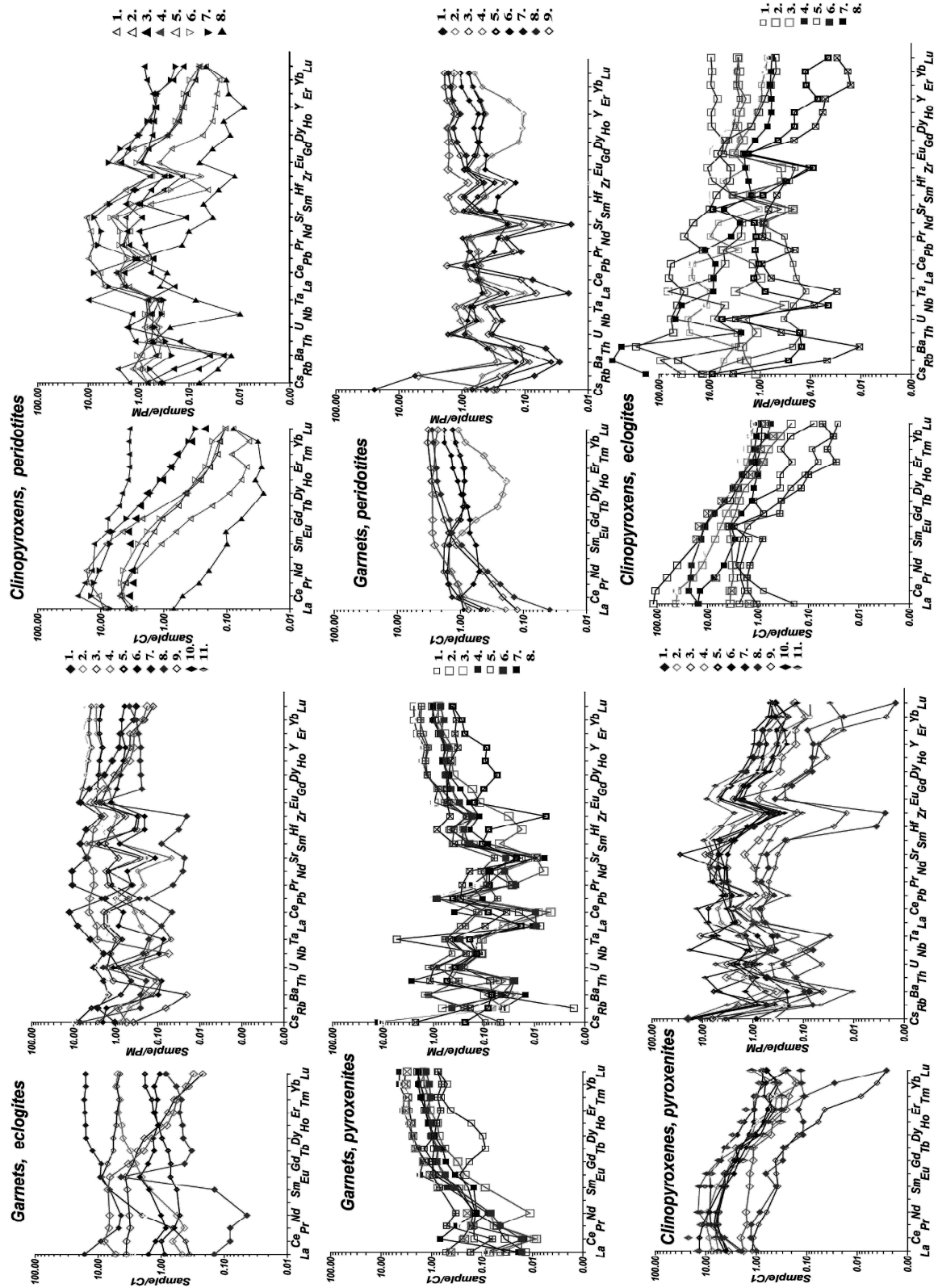


Fig. 9. TRE spectra for the minerals from deep seated inclusion from Udachnaya pipe

Garnets from pyroxenites demonstrate the nearly straight line incline patterns and fluctuations in Ce due to different oxidation state. They show high Pb peaks elevated Ta, Nb as typical for remelted metasomatic and small Sr depressions.

Eclogitic garnets are La, Ce enriched. Those with lower REE demonstrate HFSE depletion.

The orthopyroxenes show mostly flattened patterns with the small negative inclination but those with the lower concentration of TRE reveal  $La/Yb > 1$ . REE patterns for the olivines are similar but one order lower with the gentle depression and inflections. Ba, Th depressions are typical for them. The TRE patterns for the phlogopites reveal high inclination in general. The TRE are jagged with the picks in LILE components and Sr, Pb and depression in Th and some HFSE.

## DISCUSSION

### Structure of the mantle.

Detail thermobarometry for the mantle section beneath Udachnaya and the comparisons with the petrographic features visible in thin section allows reconstructing the set of the rocks in each level in the mantle columns. The uppermost horizon from 10 to 20 kbars is compiled from the coarse grained relatively depleted lherzolites and harzburgites. Pyroxenites are rare but they are abundant just near the Garnet -Spinel boundary close to 20 kbars. They belong both to the Cr-diopside Fe-Ti rich cumulates. Phlogopites occurs as symplectites with the pyroxenes and spinels. The xenoliths from 20 to 30 kbars are represented by the peridotites with the relatively scarce garnets grains, they became more abundant in 30-40 kbar interval. Pyroxenites [47] and lherzolites [34] there contain the pyroxenes enriched in Al but the Cr content is not high. The level near 30 kbars again is enriched in pyroxenites and some Fe – rich eclogites [21, 22, 35, 49, and 50] and as well as harzburgites and dunites and should be the border of two subduction slices or phase boundary which is correspondent by melting and crystallization processes. Relative Ti enrichment is demonstrated by the Cr – spinels from this interval, peridotites are mostly very heterogeneous lherzolites. The boundary from 37 to 42 kbar is probably the most sharp in the mantle section. Many of pyroxenites and Fe- lherzolites as well as depleted veined dunite rocks are correspondent to this boundary. The level between 57 and 42 kbars is very heterogeneous. Garnets Cr- pyroxenites [28-30] show the increase of the Cr upward and Ca downward in the mantle section. Dunites- harzburgites are coinciding in the pressure with the eclogites and pyroxenites showing the very high variations in the Fe in pyroxenes and Ca in garnets. The level between 50 and 40 kbars possibly represent the collage of the 4 separate slices showing the trends for the Ca increase in garnets with the calculated pressure. The first is for dunites then for harzburgites and the last one for pyroxenites. Phlogopite metasomatism is developed as the rims of the garnets mainly and rare veins with the ilmenites. There are also 4 trends of the Fe# decrease in this direction for the Cr- low clinopyroxenes. Two most Fe# rich are coinciding with the same trends for ilmenites and thus should reflect the two stages of the protokimberlite melt percolations, the higher in Fe# corresponds to the HT diamond bearing eclogites [21, 22, 35, 49, 50]. Some explorers suggest the protokimberlites at the level near

40 kbars to be essentially carbonatitic [64, 69]. More Fe rich eclogites compositions also containing diamonds but more LT are probably of the primary subduction origin. Cr-spinel bearing relatively fertile lherzolites with the chains or veinlets of the Garnet and Cpx and Chr probably are marking the ways of the melt migration and refertilization judging by the relatively high Ti in Chr. The high Cr content of the Cpx is probably marking the levels of the depletions and specific Na-Cr metasomatism which is more typical for the Alakite pipes [4]. This level is coinciding with the presence of the Gar harzburgites.

The boundary 48-50 kbars is characterized by the appearance of the abundant rather LT eclogites. They all are diamondiferous and differ in Fe contents [21, 22, 35, 49, 50] separating in 4 groups. Two of the ilmenites bearing probably are cumulates from the protokimberlites. The group of the eclogites with the Fe# 20 - 30 is probably of subduction origin – the intermediate range may correspond to the submelted varieties [49]. The horizon between 50 and 65 kbar is marking the so called kink of the geotherm. The range of the 1200 to 1000° is coinciding for the eclogites [53-56], Chr from the diamond inclusions and harzburgites as well as for some ilmenite pyroxenites. Most of the peridotitic rocks including harzburgites are showing the range of the Fe# from the enriched 12% to low up to 5% with the increasing of the pressures. Similar is range Fe# 8- 12% is demonstrating by the so called sheared peridotites [25, 38]. The Ca content for the garnets is rising downward the mantle section but for the amount of Cr- rich subcalcic garnets [10, 11, 69] is also increasing with the depth. Probably the subcalcic garnets are reflecting an ancient depletion event formed by the specific fluids forming megacrystalline dunites which were studied also in our collection [45-46]. This is the level of the appearance of the megacrystic Ilm pyroxenites [1, 2] which are rarely exhibiting the contacts with the deformed peridotites.

Similar lens between 65-75 kbars is characterized by the more high abundance of the Ilm pyroxenites. The Gar-dunites are less abundant but became more depleted with the depth. The sheared peridotites are more HT and show the veins of the magmatic Cpx, Opx and even garnets. They are coinciding with the porphyroclastic varieties. The Ti – rich wehrlitic and harzburgitic peridotites with the newly formed Ti – enriched green garnets are result of the melts percolation which produced the chains of garnets and Cpx. The metasomatic diamond bearing Ilm lherzolite [48] with the very high Cr content in the Cpx is also correspondent to this level. Some subduction type eclogites [21, 22, and 53] are referring to the LT conditions.

The lowest detected by the xenoliths and xenocrysts level corresponds to the most Cr rich garnets found as xenocrysts and inclusions in diamonds with the high range of Ca decreasing with the pressures. More Fe – rich compositions correspond to the HT cumulates probably leaved by the protokimberlites and to the hot diamond eclogites as well as for some porphyroclastic peridotites.

## **Evolution of mantle column**

Several pipes like Yubileinaya [4] demonstrate the difference in the structure of the mantle columns reconstructed by the xenocrysts and xenoliths. Such a conclusions for Udachnaya are still absent because West part of pipe is not studied in detail due to the low amount of the fresh xenoliths. The xenoliths from the brown breccias which are in general most fresh show slightly more restricted intervals but deeper levels also. This is seems to be one of the initial stage of the pipe formations when the magmatic roots were not subjected to more developed metasomatism and melt interaction which is visible in the diagram for the whole set of the mantle samples.

Indirect evidences shows that the wide variations of the mineral compositions and the high positions of the geotherms in the deeper level even to the level of 20 kbars shows that there were abundant reaction and melt interactions in several levels of the mantle columns. The deeper were definitely undergone to the influence of the protokimberlite melts which created the two magmatic chamber – vein system near 70 and 60 kbar and course the deformations of the peridotites and high scale interactions possibly due to the hydraulic fracturing [7]. It seems that the coexistence of the relatively easy melted material like eclogites and melt conduits like dunites is not an occasion. The upper 55-40 kbar levels is correspondent mainly by the interactions around the veins which should be formed by the essentially carbonatitic compositions which may be created due to the splitting of the primary melts during the differentiation rising and cooling. Such systems containing abundant carbonates are favorable for the creation of the diamonds especially during the interactions with the reduced peridotites. Stopping of the pervasive melt percolation occurred near 40 kbar where the large dense layer of the eclogites exists. The large unites in the mantle columns were created by the subduction processes [41] and most Fe-rich eclogites should correspond to the upper parts of the subduction slabs. The physical – chemical boundary corresponds to the temperature minima of the oxidized and carbonated peridotites [64]. This should bring to the melt concentration and creation of the pyroxenite lens. The separate high temperature level appeared in the upper part near the Gar-Sp boundary which also concentrates the melts. Possibly separate most evolved protokimberlite melt portion reached this level. But it also possible that it is correspondent to the close stages of the basalt creation which are abundant as the xenoliths in kimberlites.

## **Phlogopite metasomatism**

The nature of the phlogopite metasomatism is debatable. They occur in the most deep levels correspondent to Cr-rich diamond inclusions [61]. Those with  $\text{FeO} > 4.5\%$  are produced by melt metasomatism referred probably to protokimberlites. This type which is also higher in  $\text{Na}_2\text{O}$  should be referred to the melts interaction. They are close to the varieties fond in the Phl bearing deep seated breccia. There are two types of the Phl according to the Ti content which can mark the interaction with the melts percolating through the mantle. Phlogopite

microveins with the low TiO<sub>2</sub> content may be south to be related to the melts though some of them show the primary origin according to the well equilibration with the other minerals. Example of the mantle phlogopites from the Alakite fields are correspondent to the earlier Precambrian stages close to Rodinia break up. Nevertheless large part of phlogopites in Udachnaya peridotites should be related to the later events correspondent to the protokimberlite melts

The phlogopites from the breccia have enriched Na and Ti content but they do not have Ba and Cl as well as F. One can suggest that there is not relation to the subduction related rocks or melts. But intergranular material in this breccia contains barite and stroncianite as well as abundant apatites, rare sulfides. Amphiboles referred to the Na - richterites and kaersutites as well as some CPx, presence of the picroilmenites (MgO~10) as well as the debris of sheared peridotites evidences about very deep origin of this rocks and polybaric crystallization of this melts. Thus the channels of the f the protomagmatic systems before the rising to the surface were subjected to the interaction with the H<sub>2</sub>O rich fluid rise from the levels of more then 80 kbars. So the K – rich fluids founds also in diamonds were wide spread and concentrated in the mantle just before the eruption. Many porphyroclastic rocks and even sheared peridotites contain intergranular phlogopites especially in he rims around the garnets.

There are now still geochemical – trace element or isotopic evidences about the nature of this rocks. But one can suggest that they are related to the kimberlite II melts which appeared in the Daldyn field the kimberlite melts from the deep 410 km boundary [26]. Another possibility is that are developed due to the submelting of some subducted sediments reactivated by the kimberlites.

### **Melt rising and capturing**

The adiabatic branches traced by the secondary Cpx PT conditions show that there were several intermediate levels during to the rise of the kimberlites to the surface. They should be created near the boundary of the layering in the mantle, The several separate intervals (5) see (Fig 6-7) of the pressures which are marked by the xenoliths from the brown breccia possibly refer to such a chambers.

### **Trace element evidences**

TRE content of the rocks and minerals usually is using for the recognition of the genetic signatures and links of the studied rocks as well as the degree of melting or differentiation , contamination and characteristics of the melting sources. The trace elements for the mantle peridotites from Udachnaya [20] evinces about the preference of the CPX input in the bulk rock composition. The sheared peridotites more enriched in HREE possibly refer to the interaction with the melts [19] with the less inclined TRE which were protokimberlites.

The Cpx and Gar are the major concentrator of the TRE in the peridotites. Cpx shows different levels of REE which is higher together with the La/Yb ratios reflecting the both increasing the Gar/Cpx ratios and decreasing melting degree in

the mantle columns with the depth. The melting degree is less than 0.1 according to the La/Ce ratios. This evidences about the low degree melting usually correspondent to the infiltration of the fluids. Presence of the S - type garnets [51] possibly reflect the same processes of the fluid LREE rich melting. The complex shapes of the REE and TRE diagrams and inflection and local dips or elevations in MREE or MHREE parts of the diagrams may mean that there were several stages of the melt fluid percolations through the mantle rocks especially in the lower part of the mantle column and changes of the volatile content from the CO<sub>2</sub> or H<sub>2</sub>O or H<sub>2</sub> rich. It also subjected to the pervasive HFSE metasomatism [16-17] The permanent dips in Zr may also suggest that the rocks initially were melted in a high activity of P creating apatites or zircons.

### CONCLUSIONS.

1. The brown breccia from the most deep level of the Udachnaya kimberlite quarry contains the most deep and fresh mantle xenoliths in the pipes captured from the levels of about 80 kbar and representing separate capturing intervals.
2. Phlogopite metasomatism is developed in the whole section of the mantle column beneath the pipe. Melt related phlogopites from the probably are related to the ancient stages of the melt percolation as in Alakite field or to the basaltic stages preceding kimberlite magmatism. The deeper levels probably are correspondent to the deep seated melts close to kimberlite II were appeared from the deep level of the mantle. The deep seated phlogopite breccia was formed at the deep level of the mantle column due to the H<sub>2</sub>O rich fluid interaction with the mantle peridotites.
3. The protokimberlite melt interaction with the deeper level was responsible for peridotite shearing and wide scale interaction the remelting of the deep eclogites, and possibly creation of some population of the diamonds. The phlogopite metasomatism is accompanied these interaction.

### REFERENCES:

1. **Alymova, N.A.** Peculiarities of ilmenites and ilmenite – bearing association from kimberlites of Yakutian province. PHD dissertation thesis. Irkutsk. // Institute of Geochemistry SB RAS. 2006. p.175.
2. **Alymova, N.A., Kostrovitsky, S. I., Ivanov, A.S., Serov, V. P.** Picroilmenites from kimberlites of Daldyn field, Yakutia. //Transactions of the Russian Academy of Sciences Earth Science Sections, 2004. v.395, pp.444-447.
3. **Artemieva, I. M.** The continental lithosphere: Reconciling thermal, seismic, and petrologic data. 2009.// Lithos v109 (1), pp.23-46
4. **Ashchepkov, I. V., Pokhilenko, N. P., Vladykin, N.V., Rotman, A.Y., Afanasiev, V.P., Logvinova, A.M., Kostrovitsky, S.I., Pokhilenko, L.N., Karpenko, M.A., Kuligin, S.S., Malygina, E.V., Stegnitsky, Y.B., Alymova, N.A., Khmelnikova, O.S.** Reconstruction of mantle sections beneath Yakutian kimberlite pipes using monomineral thermobarometry. // Geological Society, London, Special Publications, 2008. v.293. pp.335 – 352.
5. **Ashchepkov, I.V., Vladykin, N.V., Logvinova, A.M., Kuligin, S.S., Malygina, L.V., Pokhilenko, L.N., Alymova, N.V., Mityukhin, S.I.** Using of the monomineral thermobarometers for the reconstruction of the mantle lithosphere structure.// Vestn. Otd.nauk o Zemle RAN. № 1(27)'2009.

6. **Ashchepkov, I.V., Pokhilenko, N.P., Vladykin, N.V., Logvinova, A.M., Kostrovitsky, S.I., Afanasiev, V.P., Pokhilenko, L.N., Kuligin, S.S., Malygina, L.V., Alyмова, N.V., Khmelnikova, O.S., Palessky, S.V., Nikolaeva, I.V., Karpenko, M.A., Stagnitsky, Y.B.** Structure and evolution of the lithospheric mantle beneath Siberian craton, thermobarometric study. //Tectonophysics. 2010. v. 485, pp.17-41.
7. **Ave Lallement, H.L., Carter, N.L., Mercier, J.C., Ross, J.V.** Rheology of the uppermost mantle: inferences from peridotite xenoliths. //Tectonophysics. 1980. v.70, pp.221–234.
8. **Boyd, F.R., Pokhilenko, N.P., Pearson, D.G., Mertzman, S.A., Sobolev, N.V., Finger, L.W.** 1997. Composition of the Siberian cratonic mantle: evidence from Udachnaya peridotite xenoliths. //Contrib. Mineral. and Petrol. 1997, V. 128. N 2-3. P. 228-246.
9. **Brey, G.P., Kohler, T.** Geothermobarometry in four-phase lherzolites. II. New thermobarometers, and practical assessment of existing thermobarometers. //Journal of Petrology, 1990. v.31, pp.1353-1378.
10. **Burgess, S.R., Harte, B.** Tracing lithosphere evolution through the analysis of heterogeneous G9-G10 garnets in peridotite xenoliths, II: REE chemistry. //J. Petrol. 2004. V. 45. Iss. 3. P. 609-634.
11. **Dawson, J.B.** Kimberlites and their xenoliths. 1980. Springer-Verlag, Berlin Heidelberg New York.
12. **De Hoog, J.C.M., Gall, G., Cornell, D.H.** Trace-element geochemistry of mantle olivine and application to mantle petrogenesis and geothermobarometry. Chemical Geology 2010.
13. **Finnerty, A.A., Boyd, F.R.** 1987. Thermobarometry for garnet peridotites: basis for the determination of thermal and compositional structure of the upper mantle. /In: Nixon PH (ed) Mantle xenoliths. John Wiley and Sons, Chichester pp 381±402.
14. **Gaul, O.F., Griffin, W.L., O'Reilly, S.Y., Pearson, N.J.** Mapping olivine composition in the lithospheric mantle.//Earth Planet. Sci. Lett. 2000. v.182, pp.223–235.
15. **Gregoire, M., Bell, D.R., Le Roex, A.P.** 2003. Garnet lherzolites from the Kaapvaal Craton (South Africa): trace element evidence for a metasomatic history. //J. Petrol.2003. v.44, pp.629–657.
16. **Griffin, W.L., Cousens, D.R., Ryan, C.G., Suter G.F.** Ni in chrome garnet: a new geothermometer. //Contrib. Mineral. Petrol.1989. v.103, pp.199–202.
17. **Griffin, W.L., Ryan, C.G., Kaminsky, F.V., O'Reilly, S.Y., Natapov, L.M., Win, T.T., Kinny, P.D., Ilupin, I.P.** The Siberian lithosphere traverse: Mantle terranes and the assembly of the Siberian Craton. //Tectonophysics, 1999. v.310, pp.1–35.
18. **Griffin, W.L., Sobolev, N.V., Ryan, C.G., Pokhilenko, N.P., Win, T.T., Yefimova, E.S.** (1993) Trace elements in garnets and chromites: diamond formation in the Siberian lithosphere.// Lithos 1993. v.29, pp. 235±256
19. **Griffin, W.L., Smith, D., Boyd, F.R., Cousens, D.R., Ryan, C.G., Se, S.H., Suter, G.F.** Trace element zoning in garnets from sheared mantle xenoliths. Geochim Cosmochim Acta v.53, pp. 56±567.
20. **Ionov, D.A., Doucet, L.S., Ashchepkov, I.V.** Composition of the Lithospheric Mantle in the Siberian Craton: New Constraints from Fresh Peridotites in the Udachnaya-East Kimberlite. //J. Petrology. 2010. (in press, accepted)
21. **Jacob, D., Jagoutz, E., Lowry, D., Matthey, D., Kudrjavitseva, G.** Diamondiferous eclogites from Siberia: remnants of Archean oceanic crust.// Geochim. Cosmochim. Acta 1994. v.58, pp.5191-5207.
22. **Jagoutz, E., Lowry, D., Matthey, D., Kudrjavitseva, G.** Diamondiferous eclogites from Siberia: Remnants of Archean oceanic crust. .Geochim. Cosmochim. Acta 14. v.58, pp.5195-5207.
23. **Kamenetsky, V. S., Kamenetsky, M. B., Weiss Ya, Oded Navon O., Nielsen T.F.D., Mernagh T.P.** How unique is the Udachnaya-East kimberlite? Comparison with kimberlites from the Slave Craton (Canada) and SW Greenland.// Lithos 2009. v.112.S2. pp.

24. **Kamenetsky, V. S., Kamenetsky, M. B., Sobolev, A. V., Golovin, A. V., Demouchy, S., Faure, K., Sharygin, V. V. & Kuzmin, D. V.** Olivine in the Udachnaya-East Kimberlite (Yakutia, Russia): Types, Compositions and Origin. // *Journal of Petrology*, 2008. v.49, pp.823-839.
25. **Katayama, I., Suyama, Y., Ando, S., Komiya, T.** Mineral chemistry and P–T condition of granular and sheared peridotite xenoliths from Kimberley, South Africa: Origin of the textural variation in the cratonic mantle. // *Lithos*. 2009. v.109 (3), pp.333-340.
26. **Kawamoto, T., Herig, R.L., Holloway, J.R.** Experimental evidence for a hydrous transition zone in the early Earth's mantle. // *Earth Planet. Sci. Lett.* 1996. v.142, pp. 587–592.
27. **Kohler, T, Brey, G.P.** 1990. Calcium exchange between olivine and clinopyroxene calibrated as a geothermobarometer for natural peridotites from 2 to 60 kb with applications. *Geochim Cosmochim Acta* 54: 2375 2388.
28. **Kostrovitsky, S.I., Morikiyo, T., Serov, I.V., Yakovlev, D.A., Amirzhanov, A.A.** Isotope-geochemical systematics of kimberlites and related rocks from the Siberian Platform. // *Russian Geol. Geophys.* 2007.V.48/3, pp.272-290.
29. **Kuligin, S.S.** 1997. Complex of pyroxenite xenoliths in kimberlites from different regions of Siberian platform. /PhD thesis, United Institute of Geology Geophysics and Mineralogy, Novosibirsk. 220p..
30. **Kuligin, S.S., Malkovets, V.G., Pokhilenko, N.P., Vavilov, M.A., Griffin, W.L., O'Reilly, S.Y.** Mineralogical and Geochemical Characteristics of a Unique Mantle Xenolith from the Udachnaya Kimberlite Pipe. // *Extended Abstracts of the 8International Kimberlite Conference*. 2003. FLA\_0114.
31. **Kuligin, S.S., Pokhilenko, N.P.** Mineralogy of xenoliths of garnet pyroxenites from kimberlite pipes of Siberian platform. // *Extended Abstracts 7IKC*. Cape Town. 1998. P. 480- 482.
32. **Lavrent'ev, Yu. G., Usova, L.V.** New version of KARAT program for quantitative X-ray spectral microanalysis. // *Zhurnal Analiticheskoi Khimii*, 1994, v.5, pp.462–468.
33. **Logvinova, A.M., Taylor, L.A., Floss, C., Sobolev, N.V.** Geochemistry of multiple diamond inclusions of harzburgitic garnets as examined in-situ. // *International Geology Review*. - 2005. - Vol. 47. - № 12. - P. 1223-1233.
34. **MacGregor, I.D.** 1974. The system MgO-Al<sub>2</sub>O<sub>3</sub>-SiO<sub>2</sub>: solubility of Al<sub>2</sub>O<sub>3</sub> in enstatite for spinel and garnet peridotite compositions.// *Am Mineral.* 1974. v.59. pp. 110±119.
35. **Malygina, E.V.** 2000. Xenoliths of granular mantle peridotites in Udachnaya pipe. /PhD thesis, United Institute of Geology Geophysics & Mineralogy, Novosibirsk.187 p.
36. **Misra, K.C., Anand, M.; Taylor, L.A., Sobolev, N.V.** Multi-stage metasomatism of diamondiferous eclogite xenoliths from the Udachnaya kimberlite pipe, Yakutia, Siberia. // *Contrib Mineral Petrol.* 2004. v. 146/6. p. 696-714
37. **Nimis, P., Zanetti, A., Dencker, D., Sobolev, N.V.** Major and trace element composition of chromian diopsides from the Zagadochnaya kimberlite (Yakutia, Russia): metasomatic processes, thermobarometry and diamond potential. // *Lithos* 112, S2. pp.112 S1.
38. **Nimis, P. Taylor, W.** Single clinopyroxene thermobarometry for garnet peridotites. Part I. Calibration and testing of a Cr-in-Cpx barometer and an enstatite-in-Cpx thermometer. // *Contrib. Mineral. Petrol.* , 2000. v.139 (5), pp.541-554.
39. **Nixon, P.H., Boyd, F.R.**1973. Petrogenesis of the granular and sheared ultrabasic nodule suite in kimberlites. / In: Nixon PH (ed) Lesotho kimberlites. Lesotho Nat Dev Corp Maseru, Lesotho, pp 48-56.
40. **O'Neill, H. St. C. & Wall, V. J.** 1987. The olivine orthopyroxene-spinel oxygen geobarometer, the nickel precipitation curve, and the oxygen fugacity of the Earth's upper mantle. // *Journal of Petrology*, 1987. v. 28, pp.1169-1191.
41. **O'Neill, H.St.C, Wood, B.J.** 1979. An experimental study of Fe-Mg- partitioning between garnet and olivine and its calibration as a geothermometer. // *Contrib. Mineral. Petrol.* 70, 5970.

42. **Pearson, D.G.** The age of continental roots., 1999.// *Lithos*, 1979. v.48, pp.171-194.
43. **Pokhilenko, N.P., Boyd, F.R., Ashchepkov, I.V., Kuligin, S.S., Malygina, E.V.** Layered mantle beneath Udachnaya pipe: OPX thermobarometry. // *Geophysical Research Abstracts*, 2000, v.2, p.154.
44. **Pokhilenko, N.P., Sobolev, N.V., Boyd, F.R., Pearson, D.G., Shimizu, N.** 1993. Megacrystalline pyrope peridotites in the lithosphere of the Siberian platform: mineralogy, geochemical peculiarities, and the problem of their origin. // *Russian J Geol Geophys* 34 (1): 50-62.
45. **Pokhilenko, L.N.** 2006. Volatile composition and oxidation state of mantle xenoliths from Siberian kimberlites. /PhD thesis, United Institute of Geology Geophysics and Mineralogy, Novosibirsk. 225 p.
46. **Pokhilenko, N. P., Pearson, D. G., Boyd, F. R. & Sobolev, N. V.** Megacrystalline dunites: sources of Siberian diamonds. /*Carnegie Inst. Washington Yearbook*, 1991. pp.11-18.
47. **Pokhilenko, N. P., Sobolev, N. V., Boyd, F. R., Pearson, D. G. & Shimizu, N.** Megacrystalline pyrope peridotites in the lithosphere of the Siberian platform: mineralogy, geochemical peculiarities and the problem of their origin. // *Russian Geology and Geophysics* 1993. v.34, pp. 56-67.
48. **Pokhilenko, N. P., Sobolev, N.V., Kuligin, S. S., Shimizu, N.** 1999. Peculiarities of distribution of pyroxenite paragenesis garnets in Yakutian kimberlites and some aspects of the evolution of the Siberian craton lithospheric mantle.// *Proceedings of the VII International Kimberlite Conference. The P.H. Nixon volume. P. 690-707.*
49. **Pokhilenko, N.P., Sobolev, N.V., Sobolev, V.S., Lavrentiev, Yu.G.** Xenolith of diamond bearing ilmenite-pyrope lherzolite from the Udachnaya kimberlite pipe, Yakutia.// *Doklady AN SSSR*, 1976, v.231, pp.149-151.
50. **Shatsky, V., Ragozin, A., Zedgenizov, D., Mityukhin, S.** 2008. Evidence for multistage evolution in a xenolith of diamond-bearing eclogite from the Udachnaya kimberlite pipe.// *Lithos* 2008, v.105, pp. 289–300.
51. **Shatsky, V. S., Buzlukova, L.V., Jagoutz, E., Koz'menko, O. A. & Mityukhin, S. I.** Structure and evolution of the lower crust of the Daldyn-Alakit district in the Yakutian Diamond Province (from data on xenoliths). // *Russian Geology and Geophysics*, 2005. v.46, pp.1252-1270.
52. **Shimizu, N., Pokhilenko, N. P., Boyd, F. R. & Pearson, D. G.** Geochemical characteristics of mantle xenoliths from the Udachnaya kimberlite pipe.// *Russian Geology and Geophysics* 1997. v.38, pp. 205-217.
53. **Shimizu, N., Sobolev, N.V., Yefimova, E.S.** 1997b. Chemical heterogeneities of inclusion garnets and juvenile character of peridotitic diamonds from Siberia. // *Russ. Geol. Geophys.* V.38-2, pp.356– 372.
54. **Snyder, G.A., Taylor, L.A., Crozaz, G., Halliday, A.N., Beard, B.L., Sobolev, V.N.** 1997. The Origins of Yakutan Eclogite Xenoliths.// *J. Petrol.*, 1997. v.38, pp.85-113.
55. **Sobolev, N.V., Logvinova, A.M., Zedgenizov, D.A., Pokhilenko, N.P., Malygina, E.V., Kuzmin, D.V., Sobolev, A.V.** Petrogenetic significance of minor elements in olivines from diamonds and peridotite xenoliths from kimberlites of Yakutia.// *Lithos*, 2009. v.112 S1 pp.
56. **Sobolev, V.N., Sobolev, N.V.** Nd and Sr isotopes from diamondiferous eclogites, Udachnaya kimberlite pipe, Yakutia, Siberia: evidence of differentiation in the early Earth? // *Earth Planet. Sci. Lett.* 1993. v.118, pp.91–100.
57. **Sobolev, V.N., Taylor, L.A., Snyder, G.A., Sobolev, N.V.** Diamondiferous eclogites from the Udachnaya pipe, Yakutia. // *International Geology Review*, 1994, v. 36, N 1, pp. 42-64.
58. **Sobolev, N. V., Logvinova, M., Zedgenizov, D. A., et al.** Mineral inclusions in microdiamonds and macrodiamonds from kimberlites of Yakutia: a comparative study. // *Lithos*, 2004. v. 77, pp.225–242.

59. **Sobolev, N. V., Pokhilenko, N. V. & Efimova, E.S.** Xenoliths of diamond bearing peri-dotites in kimberlites and problem of the diamond origin. //Russian Geol. Geophys. 1984, V.25/12, pp.63-80.
60. **Sobolev, N.V.** 1977. Deep-Seated Inclusions in Kimberlites and the Problem of the Composition of the Mantle./Amer. Geophys.Union, Washington, DC. 279 p.
61. **Sobolev, N.V., Logvinova, A.M., Efimova, E.S.** Syngenetic phlogopite inclusions in kimberlite-hosted diamonds implications for role of volatiles in diamond formation. Russian.// Geology and Geophysics 2009..v.50 pp.1234–1248.
62. **Solovjeva, L.V., Egorov, K.N., Markova, M.E., Kharkiv, A.D., Popolitov, K.E., Barankevich, V.G.,** 1997. Mantle metasomatism and melting in mantle-derived xenoliths from the Udachnaya kimberlite; their possible relationship with diamond and kimberlite formation.// Russian Geology and Geophysics 38 (1), pp.172–193.
63. **Solov'eva, L.V., Lavrent'ev, Yu.G., Egorov, K.N., Kostrovitskii S.I., Korolyuk V.N., Suvorova L.F.** 2008. The genetic relationship of the deformed peridotites and garnet megacrysts from kimberlites with asthenospheric melts. //Russian Geology and Geophysics. 2008. v.49, pp. 207–224.
64. **Spetsius, Z. V. & Serenko, V. P.** Composition of the continental upper mantle and lower crust beneath the Siberian Platform. 272 (in Russian) p. /Moscow: Nauka. 1990, 200 p .
65. **Tappe, S., Foley, S. F., Stracke, A., Romer, R.L., Kjarsgaard, B.A. Heaman, L.M., Joyce, N.** Craton reactivation on the Labrador Sea margins: 40 Ar/39 Ar age and Sr-Nd-Hf-Pb isotope constraints from alkaline and carbonatite intrusives.// Earth and Planetary Science Letters. 2007. v. 256. pp. 433-454.
66. **Taylor, W.L., Kamperman, M., Hamilton, R.** New thermometer and oxygen fugacity sensor calibration for ilmenite and Cr-spinel-bearing peridotite assemblage. In: Gurney, J.J., Gurney, J.L., Pascoe, M.D., Richardson, S.H. (Eds.)//7th International Kimberlite Conference. In: Red Roof Design, Capetown, 1998. pp.986–988.
67. **Turkin, A.I., Sobolev, N.V.** Pyrope–knorringite garnets: overview of experimental data and natural parageneses. //Russian Geology and Geophysics 50 (2009) pp.1169–1182.
68. **Zedgenizov, D.A., Kagi, H., Shatsky, V.S., Sobolev N.V.** Carbonatitic melts in cuboid diamonds from Udachnaya kimberlite pipe (Yakutia): evidence from vibrational spectroscopy. //Miner. Magazine 2004 v.68, pp.61-73.
69. **Zinchuk, N. N., Spetsius, Z. V., Zuenko, V. V. & Zuev, V. M.** Kimberlite Pipe Udachnaya. 46 (in Russian) /Novosibirsk: Novosibirsk University. 1993, 185 p.

## **Alkali lamprophyres of the Palaeozoic igneous complex of Belarus**

Mikhailov N. D.<sup>1</sup>, Laptsevich A. G.<sup>1</sup>, Vladykin N.V.<sup>2</sup>

<sup>1</sup>*Republican Unitary Enterprise «Belarusian Research Geological Exploration Institute», Kuprevich str., 7, Minsk, 220141, Belarus, mihailov@igig.org.by.*

<sup>2</sup>*A. P. Vinogradov Institute of Geochemistry, Siberian Branch of the Russian Academy of Sciences, Favorsky str., 1a, Irkutsk, Russia, vlad@igs.irk.ru.*

### **ABSTRACT**

Within the Upper-Devonian rift alkali igneous formation lamprophyres as representatives of the earliest phase of magmatism ( $D_{3rch}$ ) were identified in two areas—Pripyat graben and North-Pripyat magmatic region, including the southern part of the Zlobin saddle and the northern zone of the Gomel structural dam. Feldspathoid, feldspathic and melilite (alnoite) subfamilies were identified among alkali rocks of the lamprophyric family. Lamprophyres are mostly patassic rocks, but some increase of the sodium amount is observed in melilite lamprophyres. Feldspathic lamprophyres are described by moderate alumina contents, whereas alnoites are low in alumina, but both are of miaskite nature. Feldspathic lamprophyres were determined to be described by rather high Nd, Zr, Sm, Eu, Hf, Yb and rather low Ni, Co, Cr, Pb, Nb concentrations. Melilite lamprophyres are inherent in the higher of Cr, Ni, Nb, and lower Nd, Sm, Eu contents. Alnoites are distinguished by the maxima of Cr, Ni, La and Ba in the range of elements.

### **INTRODUCTION**

Among petrographically diverse alkali igneous rocks found in the territory of Belarus rocks of the lamprophyric family described by the presence of micas, biotite and phlogopite in their mineral composition along with considerable amounts of ore minerals were rare in occurrence until the present time. These rocks belong mainly to hypabissal formations that essentially do not have analogues among volcanites and plutonites. Alkali rocks related to this group are identified as isolated formations looking like small sills, dikes and stocks in the Pripyat Trough and North-Pripyat magmatic region [1, 2].

Within the Pripyat Trough lamprophyres were identified among rocks of the Vasilievsk (Artukovskaya 3 borehole), Vetkhino (Vetkhinskaya 1 borehole), and Dnieper (Dnieprovskaya 1 borehole) palaeovolcanoes. Within the North-Pripyat magmatic region lamprophyric rocks are revealed in the southern part of the Luchin cluster of the Zhlobin diatreme field and the northern edge of the Gomel structural dam (Urtskaya 63d 1 borehole).

### **TYPES OF LAMPROPHYRES**

Among the studied alkali lamprophyres found in the territory of Belarus the subfamilies of feldspathic, melilite and feldspatoid lamprophyres are distinguished.

Feldspathic lamprophyres are rocks forming the igneous complex of the Pripyat graben. In the Vetkhinskaya 1 borehole lamprophyres (vogesites after V.P. Korzun) were exposed in deposits of the Semiluki horizon (at a depth of 4.565-4.582m), where these form a small dike about 20 m in thickness. The rock is fine-

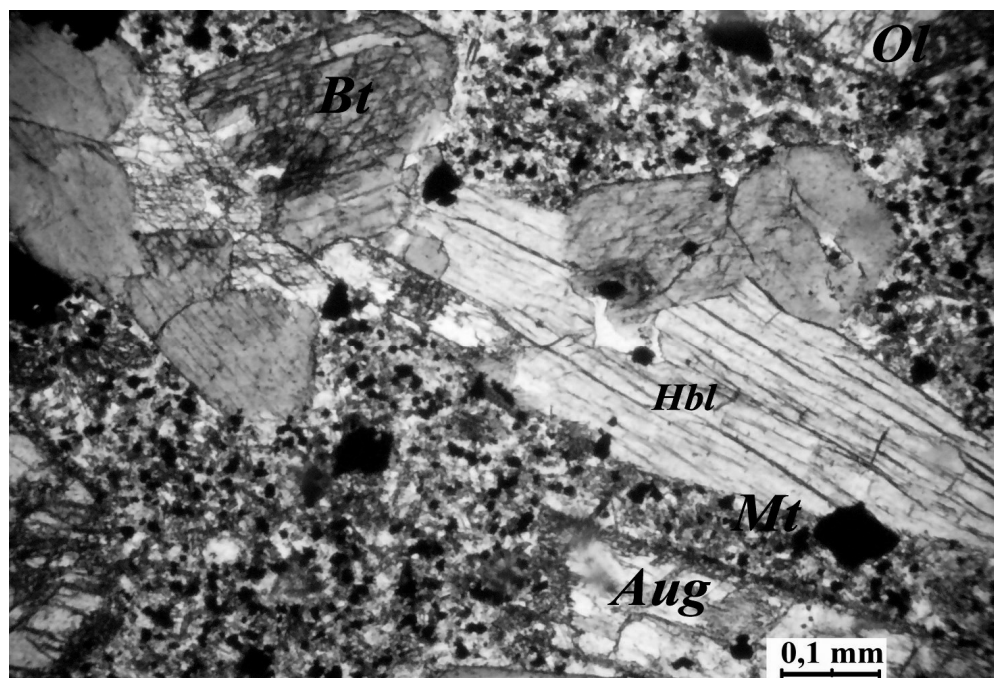
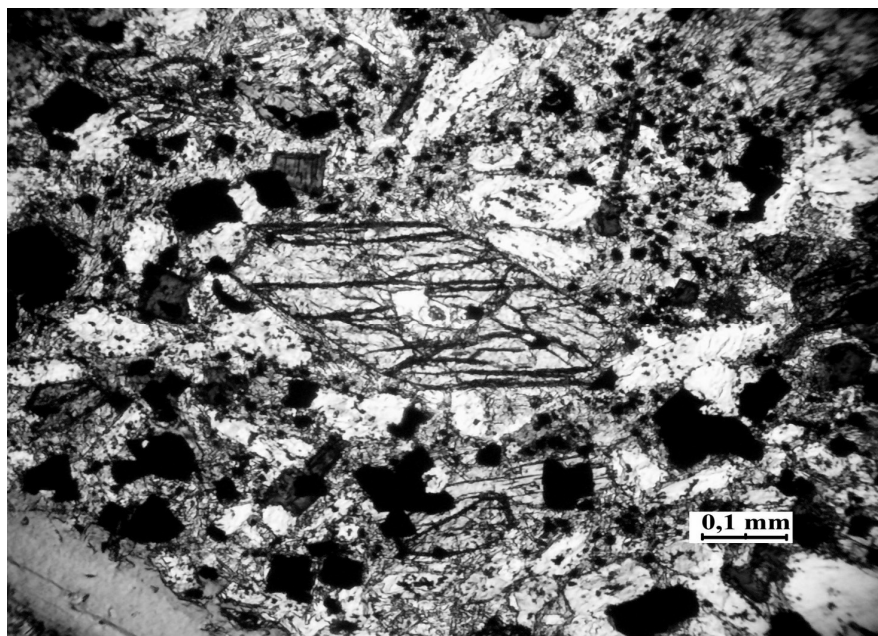


Fig. 1a. Feldspathic lamprophyre. Pripyat graben, Artukovskaya 3 borehole, depth of 4,514-4,518.

grained. The rock structure is lamprophyric due to porphyries of hornblende substituted by calcite and chlorite (penninite). The rock groundmass is composed of leistes of potassium-sodium feldspar sometimes of trachtyoid texture. The rock is abundant in biotite scales confined to feldspar leistes or occurring as microporphyries. There are numerous impregnations of ore minerals – titanomagnetite and magnetite, the first one being dominant. Femic, salic mineral and feldspar contents of the rock are generally similar.

Lamprophyres from the Artukovskaya 3 borehole adjacent from the north to the Vetkhino palaeovolcano (Artukovskaya 3 borehole, depth of 4,514 to 4.518m) occur similarly in the geological section and form there a small (about 2 m thick) vein in the Semiluki deposits. By the mineral composition these are similar to feldspathic lamprophyres from the Vetkhino palaeovolcano, but the porphyries of coloured minerals are larger in size and the idiomorphic texture is more pronounced there (Fig.1a). Lamprophyres also occur as an about 5m thick dike among quartzitic sandstones in the northwestern area of the Pripyat graben magmatism developed in the rocks of the Dnieper palaeovolcano (Dnieprovskaya 1 borehole, depth of 3,564 m).

The rock is a finely crystalline feldspar matrix, where coloured minerals form the lamprophyric structure, and femic minerals represented by hornblende, biotite



**Fig. 1b. Feldspathic lamprophyre with olivine and porphyries. Pripyat graben, Dneprovskaya 1 borehole, depth of 3,564 m.**

and a variety of ore minerals comprise about 60% of the rock groundmass. The pleochroic biotite light yellow to dark-brown in colour together with porphyries and an association of ore minerals form there abundant spot impregnations. Porphyries of strongly altered olivine and pyroxene (Fig.1b) often occur in the rock.

The North- Pripyat magmatic region is the second area where lamprophyres were determined in the southern part of the Zlobin diatrem field and in the northern edge of the Gomel structural dam. Within the Zlobin Saddle lamprophyres were identified in boreholes drilled within the anomaly zone named «Shliakh Selianina». By the mineral composition these correspond to the melilite subfamily of the lamprophyric family and are represented by two rock varieties. The rocks occur in two boreholes 761 (depth interval from 104 to 196 m and from 229 to 243 m) drilled within the abovesaid anomaly. In the borehole 763 lamprophyres (alnoites) are underlain and overlain by breccias formed by the same rocks. Igneous rocks exposed in the borehole 761 at a depth of 194 m may be related to the first variety of the melilite subfamily of lamprophyres (polzenites) [3]. The rock groundmass is represented by elongated-tabular, strongly altered (to carbonate) melilite crystals, as well as by tabular, often elongated mica crystals yellow-brown to light-brown in colour, frequently with pronounced zoning structure peculiar to micas entering in

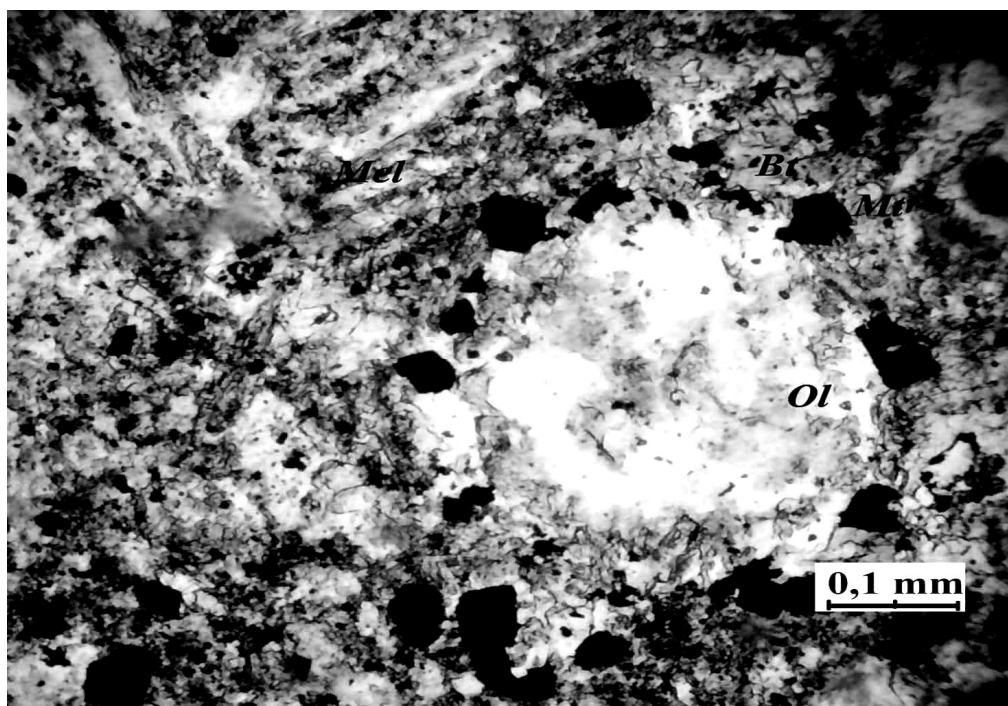


Fig. 2a. Melilite lamprophyre of trachytoid structure. Luchin 761 borehole, depth of 194 m.

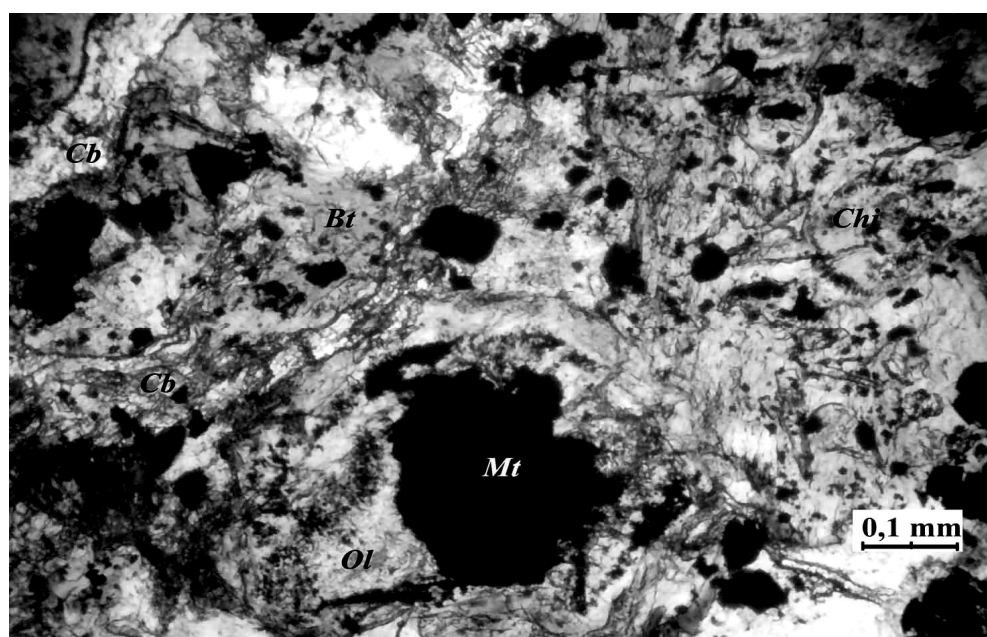
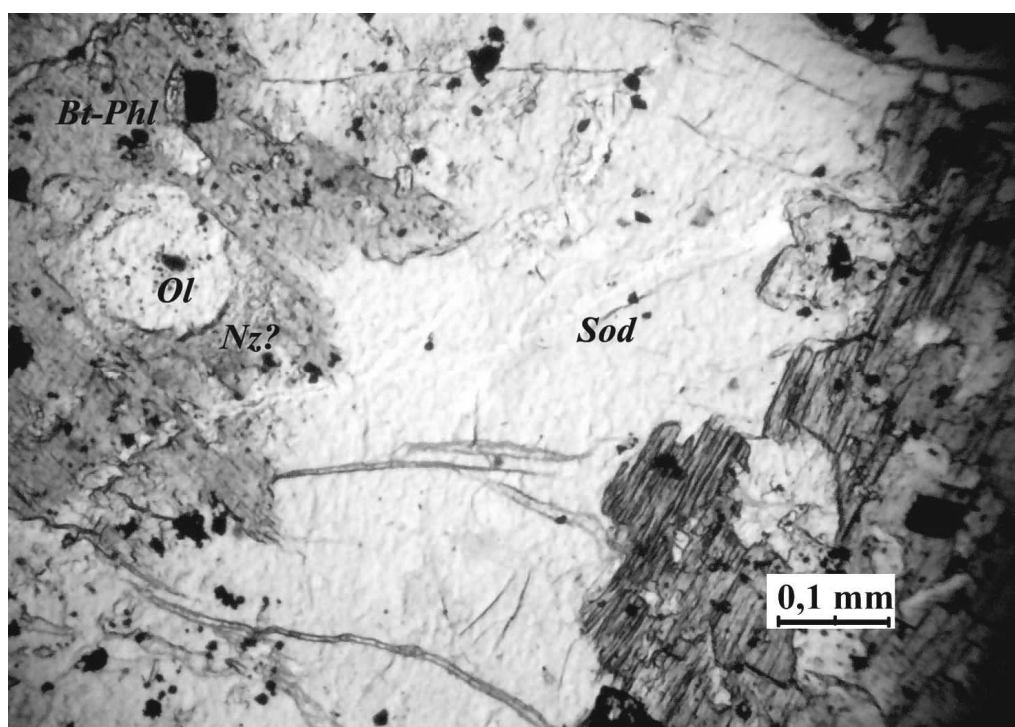


Fig.2b. Alnoite lamprophyre. Luchin 761 borehole, depth of 237.5 m.

the composition of the lamprophyres, or to phlogopite [4]. Magnetite grains are scattered in the rock forming an uneven impregnation and fringe olivine pseudo morphs around the periphery. When melilite and phlogopite flow around olivine



**Fig. 2c. Lenticular sodalite veinlet in alnoite. Luchin 761 borehole, depth of 231 m.**

porphyries the rock shows a slightly trachytoid texture (Fig. 2a). Alnoites stripped by the borehole 761 in the low part of the section (227-233 m) is the second variety of lamprophyres of the melilite subfamily. These rocks are grey, dark-grey to black in colour showing massive texture and microcrystalline, often aphanitic structure. The rock groundmass is composed of argillic glass altered to hydromica, serpentinous olivine, chlorite, carbonate. Porphyry impregnations are represented by phlogopite (biotite) and magnetite (Fig.2b). A light yellowish-green isotropic mineral with a low refractive index which can be qualified as sodalite by its optical properties occurs in the rock within the depth range from 231 to 232 m. This mineral often forms irregularly shaped lenticles and clasts in association with phlogopite and a blue mineral of similar properties (nosean?), which was probably developed on alkali glass (Fig. 2c). As it was mentioned above lamprophyres in the borehole 763 are underlain and overlain by breccias of melilite- lamprophyric composition. In lamprophyres (polzenites) of the upper part of the section melilite pseudomorphs are infilled with greenish chlorite. The rock groundmass is carbonate with melilite, hydromica and chlorite pseudomorphs. Femic minerals are represented by phlogopite (biotite) and magnetite. Lamprophyres from the lower part of the section are of the alnoite composition with olivine and sodalite, pyroxene porphyries occur sometimes (Fig.2d). Carbonate constitutes the most part of the alnoite groundmass, which is just peculiar to this type rocks [5]. A distinguishing feature of all igneous rocks from the Shliakh Selianina anomalous zone is their rather strong carbonatization.

Lamprophyres of the feldspathoid subfamily represented by monchiquite were

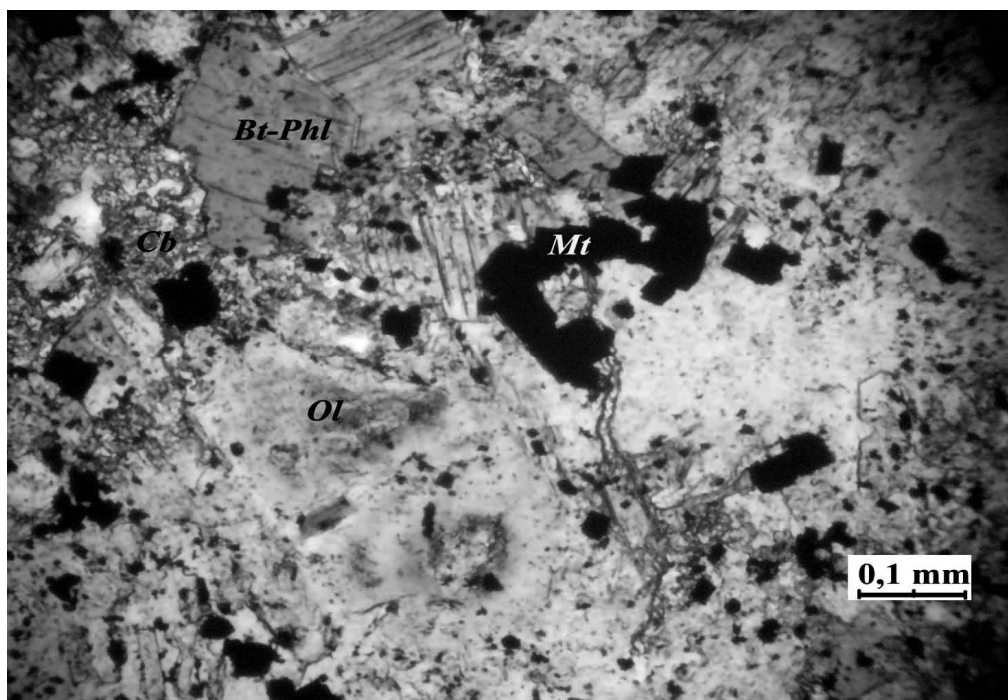


Fig. 2d. Olivine impregnations in alnoite lamprophyre. Luchin 763 borehole, depth of 229 m.

determined in the borehole 63d within the territory of the Gomel structural dam.

According to H. Williams [5] monchiquites differ from feldspathoid camptonites by the absence of feldspar which is replaced by a colourless isotropic mineral, sodium glass, or analcime appeared in the felsic matrix. Lamprophyres exposed in the borehole 63d are represented by a black rock of porphyritic texture. The rock groundmass is built by slightly decrystallized glass and elongated-prismatic greenish-yellow crystals of alkali pyroxene with analcime and apatite impregnations (Fig. 3a). Rhombic pyroxene porphyries rarely occur, but these are short-prismatic and smaller in size. The rock shows abundant magnetite, more seldom, ilmenite impregnations and corresponds to pyroxene-magnetitic monchiquite by its mineral and chemical composition. The second lamprophyre variety, or the rock transition found in the borehole 63d is monchiquite with vitrophyre-olivine-pyroxene nodules underlying pyroxene-magnetitic monchiquites. The major composition of this rock is similar to that of monchiquites described above, but pyroxene and magnetite form a subtrachytic texture around nodules (Fig. 3b). The nodules originally microstructure, when their major part is built by iddingsite surrounded by an envelope of olivine in composition are transformed to become orange-brown in colour (iddingsite-biotite like mineral according to Lodochnikov) and show a corona of pyroxene and magnetite (Fig. 3c).

There are lenticular and drop-like residual glass xenoliths, with impregnations of two pyroxene generations— acicular crystals and phenocrysts of prismatic clino- and orthopyroxenes (Fig. 3d).

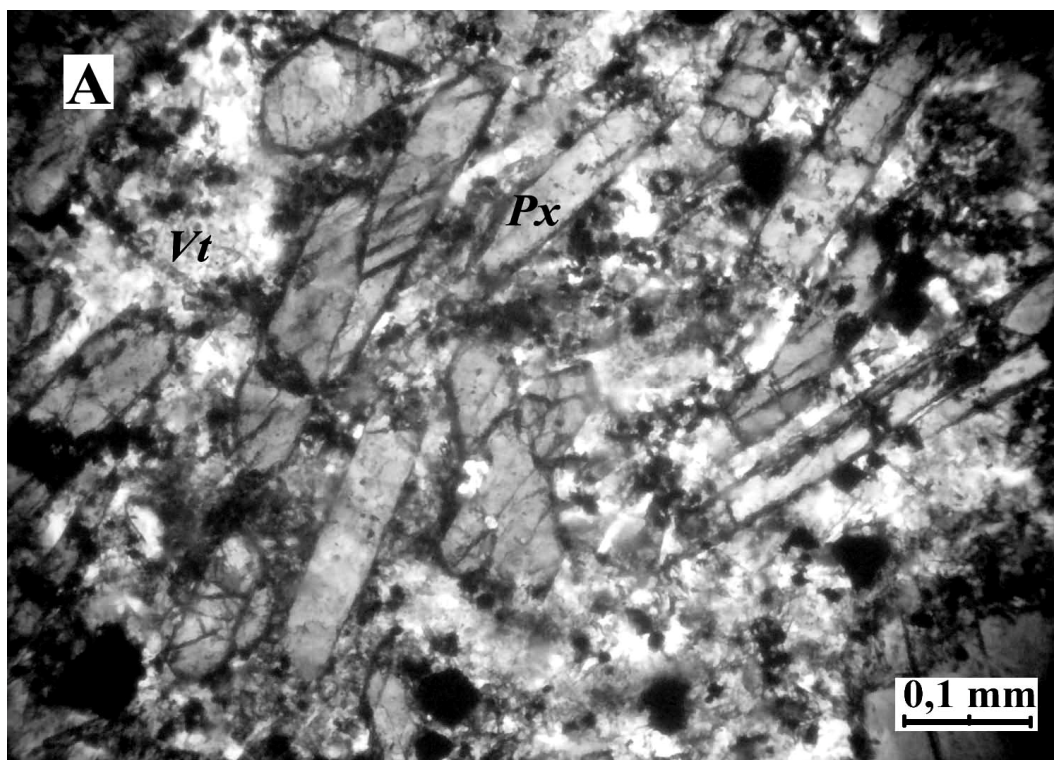


Fig. 3a. Vitrophyre-pyroxenic composition of the monchiquite groundmass (borehole 63d, depth of 260 m, section, parallel nicols).

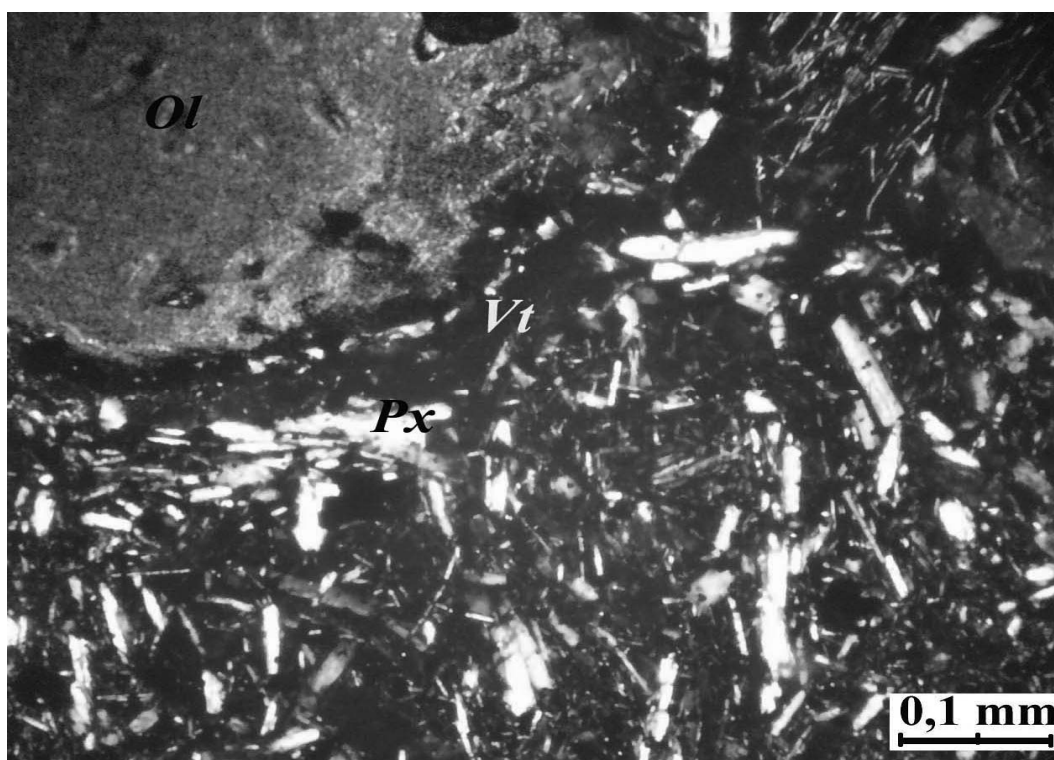


Fig.3b. Trachytoid texture of monchiquite-camptonite around olivine nodules (borehole 63d, depth of 262 m, section, parallel nicols).

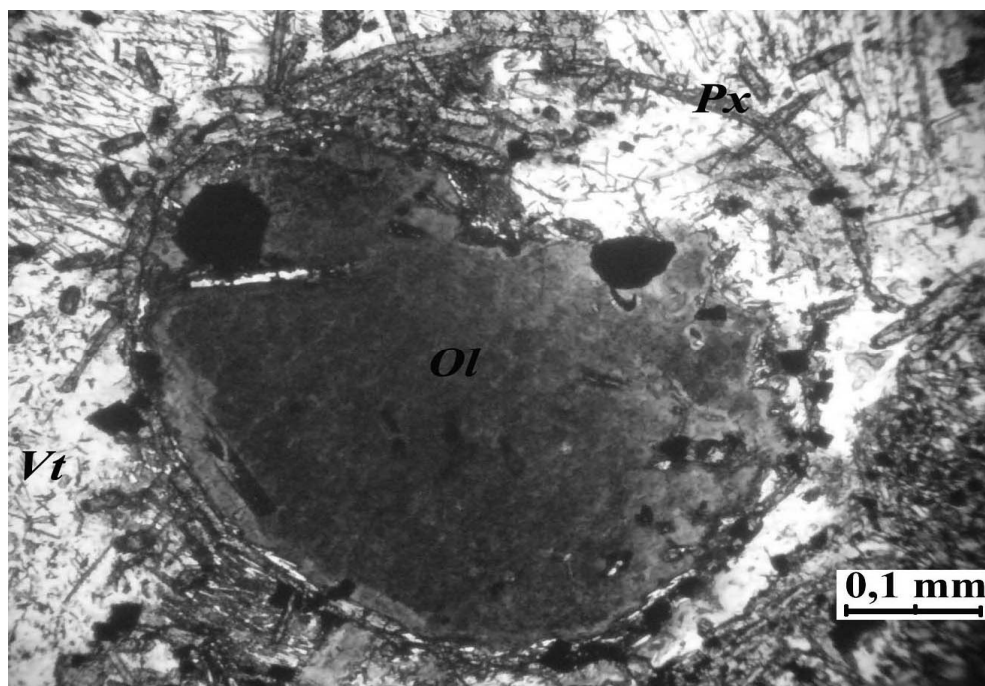


Fig. 3c. Olivine nodule altered to iddingsite fringed by pyroxene and magnetite crystals in monchiquite (borehole 63d, depth of 262 m, section, parallel nicols).

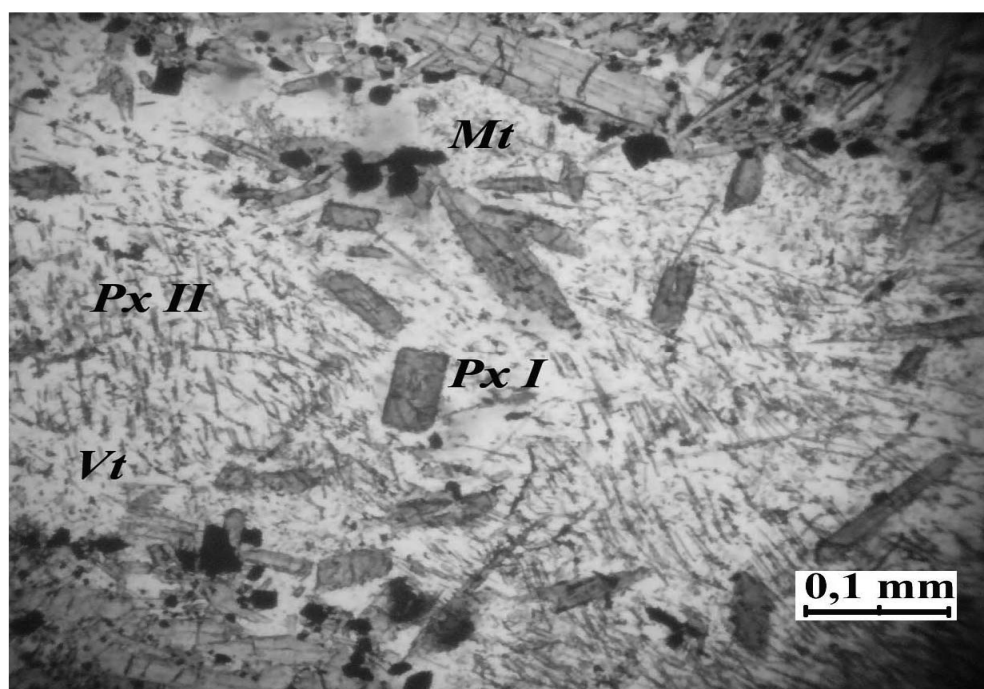


Fig. 3d. Two pyroxene generations (acicular and short prismatic-rhombic ones) in residua; glass xenolites observed in monchiquite (borehole 63d, depth of 262 m, section, parallel nicols).

Chemical composition of alkali lamprophyres (wt.%)

Oxides	Feldspathic lamprophyre of the Pripyat graben				Feldspathoid 5a	Melilit lamprophyres							
						pyroxene-free melilit lamprophyres				melilit lamprophyres (alnoites)			
	1	2	3	4		5	6	7	8	9	10	11	13
SiO <sub>2</sub>	39.23	38.69	39.6	44.53	44.56	34.9	34.75	37.03	36.7	35.76	35.16	34.58	35.72
TiO <sub>2</sub>	2.09	3.55	2.77	3.11	3.32	2.12	2.03	2.06	2.19	1.84	2.1	2.14	2.23
Al <sub>2</sub> O <sub>3</sub>	8.17	9.83	11.16	9.85	13.07	5.1	5.24	4.4	4.4	3.9	4.6	4.3	4.31
Fe <sub>2</sub> O <sub>3</sub>	10.12	16.12	13.99	10.97	12.89	15.57	16.05	15.46	16.12	14.4	15.15	14.49	13.92
MnO	0.12	0.13	0.09	0.08	0.12	0.19	0.13	0.17	0.17	0.2	0.24	0.23	0.24
MgO	12.65	9.16	15.18	10.73	4.98	18.86	15.31	22.87	23.51	26.52	21.7	21.74	18.55
CaO	12.37	10.67	2.94	5.74	8.36	7.21	10.97	1.63	2.13	2.44	6.0	7.52	9.45
SrO	0.05	0.09	0.04		0.17	0.14	0.14	0.08	0.1	0.11	0.1	0.12	0.09
BaO	0.25	0.09	0.13		0.13	0.1	1.0	0.05	0.05	0.05	0.05	0.05	0.10
Na <sub>2</sub> O	0.36	1.08	0.59	1.89	4.11	0.49	0.78	0.5	0.55	0.23	0.39	0.3	0.35
K <sub>2</sub> O	2.76	3.00	3.46	6.67	2.72	2.29	0.87	2.19	1.99	1.99	2.63	2.58	2.20
P <sub>2</sub> O <sub>5</sub>	0.45	0.74	0.61	0.61	0.79	0.73	0.61	0.6	0.6	0.55	0.61	0.6	0.58
H <sub>2</sub> O	4.65	3.76	6.76	0.00	4.56	6.50	6.98	11.35	9.53	9.59	6.43	6.17	
CO <sub>2</sub>	6.13	2.83	2.55		0.05	5.01	4.22	1.02	1.14	1.61	4.04	4.85	
F	0.34	0.26	0.23	0.07	0.09	0.35	0.23	0.31	0.32	0.35	0.34	0.32	
П.п.п	10.48	6.11	8.83		4.12	11.51	11.20	12.37	10.67	11.20	10.47	11.02	12.11
сумма	99.77	100.04	100.11	94.25	99.92	99.62	99.46	99.76	99.50	99.50	99.60	100.02	99.85
Na <sub>2</sub> O+K <sub>2</sub>	3.12	4.08	4.05	8.56	6.83	2.78	1.65	2.69	2.54	2.22	3.02	2.88	2.55
Na <sub>2</sub> O/K <sub>2</sub>	0.13	0.36	0.17	0.28	1.51	0.21	0.90	0.23	0.28	0.12	0.15	0.12	0.16
al'	0.36	0.39	0.38	0.45	0.73	0.15	0.17	0.11	0.11	0.10	0.12	0.12	0.13
Ka	0.38	0.42	0.36	0.87	0.52	0.55	0.31	0.61	0.58	0.57	0.66	0.67	0.59

Note: 1) analysis №: **1-4 Feldspathic lamprophyres of the Pripyat graben**: 1- Artukovskaya 3 borehole, sample 27, depth of 4,384 m; 2- Artukovskaya 3 borehole, sample 40-a, depth of 4,518m; 3- Dnieprovskaya 1 borehole, sample 1d, depth of 3,564-3,567m; 4- Vetkhinskaya 1 borehole, sample 85b, depth of 4,565m; 5-14- **Lamprophyres of the North-Pripyat region**; 5-6 – melilit lamprophyres from the southern part of the Zlobin saddle: 5- Luchin borehole 761, sample 9, depth of 194m; 6- Luchin borehole 761, sample 8, depth of 193m; 7-14 – alnoites from the southern part of the Zlobin saddle: 7- Luchin borehole 761, sample 20, depth of 231m; 8- Luchin borehole 761, sample 20a, depth of 232m; 9- Luchin borehole 761, sample 21, depth of 236m; 10- Luchin borehole 761, sample 23, depth of 238m; 11- Luchin borehole 761, sample 24, depth of 241m; 12- carbonate alnoite Luchin borehole 763, sample 9, depth of 227m.; 13 - Luchin borehole 763, sample 12, depth of 228m; 14- Luchin borehole 763, sample 15, depth of 229m;

2) rock-forming pxides were determined by X-ray fluorescence analysis at the A. P Vinogradov Institute of Geochemistry Irkutsk, Russia .

3) Fe<sub>2</sub>O<sub>3</sub> –indicates a sum of iron oxides.

Table 2

## Trace elements contents (ppm) of lamprophyres from the Paleozoic igneous complex of Belarus

elements	1	2	3	4	5	6	7	8	9	10	11	12	13	14
Be	2.9	3.7	6.2	7.5	9.1	7.3	5.7	4.5	4.8	7.5	8.3	7.5	9.0	5.6
V	436.1	259.0	288.5	288.8	284.6	245.9	243.4	244.4	163.7	266.9	228.8	228.7	270.3	366.6
Cr	60.8	121.4	606.5	286.8	316.8	679.4	669.2	673.3	434.7	947.7	887.3	871.6	867.9	985.6
Co	59.0	33.6	67.1	49.5	55.5	69.9	65.3	73.7	51.5	75.5	73.0	63.8	76.9	82.1
Ni	49.5	63.9	295.8	117.6	124.7	332.2	271.9	332.5	199.9	400.7	366.5	301.4	354.2	368.1
Cu	253.1	21.7	358.7	399.6	429.5	368.7	368.0	421.0	282.3	403.3	389.6	354.5	401.6	409.3
Zn	181.3	31.2	71.4	146.0	131.4	77.0	146.4	119.1	80.2	96.6	100.5	118.9	138.2	105.9
Ga	20.9	21.7	12.9	12.1	12.8	12.1	12.5	13.6	9.4	11.7	11.7	10.7	11.2	13.0
Rb	49.0	51.5	68.2	28.0	41.8	52.9	48.2	51.4	44.7	41.9	37.9	46.0	43.1	47.3
Sr	1179	481	1276	1722	1296	859	887	804	815	778	895	1000	788	1173
Y	23.8	30.4	13.6	13.8	16.9	11.8	12.4	13.2	9.7	13.6	13.1	12.8	12.4	15.2
Zr	231.0	250.7	161.9	117.1	116.7	139.8	128.1	128.0	92.2	104.8	116.1	112.3	118.1	110.6
Nb	54.9	75.5	81.4	85.1	87.5	80.7	78.2	82.2	55.2	79.0	79.2	72.0	82.3	82.5
Ba	914	1103	1131	10971	1882	2154	899	967	647	986	887	893	1127	1164
La	57.4	66.2	42.4	115.4	106.2	71.5	82.2	95.9	65.9	72.2	69.7	60.7	116.3	96.2
Ce	123.1	131.4	75.4	174.8	171.1	129.5	142.7	161.8	115.1	108.3	139.2	104.7	168.1	137.3
Pr	13.9	11.9	7.3	17.2	16.3	11.8	12.7	14.7	10.3	10.7	13.4	10.5	16.3	14.6
Nd	60.0	58.4	25.3	52.1	49.5	41.1	44.1	50.8	34.8	32.3	41.6	31.6	46.8	46.7
Sm	10.6	9.8	3.9	7.4	7.2	5.7	6.0	6.8	4.6	5.0	5.9	4.3	5.8	7.0
Eu	3.0	3.4	1.1	2.5	1.9	1.7	1.6	1.9	1.2	1.5	1.7	1.5	1.7	2.1
Gd	9.4	8.0	4.1	7.0	6.3	6.0	6.0	6.9	4.6	4.5	5.3	5.2	5.8	6.8
Tb	1.1	0.9	0.5	0.8	0.9	0.6	0.6	0.6	0.4	0.7	0.7	0.6	0.7	0.8
Dy	5.7	4.9	3.0	3.6	4.5	3.1	3.2	3.3	2.2	3.3	3.3	3.2	3.5	4.0
Ho	1.0	1.0	0.6	0.6	0.8	0.5	0.5	0.5	0.4	0.6	0.6	0.5	0.5	0.7
Er	2.3	2.1	1.6	1.5	2.0	1.6	1.6	1.4	1.1	1.6	1.5	1.5	1.1	1.6
Tm	0.3	0.3	0.2	0.2	0.2	0.2	0.2	0.2	0.1	0.2	0.2	0.2	0.2	0.2
Yb	1.7	2.0	1.3	1.3	1.7	1.1	1.0	0.9	0.7	1.2	0.9	1.3	1.0	1.4
Lu	0.2	0.3	0.2	0.2	0.2	0.2	0.1	0.1	0.1	0.2	0.2	0.2	0.1	0.2
Hf	5.2	6.3	3.9	3.5	3.1	3.3	3.1	3.2	2.2	2.8	2.9	3.0	3.0	2.6
Ta	3.9	4.7	4.6	4.6	4.5	5.0	4.9	5.2	3.6	4.0	4.1	4.0	4.3	3.6
Pb	4.1	3.2	5.1	4.8	12.4	5.5	169.5	14.8	4.3	6.3	7.8	16.0	9.3	14.4
Th	6.2	8.3	8.5	11.4	11.8	8.4	8.5	8.3	6.6	9.3	8.6	9.8	11.4	7.5
U	1.2	1.7	1.8	2.3	2.4	2.3	1.4	1.4	0.7	2.2	1.9	1.6	1.8	1.6

Note I) **Feldspathic lamprophyres**: 1— Artukovskaya 3 borehole, sample 40-a, depth of 4,518m; 2— Vetkhinskaya 1 borehole, sample 85b, depth of 4,565m; II) **melilit lamprophyres**: 3 — Luchin borehole 763, sample 8, depth of 225m; 4—Luchin borehole 761, sample 8, depth of 193m; 5— Luchin borehole 761, sample 9, depth of 194m; III)— **alnoites**: 6— carbonate alnoites, Luchin borehole 763, sample 9, depth of 227m.; alnoites : 7— Luchin borehole 763, sample 13, depth of 229 m; 8— Luchin borehole 763, sample 15, depth of 229m; 9— Luchin borehole 763, sample17, depth of 232m; 10— Luchin borehole 761, sample depth of 231 m; 11 Luchin borehole 761, sample depth of 232m; 12— Luchin borehole 761, sample depth of 236 m; 13— Luchin borehole 761, sample depth of 238m; 14— Luchin borehole 761, depth of 241m; IV) trace-elements were determined by ICP-MS at the A. P Vinogradov Institute of Geochemistry Irkutsk, Russia.

## TRACE ELEMENTS AND ISOTOPES

Data obtained for the composition of lamprophyres and the trace element distribution in them suggest that each lamprophyre variety is described by its own geochemical features (Tables 1, 2). Their common features are high titanium, iron

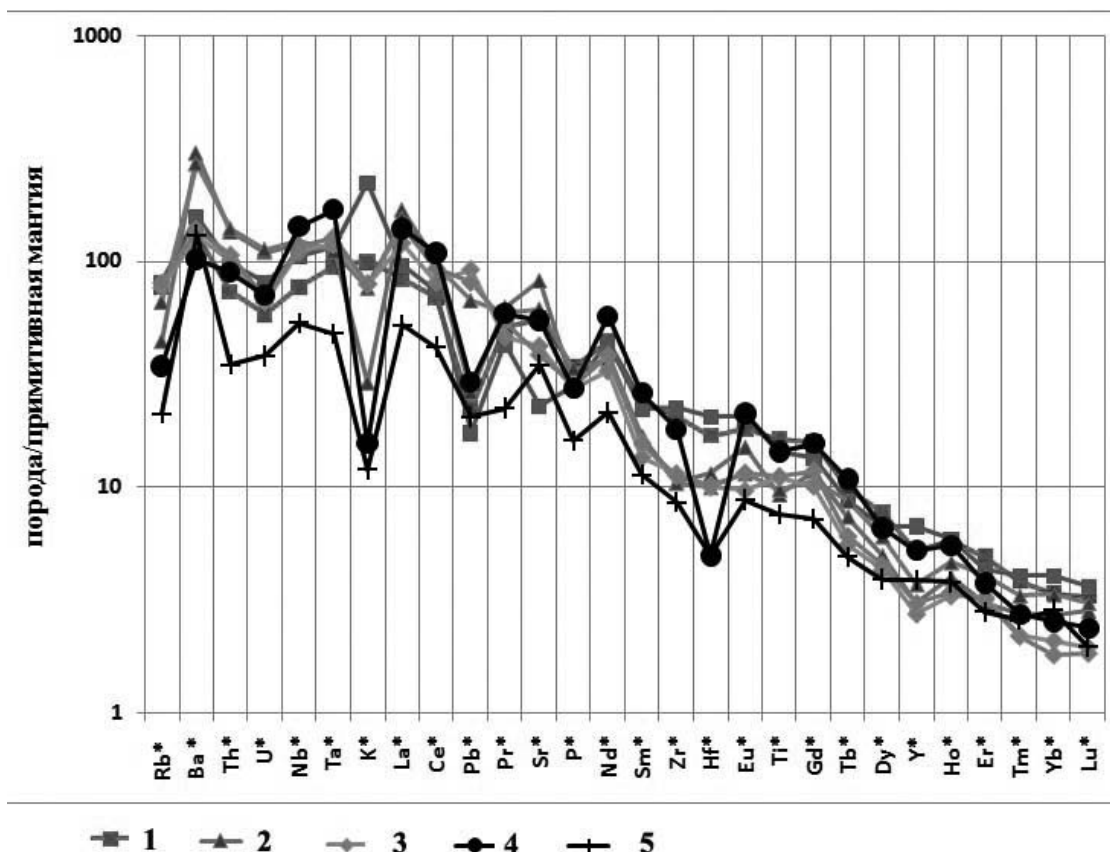


Fig. 4 Primitive mantle normalized [6] rare element distribution in lamprophyres of the Palaeozoic igneous complex of Belarus.

1- feldspathic lamprophyres of the Pripyat graben; 2- pyroxene-free melilite lamprophyres; 3- melilite lamprophyres- alnoeit; 4- alkali picrite of the Pripyat graben; 5-alkali picrite of the North-Pripyat region.

content and alkalinity. The highest alkalinity is determined in feldspathic lamprophyres of the Pripyat graben ( $\text{Na}_2\text{O}+\text{K}_2\text{O}= 3.12\text{--}8.56$  mas. %) and monchiquites ( $\text{Na}_2\text{O}+\text{K}_2\text{O}=6.9$  mas.%). Lamprophyres are generally potassic ( $\text{Na}/\text{K}=0.2\text{--}0.4$ ), but melilite lamprophyres show a slight increase in the sodium amount ( $\text{Na}/\text{K}=0.94$ ), while feldspathoid lamprophyres are distinguished by their preferentially sodium composition. Various groups of lamprophyres were shown to differ in their alumina contents. Feldspathoid lamprophyres are highly aluminous ( $\text{al}'=0.73$ ), feldspathic lamprophyres (Pripyat graben) can be related to medium-aluminous rocks ( $\text{al}'\approx 0.4$ ), while melilitite lamprophyres (alnoites) are low aluminous ( $\text{al}'\approx 0.1$ ). However, all lamprophyres are of miaskite nature ( $\text{Ka}<1$ ), sometime, slightly modified to the agpaitic one (Vetkhinskaya 1 borehole,  $\text{Ka}=0.7$ ). In general, feldspathic lamprophyres show high  $\text{SiO}_2$ ,  $\text{TiO}_2$ ,  $\text{Al}_2\text{O}_3$  and

low Fe<sub>2</sub>O<sub>3</sub>, and MgO contents. Feldspathoid lamprophyres are described by the highest SiO<sub>2</sub>, Al<sub>2</sub>O<sub>3</sub> and lowest MgO concentrations, but their aluminium content is slightly increased. Melilite lamprophyres are mostly magnesian and poor in alumina. All the above chemical features of various groups of lamprophyres are due to their mineral composition.

The geochemical features of lamprophyres are shown in a diagram of the distribution of trace elements normalized to the primitive mantle. With the rather similar distribution of trace elements feldspathic lamprophyres from the Pripyat graben typically show the K, Na, Ba maxima and the U, Th, Pb minima, melilitite lamprophyres are described by the Th, Ce, P maxima and the U, Da, La minima (Fig. 4). Alnoite is distinguished by the La and Ba maxima (especially in carbonate alnoites, where the barium concentration in rock is nearly 1% } and the U, Pb, Zr and Hf minima. For comparison Fig 4 shows also spectra of the trace elements distribution in alkali picrites of the Pripyat graben and Zhlobin saddle with their typical well-defined K and Hf minima. An analysis of the trace element distribution in alkali picrites and lamprophyres suggests a specific geochemical nature of lamprophyres.

Table 3

**Isotopic composition of strontium and neodymium from Paleozoic lamprophyres of Belarus**

Sample	<sup>87</sup> Sr/ <sup>86</sup> Sr measured	<sup>87</sup> Sr/ <sup>86</sup> Sr 0	εSr	<sup>143</sup> Nd/ <sup>144</sup> Nd measured	<sup>143</sup> Nd/ <sup>144</sup> Nd <sub>0</sub> расч	eNd (0)	eNd (t)	T (DM)	T (DM-2)
<b>Bel--6</b>	0,707190	0,705559	<b>21,2</b>	0,512302	0,512049	<b>-6,6</b>	<b>-2,0</b>	1152	1308
<b>OOP 40a</b>	0,70555	0,704758	<b>9,8</b>	0,512550	0,51228	<b>-1,7</b>	<b>2,4</b>	890	942
<b>Luch-13</b>	0,704441	0,703614	<b>-6,4</b>	0,512468	0,512270	<b>-3,3</b>	<b>2,1</b>	791	962

Bel-6,— Vetkhinskaya 1 borehole, depth of 4,565m, lamprophyre; OOP40a— Artukovskaya 3 borehole, depth of 4,518m monchiquite; Luch-13 — Luchin borehole 763, depth of 229m, alnoite

The Sr—Nd isotope ratios in the studied samples of Palaeozoic lamprophyres (Table 3) place the rock under examination in a field restricted between the PREMA and enriched mantle source EM I isotope characteristics. Feldspathic lamprophyres of the Vetkhino structure of the Pripyat graben are described by the heavier strontium isotope composition (εSr=21.2), and alnoites are depleted in radiogenic Sr. There are also differences in the Nd isotope distribution, εNd varies in the range of values from–2.2 (feldspathic lamprophyres from the Vetkhino structure) to +2.1—+2.4 (alnoites, monchiquite).

The simulated Sm-Nd age of lamprophyric rock sources corresponds to the age interval T<sub>DM</sub>=0.79–1.15, T<sub>DM2</sub>= 0.95–1.31 and represents the age of the rock source metasomatic enrichment. The simulated age was noted to be dependent on the εNd value; lamprophyre with a negative εNd value is older in age.

## CONCLUSION

Three subfamilies of lamprophyric varieties of alkali rocks mostly related to the hypabyssal facies of magmatism and distinguished almost in every region of magmatism development suggest that the process of this rock magmatic source differentiation occurred on a large scale. This condition together with the data obtained earlier [7,8] does not exclude the possibility that kimberlitic and lamproitic magmatism similar in composition to that observed in the Arkhangelsk province would have developed within the Palaeozoic alkali igneous formation of Belarus.

The research was performed under the financial backing of the BRFFI, grant X08P-087.

## REFERENCES:

1. **Korzun V.P., Makhnach A.S.** Upper-Devonian alkali volcanogenic formation of the Pripyat Trough. Minsk, Nauka i Tekhnika Publ. 1977. 164 p. (in Russian).
2. **Veretennikov N.V., Laptsevich A.G., Vladykin N.V., Mikhailov N.D.** Association of alkali lamprophyres and carbonatites of the Luchin diatreme cluster as a positive magmatic criterion of forecast of and search for potentially diamondiferous kimberlites // *Innovations in Geological Science – a Way of Efficient and Multipurpose Utilization of Mineral Resources*. Minsk, 2007. P.55-58 (in Russian).
3. **Petrographic code** of Russia magmatic, metamorphic, metasomatic, impact rock assemblages. St. Petersburg, 2008, 200p. (in Russian).
4. **Lodochnikov V. N.** Major rock-forming minerals. Moscow, 1974, 248 p. (in Russian).
5. **Williams H., Turner F., Gilbert Ch.** Petrography. Vol.1. Moscow, 1985. 301 p. (in Russian).
6. **Sun S.S., McDonough W.F.** Chemical and isotopic systematics of oceanic basalts: implications for mantle composition and processes // *Magmatism in the Ocean Basins*. Geol. Soc. London Spec. Publ.–1989.–Vol. 42.– P. 313-346.
7. **Mikhailov N. D., Vladykin N.V., Laptsevich A.G.** Geochemical features of alkali rocks of Palaeozoic magmatism of Belarus // *Deep-seated magmatism, its sources and plumes*// Vladivostok, Irkutsk 2008. P.169-180.
8. **Mikhailov N. D., Laptsevich A.G.** Distribution of radioactive elements (U, Th) in Paleozoic alkali igneous rocks of Belarus // *Lithosphere*, №1 (30), 2009, P.. 126-133 (in Russian).  
(in Russian).

## **Lamprophyres of South Sikhote-Alin**

L.L. Petukhova, Prikhod'ko V.S.

*Yu.A. Kosygin Institute of Tectonics and Geophysics, Far East Branch, Russian Academy of Sciences, Khabarovsk, Russia, e-mail: [Ludmila.pet.@mail.ru](mailto:Ludmila.pet.@mail.ru)*

### **ABSTRACT**

The paper describes petrogeochemical and mineralogical features of the rocks which compose dykes and volcanic pipes among the Jurassic terrigenous deposits of the volcanogenic-sedimentary unit of the Ariadnensky formation (South Sikhote-Alin). K-Ar isotope age of the magmatic rocks varies in a range between 152-159 Ma. The magmatic rocks present grayish-greenish rocks of porphyry structure and globular texture. Amphibol, mica, clinopyroxene are alloliths, the groundmass is composed of fibrous-diverse aggregates of kersutite, phlogopite, clinopyroxene, ilmenite, and magmatic calcite. Olivine was not recorded in these rocks. The studied rocks which were originally referred to the meymechite-picritic complex have a number of specific features such as a) the presence of matrix; b) mica and amphibole enrichment; c) the absence of olivine among the matrix; d) porphyric structure that allows us to assign them to lamprophyres. They bear great similarities to the lamprophyres of the Kosvozh complex of the Polar Urals. Mineralogical and geochemical features of the described rocks are more close to an alkali series of an alnoite-type lamprophyres family or most probably, its carbonatized variety – aillikite.

### **INTRODUCTION**

Diamond occurrences in placers and rocks of meymechite-picrite complex of the Sikhote-Alin orogenic belt [1, 8] attract considerable interest of the researchers to these rather rare magmatic formations and promote searching for potential diamond-bearing rocks such as kimberlites, lamproites and lamprophyres in the region. Rocks discovered in dikes and volcanic pipes near the Ariadnoe settlement (Primorye) were primarily ascribed to picrites [7]. An integrated study has revealed definite specific features of the rocks. This allowed their classification with the lamprophyres. Rocks with similar composition and structure were found by one of the authors in the Kedrovka river alluvial sediments.

### **GEOLOGICAL SETTING**

Southern Sikhote-Alin is a heterogenic collage of different in structure and origination terranes – fragments of accretionary prisms. The latter consist of lenticular packets of Triassic to Jurassic terrigenous-volcanogenic-siliceous complexes embedded into Late Jurassic to Early Cretaceous turbidite matrix [2]. The Bikin and Samarka accretionary prisms of Sikhote-Alin are known for exposures of small-sized bodies of exotic mafite-ultramafite rocks close to kimberlites, meymechite, lamproite, lamprophyres in petrogeochemical and mineralogical peculiar features. In the vicinity of Ariadnoe settlement micaceous

mafite-ultramafites constitute a series of small dikes persistent along the strike (near-latitudinal) with 8-10 m in width and 100-300 m in extent. We observed similar rocks along the left side of the Malinovka river, between the Pad' Malaya Pozhiga and Todokhov Pad' creeks, where they constitute a thin subvertical

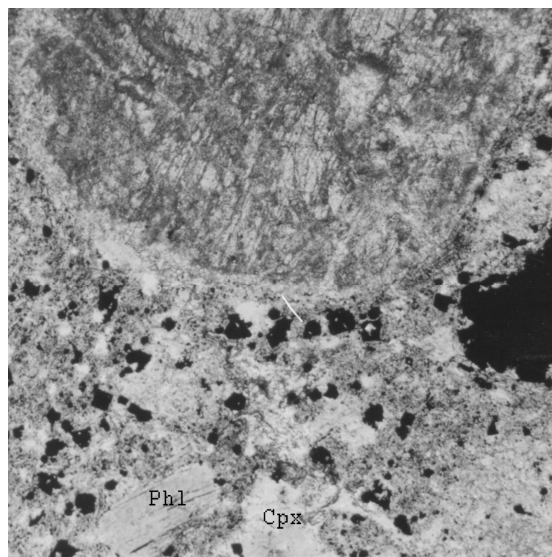


**Fig.1. Globular structure of picrites. x 54.**

dike and a small volcanic pipe within the Jurassic terrigenous deposits (sandstones and siltstones) of the volcanogenic-sedimentary sequence of the Ariadne formation. K-Ar age of the co-existing kaersutite and Ti-biotite from the rocks exposed near the Ariadne settlement varies from 152 to 159 Ma [10]. Near the contact with host rocks brecciated varieties of picrite are developed, the fragments of which are dominated by sandstones. The central part of the dike consists of rather massive rocks with large-sized (occasionally giant-sized) impregnations of amphibole and mica, and carbonate globules. The rocks are enriched in biotite, quartz, and carbonate and penetrated by thin barite veinlets. The volcanic pipe is filled with altered and weathered rocks thus it is difficult to judge about its inner structure.

## **ANALYTICAL METHODS**

The chemical composition of the rocks has been analyzed at the Central Laboratory of PA "Dalgeologiya" using a "wet" chemistry method. The REE contents and rare elements were determined at the Analytical Center of Yu.A. Kosygin Institute of Tectonics and Geophysics of the Far East Division of the Russian Academy of Sciences in Khabarovsk, analysts V.E. Zazulina and D.V. Avdeev, using ISP-MS method. The chemical composition of rock-forming and accessory minerals was measured using JX-50 X-ray spectral microanalyzer at the Institute of Volcanology and Sedimentology in Petropavlovsk-Kamchatsky, analyst V.M. Chubarov.

Table 1.

**Chemical compositions (wt.%) and contents of trace components of lamprophyres (g/t) from South Silhote-Alin.**

Component	AP 02-01	AP02-02	AP02-04	AP 02-05	AP 02-06	AP 02-08	AP 02-09	AP 02-13	AP02-15	AP 02-17
SiO <sub>2</sub>	36,9	37,29	35,21	36,10	36,57	37,6	36,00	33,86	31,19	33,03
TiO <sub>2</sub>	3,49	3,30	3,35	3,58	3,38	3,25	3,37	3,83	3,46	3,26
Al <sub>2</sub> O <sub>3</sub>	7,23	7,13	6,62	7,14	7,59	8,97	7,04	7,61	8,55	7,25
Fe <sub>2</sub> O <sub>3</sub>	8,59	8,73	7,79	7,87	7,00	5,67	7,24	3,97	4,10	5,54
FeO	8,10	7,76	7,53	7,85	8,11	8,50	7,77	10,12	11,95	7,52
MnO	0,26	0,28	0,26	0,26	0,24	0,22	0,28	0,19	0,20	0,30
MgO	16,17	16,31	17,11	16,98	15,07	15,15	15,72	12,82	13,04	10,75
CaO	10,10	9,42	11,35	10,23	11,23	9,97	11,22	8,43	8,61	13,26
Na <sub>2</sub> O	1,39	1,44	1,34	1,25	0,98	1,44	1,25	0,30	0,26	0,44
K <sub>2</sub> O	1,39	1,38	1,30	1,26	1,77	1,71	1,34	0,55	0,54	0,88
P <sub>2</sub> O <sub>3</sub>	0,53	0,20	1,11	1,35	1,59	1,05	1,25	1,76	1,83	2,37
SO <sub>3</sub>	<0,1	<0,1	<0,10	0,23	<0,10	0,10	0,29	0,44	1,23	0,49
CO <sub>2</sub>	3,06	2,75	4,34	2,06	3,03	1,77	2,80	9,10	8,19	9,36
H <sub>2</sub> O <sup>x</sup>	2,64	2,91	2,89	3,13	3,27	3,21	3,27	5,83	5,55	4,27
н.п.п.	4,95	4,66	6,06	4,18	5,01	3,69	4,84	12,65	12,12	11,87
Sc	30,71	33,21	32,95	32,29	31,26	29,83	32,15	31,23	35,10	26,72
Ti	24338	23784	24230	24612	24949	23466	26070	27773	28731	21135
V	254,20	258,76	249,33	254,20	269,65	299,01	274,94	464,19	430,95	336,91
Cr	587,08	649,60	620,90	558,29	509,88	455,29	579,83	510,81	497,58	363,38
Mn	2407,18	2533,2	2639,4	2283,05	2337,76	1906,22	2573,56	1711,24	1771,0	2492,38
Co	71,22	70,08	69,29	68,86	63,67	65,81	73,05	59,48	72,74	52,65
Ni	469,09	474,36	433,22	408,44	369,49	434,59	453,67	387,81	438,88	320,01
Cu	45,24	50,56	48,57	45,34	50,76	83,54	49,24	66,15	84,06	70,84
Zr	435,22	443,57	424,97	423,00	453,49	486,99	434,34	315,40	447,12	265,00
Nb	113,40	119,40	110,83	129,39	184,22	116,87	135,34	222,07	379,89	182,42
La	159,31	139,72	147,41	180,84	182,11	99,96	176,00	150,93	139,79	211,62
Ce	390,31	343,60	366,21	406,13	409,47	228,88	413,95	325,59	301,86	467,16
Pr	45,04	39,00	41,13	45,87	47,01	27,31	47,51	38,05	34,87	52,28
Nd	169,39	144,01	157,43	173,76	181,64	110,61	183,71	153,18	140,32	207,05
Sm	27,59	22,76	26,60	30,52	34,10	22,52	32,84	30,72	29,92	40,49
Eu	7,41	6,23	7,46	8,75	9,93	6,81	9,22	9,17	9,06	11,32
Gd	24,73	20,89	24,84	29,10	32,35	21,09	30,08	28,52	29,83	37,99
Tb	2,65	2,22	2,73	3,25	3,77	2,66	3,41	3,75	4,43	4,47
Dy	10,28	8,64	10,83	13,38	15,73	11,16	13,74	17,88	23,33	19,48
Ho	1,69	1,42	1,77	2,20	2,54	1,83	2,21	3,18	4,25	3,40
Er	4,26	3,69	4,46	5,30	6,00	4,22	5,22	7,89	10,38	8,36
Tm	0,51	0,44	0,51	0,59	0,73	0,54	0,57	0,87	1,20	0,92
Yb	2,73	2,50	2,83	3,13	3,71	2,80	3,08	4,50	6,27	4,88
Lu	0,41	0,39	0,40	0,43	0,56	0,43	0,42	0,58	0,83	0,60
Hf	9,31	9,22	9,18	9,72	10,46	11,76	9,99	6,74	9,89	5,97

*Note.* Chemical analyses were carried out at Central laboratory «Dalgeologiya», trace elements were established using ISP-MS method at Analytical Centre of T&G FEB RAS (Khabarovsk).

**PETROGEOCHEMICAL CHARACTERISTICS OF THE ROCKS**

The magmatic rocks present grayish-greenish rocks of porphyry structure and globular texture. Amphibole, mica, clinopyroxene represent alloliths, the groundmass of the rocks is composed of fibrous-diverse aggregates of kersutite, phlogopite, clinopyroxene, ilmenite, and magmatic calcite. Olivine was not established in these rocks.

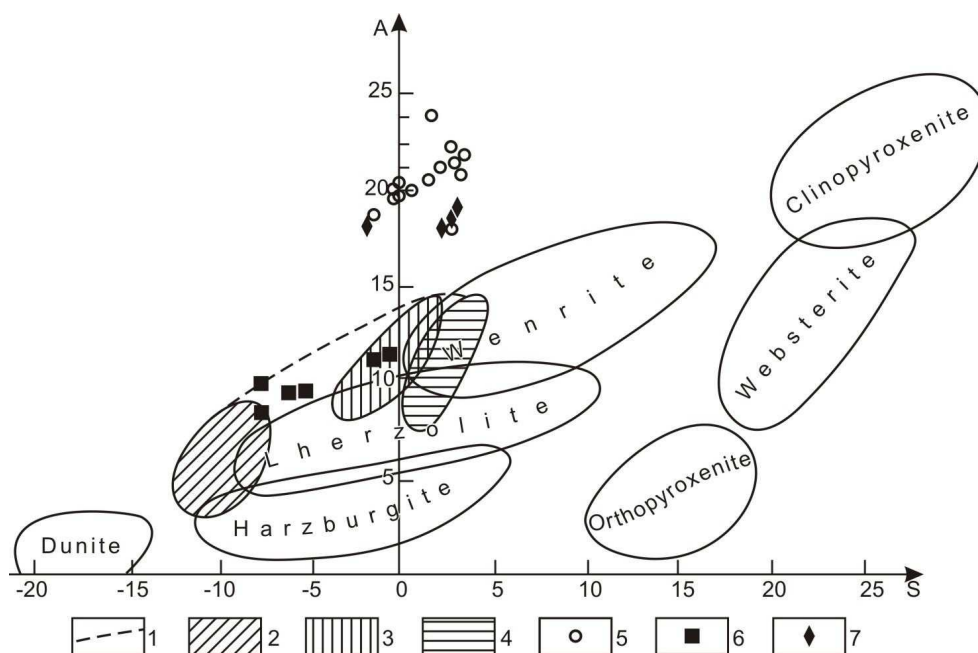


Fig. 2. Location of figurative points of lamprophyres compositions of South Sikhote-Alin plotted on the diagram in coordinates  $A=Al_2O_3+CaO+Na_2O+K_2O$  and  $S=SiO_2+(Fe_2O_3+FeO+MgO+MnO+TiO_2)$ . (wt %.).

1 – field of compositions of volcanic and hyperbyssal rocks of a picrite family; 2 - meimechites; 3 – picrites; 4 – peridotite comatiites; 5 – points of lamprophyres compositions of South Sikhote-Alin; 6 – points of meimechite compositions of Sikhote-Alin; 7 – points of lamprophyres compositions of the Polar Urals.

Based on their chemical composition (Table 1), the rocks are referred to as ultrabasic group ( $SiO_2$  – 31.19-37.6 wt %) and characterized by a rather high content of alkali sum varying in a broad range from 0.7 to 3.3 wt %. They are related to K-series ( $Na_2O/K_2O = 0.48-1.04$ ).  $TiO_2$  contents vary from 2.8 to 5.0 wt %, FeO total – 11.4 - 20.8 wt %, CaO – 6.9 – 13.5 wt %,  $Al_2O_3$  – 4.6 - 9.1 wt %, and MgO – from 10.9 to 17.11 wt %. To compare the chemical composition of the considered rocks with other types of ultramafites, the known diagram by V.A. Barsukov and L.V. Dmitriev (Fig. 2) was utilized which indicates that figurative points of the described rocks composition are plotted in the field of lamprophyres of the Kosvozh complex of the Polar Urals and remote from the field of picrites [6]. On the ternary diagram in coordinates MgO –  $Al_2O_3$  – FeO (Fig. 3), micaceous rocks and the Polar Urals lamprophyres are plotted in the field of alnoites and aillikites [9]. It was quite possible that the primary chemical composition of the studied rocks was distorted due to secondary transformations. As the ratios of Zn/Hf and other elements (Zn/Hf, Ni/Co, and Cr/V) are sufficiently constant, this process hardly disturbs the petrogeochemical structure of the rocks.

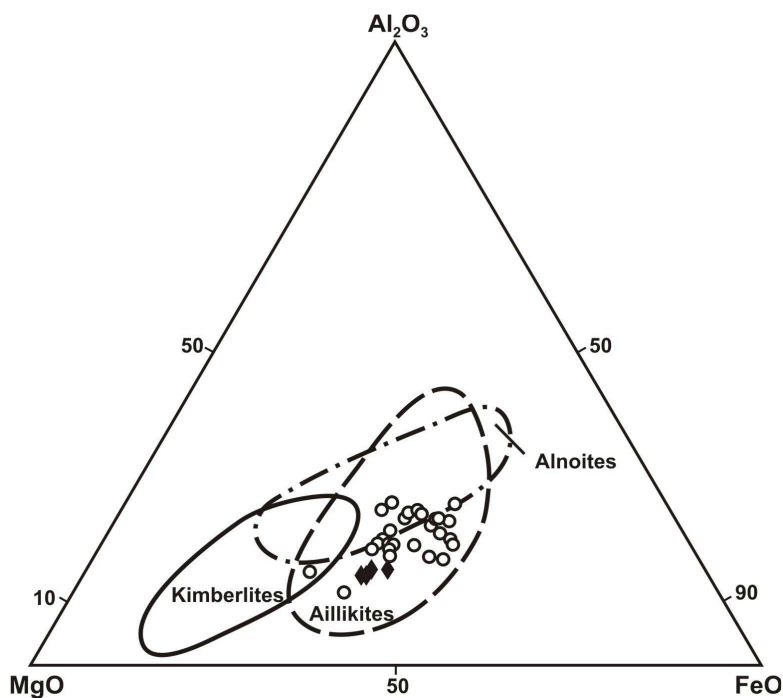


Fig. 3. Fields of ultramafic lamprophyres and kimberlites compositions from (9) and variations of lamprophyres compositions from the Polar Urals and South Sikhote-Alin (for symbols see Fig. 2).

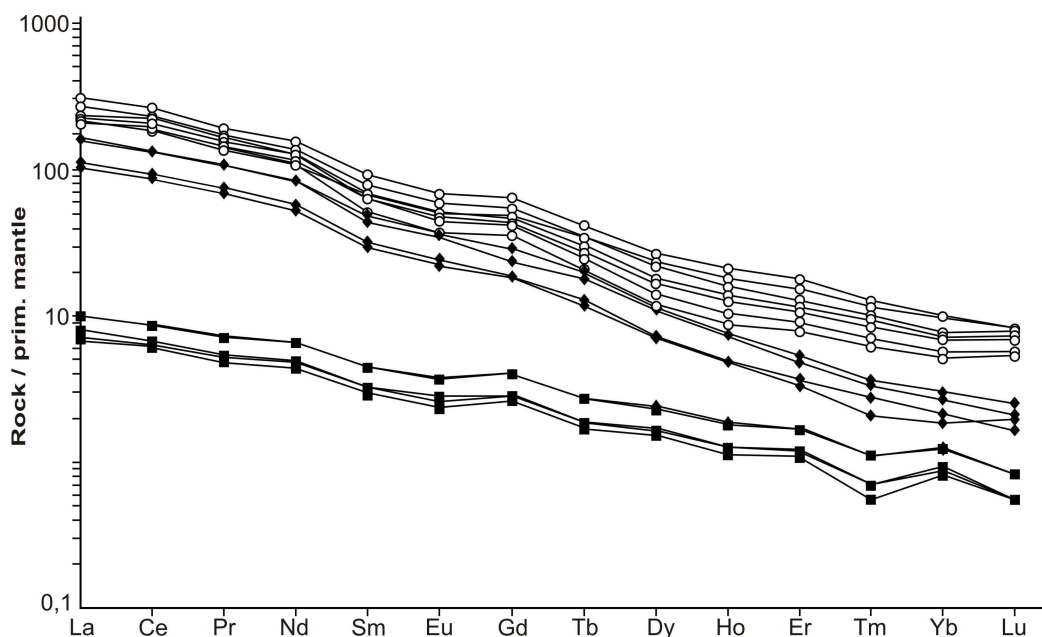


Fig. 4. Rare earth spectra of ultrabasic lamprophyres from the Polar Urals and South Sikhote-Alin, and meimechites from Sikhote-Alin. (for symbols see Fig. 2).

The contents of the coherent elements (Cr, Co, Ni) in these rocks occupy the intermediate position between ultrabasites and basites. The ratio Ni/Co varies from 4.7 to 6.5, whereas Ni/Co ratio in hyperbasites varies in a wider range from 10 to 25, and from 6 to 16 in lamproites [3]. The Cr/V ratio changes

insignificantly, from 1 to 2.4, that is typical of the Polar Urals lamprophyres and alnoites [6].

Micaceous picrites from the Ariadne settlement demonstrate a high enrichment in LREE at a lowered level of HREE accumulation (Fig. 4). The value of La/Yb ranges from 33 to 58. The REE spectrum of these rocks exhibits a negative gently sloping inclination at slightly manifested Gd anomaly. The REE total contents in the studied rocks are very high (775-1017 g/t) and comparable with total contents in the lamprophyres of the Kosvozh complex in the Polar Urals [6]. In general, they are tens times higher than in typical picrites and meymechites. Fig. 4 shows distinct differences in REE distribution in the meymechites and micaceous picrites from Sikhote-Alin. Judging from the Sm and La/Yb ratios, the considered rocks, like the lamprophyres of the Kosvozh complex from the Polar Urals, are plotted in the field of ultramafic lamprophyres (Fig. 5) [9].

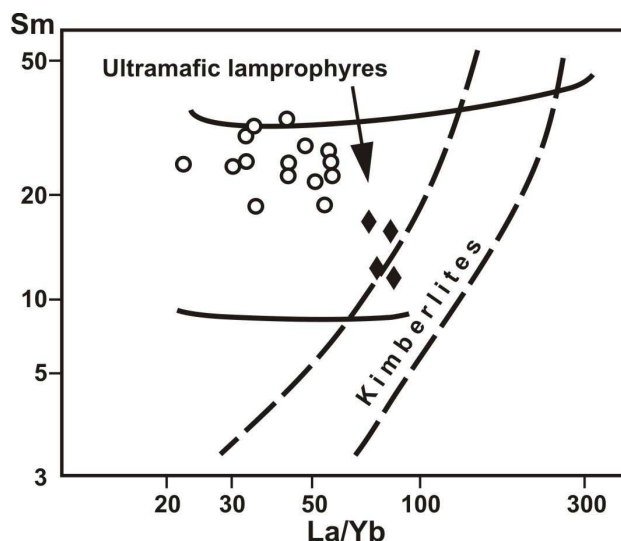


Fig. 5. Sm and La/Yb ratio for kimberlites and ultramafic lamprophyres (for symbols see Fig. 2).

The geochemical composition of the considered rocks is characterized by increased concentrations of high-charged lithophilous elements such as Ti, Sc, Ta, Nb, Zr, Hf, and high ratio values Zr/Hf (43-47), Nb/Ta (14-22). This is the case for the alkali rocks and kimberlites.

## MINERALOGY OF THE ROCKS

Chemical analyses (Table 2) of the minerals of the studied rocks give an idea of their compositional peculiarities.

*Clinopyroxenes* represented by low-alumina doopside-augites are partly plotted in the field of pyroxene distribution from ultramafic lamprophyres and

Table 2.

## Chemical composition of the lamprophyres minerals from South Sikhote-Alin

Pyroxenes												
oxides	1	2	3	4	5	6	7	8	9	10	11	12
SiO <sub>2</sub>	50,85	51,48	50,42	51,28	51,01	51,64	52,82	50,72	53,39	53,55	52,86	52,51
TiO <sub>2</sub>	1,78	1,16	1,17	1,26	1,03	1,15	1,30	1,93	1,08	0,65	0,69	0,68
Al <sub>2</sub> O <sub>3</sub>	2,91	2,17	3,47	2,81	3,42	3,63	2,08	3,12	0,97	3,61	3,75	3,50
FeO	4,95	5,69	6,39	5,66	6,56	6,26	6,22	6,74	9,73	6,21	5,67	6,06
Cr <sub>2</sub> O <sub>3</sub>	0,00	0,10	0,15	0,12	0,16	0,19	0,00	0,00	0,00	0,60	0,68	0,64
MgO	14,71	15,79	16,09	14,56	15,18	15,37	14,97	13,74	11,84	16,38	16,46	16,18
CaO	22,92	22,31	21,11	22,01	21,04	19,29	20,99	23,49	20,12	18,88	18,61	18,56
Na <sub>2</sub> O	0,93	0,59	0,97	0,81	0,66	0,96	0,77	1,07	2,74	0,98	1,05	1,39
K <sub>2</sub> O	0,00	0,04	0,01	0,01	0,02	0,00	0,02	0,02	0,02	0,05	0,04	0,04
MnO	0,01	0,00	0,01	0,00	0,00	0,10	0,08	0,12	0,32	0,00	0,00	0,00
<b>Total</b>	99,06	99,33	99,79	98,52	99,08	98,59	99,25	100,95	100,21	100,91	99,81	99,56

Mica												
oxides	1	2	3	4	5	6	7	8	9	10	11	12
SiO <sub>2</sub>	37,71	37,73	38,43	38,91	37,32	38,89	37,82	37,56	38,04	38,47	36,99	35,63
TiO <sub>2</sub>	6,00	5,79	3,57	2,76	4,55	3,43	3,78	5,42	5,68	3,71	6,08	5,00
Al <sub>2</sub> O <sub>3</sub>	15,39	15,31	13,17	12,47	15,47	15,89	15,55	15,7	16,02	15,05	15,34	15,38
FeO	9,31	9,05	12,87	14,13	9,29	7,39	7,41	9,35	8,81	8,04	9,13	12,86
Cr <sub>2</sub> O <sub>3</sub>	0,21	0,28	0,00	0,01	0,10	0,00	0,00	0,51	0,90	0,00	0,43	0,52
MgO	17,76	17,91	18,49	17,44	18,94	20,76	20,18	18,53	19,00	20,53	18,42	17,26
CaO	0,04	0,03	0,26	0,13	0,02	0,00	0,00	0,01	0,00	0,03	0,00	0,04
Na <sub>2</sub> O	0,4	0,72	0,29	0,06	0,71	0,6	1,05	0,65	0,54	0,59	0,48	0,19
K <sub>2</sub> O	9,67	9,77	8,97	9,09	9,19	8,82	8,99	9,48	8,81	7,99	9,79	7,91
MnO	0,03	0,02	0,23	0,25	0,01	0,01	0,00	0,00	0,03	0,05	0,02	0,01
<b>Total</b>	96,52	96,61	96,28	95,25	95,6	95,79	94,78	97,21	97,83	94,46	96,68	94,8

Amphibole				Spinel
oxides	1	2	3	4
SiO <sub>2</sub>	41,30	42,40	45,80	37,90
TiO <sub>2</sub>	4,70	3,10	2,90	3,60
Al <sub>2</sub> O <sub>3</sub>	12,10	11,10	8,40	15,60
FeO	9,70	14,50	10,00	7,30
Cr <sub>2</sub> O <sub>3</sub>	0,00	0,00	0,00	0,00
MgO	14,50	12,20	16,30	21,40
CaO	11,60	10,80	9,90	0,10
Na <sub>2</sub> O	3,00	3,00	4,60	0,80
K <sub>2</sub> O	1,70	1,90	0,90	9,00
MnO	0,00	0,10	0,20	0,00
<b>Total</b>	98,60	99,10	99,00	95,70

*Note* : Analyses were made using microanalyzer «Camebax», analyst V.M. Chubarov (IV&S FEB RAS, Petropavlovsk-Kamchatsky).

pyroxenes from lamprophyres of the Polar Urals (Fig. 6) [6]. Figure 7 illustrates variations of major oxides such as Ti, Fe, Ca, Si, Al, and Na in diopside-augites depending on the MgO content. The pair MgO-CaO shows the lowest ratio, while other pairs (MgO - TiO<sub>2</sub>, MgO - FeO, MgO - SiO<sub>2</sub>, MgO - Al<sub>2</sub>O<sub>3</sub>) demonstrate the presence of two groups of pyroxenes with different pattern of variation trends. Large-sized phenocrystals of the pyroxenes have a higher Mg content. On the contrary, small-sized clinopyroxene grains (needles in the groundmass) are

characterized by high Fe and Ti contents. Agyrin component was not found in the pyroxenes, with  $\text{Na}_2\text{O} = 2.74\%$  only in one sample.

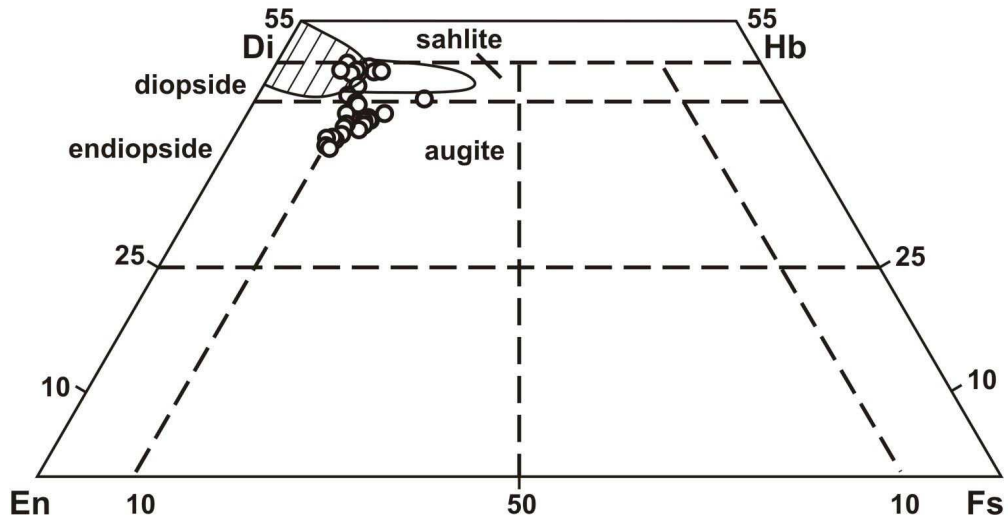


Fig. 6. Compositions of monoclinic pyroxenes from lamprophyres of the Polar Urals (shaded area) and South Sikhote-Alin (for symbols see Fig. 2), and ultramafite lamprophyres (unshaded area).

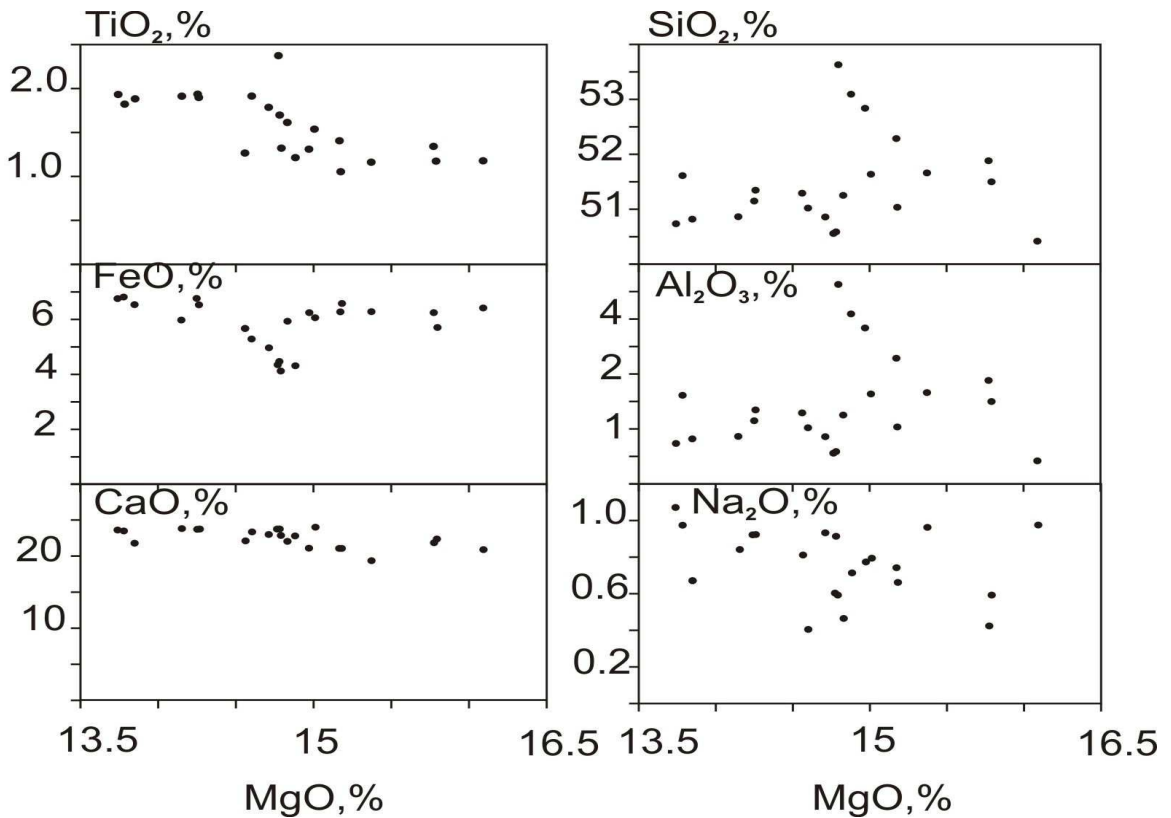


Fig. 7. Variations in basic oxides (Ti, Fe, Ca, Si, Al, Na) in clinopyroxenes from lamprophyres of South Sikhote-Alin in dependence of MgO concentration.

**Calcic amphiboles** are represented by titaniferous pargasite-magnesiohastingsites (Fig. 8) which are parts of the primary minerals (from phenocrysts to microliths of the groundmass), as well as magnesioferrous and actinolitic hornblendes. The latter are distributed along clinopyroxene and pargasite. In large-sized amphibole grains chemical zonation has been distinguis-

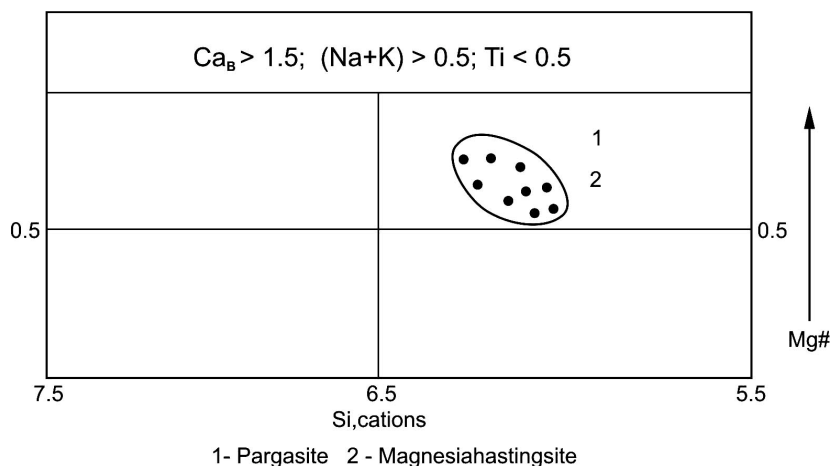


Fig. 8. Points of amphibole compositions of lamprophyres from South Sikhote-Alin in coordinates Si (cations) and Mg#.

hed as follows: the Ti and Mg contents increase from the centre to the edges, while the Al, Fe, and K contents decrease. In the pargasites a constant negative correlation between the Na and Al and K contents has been established.

**Mica** is one of the major rock-forming minerals. It occurs in the groundmass both as large phenocrysts and small laths. Isolated samples reach several cm in size. Based on the chemical composition (Fig. 9), mica falls in the field of the mica distribution from lamprophyres, according to [10]. The phlogopite is enriched in Ti – from 1.84 to 6 wt % with the average content = 4.43 wt %. The Al<sub>2</sub>O<sub>3</sub> content varies in a range from 12.4 to 16 wt %. Micas exhibit different chemical zonation pattern, as compared to amphiboles. The higher Ti, Mg and Al contents and lower Fe and K contents were established in the core areas of the mica grains. Figure 10 shows the variation trends of phlogopite compositions from kimberlites, lamproites, and minettes, according to [4]. Concentration points of the compositions of the studied mica and those from lamprophyres of the Polar Urals are plotted near the minette trend, where against the background of TiO<sub>2</sub> increase the Al<sub>2</sub>O<sub>3</sub> content is slightly elevated. In addition, they considerably differ from the trends of mica from kimberlites and lamproites.

**Chrome-spinel** occurs in two modifications: high-titanium and high-chrome low-titanium. The compositional points of titanium-bearing chrome-spinelides fall near the trend of chrome-spinelids from meymechites of Sikhote-Alin. *Ilmenites* of the groundmass exhibit insignificant amounts of Mg, Al, and Cr (< 0.25 wt %) with high content of the pyrophanite molecular (MnO = 5.86 wt %). *Ore minerals* are

represented by pyrite, chalcopyrite, and pentlandite, and accessory minerals by apatite, sphene, monazite, and orthite.

## RESULTS

The considered rocks which were primarily related to the representatives of meymechite-picrite magmatism are characterized by a number of mineralogical

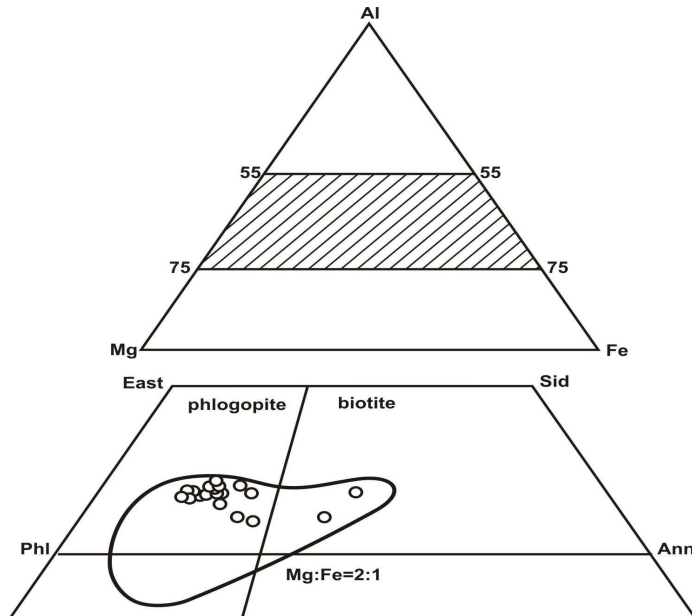
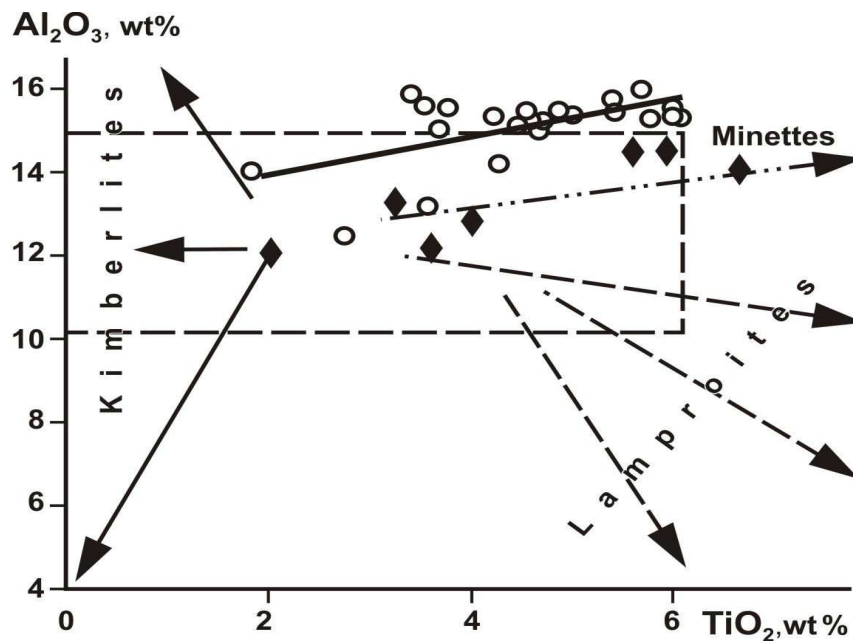


Fig. 9. Mica composition from ultramafite lamprophyres (unshaded area) (9) and lamprophyres from South Sikhote-Alin.



**Fig. 10. Variations in phlogopite compositions from lamprophyres of South Sikhote-Alin and Polar Urals (for symbols see Fig. 2).**

peculiar features such as (a) presence of magmatic phlogopite; (b) enrichment in mica and amphibole; (c) absence of olivine in the impregnations; (d) presence of the porphyry structure that brings them closer to lamprophyres. In the diagrams (Figs. 3, 4), the data points of their compositions are located in the field of the distribution of the lamprophyres from the Polar Urals, and together with the Polar Urals rocks they plot in the field of the alnoite and aillikite distribution. The studied rocks cannot be ascribed to lamproites as they are distinguished by a lowered K content, absence of the K phases, the elevated Fe and Ca contents, and lower Zr, Sr, and Ni concentrations, as compared to the latter [11]. These rocks exhibit some similar geochemical features (close content and pattern of REE distribution) to kimberlites, but differ from them by the absence of olivine, barophilic accessory minerals as well as high Ti, Fe, Ca contents and lowered MgO, Cr, and Ni contents.

As mentioned above, the described rocks bear similarities to the lamprophyres of the Kosvozh complex of the Polar Urals. A close pattern of the REE distribution curves in the lamprophyres of southern Sikhote-Alin and Polar Urals, medium and light in particular, can indicate to the similar geochemical mantle sources of the original magmas. In terms of their mineralogical and geochemical features, the described rocks are ascribed to the alkaline series of alnoite-type lamprophyres, most likely, to its carbonitized variety –aillikite.

The lamprophyre exposures nearby the Ariadne settlement, like the localities of the similar rocks from the Kedrovka river alluvium, are located along one line of NE strike together with the known exposures of meymechite magmatism [7]. Rocks close in composition and structure, are found to the north, in the territory of the Khabarovsk Krai, where judging from the geological survey results, dikes of camptonite, limburgite, monchiquite, augitite, and other exotic rocks are found. The age range of the lamprophyres from the Ariadne settlement varies in the interval from 152 to 159 Ma, while the augitite dike from the northern Sikhote-Alin orogenic belt (K-Ar method) is 151 Ma. The K-Ar datings constrain the age of meymechites from the Barakhtinsky section to 134.4 Ma [5]. One can suggest that the accretionary processes in Sikhote-Alin were accompanied with a long period of mafite-ultramafite magmatism, primarily, lamprophyric, and then meymechite-picritic.

The presented petro-geochemical analyses data demonstrate that the studied lamprophyres are enriched in K, Ti, Nb, Zr, and REE, consequently, they can be proposed as the products of K-bearing ultramafite melts originated from metasomatically altered (hydrous, carbonatized) depleted mantle source.

## **CONCLUSIONS**

It has been established that the studied rocks of the Ariadne settlement in their mineralogical, petrochemical, and geochemical features do not belong to the representatives of the meymechite-picritic complex of Sikhote-Alin, and correspond to lamprophyres of alnoite and aillikite affinity.

## REFERENCES

1. **Ivanov, V.V., Kolessova, L.G., Khanchuk, A.I. et al.** Occurrence of diamonds in the Jurassic rocks of the meymechite-picritic complex of Sikhote-Alin orogenic belt // Doklady of Akademii Nauk, 2005. V. 404, N 1. p. 72-75.
2. **Khanchuk, A.I.** Geodynamics, magmatism and metallurgy of East Russia. Book 1. (Ed.). Vladivostok: Dalnauka, 2006. 572 p.
3. **Bogatikov, G.A., Ryabchikov, I.D., Kononova, V.A. et al.** Lamproites /M.: Nauka, 1991. 302 p.
4. **Mitchell, R.X.** Lamproites – the family of the alkaline mountain rocks // Notes of All-Union Mineralogical Society, 1988. P. CXVII. Issue 5. P. 575-586.
5. **Prikhod'ko, V.S., Petukhova, L.L., Soldatov, A.I.** Meymechites from the Sikhote-Alin mantle-folded system: the distribution area, age, and mantle sources // Volcanism and geodynamics: Proceedings of the IV All-Russian Symposium on Volcanology and Paleovolcanology. Petropavlovsk-Kamchatsky, . V. 2. p. 467-470.
6. **Soboleva, A.A., Shishkin, M.A., Romanova, N.V. et al.** Ultrabasic lamprophyres from the western slope of the Polar Urals // Herald of the Komi Scientific Center: Institute of Geology, 2007. N 3, p. 2-7.
7. **Shcheka, S.A.** Basite-hyperbasite intrusions and impregnations in the effusives of the Far East. M.: Nauka, 1983.
8. **Shcheka, S.A., Ignatiev, A.V., Nechaev, V.P., and Zvereva, V.P.** The first diamond findings in placers of Primorye // petrology. 2006. V. 14, N 3. P. 319-336.
9. **Rock, N.M.S.** The nature and origin of ultramafic lamprophyres: Alnoites and allied rocks // Journal of Petrology. 1986. V. 27, Pt1. P. 155-196.
10. **Shcheka, S.A., Vrzhosek, A.A., Vytsoskiy, S.V.** Jurassic meymechite-picrite complexes of Prymorye, Russia: Comparative study with komatite and Japanese picrite suites // Plumes and problems of deep sources of alkaline magmatism. Khabarovsk, 2003. P. 184-200.
11. **Wooley, A.R., Bergman, S.C., Edgar, A.D et al.** Classification of lamprophyres, lamproites, kimberlites, and the kalsilitic and leucitic rocks // The Canadian Mineralogist. 1996. V. 34. P. 175-186.

12.